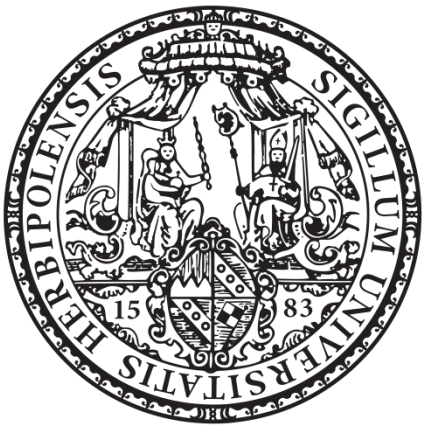

Hypoxia and hypoxia-inducible factor 1α modulate the immune response of human dendritic cells against *Aspergillus fumigatus*

Dissertation zur Erlangung des

naturwissenschaftlichen Doktorgrades

der Julius-Maximilians-Universität Würzburg

vorgelegt von

Mirjam Fließer

Geboren in Nürnberg

Würzburg 2015

Eingereicht am: 11. August 2015

Mitglieder der Promotionskommission:

Vorsitzender: Herr Prof. Dr. Thomas Dandekar

Gutachter : Herr Prof. Dr. Jürgen Löffler

Gutachter: Herr Prof. Dr. Thomas Rudel

Tag des Promotionskolloquiums: 14. Oktober 2015

Doktorurkunde ausgehändigt am:

Contents

Summary

The mold *Aspergillus fumigatus* causes life-threatening infections in immunocompromised patients. Over the past decade new findings in research have improved our understanding of *A. fumigatus*-host interactions. One of them was the detection of localized areas of tissue hypoxia in the lungs of mice infected with *A. fumigatus*. The transcription factor hypoxia-inducible factor 1α (HIF-1α) is known as the central regulator of cellular responses to hypoxia. Under normoxia, this constitutively expressed protein is degraded by oxygen-dependent mechanisms in most mammalian cell types. Interaction with pathogens can induce HIF-1α stabilization under normoxic conditions in innate immune cells. Bacterial infection models revealed that hypoxic microenvironments and signaling via HIF-1α modulate functions of host immune cells. Moreover, it was recently described that in murine phagocytes, HIF-1α expression is essential to overcome an *A. fumigatus* infection. However, the influence of hypoxia and the role of HIF-1α signaling for anti-*A. fumigatus* immunity is still poorly understood, especially regarding dendritic cells (DCs), which are important regulators of anti-fungal immunity. In this study, the functional relevance of hypoxia and HIF-1α signaling in the response of human DCs against *A. fumigatus* has been investigated.

Hypoxia attenuated the pro-inflammatory response of DCs against *A. fumigatus* during the initial infection as shown by genome-wide microarray expression analyses and cytokine quantification. The up-regulation of maturation-associated molecules on DCs stimulated with *A. fumigatus* under hypoxia was reduced; however, these DCs possessed an enhanced capacity to stimulate T cells. This study thereby revealed divergent influence of hypoxia on anti-*A. fumigatus* DC functions that included both, inhibiting and enhancing effects.

HIF-1α was stabilized in DCs following stimulation with *A. fumigatus* under normoxic and hypoxic conditions. This stabilization was partially dependent on Dectin-1, the major receptor for *A. fumigatus* on human DCs. Using siRNA-based HIF-1α silencing combined with gene expression microarrays, a modulatory effect of HIF-1α on the anti-

fungal immune response of human DCs was identified. Specifically, the transcriptomes of HIF-1α silenced DCs indicated that HIF-1α enhanced DC metabolism and cytokine release in response to *A. fumigatus* under normoxic and hypoxic conditions. This was confirmed by further down-stream analyses that included quantification of glycolytic activity and cytokine profiling of DCs. By that, this study demonstrated functional relevance of HIF-1α expression in DCs responding to *A. fumigatus*. The data give novel insight into the cellular functions of HIF-1α in human DCs that include regulation of the anti-fungal immune response under normoxia and hypoxia. The comprehensive transcriptome datasets in combination with the down-stream protein analyses from this study will promote further investigations to further characterize the complex interplay between hypoxia, activation of Dectin-1 and HIF-1α signaling in host responses against *A. fumigatus*.

Zusammenfassung

Der Schimmelpilz *Aspergillus fumigatus* verursacht lebensbedrohliche Infektionen in immunsupprimierten Patienten. Im letzten Jahrzehnt haben neue Forschungsergebnisse unser Verständnis der Interaktion von *A. fumigatus* mit seinem Wirt verbessert. Dazu zählt die Beschreibung von lokalisierten Arealen der Hypoxie im Lungengewebe von Mäusen die mit *A. fumigatus* infiziert wurden. Der Transkriptionsfaktor Hypoxie-induzierbarer Faktor 1α (HIF-1α) ist schon lange als der zentrale Regulator der zellulären Antwort gegenüber Hypoxie bekannt. Unter Normoxie wird dieses konstitutiv exprimierte Protein in den meisten Körperzellen durch sauerstoffabhängige Prozesse abgebaut. In angeborenen Immunzellen kann die Interaktion mit Pathogenen zu einer Stabilisierung von HIF-1α unter normoxischen Bedingungen führen. Bakterielle Infektionsmodelle haben gezeigt, dass hypoxische Mikromilieus und der HIF-1α Signalweg die Funktion von Immunzellen des Wirtes beeinflussen können. Zudem konnte kürzlich nachgewiesen werden, dass die Expression von HIF-1α in murinen Phagozyten während einer Infektion mit *A. fumigtus* essentiell für eine effektive Bekämpfung des Pilzes ist. Der Einfluss der Hypoxie und die Rolle von HIF-1α für die gegen *A. fumigatus* gerichtete Immunantwort sind jedoch immer noch unzureichend charakterisiert. Das trifft besonders auf die für die Regulation der anti-fungalen Immunantwort wichtigen dendritischen Zellen (DCs) zu. In dieser Studie wurde die funktionale Bedeutung der Hypoxie und des HIF-1α Signalweges für die Antwort humaner DCs gegenüber *A. fumigatus* untersucht.

Hypoxie hatte einen abschwächenden Effekt auf die initiale pro-inflammatorische Antwort von DCs gegen *A. fumigatus.* Dies konnte durch genomweite Microarray Expressionsanalysen sowie Zytokinbestimmungen gezeigt werden. Die Hochregulation von Markern, die mit einer Maturierung von mit *A. fumigatus*-stimulierten DCs assoziiert sind, war unter Hypoxie reduziert. Jedoch zeigten diese DCs eine erhöhte Fähigkeit zur Stimulation von T Zellen. Damit wurden in dieser Studie divergente Effekte der Hypoxie auf die gegen *A. fumigatus* gerichtete Immunantwort humaner DCs aufgedeckt. Dies beinhaltete sowohl einen inhibierenden als auch einen verstärkenden Einfluss in Abhängigkeit der untersuchten DC Funktion.

HIF-1α wurde in DCs nach Stimulation mit *A. fumigatus* unter normoxischen als auch hypoxischen Bedingungen stabilisiert. Diese Stabilisierung war teilweise abhängig von Dectin-1, dem wichtigsten Rezeptor für *A. fumigatus* auf humanen DCs. Durch eine Kombination aus RNAi-vermittelter Herunterregulation von HIF-1α und Genexpressions-Microarrays wurde ein modulierender Effekt von HIF-1α auf die anti-fungale Immunantwort humaner DCs identifiziert. Die Transkriptomanalyse von HIF-1α herunterregulierten DCs deutete darauf hin, dass HIF-1α den Metabolismus und die Zytokinfreisetzung in DCs während der Antwort auf *A. fumigatus* unter normoxischen als auch hypoxischen Bedingungen verstärkt. Dieser Befund wurde durch weiterführende Analysen bestätigt, die eine Quantifizierung der glykolytischen Aktivität sowie die Erstellung eines Zytokinprofils der DCs beinhalteten. Damit konnte in dieser Studie eine funktionale Relevanz der Expression von HIF-1α in DCs für die gegen *A. fumigatus* gerichtete Immunantwort aufgedeckt werden. Diese Daten geben einen neuen Einblick in die zellulären Funktionen von HIF-1α in humanen DCs, die eine Regulierung der anti-fungalen Immunantwort beinhalten. Die umfassenden Transkriptom-Datensätze dieser Studie, die durch Proteinanalysen funktional ergänzt wurden, bilden die Grundlage für weiterführende Untersuchungen. Damit wird es möglich sein, das komplexe Zusammenspiel aus Hypoxie, Aktivierung von Dectin-1 und Signalübertragung über HIF-1α in der Immunantwort gegen *A. fumigatus* über die Ergebnisse dieser Studie hinaus noch besser zu charakterisieren.

1 Introduction

1.1 *Aspergillus fumigatus* as a human pathogen

1.1.1 Clinical relevance of *A. fumigatus* infections

Fungi are the least well studied pathogens of man [1]. This may be due to the fact that healthy people seldom develop severe fungal infections. However, alterations in the immune status of the (human) host may cause life-threatening invasive fungal diseases. Over the past decades, systemic fungal infections have become more common. This is due to an increase in immunocompromised patients as a consequence of modern medicine. The risk cohort includes patients receiving chemotherapy, solid organ or hematopoietic stem cell transplantation (HSCT), but also intensive care unit as well as surgical or HIV/AIDS patients [1]. Only very few of the known fungal species are truly pathogenic. The majority of lethal invasive fungal infections in immunocompromised patients are opportunistic infections caused by normally commensal or saprophytic fungi, primarily species of *Aspergillus, Candida, Cryptococcus* and *Pneumocystis* [1].

Among those fungi, *Aspergillus* species are responsible for one of the most feared invasive fungal infections. The disease, known as invasive (pulmonary) aspergillosis (IA), is rapidly progressive, very difficult to treat and has the highest rate of mortality among invasive fungal infections [2, 3]. IA is predominantly caused by the species *A. fumigatus*. Depending on the patient cohort and the underlying disease, mortality rates of IA range between 30 to 95 % in infected populations [4]. IA is one leading cause of death in patients receiving HSCT [5, 6]. Given the threat of *A. fumigatus* infections especially for HSCT and other immunocompromised patients, various research projects aimed to shed light on the host immune response against *A. fumigatus* and the factors influencing the progression and outcome of IA. Over the last decades, much progress has been made in understanding fungal-host interactions. However, the treatment outcome of IA remains poor and the mortality rate is still high.

The successful treatment of IA is challenged by emerging drug resistant strains. In the last years, azole resistant *A. fumigatus* isolates have been identified. Azoles represent one major class of anti-fungal agents and resistance may become a critical problem in handling IA [7]. Therefore, research is aiming at developing new antifungal treatments by identifying new drug targets. A second research strategy is to unravel the still not fully understood immune response against *A. fumigatus* and to develop therapies that improve the host defense in immunocompromised patients, including cell based therapies. Therefore, further extensive studies on the critical factors influencing the host immune response against *A. fumigatus* may help to identify and improve novel therapeutic strategies to boost host resistance and to manage the disease.

1.1.2 Biology and life-cycle of *A. fumigatus*

A. fumigatus is a saprophytic mold and one of several hundred species of the genus *Aspergillus*. It belongs to the phylum Ascomycota. Most of the *Aspergillus* species are not pathogenic and several are utilized in industrial biotechnology, e.g. for the production of food (*A. oryzae*) and pharmaceuticals (*A. terreus*) [8]. Among the species that may cause diseases in humans, *A. fumigatus* is the primary causative agent of most of these infections. As a ubiquitous filamentous saprophyte, *A. fumigatus* is commonly found in soil and decaying matter where it grows and recycles carbon and nitrogen [9]. In contact with air, its mycelium forms conidiophores. These are specialized structures that produce large numbers of asexual spores, so-called conidia, which are dispersed through the air [2]. In a suitable environment, these airborne, dormant conidia can swell and germinate, forming so-called germ tubes, which will then outgrow into branching hyphae and form a mycelium. Besides this asexual life cycle, in 2008 O'Gorman *et al.* discovered a sexual reproduction cycle that leads to the formation of cleistothecia and ascospores. It requires isolates of complementary mating types and increases genotypic variation [10].

Airborne *A. fumigatus* conidia are ubiquitous in the environment. It is estimated that humans inhale several hundred conidia per day. Due to their small diameter of 2 to 3 µm, they can reach the lung alveoli [6]. *A. fumigatus* does not possess true virulence factors; however, its ability to survive, overcome and grow in hostile microenvironments encountered in its natural habitat, e.g. a compost heap, as well as in the human lung, the primary site of infection, distinguishes it from other non-pathogenic saprophytic molds.

A. fumigatus is very thermotolerant and germinates and grows optimal at temperatures around 37 °C. Furthermore, it has a high nutritional versatility and utilizes a variety of nitrogen and carbon sources. Another important virulence attribute includes its ability to survive and generate energy in low oxygen environments. Thus, the characteristics that enable *A. fumigatus* to grow in its natural habitat also enable it to live as an opportunistic pathogen [8].

1.1.3 *A. fumigatus* associated diseases

A. fumigatus is not truly pathogenic and an immune competent host is very unlikely to develop an infection. In individuals with a compromised immune response, however, *A. fumigatus* may cause severe invasive infections. As mentioned in the first paragraph, IA is the most severe fungal infection in immunocompromised patients. There are several major risk factors for developing IA, including prolonged neutropenia or neutrophil dysfunction, high-dose corticosteroid therapy, transplantation (especially lung and bone marrow), hematological malignancy (especially leukemia), cytotoxic therapy and advanced AIDS (low CD4 count) [11]. IA usually starts in the lung with the germination of inhaled conidia in the alveoli of the lower respiratory tract. In neutropenic patients, IA is marked by invasive growth of *A. fumigatus* hyphae into lung tissue and blood vessels, followed by bleeding, tissue necrosis, thrombosis and collapse of alveoli. In patients under corticosteroid-therapy, initiation of the inflammatory response induces tissue damage and excessive inflammation (Figure 1). If not treated, IA usually results in pneumonia and the infection disseminates hematogenously, infecting other organs such as the brain and leading to the death of the patient in the end.

Clinical symptoms of IA are rather unspecific and include fever, chest pain, dyspnoe, cough and hemoptysis (the coughing up of blood) [12]. Diagnostic methods include the serologic marker galactomannan (a fungal cell wall component that is also present in non-*Aspergillus* species), detection of fungal DNA or RNA in serum or whole blood via PCR, radiology (CT scans), isolation of the fungus from materials such as bronchoalveolar lavage fluid (BAL) and histopathological diagnosis from biopsy samples. However, diagnosis remains difficult due to nonspecific serology and radiologic testing. Several compound classes are available for anti-fungal therapy, including triazoles, polyenes and echinocandins. As already mentioned in the first paragraph, emerging resistance to azoles

poses a problem in antifungal therapy. The earlier the treatment is given, the better is the chance to survive IA. Furthermore, even though there is no common consensus, many physicians recommend administering antifungal prophylaxis to high risk patients to ensure a better control of IA [13].

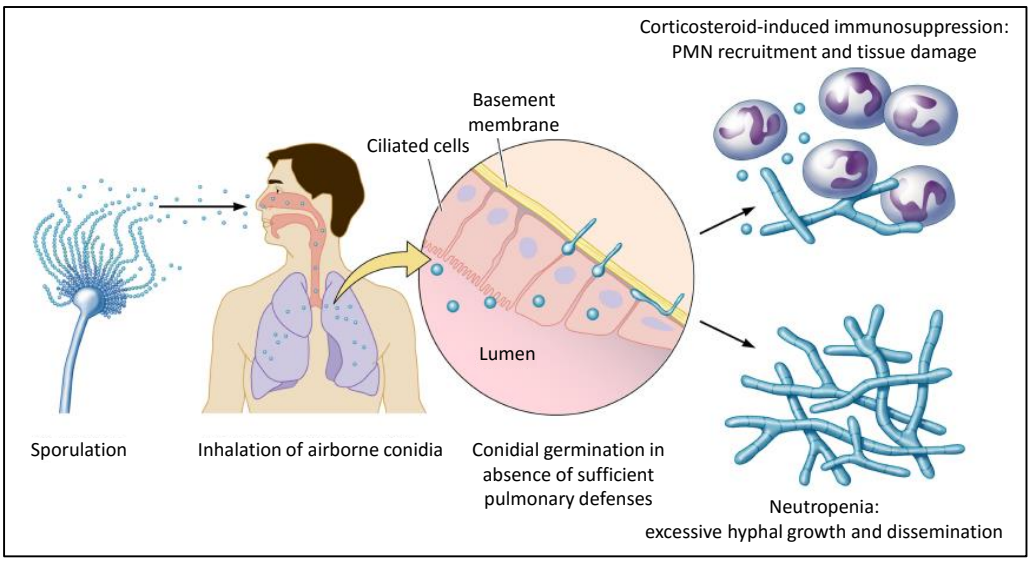

Figure 1 I Invasive Aspergillosis following pulmonary infection with *A. fumigatus*.

A. fumigatus conidia are released into the air via asexual reproduction and are ubiquitous in the environment. Inhalation by immunocompromised individuals may result in conidial germination in the lung alveoli, leading to either PMN-mediated fungal control with significant inflammation (in patients under corticosteroid therapy) or uncontrolled hyphal growth with a lack of PMN infiltrate and, in severe cases, dissemination (in neutropenic patients). PMN, polymorphonuclear leukocyte (in this case, neutrophils). Figure modified by [8].

Besides IA, *A. fumigatus* may cause a range of other diseases in humans, dependent on the immune status of the host and the presence of underlying diseases (Figure 2). Chronic necrotizing aspergillosis (CNA, also called semi-invasive or subacute invasive aspergillosis) is slowly progressive (weeks and months). In contrast to IA, vascular invasion or dissemination to peripheral organs are uncommon. In general, CNA is a rare syndrome that might affect patients with other underlying (chronic) lung diseases [11].

An aspergilloma is described as a conglomeration of condensed hyphae, also called a fungal ball, and is usually located in a preexisting (thoracic) cavity. Therefore, a predisposing factor is cavitary lung disease. Patients with an aspergilloma are mostly asymptomatic. Episodes of hemoptysis caused by hyphal invasion of bronchial arteries, however, are possible life-threatening complications [14].

A. fumigatus can also be the causative agent for episodes of asthma and allergic bronchopulmonary aspergillosis (ABPA). Both are hypersensitivity reactions against *A. fumigatus* antigens. ABPA is most common in patients already suffering from asthma or cystic fibrosis. This severe form of allergic disease may lead to irreversible pulmonary damage. Treatment is aimed at reducing the exaggerated immune response against the constantly inhaled *A. fumigatus* antigens by oral corticosteroid therapy [11].

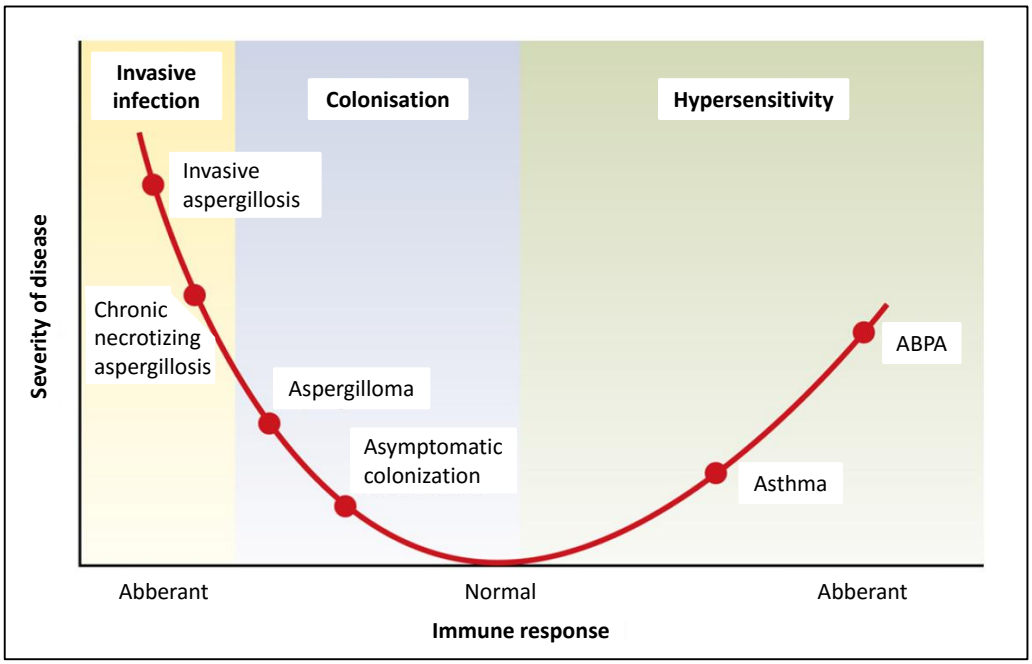

Figure 2 I Diseases attributable to *A. fumigatus*, depending on the host immune status.

A. fumigatus may cause a range of diseases in humans. Individuals with a severely compromised immune system are most likely to develop an invasive aspergillosis. Patients with mild immunosuppression or chronic lung disease are susceptible to chronic necrotizing aspergillosis, whereas aspergillomas are mostly found in hosts with cavitary lung disease. Asymptomatic colonization may occur in individuals with a normal immune response. Constant exposure to *A. fumigatus* is a risk factor for the development of asthma. A severe form of hypersensitivity against *A. fumigatus* allergens is allergic bronchopulmonary aspergillosis (ABPA), which may develop in patients with atopic asthma or cystic fibrosis as underlying disease. Figure modified by [5].

1.2 Host immune responses against *A. fumigatus*

1.2.1 Components of the anti-fungal immune response

Humans live under constant exposure to inhaled *A. fumigatus* conidia that contain antigens and allergens; however, these conidia do not activate the innate immune system continuously or induce inflammatory responses [15]. That is in part due to defense mechanisms in the lung that remove inhaled conidia before they get in contact with immune cells. The mucociliary clearance of the upper respiratory tract removes inhaled particles. Another important barrier is the mucosal epithelial cell surface of the respiratory tract. The fluid lining the airway epithelium contains cellular secretions that contribute to effective mucociliary clearance. Furthermore, the pulmonary fluid contains opsonic proteins such as collectins (released by type II lung epithelial cells), pentraxin 3 (PTX3, produced by phagocytes) and complement proteins. All these serum proteins opsonize inhaled conidia and thereby contribute to host defense [8]. Due to their small size, conidia may escape clearance by these lung specific defense mechanisms and reach the lung alveoli, where they encounter cells of the immune system.

Generally, the immune system in higher animals can be divided into innate immunity, acting as the front-line defense against a broad range of pathogens, and adaptive immunity, providing pathogen-specific responses and immune memory. Cells of the innate immune system include macrophages, neutrophils, natural killer (NK) cells and monocytes. Dendritic cells (DCs) bridge innate and adaptive immunity and have both innate (antigen uptake, cytokine release) and adaptive (antigen presentation and T cell activation) characteristics. Lymphocytes (B and T cells) are antigen specific cells and part of the adaptive immune system.

In the course of an immune response against *A. fumigatus*, first of all phagocytes, most importantly alveolar macrophages, promote immune activation and fungal clearance (Figure 3). They release cytokines and chemokines to recruit other effector immune cells to the site of the infection. This includes neutrophils, NK-cells and monocytes. DCs are either recruited via the bloodstream or are already patrolling the intestine space. Through recognition and uptake of *A. fumigatus* antigens, DCs release

pro-inflammatory cytokines at the site of the infection. In addition, they mature and migrate to the peripheral lymph nodes to promote anti-fungal T cell responses. Therefore, DCs bridge the innate and adaptive immunity.

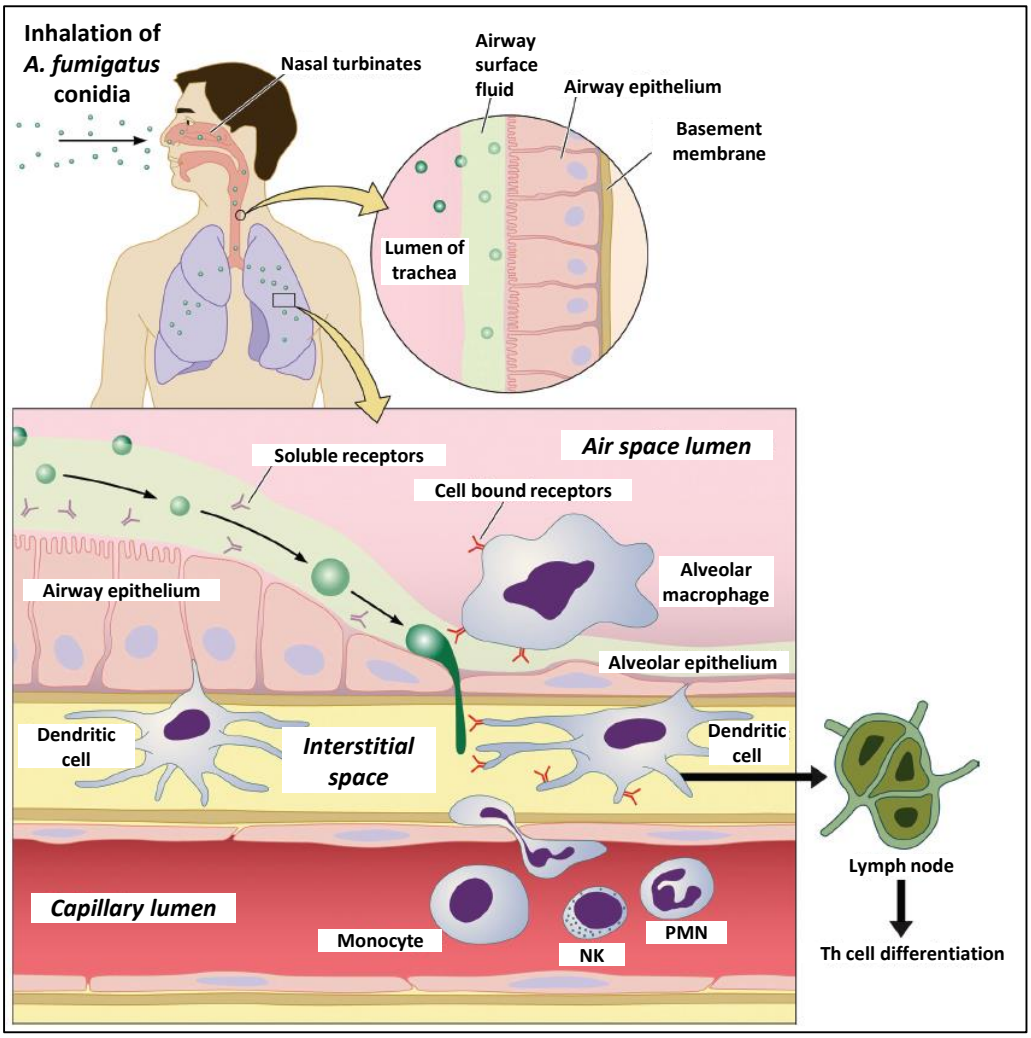

Figure 3 I Components of the host response to inhaled and germinating *A. fumigatus* conidia.

The first line of defense against inhaled conidia is the mucociliary clearance and the surface fluid of the airway epithelium. Soluble and cell bound receptors contribute to phagocytosis of dormant and germinating conidia by alveolar macrophages. Other immune cells are recruited to the site of the infection once the conidia start germinating, including monocytes, NK cells, PMNs and dendritic cells (DCs). They all contribute to innate anti-fungal defense mechanisms. DCs play a central role in the initiation of adaptive immunity in their function as professional antigen presenting cells. DCs take up *A. fumigatus* conidia and germ tubes, they maturate and move to draining lymph nodes to induce Th cell responses against the fungus. NK, natural killer cell; PMN, polymorphonuclear leukocyte (neutrophil); Th, T helper. Figure modified by [5]

Table 1 summarizes selected effector functions of the different immune cell populations during immune responses against *A. fumigatus*.

Table 1 I Effector functions of different immune cell populations against *A. fumigatus*.

Cell type	Selected functions/ characteristics
(Alveolar) macrophages	- Phagocytosis of inhaled conidia, intracellular killing by acidification of the phagosome and cathepsin D activation - Coordination of the early inflammatory response - Monocyte and neutrophil recruitment
Monocytes	- Phagocytosis of conidia and inhibition of germination - Progenitors of macrophages and inflammatory DCs - Production of pro-inflammatory cytokines
Neutrophils (PMNs)	- Phagocytosis of conidia and germ tubes, fusion of antimicrobial granules - Intracellular and extracellular activity against germ tubes and hyphae - Formation of neutrophil extracellular traps (NETs)
NK cells	- Direct antifungal response against hyphae (release of antimicrobial molecules) - Production of proinflammatory cytokines - Release of IFN-γ (indirect and direct antifungal activity)
DCs	- Recognition and uptake of *A. fumigatus* conidia and germ tubes, antigen processing - Production of pro-inflammatory cytokines - Activation of $CD4^+$ T cells through presentation of fungal antigens on MHC-II - Diverse subtypes of DCs exist *in vivo* (details in paragraph 1.2.3, p. 20ff.)
T cells	- Diverse subtypes of *A. fumigatus*-specific $CD4^+$ T cells (Th1, Th2, Th17, Treg) - Th1 and Th17 responses are considered to be protective - Th2 responses are associated with destructive allergic immunity - Adoptive T cell therapy is a therapeutic strategy - Details in paragraph 1.2.3.3, p. 25ff.

The content of this table is summarized in [16].

1.2.2 Pattern recognition of *A. fumigatus*

1.2.2.1 The fungal cell wall is the target for immune recognition

Macrophages and DCs encounter *A. fumigatus* conidia that have reached the alveoli. Interestingly, these phagocytes bind and ingest dormant as well as germinating conidia but only the latter ones induce further immune responses including activation of the central immune-regulating transcription factor NF-κB, secretion of proinflammatory cytokines and production of reactive oxygen species (ROS) [17]. From the host point of view, that prevents unnecessary and excessive immune responses since only germination makes *A. fumigatus* an invasive pathogen while the dormant conidia are largely innocuous. Dormant airborne conidia are not recognized by immune cells due to a layer of surface hydrophobin, the so-called rodlet layer, which contains RodA proteins (Figure 4). Once the conidia start germinating in a suitable environment, they lose the masking rodlet cover and expose cell wall components, such as the carbohydrate β(1,3)-glucan, which are recognized by innate immune cells [15].

Figure 4 I Electron microscopy section of the conidial wall.

A layer consisting of regularly arranged hydrophobic rodlet proteins covers dormant *A. fumigatus* conidia. Through this surface hydrophobin layer, conidia avoid immune recognition. Another component of the outer, electron dense membrane is melanin. The translucent inner layer contains structural polysaccharides and proteins that are immunogenic. Germinating conidia lose their rodlet layer and induce immune activation. Figure modified by [18].

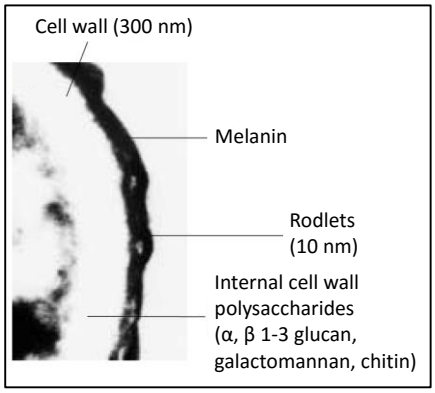

Components of the fungal cell wall comprise ideal targets for recognition of *A. fumigatus* by innate immune cells as these structures are fungal specific and not found in the human host [19]. In general, immune cells have to differentiate between self and non-self in order to properly defend the host against invading pathogens but not attack own body cells. Alveolar macrophages and DCs discriminate between self and non-self (and between innocuous dormant and potentially hazardous germinating conidia) by expression of cell bound patter recognition receptors (PRRs). Some of these PRRs specifically bind to components of the fungal cell wall. Therefore, innate and adaptive immunity to fungal infections is critically dependent on fungal recognition by PRRs [1].

1.2.2.2 PRRs are crucial for the recognition of A. fumigatus

PRRs are germ line encoded proteins and either secreted or localized on the cell surface or intracellular. They recognize highly conserved structures on microorganisms (pathogen associated molecular patterns, PAMPs) and are part of the innate immune system. Among the four major families of PRRs, namely C-type lectin receptors (CLRs), Toll-like receptors (TLRs), nucleotide-binding oligomerization domain receptors (NOD-like receptors, NLRs) and RIG-I-like receptors (RLRs), especially CLRs and TLRs seem to be important for the recognition of *A. fumigatus* [20]. They are expressed on macrophages, PMNs, monocytes and DCs. PRR activation induces various immune effector functions, including the release of specific chemokines and cytokines, production of ROS in macrophages and neutrophils and maturation of DCs, enabling them to induce anti-fungal T cell responses. The central proinflammatory transcription factor NF-κB is the key transcriptional activator downstream of PRR signaling. Table 2 summarizes PRRs that have been identified in recognition of *A. fumigatus* molecules.

Table 2 I PRRs involved in recognition of *A. fumigatus*.

PRR	*A. fumigatus* ligand *	Expressed on (examples)
Dectin-1 (a CLR)	β(1,3)-glucans	DCs, macrophages, monocytes, B cells
DC-SIGN (a CLR)	Galactomannans	DCs, macrophages
TLR2	unknown	DCs, macrophages, monocytes, PMNs, B and T cells
TLR4	unknown	DCs, macrophages, monocytes, PMNs, B and T cells
CD14	(cooperates with TLR2/TLR4)	macrophages, monocytes

* Many *A. fumigatus* ligands/ molecules responsible for PRR activation are still unknown. DC-SIGN, Dendritic Cell-Specific Intercellular adhesion molecule-3-Grabbing Non-integrin. Other abbreviations are described in the text. Table adapted from [21].

Murine knockout models, some of which will be described below, demonstrated an important role of PRRs in anti-*A. fumigatus* host response. These models are either immune competent knockout mice or immunosuppressed mice that are susceptible for infections with *A. fumigatus*. Mice immunosuppressed with corticosteroids or neutropenic mice are commonly used models to study the pathogenesis of IA. In line with these knockout models, several human genetic variants (single nucleotide polymorphisms, SNPs) in PRRs have been associated with an increased risk to develop IA, especially in HSCT recipients (reviewed in [22]). This includes SNPs in Dectin-1 [23], DC-SIGN [24], TLR4 [25] and PTX3 [26].

1.2.2.3 Dectin-1 is the major PRR for recognition of A. fumigatus

Dectin-1 is the major CLR involved in the recognition of *A. fumigatus* and binds to β(1,3)-glucans on the surface of germ tubes and hyphae [27]. It is a transmembrane protein with a single C-type lectin domain in the extracellular region and an immunoreceptor tyrosine-based activation motif (ITAM)-like motif in its intracellular tail [28]. Several signaling pathways downstream of Dectin-1 have been identified. The two major downstream signaling pathways are the spleen tyrosine kinase/-caspase recruitment domain containing protein 9 (SYK/CARD9) and the RAF1 pathway. Both act synergistically to induce and fine-tune canonical and non-canonical NF-κB activation, leading to cytokine expression [29]. Details are depicted and described in Figure 5.

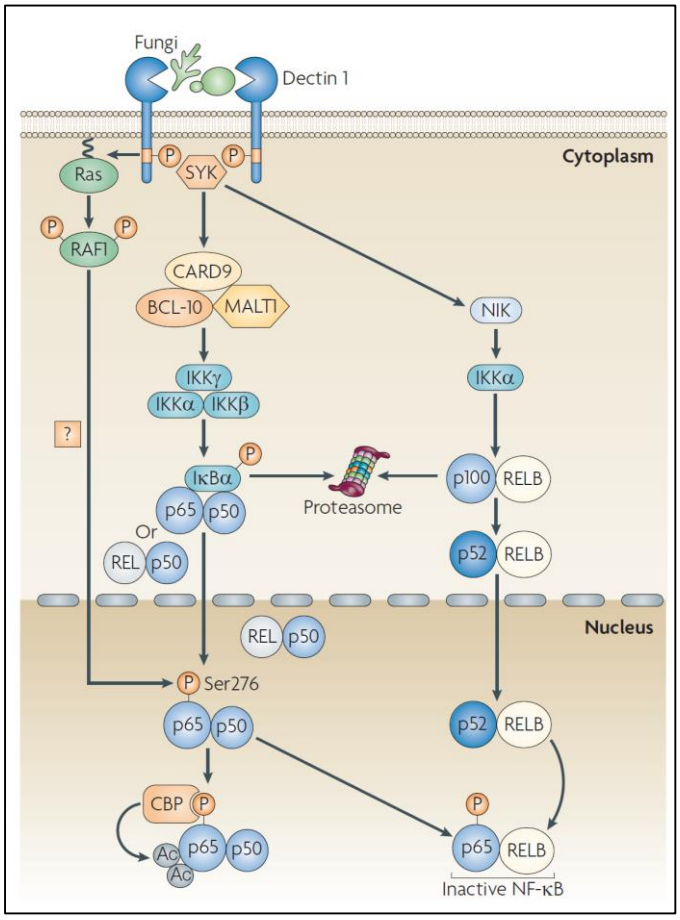

Figure 5 I Dectin-1 signaling through SYK and RAF1 induces NF-κB.

Dectin-1 binds to β-glucans, carbohydrates in the fungal cell wall, which induces phosphorylation of its ITAM-like motif and receptor dimerization. SYK is recruited, leading to the formation of a complex (CARD9/ BCL-10/ MALT1) that in turn induces activation of the canonical IKK complex. IKKβ phosphorylates IκBα, thereby targeting it for proteasomal degradation and releasing NF-κB, which consists of either p65-p50 or REL-p50 dimers which then translocate to the nucleus. SYK also activates non-canonical NF-κB via NIK and IKKα, which process p100 to p52, leading to nuclear translocation of p52-RELB dimers. In a SYK dependent manner, RAF1 is activated by Ras proteins, which leads to phosphorylation of p65 at Ser276, thereby providing a binding site for CBP to acetylate p65 at different lysine residues and thus increasing transcriptional activity of the p65-p50 dimers. Ser276 phosphorylated p65 dimerizes with RELB to form inactive dimers that cannot bind DNA, thereby providing a cross-regulatory mechanism between canonical and non-canonical NF-κB. BCL-10, B cell lymphoma 10; CARD9, caspase recruitment domain family member 9; CBP, CREB binding protein; IκB, inhibitor of NF-κB; IKK, IκB kinase; ITAM, immunoreceptor tyrosine-based activation motif; MALT1, mucosa-associated lymphoid tissue lymphoma translocation 1; NIK, NF-κB inducing kinase; SYK, spleen tyrosine kinase. Figure adapted from [29].

In addition to induction of NF-κB through SYK and RAF1, Dectin-1/SYK signaling couples to NLRP3, a protein belonging to another group of PRRs, the NLRs that are localized intracellular (not shown in Figure 5). NLRP3 is involved in the activation of the inflammasome, a multiprotein complex crucial for the induction of IL-1β, a key pro-inflammatory factor in innate antifungal immunity [30]. Although much progress has been made in understanding of Dectin-1 signaling, some steps are still unclear and regulatory mechanisms are poorly understood [28].

The essential relevance of Dectin-1 signaling for a functional immune response against *A. fumigatus* was demonstrated in 2009 using a murine *Clec7a*$^{-/-}$ model [31]. *Clec7a* is the gene encoding Dectin-1. Non-immunosuppressed *Clec7a*$^{-/-}$ mice show increased mortality after intratracheal challenge with *A. fumigatus* conidia compared to wild type mice. That is due to an impaired production of several pro-inflammatory cytokines, resulting in decreased neutrophil recruitment and uncontrolled fungal growth in the lungs. In *Clec7a*$^{-/-}$ mice, alveolar macrophages produce less pro-inflammatory mediators and neutrophils show a decreased release of ROS, resulting in impaired killing of *A. fumigatus* in response to the administration of conidia.

Furthermore, the authors provide evidence of a Dectin-1 dependent production of IL-17 in the lung after stimulation with *A. fumigatus* and evidence that neutralization of IL-17 impairs the early clearance of the fungus in wild type mice. This is in line with an earlier study from 2007 demonstrating the induction of Th-17 cells through Dectin-1/SYK/CARD9 mediated activation of DCs [32].

Besides Dectin-1, other CLRs are involved in the recognition of *A. fumigatus*. DC-SIGN (dendritic cell-specific intercellular adhesion molecule 3-grabbing nonintegrin) is expressed on DCs and macrophages. DC-SIGN recognizes fungal galactomannan and thereby mediates binding and internalization of *A. fumigatus* conidia [33]. The mannose receptor pathway [34] and Dectin-2 [35] seem to recognize *A. fumigatus* antigens as well. The specific fungal ligands recognized by these CLRs and their overall importance in anti-*A. fumigatus* host defense remain to be fully elucidated.

1.2.2.4 TLRs play a role in the recognition of A. fumigatus

The second class of PRRs important for recognition of *A. fumigatus* are the TLRs. The Drosophila protein Toll was originally recognized as a protein essential for establishing dorsoventral polarity during embryogenesis [36]. Lemaitre *et al.* discovered in 1996 that Toll also plays a crucial role in immune responses directed against *A. fumigatus*, which is a pathogen for drosophila [37]. One year later, the mammalian homolog of Toll, the Toll-like receptors, were identified [38].

Human TLR2 and TLR4 are the major surface TLRs involved in the recognition of *A. fumigatus*. Nonetheless, it is currently unknown which fungal structures are the ligands for TLR2 and TLR4, since fungal polysaccharides are structurally distinct from the prototypical ligands of TLR2 and TLR4 [21, 39]. In a murine model of IA (i.e., immunosuppressed mice), mice lacking TLR2, TLR4 or the downstream molecule MyD88 show decreased cytokine release and higher fungal burden compared to immunosuppressed wild-type (WT) mice [40, 41]. However, following pulmonary *A. fumigatus* challenge, immunocompetent *Tlr2*$^{-/-}$, *Tlr4*$^{-/-}$ or *Myd88*$^{-/-}$ knockout mice showed the same viability compared to WT mice, suggesting that these molecules are dispensable for the clearance of *A. fumigatus* under immunocompetent conditions [42]. It is important to note that this is in contrast to the reduced viability of *Clec7a*$^{-/-}$ mice [31].

Both TLR1 and TLR6 can form heterodimers with TLR2. In 2012, Rubino *et al.* reported that the detection of *A. fumigatus* involves both TLR1 and TLR6 in mice and TLR1 but not TLR6 in humans and confirmed the role of TLR2 and TLR4 for the detection of *A. fumigatus* in both species [43]. CD14 was originally described as a receptor for LPS (a major cell wall component of Gram-negative bacteria) [44]. It contributes to immune responses by loading of TLR4 and TLR2 with their ligands [21]. In addition, CD14 seems to be involved in the activation of human monocytes by *A. fumigatus* hyphae [45], although the mechanisms by which CD14 promotes anti-fungal responses in leukocytes are still largely unknown [21].

A. fumigatus itself seems to modulate TLR signaling and thereby influences the immune response. Co-stimulation of TLR2 or TLR4 with *A. fumigatus* conidia and Pam3Cys (a TLR2 ligand) or LPS (a TLR4 ligand) reduces the proinflammatory cytokine release in comparison to stimulation with the respective ligand alone, thus suggesting that

A. fumigatus conidia attenuate host proinflammatory responses through modulation of TLR2 and TLR4 signaling [46, 47]. On the other hand, Dectin-1 seems to collaborate with TLR2- and TLR4-dependent pathways, leading to enhanced proinflammatory responses upon simultaneous TLR2/4 and Dectin-1 ligation [48, 49]. Taken together, the immune signaling pathways induced by TLR2 and TLR4 in response to *A. fumigatus* are rather complex and seem to include several regulatory mechanisms.

The intracellular TLR3 and TLR9 also seem to play a role in host defense against *A. fumigatus*. TLR3 recognizes *A. fumigatus* RNA and signals through the adaptor molecule TRIF (TIR-domain-containing adaptor-inducing interferon-β). *Trif*$^{-/-}$ and *Tlr3*$^{-/-}$ mice are highly susceptible to be infected with *A. fumigatus* and develop *A. fumigatus* induced-inflammation in a non-immunosuppressed intranasal infection model or show increased mortality under immunosuppression, respectively [50, 51]. In patients receiving HSCT, TLR3 mediated protective class I-restricted memory $CD8^+$ T cell responses against *A. fumigatus* [50]. TLR9 mediates immune activation by recognizing unmethylated CpG motifs in *A. fumigatus* DNA [52] and is actively recruited to phagosomes containing *A. fumigatus* conidia [53]. However, as *Tlr9*$^{-/-}$ mice survive an infection with *A. fumigatus,* TLR9 seems to be unessential for resistance [41].

1.2.2.5 Soluble PRRs involved in anti-A. fumigatus responses

Several soluble PRRs are involved in anti-*A. fumigatus* responses. The collectins surfactant protein A (SP-A) and D (SP-D) are soluble C-type lectins produced by pneumocytes in the lung. SP-A and SP-D opsonize *A. fumigatus* conidia, thereby enhancing phagocytosis and killing through neutrophils and macrophages. SP-A and SP-D seem to play a role in the prevention of hypersensitivity reactions to inhaled *A. fumigatus* antigens [54]. In addition, intranasal administration of human SP-D protected immunosuppressed mice against otherwise lethal infection with *A. fumigatus* [55]. Contrary to the protective effect of SP-D, mice with a deletion of SP-A acquire resistance to IA [56].

Mannose-binding lectin (MBL) is a plasma protein that binds to *A. fumigatus* and activates the lectin complement pathway [57]. Its relevance during an *A. fumigatus* infection seems to be dependent on the host immune status. While immunocompetent MBL knockout mice are resistant to experimental systemic aspergillosis [58],

immunosuppressed mice that received human recombinant MBL had a clear survival benefit when infected with *A. fumigatus* [59]. Pentraxin 3 (PTX3) is another soluble PRR that can bind to *A. fumigatus* conidia, and thereby mediates recognition through macrophages and DCs [60]. PTX3 knockout mice are more susceptible for an *A. fumigatus* infection as demonstrated in a murine model of IA [60].

1.2.3 Dendritic cells and initiation of acquired immunity

1.2.3.1 Recent developments in the classification of human DC subsets

DCs are professional antigen presenting cells that bridge innate and adaptive immunity and are essential for the initiation of acquired immunity by establishing a functional T cell response [61]. They were first described by Steinman *et al.* in 1973 [62]. Most of the current knowledge regarding DC biology and function stems from murine models or human monocyte-derived DCs, a model system for human DCs.

In general, immature DCs (i.e., DCs that have not been activated by foreign antigens) continuously scan their environment and take up antigens. In a process called maturation, DCs process the antigens intracellular and migrate to the lymph nodes to stimulate T cells, thereby changing their major function from antigen capture (immature DCs) to antigen presentation (mature DCs). A second major function of DCs is the release of cytokines and chemokines to recruit other immune cells to the site of the infection (e.g., neutrophils, macrophages and NK cells) and to fine-tune the immune response. DCs express high levels of major histocompatibility complex (MHC) class II molecules, in humans called human leukocyte antigen (HLA)-DR, to present foreign peptide antigens. Human DCs lack typical lineage markers (Lin) like CD3 (T cells), CD19 (B cells) and CD56 (NK cells) and are therefore classically characterized as Lin^- / $HLA\text{-}DR^+$ cells.

Physiological human DCs are heterogeneous and comprised of different sub-populations which are similar but not identical to murine DC sub-populations. In the last years, transcriptional profiling helped to dissect the taxonomy of human DC populations and their homology to the murine system. However, these approaches also uncovered even more complexity in the origins and specialized functions of human DCs [63]. Figure 6 summarizes the current (2014) textbook knowledge of human DC development.

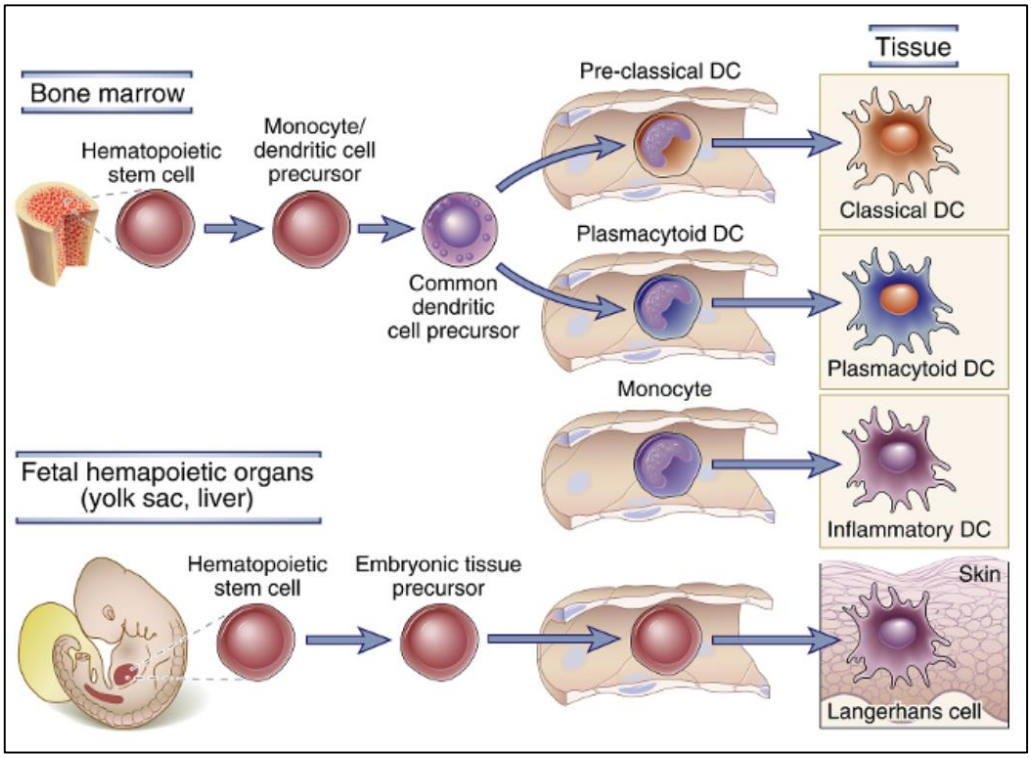

Figure 6 I Human DC development.

DCs arise from a common myeloid DC progenitor in the bone marrow and further differentiate into subsets, the major ones being classical DCs and plasmacytoid DCs. Inflammatory DCs may arise from monocytes in inflamed tissue, whereas tissue-resident DCs, such as Langerhans cells in the epithelia, may develop from embryonic precursors. Figure adapted from [64].

A common DC progenitor is thought to give rise to the two major subsets of human DCs circulating in the blood, classical DCs (cDCs, $CD11c^+$) and plasmacytoid DCs (pDCs, $CD11c^-$). cDCs and pDCs both lack expression of CD14 (which is mainly expressed on monocytes). pDCs comprise the most numerous blood DCs and express CD123, CD303 and CD304 [63]. pDCs secrete large amounts of type I interferons (IFN-α/β) in response to viral infections and are generally considered to be important effector cells in antiviral immune responses through recognition of viral RNA and DNA with the endosomal located TLR7 and TLR9, respectively [65].

cDCs (also called conventional or myeloid DCs) can be divided into two sub-populations: the major subset of mDC1 ($CD1c^+$) and a minor subset of cross-presenting (i.e. presentation of extracellular antigens on MHC class I molecules to $CD8^+$ T cells) mDC2 ($CD141^+$) [63]. The postulated major function of these DCs is the induction of T cell responses.

Classical $CD14^+$ monocytes may also give rise to DC sub-populations. $CD14^+$ DCs are a steady-state DC population found in tissues and lymph nodes. They express CD11c but lack CD1c and CD141 and were originally described as interstitial or dermal DCs; however, in healthy humans, interstitial tissue contains $CD1c^+$ (mDC1) and $CD141^+$ (mDC2) cDCs as well. $CD14^+$ DCs are more similar to monocytes and macrophages than to mDCs and their functions have not yet been finally clarified [63]. Furthermore, during inflammation, monocytes that are recruited to the site of infection may give rise to inflammatory DCs. Evidence from the literature suggests that, depending on the different infection environments, DC subsets with distinct functions may arise and may include inflammatory dendritic epidermal cells (IDECs) and TNF and inducible nitric oxide synthase-producing (TiP) DCs [63].

Langerhans cells (LCs) comprise a specialized DC population found in the epidermis and other stratified squamous epithelia like the bronchus. Until now it was commonly assumed that LCs arise from monocytes. A recent Nature publication, however, suggests that this self-renewing cell population stems from yolk-sac-derived erythroid-myeloid progenitors and characterizes them as adult tissue-resident macrophages ([66] and Figure 6).

In addition, more human DC populations have been described in the last years. This includes non-classical monocytes expressing CD16 and some MHC-II and other co-stimulatory molecules as well as a subset of $CD16^+$ monocytes expressing the antigen 6-Sulpho LacNAc (SLAN) DCs [63]. However, not all researchers agree with the classification of these cell populations as DCs.

Taken together, the definition of human DC populations is a challenging field of research. Much remains to be uncovered about human DC hematopoiesis in healthy individuals and the consequences of the differentiation of inflammatory DCs from monocytes during an infection [63].

1.2.3.2 Role of DCs in anti-A. fumigatus immune responses

As mentioned in the previous section, most of our current knowledge about DC functions is deviated from either murine or human DC model systems. These models provided an insight into the role of DCs in anti-*A. fumigatus* immune responses and established them as a cell type of particular interest in the context of IA, especially in neutropenic hosts. In the following, the known effector functions that are initiated by DCs in response to *A. fumigatus* will be summarized.

Several PRRs are expressed on the surface of DCs. Among them, TRL2 and TLR4 [67, 68] and the CLR Dectin-1 [69] recognize *A. fumigatus.* Upon encounter with *A. fumigatus*, immature DCs maturate and release proinflammatory mediators, upregulate MHC-II (HLA-DR) and co-stimulatory molecules (among them CD40, CD80 and CD86) on their surface and migrate to peripheral lymphoid organs to initiate anti-*A. fumigatus* T cell responses [69, 70].

Interestingly, in neutropenic hosts, inflammatory DCs seem to play an important role in fungal clearance that is associated with DC responses directly at the site of infection rather than the initiation of adaptive immunity. In a murine model of neutropenic IA, inflammatory DCs rapidly accumulate in response to an *A. fumigatus* infection in the lung and mediate protective responses [71]. Accumulation of DCs at the site of infection seems to be mediated by a positive feedback loop initiated by elevated levels of DC-derived TNF in the lung, which in turn drives the local production of the chemokines CCL2 and CCL20, inducing the further recruitment of TNF-producing DCs to the lung [71]. The protective effect of inflammatory DCs during IA is supported by the finding that adoptive transfer of DCs into neutropenic mice decreases fungal growth, an effect that is even more pronounced with *Ccr7*$^{-/-}$ DCs [72]. The chemokine receptor CCR7 is required for DC trafficking to the lymph nodes and is upregulated on maturing DCs, concomitant with a down-regulation of CCR6, which is the receptor for CCL20 and mediates trafficking of immature DCs to the infected lung tissue [72]. The authors suggest a trapping of *Ccr7*$^{-/-}$ DCs at the site of infection (i.e., the lung) that may lead to a cytokine milieu that favors effective fungal clearance, probably through a better balance between pro- and anti-inflammatory signals.

Few studies investigated the role of specific human DC subpopulations (Figure 6) in the context of *A. fumigatus* infections. LCs are activated after binding to *A. fumigatus* conidia *in vitro* [73] and possess the ability to differentiate into migratory DCs; however, their possible role for antigen presentation in the course of an *A. fumigatus* infection is uncertain. Ramirez-Ortiz *et al.* suggested that pDCs may play a role in host responses against *A. fumigatus*, although their major function lies in the establishment of anti-viral immunity [74]. Contrary to this study, our group recently published data demonstrating that pDCs are not activated by different *A. fumigatus* morphologies *in vitro* [75]. The divergence in these studies might be explained by different methods applied for the isolation of the pDC population from human peripheral blood. Taking into account all these data, the significance and role of pDCs in anti-*A. fumigatus* immunity remain unclear. Interestingly, data from our group demonstrate that $CD1c^+$ cDCs (mDC1) are activated by and respond to *A. fumigatus in vitro* in a similar way compared to *in vitro* generated monocyte-derived DCs [75]. This underlines the comparability of moDCs as a model system and blood mDC1 and suggests that both DC subtypes might be suitable for immunotherapy.

DCs are currently in the focus of immune-cell based, adoptive therapies for high risk patients, such as HSCT recipients. The first demonstration of a DC based vaccine against IA in a murine model was reported over a decade ago. In 2002, Bozza *et al.* showed that DCs phagocytose and transport *A. fumigatus* conidia and hyphae to the draining lymph nodes and initiate helper T cell (Th) responses against the fungus [70]. One year later, the same authors used fungus-pulsed DCs to induce activation of protective CD4 Th1 responses on adoptive transfer in a murine IA model of HSCT recipients [76].

In general, DCs as professional antigen-presenting cells are capable to induce T cell responses against *A. fumigatus*, although the specific contributions of the different DC subsets (Figure 6) are currently unclear. *In vitro* generated monocyte-derived DCs that are loaded with antigen and transferred to the host are considered a versatile tool in the development of anti-fungal vaccines [77]. Figure 7 summarizes adaptive, $CD4^+$ T cell mediated immune responses that are initiated by DCs that mature through downstream signaling of PRRs after ligation to different fungal morphologies.

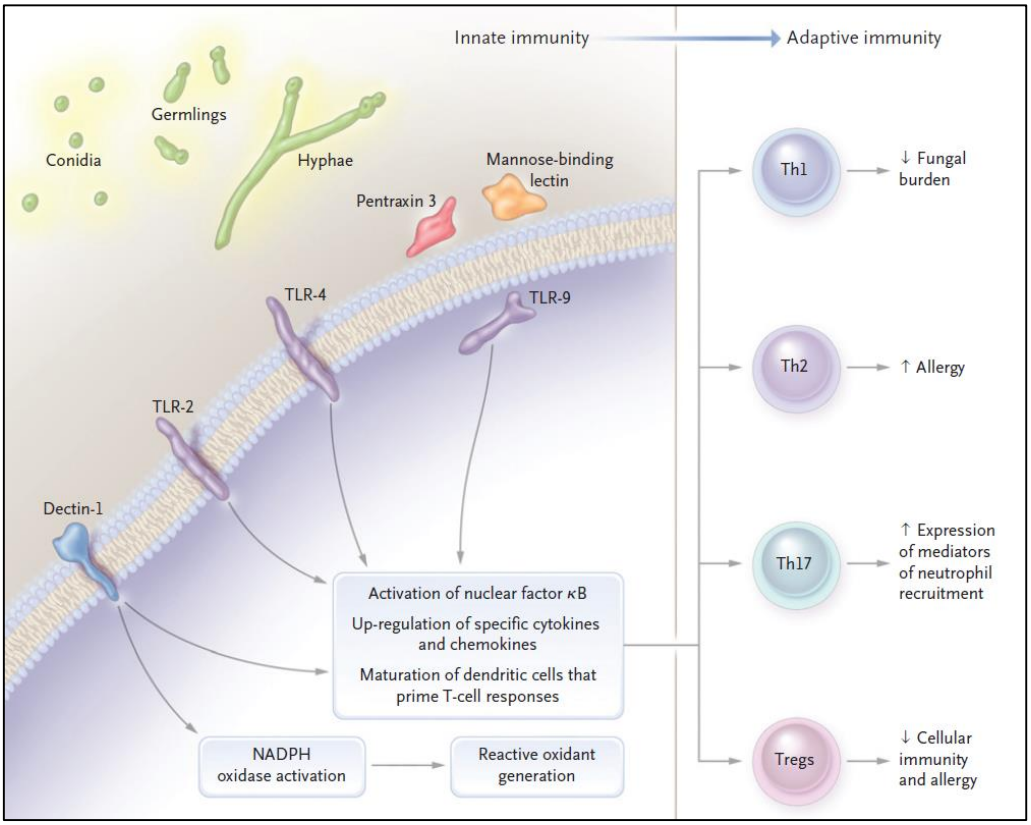

Figure 7 I Pattern recognition, innate and adaptive immune responses to *A. fumigatus*.

Immune cells like macrophages, neutrophils and DCs express cell associated PRRs like dectin-1 and TLRs and soluble PRRs like pentraxin 3 and mannose-binding lectin that recognize fungal morphologies (conidia, germ tubes and hyphae). Ligation of PRRs leads to activation of NF-κB and induction of chemokines and cytokines that activate and recruit further inflammatory cells to the site of infection. NADPH oxidase can be activated by dectin-1 and leads to generation of reactive oxygen species. DCs mature after ligation of PRRs and stimulate antigen-dependent responses in helper T cells (Th) and regulatory T cells (Tregs). The different T cell subsets have diverse effector functions in response to *A. fumigatus*. These functions can be beneficial or detrimental for the host. Figure adapted from [78].

1.2.3.3 T cell responses and adaptive immunity against A. fumigatus

In a study analyzing T cell responses against *A. fumigatus* in healthy individuals and in patients after HSCT with proven or probable IA, most of the healthy cohort and the patients surviving IA displayed a positive lymphoproliferative response to *A. fumigatus* antigens with a dominant release of IFN-γ in culture supernatants [79]. This study demonstrates the presence of adaptive immunity against *A. fumigatus* in the healthy host and provides proof of an important role of a Th1-type cellular immune response in controlling IA in patients with hematologic malignancies.

Effector functions of anti-fungal T cell immunity are largely mediated through release of cytokines, the principal ones being IFN-γ, TNF and IL-17, which enable the host to restrict fungal growth [80]. Th1 cells play a central role in the decrease of fungal burden through the release of IFN-γ, TNF and GM-CSF. These cytokines prompt the release of nitric oxide (NO) and stimulate ROS production through the activation of pro-inflammatory macrophages [80]. Contrary, a Th2 response induces release of IL-4 and IL-13 and promotes allergy. In ABPA (paragraph 1.1.3, p. 7), an *A. fumigatus* specific Th2 response contributes to the progression of the disease [81]. In IA patients, Th2 cytokine responses were associated with unfavorable outcomes compared to Th1 responses whereas Th1 responses enhanced anti-fungal host defense in a murine model of IA [78].

Th17 responses are initiated during fungal infections (not only *A. fumigatus* but including other fungal pathogens such as *Candida albicans*) through SYK/CARD9, MYD88 and mannose receptor signaling pathways in DCs and macrophages [82]. The hallmark cytokine of Th17 responses is IL-17. In contrast to the Th1 cytokines, the activities of IL-17 are not yet fully understood in the context of a fungal infection and remain controversial as both, beneficial and harmful effects, have been reported. IL-17 promotes neutrophil recruitment, which are central in the defense against invading *A. fumigatus* hyphae, but IL-17 has also been reported to impair anti-*A. fumigatus* immune resistance [83]. This might be explained by recent evidence that different sub-populations of Th17 cells exist. Depending on the release of IL-10 or GM-CSF, they are segregated into nonpathogenic and pathogenic Th17 cells [80]. Although Rivera *et al.* reported that *A. fumigatus* induced Dectin-1 signaling may favor Th17 and suppress Th1 responses [84], Chai *et al.* found that *A. fumigatus* induced only weak Th17 responses and provided evidence that the human anti-*A. fumigatus* host defense relies more on Th1 than on Th17 cellular responses [85]. Therefore, the role of Th17 responses during IA remains controversial.

Regulatory T cells (Tregs) protect against allergic responses towards *A. fumigatus* antigens and mediate tolerance (control of inflammation) through the release of IL-10 and TGF-β that lead to reduction of inflammation, NO release and macrophage activation. Hence, Tregs seem to be responsible for the fine regulation of adaptive cellular immunity to avoid excessive tissue damage but provide effective fungal clearance [82].

Besides $CD4^+$ T cells, *A. fumigatus* specific $CD8^+$ T cells are also present in mice and humans. Carvalho *et al.* provide data demonstrating the importance of TLR3 mediated protective memory $CD8^+$ T cell responses against *A. fumigatus* in HSCT recipients [50]. However, much is still to be learned about the functions and relevance of $CD8^+$ T cells in anti-*A. fumigatus* immunity.

The role of B cells in anti-*A. fumigatus* immunity is not well investigated. In general, antibody mediated immunity may play a role during fungal infections through growth inhibition of the fungus by binding of immunoglobulins to β-glucans on the fungal surface, by binding to secreted fungal proteins and toxins and by enhancing the activity of effector cells and phagocytes [86]. In a murine model of IA monoclonal IgG1, directed against *A. fumigatus* cell wall glycoprotein, indeed had a protective effect [87]. Taken together, although the therapeutic potential of immunoglobulins for prevention of IA in risk patients has been acknowledged, this research field is still in its infancies.

1.2.4 Model systems for studying human DCs and macrophages

Circulating human DC subsets (cDCs and pDC, Figure 6, p. 21) comprise physiological DC populations. Nonetheless, their numbers in peripheral blood are regularly too low to perform experiments which require a certain cell number and their isolation is very cost-intensive. Therefore, experiments with these *in vivo* DC subsets are often not feasible for *in vitro* studies. Monocyte-derived DCs (moDCs), generated by cultivation of classical $CD14^+$ monocytes with the cytokines GM-CSF and IL-4, are commonly used to study human DC functions. In addition, moDCs are also applied *in vivo* for cancer immunotherapy [88]. These model DCs are highly functional and are potent stimulators of $CD4^+$ T cells. They cross-present to $CD8^+$ T cells and produce key inflammatory cytokines such as IL-1, IL-6, IL-12 and TNF [63]. However, these *in vitro* generated DCs may be most similar to inflammatory DCs (Figure 6). *In vitro* generated moDCs, cDCs, inflammatory DCs and their committed progenitors all express the zinc finger transcription factor Zbtb46 that distinguishes them from cells of other lymphoid or myeloid lineages (e.g. pDCs, macrophages and monocytes) [89]. This confirms the similarity of *in vitro* generated moDCs with physiological cDCs. This study used moDCs as a model system to investigate human DC functions. They will be simply referred to as “DCs” throughout this thesis.

Comparable to DCs, the direct isolation of human alveolar macrophages from human bronchoalveolar lavage (BAL) or tissue samples is not feasible for experimentation with larger numbers of cells. In addition, the availability of such material is very limited. However, as tissue-based macrophages, including alveolar macrophages, derive from blood monocytes *in vivo*, they can be differentiated *in vitro* by the addition of growth factors. Several protocols have been reported for the generation of monocyte-derived macrophages and the further differentiation into classically activated macrophages (termed M1) or alternatively activated macrophages (termed M2) [90]. In the present study, macrophages were used for some confirmatory experiments. Macrophages were differentiated by cultivation of monocytes with the addition of M-CSF over six days and subsequently stimulated with *A. fumigatus* or several PRR ligands, leading to classical macrophage activation (K. Czakai, unpublished data).

1.3 Hypoxia, HIF-1α and invasive aspergillosis

1.3.1 Hypoxia at sites of *A. fumigatus* infections

In a range of diseases, the mucosal surface of the lung experiences decreased oxygen tension leading to localized areas (microenvironments) of prominent hypoxia. Hypoxia can have an impact upon innate immune and subsequent infectious and pro-inflammatory processes [91]. Based on typical histopathological characteristics observed in *A. fumigatus* infected human and murine lung tissue, it was hypothesized that hypoxic microenvironments are present during IA, and that their formation may depend on the patient cohort and the model of immunosuppression, respectively [92].

In neutropenic patients (chemotherapy-treated), IA is characterized by high fungal invasion of lung tissue and a minimal inflammatory response, leading to angioinvasion, intravascular thrombosis, coagulative necrosis and intraalveolar hemorrhage, all of which might foster the development of hypoxic microenvironments. In contrast, IA in non-neutropenic patients (steroid/corticosteroid treated) is characterized by a deregulated immune response with low fungal burden and extensive infiltration of PMNs, and hypoxia may be caused by tissue damage and inflammatory necrosis (Figure 1, p. 8).

Grahl *et al.* recently demonstrated the presence of hypoxic areas at the site of *A. fumigatus* infection in three distinct murine models of IA [93]. As it is difficult to actually measure and determine oxygen levels *in vivo*, the authors employed a staining method using pimonidazole hydrochloride (hypoxyprobe-1), a hypoxia-detecting agent that specifically binds to thiol-containing proteins in hypoxic cells with oxygen levels below 1.5 % O_2 [94]. This substance was injected intravenously prior to the sacrifice of the animals and was then detected in tissue slices by immunohistological staining (Figure 8). With this method it was demonstrated that sites of *A. fumigatus* invasive growth in the lung are accompanied by tissue hypoxia, demonstrating that both host and fungal cells encounter and have to cope with hypoxic microenvironments during IA.

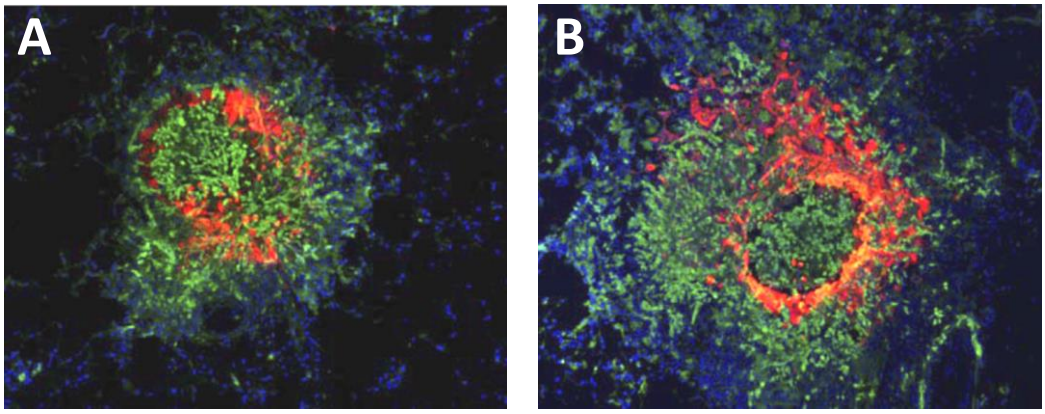

Figure 8 I Hypoxia occurs in murine models of IA.

Hypoxyprobe-1, a hypoxia detecting agent, was used to monitor *in vivo* hypoxia in two immunological distinct murine models of pulmonary IA. (A) Chemotherapy (neutropenic) model. Mice were immunosuppressed with cyclophosphamide and triamcinolone. (B) Corticosteroid model. Mice were immunosuppressed with a single dose of triamcinolone. (A+B) Mice were inoculated with *A. fumigatus* conidia. Hypoxyprobe-1 was injected intravenously prior to sacrifice on day 4 after inoculation, followed by tissue preparation and immunohistological staining. Blue, host cells (DAPI staining); green, *A. fumigatus*; red, hypoxia. Figure adapted from [93].

It is critical to understand and characterize the potential implications of hypoxic microenvironments during IA. Previous reports indicated that the efficacies of antifungal drugs may be altered under hypoxic conditions [95]. Changing oxygen levels during an *A. fumigatus* infection may also influence fungal virulence or have an impact upon the host immune response [96]. As both the fungal and host cells experience changing oxygen levels not only during disease, but also in a physiological state, they developed mechanisms to adapt to hypoxia. These mechanisms will be described in the following.

1.3.2 Hypoxic adaption by *A. fumigatus*

In contrast to other fungi like the model organism *Saccharomyces cerevisiae*, which has a facultative anaerobic life-style, *A. fumigatus* is an obligate aerobic eukaryote. Unlike in *S. cerevisiae*, the mechanisms of adaption to hypoxic conditions have not been thoroughly described for *A. fumigatus*. It is mostly unknown how pathogenic fungi respond to hypoxic microenvironments encountered at sites of infection [97]. However, as *A. fumigatus* naturally inhabits the soil and compost piles, it probably evolved mechanisms to deal with low oxygen levels commonly found in such an environment. In fact, two decades ago, Hall *et al.* observed that various pathogenic *Aspergillus* species,

including *A. fumigatus,* are capable of *in vitro* growth under very low oxygen levels ($O_2 \leq 0.5$ %) [98]. Yet, *A. fumigatus* seems to be unable to grow or germinate under strict anaerobic conditions and requires a functional respiratory chain for conidiation [99].

Only recently have scientists begun to explore the mechanism of adaption to hypoxia by *A. fumigatus*. In 2008, Willger *et al.* characterized SrbA as a fungal transcription factor that seems to be required for hypoxic adaption by *A. fumigatus*. SrbA is an ortholog of the mammalian sterol regulatory element binding protein (SREBP) [100]. The first SREBP ortholog, Sre1, was characterized in the fission yeast *Schizosaccharomyces pombe* where it functions as an oxygen sensor and principal regulator of anaerobic gene expression [101, 102]. The mutant *A. fumigatus* strain lacking SrbA is incapable of growth at 1 % O_2 and consequently did not cause disease in two distinct murine models of IA [100]. Furthermore, unlike other fungal SREBPs, *A. fumigatus* SrbA mutants show defects in cell polarity and display abnormal hyphal branching [100]. SrbA itself seems to be regulated at least in part through a group of genes that are orthologs of the *S. pombe* Dsc E3 ligase Golgi complex-coding genes that are critical for Sre1 processing in fission yeast [103]. However, the mechanisms of SrbA regulation in *A. fumigatus* and its transcriptional targets have yet to be fully elucidated.

In addition to the transcription of hypoxia regulated genes through SrbA, it is assumed that various pathways of fermentation may be employed by *A. fumigatus* when growing at sites of low oxygen levels [97]. The *S. pombe* Sre1 pathway does not regulate genes involved in respiration or fermentation; therefore, other transcription factors may exist in fungi to regulate changes in the energy metabolism under hypoxia [104]. Grahl *et al.* demonstrated that *A. fumigatus* employs ethanol fermentation under hypoxia; however, this pathway was not essential for hypoxic growth [93]. In addition, they identified a fungal alcohol dehydrogenase that influences disease pathogenesis. In a murine model, infection with the knockout mutant resulted in a significant increase of neutrophils at the site of invasive fungal growth [93]. Another group recently investigated hypoxia-inducible genes in *A. fumigatus* by transcriptome analysis and identified cellular respiration as an important contributor for the survival of the fungus under hypoxic conditions [105]. All in all, several mechanisms seem to contribute to fungal pathogenesis in a hypoxic infection microenvironment.

Very recently, Shepardson *et al.* demonstrated that growth under hypoxic conditions modulates the cell wall of *A. fumigatus*. Compared to normoxia, hypoxia-grown hyphae exhibit a thicker cell wall and the content of total and surface-exposed β-glucan is increased, while overall fungal metabolism and growth are reduced under hypoxic conditions [106]. The increase in the β-glucan content of the fungal cell wall is associated with enhanced innate immune responses of macrophages and neutrophils towards hypoxia-grown hyphae, and these effects seem to be dependent on dectin-1, the mammalian receptor for β-glucan [106]. Hence, hypoxia seems to change important virulence attributes such as the fungal cell wall, which may impact upon the host immune response and probably influence the outcome of an infection.

1.3.3 HIF-1α as the central regulator of the host hypoxic response

Immune cells have to cope with reduced oxygen availability once they have reached hypoxic sites of infection, in case of IA the infected lung tissue. While hypoxic adaption of *A. fumigatus* is not definitely characterized, it is well established how human cells respond to low oxygen levels. The hypoxia-inducible factor 1 (HIF-1) system regulates oxygen homeostasis in metazoan organisms [107]. The HIF system was first discovered as a transcriptional enhancer of the human erythropoietin (EPO) gene [108]. HIF-1 is a basic-helix-loop-helix-PAS heterodimer, composed of a constitutively expressed HIF-1β and an oxygen-regulated HIF-1α subunit [109]. Besides HIF-1α, two other α-subunits have been described, HIF-2α (encoded by *EPAS1*) and HIF-3α. HIF-3α is distantly related to the other two α-subunits and multiple isoforms have been described. It is the least well studied HIF subunit; however, it may be a negative regulator of hypoxia-induced gene expression in the human kidney [110]. HIF-2α is more similar to HIF-1α and is expressed in certain cell types, including endothelial cells [111]. A possible relevance of HIF-2α for immune cells such as DCs is largely unknown though [112]. In contrast to HIF-2α, HIF-1α is widely expressed, including essentially all innate and adaptive immune cell populations [112].

Oxygen-dependent regulation of HIF-1α occurs at the protein level (Figure 9). *HIF1A* mRNA is continuously transcribed and translated into the HIF-1α protein. However, the HIF-1α protein has a very short half-life in the presence of oxygen (< 5 min) [109]. The degradation process is initiated by oxygen-dependent hydroxylation of the HIF-1α proline

residues Pro402 and Pro564 by prolyl hydroxylases (PHDs). This hydroxylation increases the affinity of the von Hippel-Lindau tumor suppressor protein (VHL) and results in binding of VHL to HIF-1α. VHL itself is the recognition component of an E3 ubiquitin ligase complex that mediates polyubiquitination of HIF-1α and thereby targets it for proteolysis by the ubiquitin-proteasome pathway [113]. In addition to the proteasomal degradation initiated by PHDs, factor inhibiting HIF (FIH) hydroxylates HIF-1α at asparagine 803 [114] which blocks its interaction with the coactivators of target gene transcription (p300/CBP), thereby inhibiting the transactivation function of HIF-1α [115]. PHDs and FIH require oxygen and divalent ferrous iron as cofactors. Hypoxia or iron deprivation decrease the activity of PHDs and FIH. As a consequence, HIF-1α protein stability is increased, leading to its dimerization with HIF-1β, translocation to the nucleus and transcriptional activation of its target genes [107]. Dimerization of HIF-1α and HIF-1β might also occur in the nucleus [116].

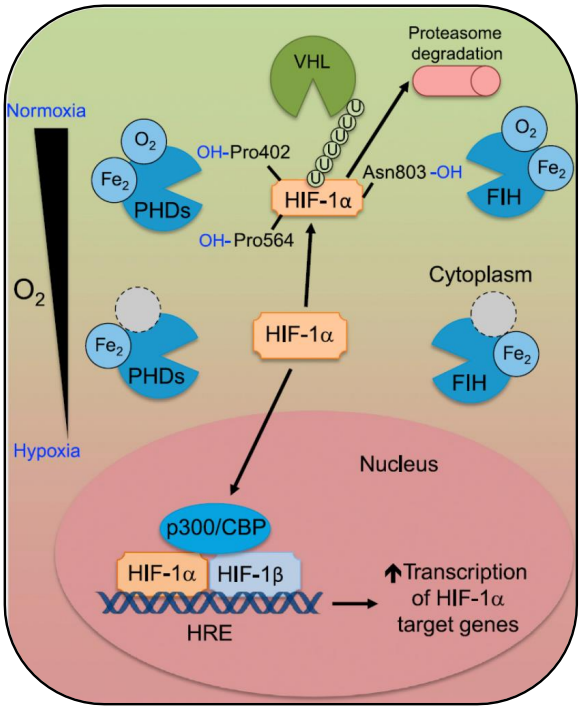

Figure 9 I O_2 dependent HIF-1α regulation.

The HIF-1 subunits HIF-1α and HIF-1β are constitutively expressed. Cellular HIF-1α levels are controlled by oxygen-dependent prolyl hydroxylases (PHDs) and factor inhibiting HIF (FIH). These enzymes require divalent ferrous iron (Fe_2) as co-factors. The PHDs hydroxylate HIF-1α at specific proline residues, leading to recognition of HIF-1α by von Hippel-Lindau tumor suppressor protein (VHL). VHL in turn mediates polyubiquitination of HIF-1α, targeting it for degradation by the cellular proteasome. Hydroxylation of HIF-1α by FIH blocks the binding site of the coactivators of gene expression (p300/CBP). When oxygen levels decrease, the hydroxylases become less active, leading to stabilization of HIF-1α. It translocates to the nucleus and forms a complex with HIF-1β and p300/CBP. In this complex, HIF-1α can activate target genes that harbor a hypoxia-response elements (HRE). Figure adapted from [112].

HIF-1α mediates adaptive responses to hypoxia including erythropoiesis, angiogenesis, and metabolic adaption [107]. Consistent with the central role of the HIF system in the hypoxic response, targeted inactivation of HIF-1α in mice results in developmental arrest and lethality by E11 of *Hif1α*$^{-/-}$ embryos due to abnormal vascular development [117]. Hypoxic microenvironments are commonly found in solid tumors,

leading to the activation of HIF-1α and the transcription of target genes including angiogenic growth factors like vascular endothelial growth factor A (VEGFA) and enzymes of the glucose metabolism. Thereby, HIF-1α promotes tumor growth. HIF inhibitors are already in clinical use to block the HIF-1α pathway in cancer therapy [113].

1.3.4 HIF-1α is involved in antimicrobial defense

The role of HIF-1α as a central transcription factor in oxygen sensing and tumorigenesis has been extensively characterized; however, a greater role of the HIF system in cell biology has been implicated. This includes the discovery of unique roles of HIF-1α in a diverse range of biological processes such as development, stem cell biology and immunity [118]. There is indeed accumulating evidence for a central role of HIF-1α as a regulator of mammalian immune defense mechanisms [119], especially in phagocytes [120]. Interestingly, the function of HIF-1α in immune cells is not limited to a hypoxic microenvironment. Stimulation of immune cells with bacterial antigens, for example, leads to stabilization of the HIF-1α protein under normoxic conditions [112].

The role of HIF-1α in innate and adaptive immunity has been most extensively studied in the context of bacterial infections. In their seminal study from 2003, Cramer *et al.* described a major role of myeloid expressed HIF-1α in the defense mechanisms initiated against bacteria (Group B *streptococci*) *in vitro* and *in vivo* [121]. The authors generated mice with a conditional deletion of HIF-1α in cells of the myeloid lineage (predominantly neutrophils and macrophages). In these HIF-1α deficient murine myeloid cells, the cellular ATP pool was drastically reduced, resulting in a profound impairment of antibacterial myeloid cell functions (aggregation, motility, invasiveness and bacterial killing) [121]. Stabilization of HIF-1α in macrophages and neutrophils upon exposure to bacterial pathogens generally seems to be a critical step for an effective antibacterial immune response. HIF-1α has been shown to play a role in a range of infections with gram-positive and gram-negative bacteria but also during viral and parasitic infections [122]. To give an example, loss of myeloid-expressed HIF-1α increases the susceptibility of mice towards invasive *Streptococcus pyogenes* infection, a gram-positive bacterium (also called Group A *Streptococcus*) [123]. Remarkably, *Chlamydia pneumoniae* interferes with the regulation of host cell HIF-1α for its own benefit. During the early phase of the infection, *C. pneumoniae* contributes to the stabilization of HIF-1α in hypoxic conditions,

thus providing energy by enhanced glucose uptake into the infected host cell. During the late phase of intracellular chlamydial replication however, *C. pneumoniae* targets HIF-1α by secretion of chlamydial protease-like activity factor, leading to the degradation of HIF-1α. These manipulations of HIF-1α by the pathogen are essential for the efficient replication of *C. pneumoniae* under hypoxia [124]. These studies demonstrate a critical involvement of HIF-1α in infectious disease pathogenesis and a functional relevance that goes far beyond mediating adaptive responses to hypoxia.

The above cited study by Cramer *et al.* identified involvement of HIF-1α in regulating the metabolic activity of myeloid cells [121]. Thereby the metabolic profile of activated immune cells resembles that of cancer cells, characterized by a shift in metabolism from oxidative phosphorylation towards aerobic glycolysis, a mechanism known as the Warburg effect [125]. These changes in cell metabolism are mediated via HIF-1α-induced transcriptional activation of genes like glucose transporter 1 (*SLC2A1*), lactate dehydrogenase A (*LDHA*), and pyruvate dehydrogenase kinase 1 (*PDK1*), whose protein products mediate a switch from oxidative to glycolytic metabolism [126]. Besides regulating metabolic activity in activated immune cells, HIF-1α has a range of other functions in myeloid immune cells. Importantly, HIF-1α signaling in these cells is connected to the NF-κB pathway. There is evidence that HIF-1α activates NF-κB and thereby mediates neutrophil survival under hypoxic conditions [127]. Furthermore, several studies reported up-regulation of *HIF1A* mRNA levels upon TLR stimulation. This transcriptional enhancement seems to be mediated via the NF-κB pathway [128, 129]. This link between hypoxia and (innate) immune signaling pathways is generally considered as an explanation for the immune-modulating functions of HIF-1α [128].

Only very few studies addressed the question of how HIF-1α signaling may influence the host response to fungal pathogens such as *A. fumigatus*. Hypoxic microenvironments had been shown to occur during *A. fumigatus* infection in the lung in distinct models of IA ([93] and Figure 8, p. 30). In infiltrating immune cells, the lack of oxygen at the site of infection as well as the interaction with *A. fumigatus* via PRRs may lead to the stabilization of HIF-1α. In a very recent publication from 2014, Shepardson *et al.* [130] were the first to describe a functional importance of HIF-1α expression in murine neutrophils and macrophages to mount an effective immune response against *A. fumigatus*. Otherwise immune competent mice with a myeloid deletion of HIF-1α died

upon infection with *A. fumigatus*. The authors used the same mouse model as Cramer *et al.* [121] and provide evidence that the role of HIF-1α in anti-fungal immune defense might defer from its role during bacterial infections. They demonstrate that HIF-1α deficient macrophages and neutrophils are not impaired in their ability to kill *A. fumigatus* conidia, as had been expected from the bacterial infection models. HIF-1α deficient mice show decreased production of the chemokine CXCL1 and increased neutrophil apoptosis. The authors conclude that these defects lead to reduced survival of these mice upon infection with *A. fumigatus*. However, in this murine model HIF-1α is deleted predominantly in mature macrophages (83-98 %) and neutrophils (near 100 %), while only partial deletion is detected in $CD11c^+$ splenic dendritic cells (16 %) [131]. Therefore, the functional relevance of HIF-1α expression in (human) DCs during an *A. fumigatus* infection remained unclear.

1.3.5 Relevance of HIF-1α and hypoxia for DC functions

Various research projects aimed at elucidating the specific role of hypoxia and HIF-1α signaling for the immune response initiated by DCs. However, divergent findings and different model systems make it difficult to interpret the data and to translate the findings to the *in vivo* situation. Most of the *in vitro* studies analyzing the effects of hypoxia and/or HIF-1α on DCs used LPS as a model stimulating agent. LPS is a prototypic TLR4 ligand and part of the outer cell membrane from gram-negative bacteria. In contrast, fungal-derived β-glucans stimulate Dectin-1, the major PRR involved in recognition of *A. fumigatus* on human DCs [69]. In addition, the available mouse models with a knockout of HIF-1α in the DC compartment only lead to partial deletion of HIF-1α or the deletion is not specific for DCs (J. Jantsch, unpublished data and personal communication). The lack of suitable murine models with a HIF-1α knockout in DCs makes it difficult to elucidate the specific role of HIF-1α in DC responses against fungal (and bacterial) pathogens.

Concluding from a number of studies, HIF-1α is commonly thought to promote maturation, activation, migration and subsequent antigen-presentation in DCs responding to bacterial antigens [132-136]. Regarding the effect of hypoxia on DC activation, previous studies yielded contradictory results and the literature provides conflicting data,

especially regarding the positivity or negativity of the effects of hypoxia on DC functions [132]. The results vary depending on the study, some studies report an enhanced TLR-induced DC maturation under hypoxia [134, 136], while another observed impaired maturation [137].

Taken together, it seems to be common consensus that HIF-1α contributes to immune responses initiated by DCs and that hypoxia has a potential influence on the activation and function of DCs. Possible implications of hypoxia and HIF-1α signaling on human DCs in the context of *A. fumigatus* infections have not yet been investigated so far.

1.4 Aim of Thesis

In bacterial infection models, hypoxia as well as HIF-1α signaling have been shown to influence the function of immune cells, including DCs [121, 138]. Hypoxic microenvironments occur during *A. fumigatus* infection in the murine lung [93]. Recently, the involvement of HIF-1α in immune responses against *A. fumigatus* has been described in a murine model of IA [130]. However, the influence of hypoxia or HIF-1α signaling on human DC responses against *A. fumigatus* is largely unknown. For these reasons, the overall aim of this thesis was to explore the functional relevance of hypoxia and HIF-1α signaling for human DCs that are stimulated with *A. fumigatus* (Figure 10).

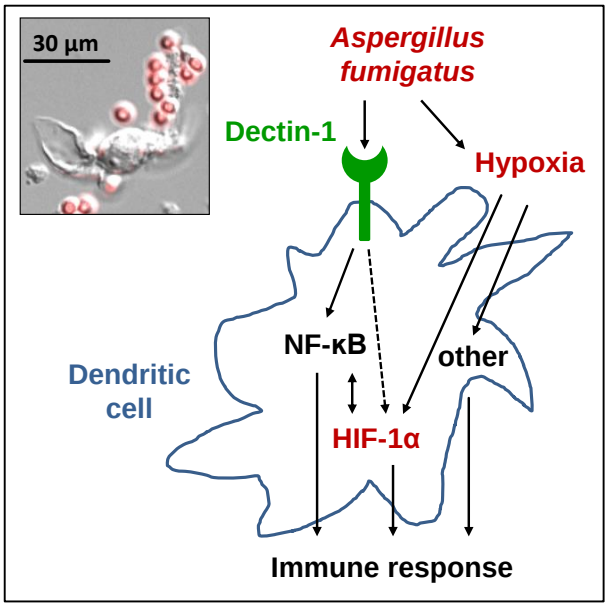

Figure 10 I Schematic representation of the interplay between *A. fumigatus*-stimulated DCs, hypoxia and HIF-1α signaling.

The influence of hypoxia and HIF-1α signaling on the immune response of human DCs against *A. fumigatus* was investigated in this study. The most important receptor for *A. fumigatus* on human DCs is Dectin-1. Downstream signaling can induce NF-κB which is known to interact with HIF-1α. *A. fumigatus* infections are accompanied by local tissue hypoxia, leading to hypoxia-dependent HIF-1α stabilization. *A. fumigatus* might induce HIF-1α by mechanisms other than hypoxia/ NF-κB signaling and hypoxia might induce (transcription) factors other than HIF-1α. **(Insert)** Microscopic picture of a DC interacting with swollen *A. fumigatus* conidia (expressing red fluorescent protein).

Using genome-wide microarray expression analyses, the influence of hypoxia should be investigated in initial experiments. The role of HIF-1α should be investigated by an RNAi mediated knockdown of HIF-1α in human DCs in combination with microarray expression analyses. With the findings gained from the hypoxia- and HIF-1α mediated DC transcriptomes, further down-stream analyses should be performed to confirm and extend the microarray results on protein level. Thereby, two major goals were pursued in this study: (I) to better characterize the DC response against *A. fumigatus* by including hypoxic culture conditions as an expected microenvironment during IA and (II) to

investigate the possible functional role of HIF-1α in human DC responses against *A. fumigatus* as a novel aspect of the human anti-fungal immune response.

This study is also significant from a translational point of view. As HIF-1α is required for an effective immune response during various bacterial infections, it is in the focus as a pharmacological target to boost innate host defense in the therapy of infectious diseases [139]. Human DCs themselves could potentially be used in novel cell-based antifungal therapy approaches [140]. Fundamental research data concerning the role of hypoxia and HIF-1α for DCs in the context of *A. fumigatus* infections are needed as a basis in the development of such novel therapeutic treatments of fungal infections.

2 Material and Methods

2.1 Material

2.1.1 Equipment and consumables

Table 3 I Equipment used in this study.

Designation	Brand name/specification	Manufacturer
Blood gas analyzer	Cobas C701	Roche
Cell culture incubator	CO2-Inkubator HERAcell 240	Thermo Scientific
Centrifuge	Centrifuge 5415 R	Eppendorf
Centrifuge	Heraeus® Multifuge® 3SR	Thermo Scientific
Centrifuge	Galaxy Mini Centrifuge	VWR
Centrifuge	MC-6400 Centrifuge	Hartenstein
Centrifuge	Rotanta 46 RC	Hettich
Electroporation pulse generator	EPI 2500	Dr. L. Fischer
ELISA Reader	GENios Microplate Reader	Tecan
ELISA Washer	hydroFLEX microplate washer for 96-well	Tecan
Flow cytometer	BD FACSCalibur	BD Bioscience
Fridge and freezer	CUP 3021 and HERAfreeze	Liebherr
Hemocytometer	Neubauer Improved	HBG Henneberg-Sander
Hypoxia workstation	Invivo2 400	Baker Ruskinn
Immunoblotting station	Standard Power Pack P25	Biometra
MACS separator	Quadro MACS Separator	Miltenyi Biotec
Magnetic stirrer	Variomag Electronicrührer	Monotherm
Microscope	Microscopes Eclipse 50i and TS 100	Nikon
Mister Frostie	Cryogenic storage system K series	Taylor-Wharton
Oxygen controllable incubator	CO_2 Incubator C60	Labotect
PCR pipetting box	DNA/RNA UV-Cleaner box UVC/T-AR	BioSan
pH Meter	pH 211 Microprocessor pH Meter	Hanna instruments
Pipettes	Pipettes Eppendorf Reference	Eppendorf
Pipettus	accu-jet pro	Brand
Protein gel casting system	Mini-PROTEAN 3 system	Bio-Rad
Protein gel electrophoresis	Power Pac Basic station	Bio-Rad
Real-time PCR machine	StepOnePlus™	Applied Biosystems
Semi-dry blotting chamber	BlueFlash-M	Serva
Sonificator	UP50H	Hielscher Ultrasonics
Spectrophotometer	NanoDrop 1000	Peqlab
Thermal cycler	9800 Fast Thermal Cycler	Applied Biosystems
Thermal cycler	Eppendorf 5341	Eppendorf
Vortexer	Vortex Genie 2	Scientific Industries
Waterbath	Waterbath Memmert	Memmert
Workbench	Herasafe HS 15	Heraeus/Kendro

Table 4 I Consumables used in this study.

Designation	Brand name/ specification	Manufacturer
12-well plate	Multiwell™ 12 well	BD Biosciences
24-well plate	Multiwell™ 24 well	BD Biosciences
6-well plate	Multiwell™ 6 well	BD Biosciences
96-well plate (ELISA)	Microplate, 96 well, PS, F-Bottom	greiner bio-one
96-well plate (PCR)	MicroAmp™ 96 well Tray for VeriFlex™ Blocks	Applied Biosystems
Blotting paper	Whatman Chromatography Paper	Whatman
Cell culture flask, T75	Cellstar Cell Culture Flasks 75 cm^2	greiner bio-one
Cell scraper	Cell Scraper 16 cm	Sarstedt
Cell strainer	BD Falcon™ Cell Strainer, 40 µm	BD Biosciences
Cryovial	CryoTube Vials	Nunc
Electroporation cuvette	Gene Pulser Cuvette 0.4 cm	Bio-Rad
Falcons (15 and 50 ml)	Cellstar Tubes	greiner bio-one
Filter tips (1000 µl)	TipOne 1000 µl XL Graduated Filter Tip	StarLab
Filter tips (20 and 100 µl)	Biosphere Filter Tips	Sarstedt
Flow cytometry tube	Polystyrene round-bottom tube, 5 ml	BD Biosciences
Glucose determination blood collection tube	Glucose FE S-Monovette, 2.7 ml	Sarstedt
MACS Separation Column	LS Column	Miltenyi Biotec
Medical X Ray Film	Fuji SuperRX	Hartenstein
Microplates for ELISA (96 wells)	Flat bottom, binding, crystal-clear	greiner bio-one
Needle (20G)	BD Microlance 3 20G needles	BD
Nitrocellulose membrane	Protran, Nitrocellulose Transfer Membrane, 0.45 µm	Schleicher-Schell
Optical adhesive cover/sealing strip (ELISA)	ELISA Plate Sealers	R&D Systems®
Optical adhesive cover/sealing strip (PCR)	Sealing tape, optically clear	Sarstedt
Pasteur pipette	Transfer pipette 3.5 ml	Sarstedt
Reaction tube	Micro Tubes (1.5 and 2 ml)	Sarstedt
Serological Pipettes (5, 10 and 20 ml)	Cellstar Serological Pipettes	greiner bio-one
Syringes (2, 5 and 10 ml)	BD Discardit II	BD

2.1.2 Commercially obtained kits

Table 5 I Commercially obtained kits used in this study.

Designation	Brand Name	Contents	Cat. No.	Manufacturer
Apoptosis detection kit	FITC Annexin V Apoptosis Detection Kit 1	10X Annexin Binding Buffer FITC Annexin V Propidium Iodide Staining Solution	556547	BD Bioscience
cDNA synthesis kit	First Strand cDNA Synthesis Kit	M-MuLV Reverse Transcriptase (20 U/µl) RiboLock RNase Inhibitor (20 U/µl) 5X Reaction Buffer 10 mM dNTP Mix Random Hexamer Primer (100 µM, 0.2 µg/ml) Water, nuclease-free	K1612	Thermo Scientific
DNA digestion kit	RNase-Free DNase Set	DNase I, RNase-Free (lyophilized), 1500 Kunitz units Buffer RDD RNase-free water	79254	Qiagen
ELISA (IFN-γ)	Human IFN-γ ELISA MAX™ Standard Sets	Human IFN-γ ELISA MAX™ Capture Antibody (200X) Human IFN-γ ELISA MAX™ Detection Antibody (200X) Human IFN-γ Standard Avidin-HRP (1000X)	430102	BioLegend
ELISA (TNF-α)	Human TNF-α ELISA MAX™ Standard Sets	Human TNF-α ELISA MAX™ Capture Antibody (200X) Human TNF-α ELISA MAX™ Detection Antibody (200X) Human TNF-α Standard Avidin-HRP (1000X)	430202	BioLegend
Monocyte isolation beads	CD14 MicroBeads	2 ml CD14 MicroBeads, human	130-050-201	Miltenyi Biotec
Nuclear extraction kit	CelLytic™ NuCLEAR™ Extraction Kit	10X Lysis Buffer, hypotonic Extraction Buffer 1 M DTT (in deionized water) Protease Inhibitor Cocktail 10 % IGEPAL CA-630 (in deionized water)	NXTRACT	Sigma-Aldrich
RNA isolation kit (< 5x10^5 cells)	RNeasy Micro Kit	RNeasy MinElute Spin Columns Buffer RLT Buffer RW1 Buffer RPE RNase-Free Water RNase-Free DNase Set	74004	Qiagen
RNA isolation kit (> 5x10^5 cells)	RNeasy Mini Kit	RNeasy Mini Spin Columns Buffer RLT Buffer RW1 Buffer RPE RNase-Free Water	74106	Qiagen
T cell isolation kit	Pan T Cell Isolation Kit	1 ml Pan T Cell Biotin-Antibody Cocktail, human 2 ml Pan T Cell MicroBead Cocktail, human	130-096-535	Miltenyi Biotec

2.1.3 Buffers, cell culture media and reagents

Table 6 I Commercially obtained buffers, cell culture media and reagents used in this study.

Designation	Brand Name	Contents/Description	Cat. No.	Manufacturer
Antibiotic (cell culture)	Refobacin®	Gentamycinsulfat 80 mg	PZN-7829173	Merck
Buffer clean (flow cytometry)	BD FACS Clean Solution	5 l Clean Solution	340345	BD Bioscience
Buffer flow (flow cytometry)	BD FACS Flow Sheath Fluid	20 l Flow Solution	342003	BD Bioscience
Buffer rinse (flow cytometry)	BD FACS Rinse Solution	5 l Rinse Solution	340346	BD Bioscience
Cell culture medium	RPMI 1640	Rosewell Park Memorial Institute 1640 medium, contains GlutaMAX™-I (glutamine) supplement, HEPES	72400-054	LifeTechnologies (Invitrogen)
Cell culture medium (electroporation)	RPMI 1640 medium, no phenol red	Rosewell Park Memorial Institute 1640 medium, contains GlutaMAX™-I (glutamine) supplement, HEPES	11835-063	LifeTechnologies (Invitrogen)
DMSO	DMSO	Dimethylsulfoxid	HN47.1	Roth
DNA ladder	100 bp DNA Ladder	0.5 ml DNA ladder 500 µg/ml	N3231L	New England Biolabs
DNA loading buffer	Gel Loading Dye, Blue (6X)	4 ml gel loading dye	B7021S	New England Biolabs
ECL western blotting substrate	Clarity Western ECL Substrate	100 ml Clarity werstern luminol/enhancer solution 100 ml peroxide solution	170-5060	Bio-Rad
EDTA	EDTA	Ethylenediaminetetraacetic acid disodium salt solution, 0.5 M	E7889	Sigma-Aldrich
Ethanol 100 %	Ethanol 100 %	---	32205-1L	Sigma-Aldrich
Ethanol 70 % (disinfection)	Ethanol 70 %	---	---	Pharmacy of the UKW
FCS	FBS	Fetal Bovine Serum	F7524	Sigma-Aldrich
Ficoll separating solution	Biocoll Separating Solution	density 1.077 g/ml, isotonic	L 6115	Biochrom
GM-CSF	Leukine® sargramostim	Recombinant yeast-expressed lyophilized GM-CSF, 250 mcg/vial, 1.4 x 10^6 IU/vial. Reconstituted with 1 ml HBSS. Stored in aliquots at 4 °C	NDC 58468-0180-2	Genzyme
HBSS	HBSS	Hanks' Balanced Salt Solution, with NaHCO3, without pheol red, calcium chloride and magnesium sulphate.	H6648	Sigma-Aldrich
IL-4	Premium grade recombinant human IL-4	Diluted 10 µg/ml in HBSS, stored in aliquots in liquid nitrogen	130-093-924	Miltenyi Biotec
LPS	LPS-EK	TLR2 and TLR4 ligand (standard lipopolysaccharide from *E. coli* K12 strain), diluted in HBSS [0.1 µg/ml], stored in aliquots at -20°C (6 months)	tlrl-eklps	InvivoGen

Table 6 (continued) I Commercially obtained buffers, cell culture media and reagents used in this study.

Designation	Brand Name	Contents/ Description	Cat. No.	Manufacturer
LPS ultrapure	LPS-EK Ultrapure	TLR4 ligand (ultrapure lipopolysaccharide from *E. coli* K12 strain), diluted in HBSS [0.1 µg/ml], stored in aliquots at -20°C (6 months)	tlrl-peklps	InvivoGen
M-CSF	M-CSF	Recombinant Human Macrophage Colony Stimulating Factor, 50 µg, diluted in HBSS [100 µg/ml]	11343115	ImmunoTools
Protease inhibitor tablets	cOmplete	Protease Inhibitor Cocktail Tablets in glass vial	11697498001	Roche Life Science
Protein gel electrophoresis buffer	10X Tris/Glycin/ SDS running buffer	25 mM Tris 192 mM glycine 0.1% SDS pH 8.3 (in 1X dilution)	1610732	Bio-Rad
Protein ladder	PageRuler Prestained Protein Ladder	2 x 250 µl prestained protein ladder, 170 – 10 kDa	26616	Thermo Scientific
Protein loading buffer	4X SDS sample buffer	2 ml 4X SDS sample buffer	70607-3	Merck (Novagen)
RNA stabilizing reagent	RNAprotect Cell Reagent	250 ml RNAprotect Cell Reagent	76526	QIAGEN
SYBR green mastermix	iTaq™ Universal SYBR® Green Supermix	2x concentrated, ready-to-use reaction qPCR master mix	172-5124	Bio-Rad
TAE-buffer, 10x	UltraPure™ TAE Buffer, 10X	400 mM Tris-acetate 10 mM EDTA	15558-042	Invitrogen
Trypan blue	Trypan Blue	Trypan Blue solution (0.4 %)	93595	Sigma-Aldrich
Water	Ampuwa® Spüllösung (Aqua ad iniectabilia)	Used for the preparation of self-made buffers	PZN-1214482	FreseniusKabi
Water, sterile, distilled	Aqua B. Braun	Used to harvest *A. fumigatus* conidia	0123	B. Braun
Zymosan	Zymosan	TLR2 and Dectin-1 ligand (cell wall from *Saccharomyces cerevisiae*), diluted in HBSS [1 mg/ml], stored at 4°C (6 months)	tlrl-zyn	InvivoGen
Zymosan Depleted	Zymosan Depleted	Dectin-1 ligand (hot alkali treated cell wall from *Saccharomyces cerevisiae*), diluted in HBSS [5 mg/ml], stored in aliquots at -20°C (1 month)	tlrl-zdzn	InvivoGen

Table 7 lists the self-made buffers and solutions used in this study. Unless specified otherwise, chemicals were dissolved in H_2O ("Ampuwa Spüllösung", see 2.1.3) and buffers and solutions were stored at room temperature (RT). 10X buffer concentrates were diluted in H_2O to 1X buffer. Buffers were mixed on a magnetic stirrer.

Table 7 I Buffers and solutions (self-made) used in this study.

Designation	Contents	Preparation
1st antibody diluent (Western blotting)	5 % TTBS milk 0.05 % Sodium acide	Dissolve antibody as desired in 10 ml TTBS milk. Add 50 µl of 10 % Sodium acide solution. Store reused solution at 4 °C.
Assay Diluent (ELISA)	1 % BSA in 1X PBS	Dissolve 1 g BSA in 100 ml 1X PBS.
Cell culture medium	RPMI 1640 supplemented with 10 % FCS and 120 µg/ml Refobacin	To one bottle RPMI 1640 (500 ml), add 1.5 ml antibiotics and 55 ml FCS
Coating Buffer (ELISA)	0.84 g $NaHCO_3$ 0.356 g Na_2CO_3	Dissolve chemicals in 100 ml H_2O.
HBSS buffer (cell isolation and flow cytometry)	HBSS supplemented with 1 % FCS and 2 mM EDTA	To one bottle HBSS (500 ml), add 5 ml FCS and 2 ml EDTA (0.5 M)
PBS, 10X	80 g NaCl 11.6 g Na_2HPO_4 2 g KH_2PO_4 2 g KCl	Dissolve chemicals in 800 ml H_2O. Adjust to pH 7.4 with 1 M HCl. Adjust volume to 1 l with H_2O.
PE-Buffer (complete)	10 ml PE-Buffer, stock 5 µl 1 M DTT 1 tablet complete mini protease inhibitor	Dissolve protease inhibitor tablet. Centrifuge and store at 4 °C until foam dissolves. Store 1 ml aliquots at -20 °C.
PE-Buffer, stock (protein extraction buffer)	40 g Urea 10 ml Glycerin 1 g SDS 1.21 g Tris	Dissolve chemicals in 80 ml H_2O. Adjust to pH 6.8. Adjust volume to 1 l with H_2O.
Ponceau solution	0.5 g Ponceau S 100 ml Acetic acid	Dissolve Ponceau S in 100 ml Acetic acid.
Resolving gel buffer (1.5 M Tris) (Western blotting)	36.3 g Tris 8 ml 10 % SDS-solution	Dissolve Tris in 100 ml H_2O. Adjust to pH 8.8. Add SDS-solution Adjust volume to 200 ml with H_2O.
SDS Solution, 10 %	10 % SDS (w/v)	Dissolve 50 g SDS in 500 ml H_2O.
Semi-dry blotting buffer (store at 4 °C)	1X Semi-dry blotting buffer 20 % methanol	Mix 100 ml 10X semi-dry blotting buffer, 200 ml methanol and 800 ml H_2O.
Semi-dry blotting buffer, 10X	29.1 g Tris 14.65 g Glycine 18.5 ml 10 % SDS solution	Dissolve Tris, Glycine and SDS-solution in 400 ml H_2O. Adjust volume to 500 ml.
Sodium acide solution, 10 %	10 % Sodium acide (w/v)	Dissolve 1 g Sodium acide in 10 ml H_2O.

Table 7 (continued) I Buffers and solutions (self-made) used in this study.

Designation	Contents	Preparation
Stacking gel buffer (0.5 M Tris) (Western blotting)	6 g Tris 4 ml 10 % SDS-Solution	Dissolve Tris in 50 ml H_2O. Adjust to pH 6.8. Add SDS-solution Adjust volume to 100 ml with H_2O.
TBS buffer (Western Blot)	1X TBS	Mix 100 ml 10X TBS with 900 ml H_2O.
TBS, 10X	60.5 g Tris 87.6 g NaCl	Dissolve chemicals in 800 ml H_2O. Adjust to pH 7.5 with 1 M HCl. Adjust volume to 1 l with H_2O
TTBS buffer (Western Blot)	1X TBS 0.1 % Tween-20	Dissolve 1 ml Tween-20 in 1 l 1X TBS.
TTBS Milk, 5 % (Western blotting)	5 g nonfat dry milk powder	Dissolve milk powder in 100 ml TTBS buffer.
Wash Buffer (ELISA)	1X PBS 0.05 % Tween-20	Dissolve 500 µl Tween-20 in 1 l 1X PBS.

2.1.4 Primers and siRNAs

Table 8 lists the sequences of the primers used for real-time PCR and Table 9 lists the siRNAs used for RNAi approaches. Primer design is described in chapter 2.2.4.2.

Table 8 I Real-time PCR primer sequences.

GENE*	ACCESSION NUMBER	SENSE	ANTISENSE
ALAS1	NM_000688	5'-GGCAGCACAGATGAATCAGA-3'	5'-CCTCCATCGGTTTTCACACT-3'
CCL3	NM_002983	5'-TGCAACCAGTTCTCTGCATC-3'	5'-TTTCTGGACCCACTCCTCAC-3'
CCL5	NM_002985	5'-GAGGCTTCCCCTCACTATCC-3'	5'-CTCAAGTGATCCACCCACCT-3'
CLEC7A	NM_197947	5'-CTGGTGATAGCTGTGGTCCTG-3'	5'-AAGAACCCCTGTGGTTTTGACA-3'
HIF1A	NM_001530	5'-TCGCATCTTGATAAGGCCTCT-3'	5'-ACAAAACCATCCAAGGCTTTCA-3'
HK2	NM_000189	5'-TTCGCACTGAGTTTGACCAG-3'	5'-TCACCAGGATAAGCCTCACC-3'
IL12B	NM_002187	5'-AAGGAGGCGAGGTTCTAAGC-3'	5'-GCAGGTGAAACGTCCAGAAT-3'
IL1A	NM_000575	5'-TGATCAGTACCTCACGGCTG-3'	5'-TGGTCTTCATCTTGGGCAGT-3'
IL1B	NM_000576	5'-GGACAAGCTGAGGAAGATGC-3'	5'-TCGTTATCCCATGTGTCGAA-3'
IL1RN	NM_173841	5'-AAGATGTGCCTGTCCTGTGT-3'	5'-CGCTTGTCCTGCTTTCTGTT-3'
IL6	NM_000600	5'-AAAGAGGCACTGGCAGAAAA-3'	5'-TTTCACCAGGCAAGTCTCCT-3'
IL8	NM_000584	5'-AAGAAACCACCGGAAGGAAC-3'	5'-ACTCCTTGGCAAAACTGCAC-3'
LDHA	NM_005566	5'-TGTTGCTGGTGTCTCTCTGA-3'	5'-TCCAATAGCCCAGGATGTGT-3'
PDK1	NM_002610	5'-GGTTGGGAACCACTCTTTCA-3'	5'-GCTTTGGTTACGTGGCATTT-3'
SLC2A1	NM_006516	5'-AGGCTTCTCCAACTGGACCT-3'	5'-CAGAACCAGGAGCACAGTGA-3'
TNF	NM_000594	5'-TGCTTGTTCCTCAGCCTCTT-3'	5'-TGGGCTACAGGCTTGTCACT-3'
VEGFA	NM_001025366	5'-AGGCCAGCACATAGGAGAGA-3'	5'-TTTCTTGCGCTTTCGTTTTT-3'

* Official gene symbol. Primers were ordered from Sigma-Aldrich as unmodified, desalted and lyophilized DNA Oligos.

Table 9 I siRNAs used for RNAi approaches in this study.

siRNA name	Description	Cat. no.*
Cell Death control siRNA	AllStars Hs Cell Death Control siRNA	1027298
Hs_CLEC7A_1	siRNA directed against human CLEC7A (Dectin-1), NM_022570	SI03069780
Hs_HIF1A_10	siRNA directed against human HIF1A, NM_001243084	SI04249308
Hs_HIF1A_11	siRNA directed against human HIF1A, NM_001243084	SI04262041
Hs_HIF1A_12	siRNA directed against human HIF1A, NM_001243084	SI04361854
Hs_HIF1A_5	siRNA directed against human HIF1A, NM_001243084	SI02664053
Hs_HIF1A_6	siRNA directed against human HIF1A, NM_001243084	SI02664431
Hs_HIF1A_7	siRNA directed against human HIF1A, NM_001243084	SI03224781
Neg. Control siRNA	AllStars Negative Control siRNA	1027281
Neg. siRNA Fluorescein	AllStars Neg. siRNA Fluorescein	1027282

* All siRNAs were ordered from Qiagen.

2.1.5 Antibodies

Table 10 lists the antibodies used for flow cytometry in this study and Table 11 lists the antibodies used for immunoblotting. Antibodies used for ELISA or immune cell isolation (MACS) were part of commercially available kits and are listed in Table 5.

Table 10 I Antibodies used for flow cytometry in this study.

Antibody	Iso-type	Conju-gation	Clone	Catalog Number	Manufacturer	Vol.*
Mouse Anti-Human **CCR7**	IgG1	APC	FR11-11E8	130-093-624	Miltenyi Biotec	5 µl
Mouse Anti-Human **CD14**	IgG2a	FITC	M5E2	561712	BD Bioscience	2 µl
Mouse Anti-Human **CD1a**	IgG1	APC	HI149	559775	BD Bioscience	2 µl
Mouse Anti-Human **CD40**	IgG1	PE	MAB89	IM1936U	Beckman-Coulter	2 µl
Mouse Anti-Human **CD80**	IgG1	APC	2D10	130-097-204	Miltenyi Biotec	4 µl
Mouse Anti-Human **CD83**	IgG1	PE	HB15e	556855	BD Bioscience	6 µl
Mouse Anti-Human **CD86**	IgG1	FITC	2331(FUN1)	555657	BD Bioscience	4 µl
Mouse Anti-Human CLEC7A (**Dectin-1**)	IgG2b	PE	259931	FAB1859P	R&D Systems	2,5 µl
Mouse Anti-Human **HLA-DR**	IgG2a	PE	G46-6	555812	BD Bioscience	2 µl
Mouse Anti-Human **ICAM1**	IgG1	FITC	BBIG-I1	BBA20	R&D Systems	2 µl
Mouse **IgG1** isotype control	IgG1	PE	X40	349043	BD Bioscience	#
Mouse **IgG1** isotype control	IgG1	FITC	X40	349041	BD Bioscience	#
Mouse **IgG1** isotype control	IgG1	APC	MOPC-21	555751	BD Bioscience	#
Mouse **IgG2a** isotype control	IgG2a	FITC	X39	349051	BD Bioscience	#
Mouse **IgG2a** isotype control	IgG2a	PE	S43.10	130-091-835	Miltenyi Biotec	#
Mouse **IgG2b** isotype control	IgG2b	PE	27-35	556656	BD Bioscience	#

* Antibodies were titrated to use optimal amounts. Volumes are indicated for flow cytometry staining of immune cells in 100 µl buffer. # Volume according to the specific antibody.

Table 11 I Antibodies used for immunoblotting in this study.

Antibody	Conju-gation	Clone	Catalog Number	Manufacturer	Dilution*
Mouse Anti-Human **HIF-1α**	none	54/HIF-1α	610959	BD Bioscience	1 : 1,000
Mouse Anti-Human **β-Actin**	none	AC-74	A 5316	Sigma-Aldrich	1 : 100,000
Rabbit Anti-Human **Dectin-1**	none	polyclonal	9051	Cell Signaling Technologies	1 : 1,000
Rabbit Anti-Human **GAPDH**	none	D16H11	5174	Cell Signaling Technologies	1 : 5,000
Rabbit Anti-Human **H3**	none	D1H2	4499	Cell Signaling Technologies	1 : 1,000
Goat Anti-Rabbit IgG	HRP		7074	Cell Signaling Technologies	1 : 1,000
Horse Anti-Mouse IgG	HRP		7076	Cell Signaling Technologies	1 : 1,000 # 1 : 10,000

* Antibodies were titrated to use optimal amounts. Dilutions were prepared in 5% TTBS milk. # A dilution of 1:10,000 was used to detect β-Actin. HRP, horseradish peroxidase.

2.1.6 Software

Table 12 I Software used in this study.

Designation	Version	Application	Manufacturer
EndNote	X7	Citation program	Thomson Reuters
FlowJo	X10	Analysis of flow cytometry data	Tree Star Inc.
GeneChip® Command Console® Software (AGCC)	4.1.2	Microarray chip reading	Affymetrix
GraphPad Prism	5	Statistical analysis, graphs	GraphPad Software
Ingenuity Pathway Analysis (IPA)	2012-2014	Analysis of differntially expressed genes (mircoarray data)	Ingenuity Systems (Qiagen)
LinReg	11.1	Calculation of PCR efficiencies	[141]
Microsoft Excel	12-15	Data management, calculation	Microsoft
Microsoft PowerPoint	12-15	Figure design, presentations	Microsoft
Microsoft Word	12-15	Thesis writing	Microsoft
NanoDrop Software	3.1.0	RNA concentration measurement	PeqLab
NCBI Pick Primers	---	Primer design using Primer3 and BLAST	NCBI
Partek Genomics Suite	6.6	Analysis of microarray data	Partek
StepOne Software	2.2.2	Real-time PCR data analysis	Applied Biosystems
XFluor	4	Absorbance measurement ELISA reader	Tecan

2.2 Methods

2.2.1 Cultivation of *A. fumigatus*

The human *A. fumigatus* isolate ATCC 46645 (American Type Culture Collection) was used. *A. fumigatus* conidia were grown on malt extract agar plates (kindly provided by the Institute for Hygiene and Microbiology, University of Würzburg) for two to three days at 37 °C until the mycelium was covered in conidia. Conidia were harvested by adding 3 ml ice-cold, sterile distilled water to the plate and using a cotton swab to carefully suspend the conidia. The suspension of conidia was passed through a 40 µm cell strainer. Conidia were counted with a hemocytometer and stored at a concentration of 1 x 10^8 conidia/ml in sterile distilled water at 4 °C. All centrifugation steps regarding fungal preparation were performed at 5,000 x g and room temperature (RT) for 10 min.

Swelling of conidia was induced by incubating conidia in RPMI 1640 cell culture medium (including antibiotics but without FCS) at a concentration of 1 x 10^6 conidia/ml in a loosely closed falcon at 200 rpm and RT overnight. Germination was induced the following day by incubation of the swollen conidia at 37 °C until germ tubes were visible under the microscope. The germ tubes were ethanol-inactivated by 30 min incubation in 100 % ethanol, followed by washing three times with sterile distilled water and one time with medium without FCS. Inactivated germ tubes were passed five times through a 20G needle to obtain a single-germ tube solution. The germ tubes were diluted to 1 x 10^8 germ tubes/ml in RPMI 1640 cell culture medium and stored at 4 °C.

2.2.2 Human immune cell culture

2.2.2.1 Isolation of PBMCs

Peripheral blood mononuclear cells (PBMCs) were isolated from leukoreduction system (LRS) chambers. LRS chambers were obtained from the Institute of Transfusion Medicine and Haemotherapy from the University Hospital Würzburg. LRS chambers are a byproduct arising during platelet donations from healthy human volunteers. Platelets collected with apheresis instruments are leukoreduced during the procedure on a

fluidized particle bed in a LRS chamber, thus allowing the separation of white blood cells from platelets. After platelet collection, the majority of white blood cells are returned to the donor while a fraction remains in the LRS chamber. The residual cell content of LRS chambers was shown to be a valuable source of viable human PBMCs [142].

PBMCs were isolated by ficoll-hypaque density gradient centrifugation. First, the blood content from the LRS chambers was transferred into 50 ml falcons and mixed with HBSS buffer (RT) to a total volume of 50 ml. Then, 25 ml each was layered over 15 ml ficoll separating solution. Density gradient centrifugation was performed at 800 x g and RT for 20 min at lowest acceleration and brake settings. The PBMC layer was carefully removed using a pasteur pipette and collected in one 50 ml falcon. PBMCs were washed two times with HBSS buffer by centrifugation at 120 x g and RT for 15 min at lowest acceleration and brake settings. This washing step helped to remove the residual platelets from the PMBCs. Cells were counted using a hemocytometer. In general, when counting cells a trypan blue staining was included to check cell viability. Unless specified otherwise, all centrifugation steps from this point onwards were performed at 300 x g and 4 °C for 10 min at highest acceleration and brake settings.

2.2.2.2 Cryopreservation of PBMCs

For the cryopreservation of PBMCs, 5 x 10^7 PBMCs were resuspended in 1 ml of ice-cold FCS containing 8 % DMSO. The cell suspension was transferred into a cryovial. The cryovials were immediately placed into a cryogenic storage system (“Mister Frostie”) and stored at -80 °C for up to two weeks. To resurrect the cells, the PBMC suspension was thawed in a waterbath and immediately transferred in 9 ml preheated HBSS containing 10 % FCS. PBMCs were counted and centrifuged at 300 x g and 4 °C for 10 min. Afterwards, PBMCs were resuspended in 4 °C cold HBSS buffer for the isolation of T cells.

2.2.2.3 Magnetic activated cell sorting

General Procedure

Primary human monocytes and T cells were isolated from PBMCs by magnetic activated cell sorting (MACS). For the isolation of T cells, cryopreserved PBMCs were used, whereas monocytes were isolated from fresh PBMCs. As buffer, 4 °C cold HBSS supplemented with 1 % FCS and 2 mM EDTA was used. All incubation steps were

performed at 4 °C and all centrifugation steps at 300 x g and 4 °C for 10 min at highest acceleration and brake settings. Magnetically labelled PBMCs were applied onto MACS separation columns for either negative selection (T cells) or positive selection (monocytes) of target cells.

Pan T cell isolation (negative selection)

T cells were isolated from cryopreserved PBMCs using a pan T cell isolation kit. For magnetic labelling, per 1 x 10^7 PBMCs, 40 µl buffer and 10 µl Pan T Cell Biotin-Antibody Cocktail were added and incubated for 5 min. Subsequently, per 1 x 10^7 PBMCs, 30 µl HBSS buffer and 20 µl Pan T Cell MicroBead Cocktail were added and incubated for an additional 10 min. The suspension was filled up to a total volume of 500 µl with HBSS buffer, followed by magnetic separation. This procedure did not require a washing step after cell labelling. A MACS separation column was placed into the magnetic field of the MACS separator and equilibrated prior to adding the cell suspension with 3 ml HBSS buffer. After equilibration, a 50 ml falcon was placed under the column to collect the unlabeled cells (the T cells). The cell suspension was applied onto the column with a maximum of 5 x 10^8 PBMCs per column. One washing step was performed by adding 3 ml HBSS buffer to rinse the column once the cell suspension had passed through the column reservoir. Isolated T cells were counted and resuspended in preheated cell culture medium at a density of 2.5 x 10^6 T cells/ml for the T cell activation assay.

$CD14^+$ monocyte isolation (positive selection)

$CD14^+$ monocytes were isolated from PBMCs using monocyte isolation beads. Per 1 x 10^8 PBMCs, 340 µl HBSS buffer and 60 µl monocyte isolation beads were added and incubated for 15 min. Subsequently, cells were washed by adding buffer up to 50 ml and centrifugation. The supernatant was discarded, the pellet was loosened and 800 µl buffer per 1 x 10^8 PBMCs were added. A MACS separation column was placed into the magnetic field of the MACS separator and equilibrated prior to adding the cell suspension with 3 ml buffer. The cell suspension was applied onto the column with a maximum of 5 x 10^8 PBMCs per column. Washing steps were performed three times by adding 3 ml buffer to rinse the column once the cell suspension had passed through the column reservoir. The column was removed from the magnet and the labelled cells were immediately flushed into a 15 ml falcon by adding 5 ml buffer and firmly pushing the plunger into the column.

2.2.2.4 DC generation from CD14+ monocytes

DCs were generated from freshly isolated $CD14^+$ monocytes. Monocytes were counted, centrifuged and resuspended in preheated cell culture medium containing 250 µg/ml GM-CSF and 10 µg/ml IL-4. Cells were cultured in 6-well plates at a density of 2.5×10^6 monocytes/well in 3 ml medium. Fresh cytokines were added on the 2nd and 4th day after monocyte isolation. Therefore, 1 ml from each well was collected in a 50 ml falcon and centrifuged at RT. The supernatant was discarded and the cell pellet was resuspended in fresh, preheated medium supplemented with GM-CSF [750 µg/ml] and IL-4 [30 µg/ml]. 1 ml of this suspension was added to every well. DCs were harvested on the 5th or the 6th day after monocyte isolation. Therefore, DCs were loosened from the cell culture vessels with a cell scraper and collected in a 50 ml falcon. Residual DCs left in the wells were collected by rinsing each well with 1 ml HBSS (4 °C, without additives). The DC suspension was centrifuged at RT, the supernatant was decanted and the pellet was loosened. DCs were resuspended in preheated cell culture medium and counted using a hemocytometer.

2.2.2.5 Macrophage generation from CD14+ monocytes

Macrophages were generated from freshly isolated $CD14^+$ monocytes. Monocytes were counted, centrifuged and resuspended in preheated medium containing 0.66 µg/ml recombinant M-CSF. Cells were cultured in 12- or 24-well plates at a density of 1×10^6 monocytes/ml. The total culture volume was 1 ml (12-well) or 0.5 ml (24-well). The medium was exchanged on the 2nd and 4th day after monocyte isolation. Therefore, the cell culture supernatant (containing non-adherent and dead cells) was replaced by fresh, preheated medium supplemented with M-CSF [0.66 µg/ml]. On the 5th or 6th day after isolation, macrophages were used for further experiments.

2.2.3 Experimental setups

2.2.3.1 Hypoxic cell culture and immune cell stimulation

Normoxic cell culture was performed in a humidified cell culture incubator under 5 % CO_2, 94 % N_2 and 37 °C. Hypoxic cell culture was performed in an oxygen-controllable, humidified cell culture incubator under 1 % O_2, 5 % CO_2, 94 % N_2 and 37 °C (Labotect C60). Experiments performed under 0.1 % O_2 were performed in a hypoxia workstation under 0.1 % O_2, 5 % CO_2, 94 % N_2 and 37 °C (Invivo2 400).

Stimulation of DCs was performed at a concentration of 1×10^6 DCs/ml in cell culture media. DCs were stimulated with *A. fumigatus* germ tubes at a multiplicity of infection (MOI) of 1. Macrophages were stimulated with 2×10^6 germ tubes/ml. LPS (1 µg/ml), ultrapure LPS (1 µg/ml), zymosan (10 µg/ml) or depleted zymosan (100 µg/ml) were used to stimulate TLR2/4, TLR4, TLR2/Dectin-1 and Dectin-1, respectively. Stimulation was carried out on the 5th or 6th day after monocyte isolation. Stimulation was for 3, 6, 9, 12 or 24 h. For 24 h stimulation, fresh cytokines were added.

2.2.3.2 T cell activation assay

DCs were matured by stimulation with *A. fumigatus* (inactivated germ tubes, MOI = 1) under normoxia or hypoxia (1 % O_2) for 24 h. Control DCs were incubated without stimulation. After 24 h, DCs were harvested, counted and resuspended in fresh cell culture media at a concentration of 2.5×10^6 DCs/ml. Subsequently, DCs were γ-irradiated (receiving approximately 55 Gy). Pan T cells were isolated from allogeneic PBMCs. DCs and T cells were co-cultured under normoxia at an effector (DCs) to target (T cells) ratio of 1:9 (2.5×10^6 cells/ml) in 24-well plates in a total volume of 500 µl cell culture media (without the addition of cytokines). After three days, ELISA analysis was performed to quantify IFN-γ in the cell culture supernatants to assess T cell activation.

2.2.4 Gene expression analysis

2.2.4.1 RNA isolation

Harvesting cells for RNA isolation

DCs and macrophages were harvested in an RNA stabilizing reagent that detached adherent cells and simultaneously stabilized nucleic acids in the samples prior to RNA isolation. Therefore, cell culture supernatants were transferred into 2 ml microcentrifuge tubes. The RNA stabilizing reagent was immediately added to the remaining cells in the plates. For 12- and 24-well plates, 500 µl and 250 µl RNA stabilizing reagent were used per well, respectively. Supernatants were centrifuged at 500 x g for 5 min to pellet the non-adherent cells. The supernatants were removed from the pelleted cells in the microcentrifuge tube and either discarded or stored at -20 °C for further analysis. Subsequently, the contents from the culture plates (containing the adherent cells) were added to the cell pellet in the microcentrifuge tube and mixed well by pipetting up and down and vortexing. RNA was either isolated immediately or samples were stored at -20 °C.

RNA isolation from samples containing at least 5 x 10^5 cells

RNA was isolated using the RNeasy Mini Kit from samples containing at least 5 x 10^5 immune cells. Cells that were stored in RNA stabilizing reagent were thawed at RT and centrifuged at 5,000 x g for 5 min. Supernatants were discarded and 350 µl RLT buffer was added per sample to lyse the cells. 350 µl of 70 % ethanol was added to the homogenized lysate and mixed well by pipetting. The sample was applied onto an RNeasy Mini spin column and centrifuged at 8,000 x g for 30 sec at RT. Unless specified otherwise, all centrifugation steps were performed in the same way. The flow through was discarded and the column was washed one time with 700 µl RW1 buffer and two times with 500 µl RPE buffer. The column was centrifuged dry at full speed (13,200 x g) for 1 min. To elute the RNA, the column was placed into a fresh 1.5 ml microcentrifuge tube, 20-30 µl RNase-free water were directly added to the column membrane and the column was centrifuged at 8,000 x g for 1 min.

RNA isolation from samples containing less than 5 x 10^5 cells

RNA was isolated using the RNeasy Micro Kit (Qiagen) from samples containing less than 5 x 10^5 immune cells. Cells that were stored in RNA stabilizing reagent were thawed

at RT and centrifuged at 5,000 x g for 5 min. Supernatants were discarded and 200 µl RLT buffer was added per sample to lyse the cells. 200 µl of 70 % ethanol was added to the homogenized lysate and mixed well by pipetting. The sample was applied onto an RNeasy MinElute spin column and centrifuged at 8,000 x g for 30 sec at RT. Unless specified otherwise, all centrifugation steps were performed in the same way. The flow through was discarded and the column was washed one time with 350 µl RW1 buffer. DNA digestion was carried out by applying a mixture of 10 µl RNase free DNase and 70 µl RDD buffer onto the column and incubating for 15 min at RT, followed by an additional washing step with 350 µl RW1 buffer. The column was then washed two times with 500 µl RPE buffer and one time with 500 µl 80 % ethanol. The column was centrifuged dry at full speed for 1 min. To elute the RNA, the column was placed into a fresh 1.5 ml microcentrifuge tube, 14 µl RNase-free water were directly added to the column membrane and the column was centrifuged at 8,000 x g for 1 min.

To determine the RNA content and assess the quality of the isolated RNA, absorbance measurements were performed using a spectrophotometer. The 260/280 and 260/230 ratios were used to assess the purity of the RNA (with a value of 2.0 and 2.0-2.2 being the optimum, respectively).

2.2.4.2 Two-step real-time reverse transcription polymerase chain reaction

First strand cDNA synthesis

First strand copy DNA (cDNA) was synthesized from 100-500 ng RNA using a first strand cDNA synthesis kit and was performed in 0.2 ml reaction tubes in a thermal cycler. Per sample, RNase free water was added up to a total volume of 10 µl. Subsequently, 10 µl mastermix containing 2 µl reverse transcriptase, 1 µl random hexamer primer, 1 µl RNase inhibitor and 4 µl 5x reaction buffer were added. The reverse transcription protocol consisted of the following incubation steps: 5 min at 25 °C, 60 min at 37 °C and 5 min at 70 °C. Samples were used immediately or stored at -20 °C.

SYBR-green based real-time PCR

Primer pairs specific for one human transcript were designed using the NCBI Pick Primers feature (based on Primer3 and including BLAST analysis). If possible, primers were designed to span an exon-exon junction and primers pairs were separated by at least one

intron on the corresponding genomic DNA. Primer sequences are listed in Table 8, p. 47. Primers were ordered from Sigma-Aldrich as lyophilized, entsalted DNA oligos. Primers were diluted in nuclease free water to a stock concentration of 100 µM and further diluted to a working concentration of 10 µM. Primers had a final concentration of 500 nM in the PCR reaction. Each transcript was measured in duplicates with 10 ng cDNA per well in a total reaction volume of 20 µl. One reaction consisted of 10 µl iTaqUniversial SYBR Green Supermix, 1 µl forward [10 µM] and 1 µl reverse [10 µM] primers, 4 µl nuclease free water and 4 µl cDNA template (diluted 1:2 to 1:10 in nuclease free water according to the RNA input into cDNA synthesis). Fast thermal cycling conditions consisted of i) polymerase activation and DNA denaturation at 95 °C for 30 sec; ii) 40 cycles of denaturation at 95 °C for 3 sec and annealing/extension and plate read at 60 °C for 30 sec and iii) melt-curve analysis with an initial step at 95 °C for 15 min and a melt curve ranging from 60 °C to 95 °C with an 0.5 °C increment.

Calculation of relative expression levels

PCR efficiencies were calculated using LinRegPCR [141]. Levels of target mRNA expression were calculated using the efficiency-corrected ΔΔCq method with *ALAS1* as the endogenous reference gene and unstimulated control DCs under normoxia as calibrators. The following equation was used to calculate the fold changes:

$$\text{Fold change} = \frac{E\ (target\ gene)^{\Delta Cq\ target\ gene\ (Cq\ calibrator - Cq\ sample)}}{E\ (reference\ gene)^{\Delta Cq\ reference\ gene\ (Cq\ calibrator - Cq\ sample)}}$$

E, Efficiency; Cq, cycle threshold; calibrator, *ALAS1* (reference gene).

Agarose gel electrophoresis

Agarose gel electrophoresis was performed to control the length and specificity of the PCR products. 2 % agarose (w/v) were added to 1X TAE buffer and heated in a microwave until the agarose was completely dissolved. The solution was cooled down to app. 60 °C, ethidium bromide (0.5 µg/ml) was added and the solution was poured into a gel chamber with appropriate combs to jell. The gel was transferred into an electrophoresis chamber filled with 1X TAE buffer, PCR products were mixed with 6x DNA loading buffer and filled into the gel pockets. 5 µl 100 bp DNA ladder was loaded in a separate pocket for each run as a length standard. Samples were separated at 130 V for 15 to 30 min. The PCR products were visualized with UV-light (322 nm).

2.2.4.3 RNA interference

Transfection of siRNA into DCs by electroporation

For electroporation, DCs were harvested at the 5th day after monocyte isolation, washed one time with HBSS (4 °C, without additives) and resuspended in RPMI 1640 (without phenol-red) to a concentration of 1 x 10^7 DCs/ml. To 100 µl DC suspension, 6.6 µl siRNA [20 µM] were added, mixed by pipetting up and down and transferred into a 4-mm electroporation cuvette. The electroporation was performed using an electroporation pulse generator (EPI 2500, Dr. L. Fischer) set to a rectangle pulse of 340 V for 10 ms. DCs were incubated for 15 min at RT afterwards and then transferred into 12-well plates with each well containing 800 µl preheated cell culture medium including fresh cytokines. The electroporation cuvette was washed one time with 100 µl medium. DCs were incubated for 24 h prior to following experiments.

Knockdown to target genes

For HIF-1α knockdown, DCs were electroporated with *HIF1A* mRNA targeted siRNA. Six different siRNA sequences were tested in preliminary experiments. One of them (Hs_HIF1A_10) was consistently leading to a *HIF1A* knockdown of over 80 % 24 h after electroporation and was chosen for all further experiments. For Dectin-1 knockdown, DCs were electroporated with *CELC7A* mRNA targeted siRNA as previously established in our group [69]. Knockdown of HIF-1α and Dectin-1 was confirmed both on mRNA and protein levels. Nonsilencing siRNAs with random nucleotides were used as a negative control in each experiment.

2.2.4.4 Gene expression profiling (microarray analysis)

Microarray analysis was performed by the MFT Services (Microarray Facility Tübingen). Therefore, DCs where harvested, frozen in RNA stabilizing reagent and shipped on dry ice to the MFT. RNA was isolated using the RNeasy Mini Kit. Gene expression was measured with a Human Genome U219 Array Plate (HG-U219 24 array plate, Affymetrix).

Array analysis was conducted by hybridizing the RNA samples to the array plates. Images of the arrays were scanned and subjected to visual inspection to control for hybridization artefacts and proper grid alignment and were analyzed with AGCC 3.0 software (Affymetrix) to generate CEL files. The software applies a grid to the array image

to specify the region and location of each probe and calculates a single intensity for each probe based on the 75th percentile of remaining pixel intensities after excluding the border pixels. The resulting files, containing a single intensity value for each probe region delineated by a grid on each array image, were imported into Partek Genomics Suite for probe set summarization and statistical analysis. Model based Robust Multichip Analysis was performed to obtain a single intensity value representing transcript abundance for each probe set. This enabled comparisons between arrays, by normalizing and logarithmically transforming array data as well as stabilizing variance across the arrays.

The mean transcript abundance values for each probe set of the microarrays are available on the supplementary data CD (file names "*0.1 % O2 all signals*" and "*1 % O2/HIF-1a silenced all signals*"). The data for the 1 % O_2 microarrays were also deposited in NCBI's Gene Expression Omnibus [143] and are accessible through GEO Series accession number GSE60729.
(http://www.ncbi.nlm.nih.gov/geo/query/acc.cgi?acc=GSE60729)

Evaluation of the statistical significance of the difference observed in mean transcript abundance for each probe set between two conditions was determined by ANOVA. A *p*-value < 0.05 indicated statistically significant differential expression. Probe sets were considered significant if they exhibited a greater than 1.5-fold or 2-fold difference in mean transcript abundance between two conditions. Additionally, all *p*-values were corrected for multiple testing with the 5 %-FDR-based method of Benjamini and Hochberg [144]. Validation of the microarrays was performed by real-time RT-PCR. Expression levels of selected genes were measured in cDNA transcribed from the same RNA samples used for microarray analysis.

Venn diagrams were created using the web application BioVenn [145]. Pathway, network, upstream regulator and regulators effects analyses were performed using Ingenuity Systems Pathway analysis (IPA, Ingenuity Systems, now owned by Qiagen).

2.2.5 Protein analysis

2.2.5.1 Flow cytometry

For analysis of surface proteins, immune cells (2 x 10^5 per tube) were diluted in 100 µl HBSS buffer and incubated with mouse anti-human fluorochrome-coupled antibodies for 15 min at 4 °C, washed one time with HBSS buffer and resuspended in 300 µl HBSS buffer. For each specific antibody, the respective isotype antibody-staining was performed in a second tube. To determine percentage of apoptotic and/or necrotic cells, cells were stained with FITC-conjugated Annexin-V and with PI according to manufacturer's instructions (BD). Fluorescence was measured by flow cytometry on a FACSCalibur (BD). Flow cytometry data were analyzed using the FlowJo software. Cell debris was excluded by gating strategies according to light-scatter signals.

2.2.5.2 Cytokine quantification

Single analyte ELISA

Levels of TNF and IFN-γ in cell culture supernatants were determined by sandwich enzyme-linked immunosorbent assays (ELISAs). A mouse monoclonal antibody directed against the specific human cytokine was coated onto a 96-well plate. Therefore, the antibody was diluted 1:200 in coating buffer and 100 µl of the solution was added to each well. The plate was incubated overnight at 4 °C. The next day, the plate was washed using an ELISA washer (4x 300 µl wash buffer per well). All reagents had RT and all incubation steps were performed at RT with the plates sealed and mounted on a plate shaker at 250 rpm. Non-specific binding sites were blocked by incubating with 200 µl assay diluent per well for 1 h. A standard curve was included on each plate. The lyophilized protein standard was reconstituted in 200 µl assay diluent and aliquots from this stock solution were stored at -80 °C. Serial standard dilutions were prepared in assay diluent with concentrations of 500, 250, 125, 62.5, 31.3, 15.6 and 7.8 pg/ml. Appropriate sample dilutions were prepared in cell culture medium. After the blocking step, the plate was washed again, followed by incubation with the standards and the samples (100 µl/well) for 2 h. Samples were measured in duplicates. Afterwards, the plate was washed again and incubated with the detection antibody (1:200 in assay diluent, 100 µl/well) for 1 h, followed by washing, incubation with the Avidin-HRP (1:1000 in assay diluent, 100 µl/well) for 30 min and washing. Then, TMB substrate solution was prepared by

mixing equal amounts of component A with component B and 100 µl were added to each well. Plates were incubated in the dark until the desired color developed (10-20 min). The reaction was stopped by adding 100 µl of stop solution to each well. Absorbance (450 nm) was measured in a plate reader. Data were analyzed in Excel. Cytokine concentrations were calculated using a 3-parameter equation according to the standard curve.

Multiplex assay

Cytokines (Table 13) in cell culture supernatant of the microarray samples and the time-course cytokine profiling experiments were quantified with Bio-Plex Pro Human Cytokine Assays and measured using the Bio-Plex 200 (Bio-Rad). These assays were performed by Dr. Kerstin Hünniger in a collaboration with the HKI Jena (Prof. Kurzai).

Table 13 I Cytokines analyzed by multiplex assays.

Cytokine	Aliases	Full name
CCL11	Eotaxin	Chemokine (C-C motif) ligand 11
CCL2	MCP-1 (MCAF)	Chemokine (C-C motif) ligand 2
CCL3	MIP-1α	Chemokine (C-C motif) ligand 3
CCL4	MIP-1β	Chemokine (C-C motif) ligand 4
CCL5	RANTES	Chemokine (C-C motif) ligand 5
CCL7	MCP-3	Chemokine (C-C motif) ligand 7
CSF1	M-CSF	Colony stimulating factor 1 (macrophage)
CSF2	GM-CSF	Colony stimulating factor 2 (granulocyte-macrophage)
CSF3	G-CSF	Colony stimulating factor 3 (granulocyte)
CXCL1	Gro-α	Chemokine (C-X-C motif) ligand 1
CXCL10	IP-10	Chemokine (C-X-C motif) ligand 10
FGF2	FGF basic	Fibroblast growth factor 2
IFN-α1	IFN-α	Interferon, alpha 1
IFN-γ	---	Interferon, gamma
IL-10	---	Interleukin 10
IL-12p70	---	Interleukin 12p70
IL-13	---	Interleukin 13
IL-15	---	Interleukin 15
IL-17	---	Interleukin 17
IL-18	---	Interleukin 18
IL1RN	IL-1ra	Interleukin 1 receptor antagonist
IL-1β	---	Interleukin 1, beta
IL-2	---	Interleukin 2
IL-2Rα	IL-2RN	interleukin 2 receptor antagonist
IL-4	---	Interleukin 4
IL-5	---	Interleukin 5
IL-6	---	Interleukin 6
IL-7	---	Interleukin 7
IL-8	---	Interleukin 8
IL-9	---	Interleukin 9
PDGFB	PDGF-BB	Platelet-derived growth factor beta polypeptide
TNF	TNF-α	Tumor necrosis factor (alpha)
VEGF		Vascular endothelial growth factor

2.2.5.3 Protein extraction and immunoblotting

Whole protein preparation from human immune cells

Denaturing sodium dodecyl sulfate (SDS)-polyacrylamide gel electrophoresis (PAGE) and immunoblotting were performed to detect specific proteins in immune cell lysates. Cell culture plates were placed on ice immediately after the experiment and cells were harvested as fast as possible to avoid HIF-1α degradation. Under normoxia, hypoxic-stabilized HIF-1α has a very short half-life (< 5 min) [109]. Cells were detached by scraping the plates with a 1000 µl pipette tip. Immune cells were pelleted in 2 ml centrifugation tubes and the supernatant was transferred into a fresh 1.5 ml reaction tube for the analysis of secreted cytokines. Pelleted cells were immediately lysed in protein extraction (PE) buffer. For approximately 1 x 10^6 cells, 30 µl PE buffer was used. To homogenize the resulting gelatinous mass, DNA was fragmented by sonification. Equal amounts of the protein suspension were mixed with 4X SDS sample buffer and incubated in a thermal cycler at 95 °C for 5 min to denature the proteins. Samples were stored at -20 °C until protein separation.

Preparation of nuclear and cytoplasmic protein fractions

For the isolation of the nuclear and the cytoplasmic protein fraction of DCs, a nuclear extraction kit was used (Sigma-Aldrich). 1 x 10^6 DCs were pelleted in a 2 ml reaction tube, the supernatant was discarded and 20 µl of 1X lysis buffer (including DTT and protease inhibitors) was added to the cell pellet and DCs were gently resuspended. To extract the cytoplasmic fraction, the cells were incubated on ice for 15 min. After that, 6 µl of IGEPAL solution were added and the tube was vortexed for 10 sec and immediately centrifuged at 10,000 x g and 4 °C for 30 sec. The supernatant, containing the cytoplasmic fraction, was transferred to a fresh tube. Nuclear proteins were extracted from the remaining pellet by adding 14 µl of extraction buffer (including DTT and protease inhibitor). The tube was mounted on a vortex mixer and agitated at high speed for 20 min. Then, the tube was centrifuged at 16,000 x g for 6 min and the supernatant, containing the nuclear fraction, was transferred into a fresh tube. Equal amounts of the cytoplasmic and the nuclear fraction were mixed with 4X SDS sample buffer and incubated in a thermal cycler at 95 °C for 5 min to denature the proteins. Samples were stored at -20 °C until protein separation.

SDS-PAGE and immunoblotting

Proteins were separated on 10 % SDS-polyacrylamide gels (Table 14). These gels were casted using the BioRad Mini Protean System and had a thickness of 0.75 mm.

Table 14 I Preparation of SDS-PAGE gels (2 gels).

Gel type	Contents
Stacking gel	3.2 ml water 0.75 ml PAA 1.25 ml 4x stacking gel buffer 50 µl 10 % APS 5 µl TEMED
Resolving gel	4.2 ml water 3.3 ml PAA 2.5 ml 4x resolving gel buffer 100 µl 10 % APS 10 µl TEMED

Gels were run at 80 V in 1X electrophoresis buffer until the dye front reached the resolving gel (app. 10 min); then the voltage was increased to 130 V and gels were run until the dye front reached the bottom of the gels. A prestained protein ladder was included as a size reference marker on each gel. The separated proteins were semi-dry electroblotted onto nitrocellulose membrane in a semi-dry blotting chamber using 1X semi-dry transfer buffer and applying 75 mA per gel for 90 min. The blotting sandwich was built up with four layers of pre-soaked blotting paper on the bottom, followed by the gel and the membrane and finished again with four layers of blotting paper.

All membrane incubation steps were performed on a vertical shaker. The membrane was blocked in 5 % TTBS milk for 1-2 h, followed by incubation with the specific primary antibody diluted in 5 % TTBS milk at 4 °C overnight. The next day, the membrane was washed three times with TTBS buffer for 5 min each and incubated with appropriate HRP labeled secondary antibodies diluted in 5 % TTBS milk at RT for 1-2 h. After incubation with the secondary antibody, the membrane was washed three times with TTBS buffer and once with TBS buffer for 5 min each. Detection was carried out using a western blotting luminol reagent. Membranes were incubated with the luminol reagent for 5 min. Then, excessive luminol reagent was removed and the membranes were exposed to medical x-ray films in the dark room with varying exposure times.

To visualize total protein on the membranes, membranes were stained with Ponceau solution after the detection of specific proteins by western blot. Therefore, membranes were washed once with VE-H_2O, covered with Ponceau solution under slight agitation and then washed several times with VE-H_2O until protein bands were clearly visible.

2.2.6 Metabolic quantification

Cell culture supernatants were collected and immediately stored at -20 °C. For metabolic quantification, 500 µl of each sample were transferred into glucose determination blood collection tubes to stabilize lactate until measurement. Glucose and lactate concentrations were measured photometrically with a blood gas analyzer (Cobas C701) by the Würzburg University Hospital central laboratory facilities.

2.2.7 Statistics

Data are presented as mean + standard deviation (SD) unless specified otherwise in the figure legend. Data were analyzed with two-tailed, paired t-test when comparing two means. When comparing multiple conditions, data were analyzed by two-way repeated measures ANOVA followed by Bonferroni's multiple comparison test. Statistical tests were calculated using the software GraphPad Prism 5. Statistical significance is indicated with asterisks as follows: * $p < 0.05$, ** $p < 0.01$ and *** $p < 0.001$.

2.2.8 Ethics statement

This study, using whole blood and LRS chamber specimens obtained from healthy human volunteers, was approved by the Ethical Committee of the University Hospital of Würzburg. Data analysis was conducted anonymously.

3 Results

3.1 Generation of monocyte-derived macrophages and DCs

This study is based on model systems of primary human immune cells. In contrast to cell lines, these models mimic circulating or tissue-resident *in vivo* immune cells more closely (see paragraph 1.2.4, p. 27ff.). Monocyte-derived DCs (and for some confirmatory experiments, monocyte-derived macrophages, see paragraph 3.3.1, p. 103ff.) were used in this study. The protocol for the generation of monocyte-derived DCs had already been established in the laboratory. The method for the generation of monocyte-derived macrophages (described in paragraph 2.2.2.5, p. 54ff.) was established by Kristin Czakai during the time-course of the present study and followed widely published standard protocols [146].

Figure 11 shows the flow cytometric analysis of the different cell populations in the course of macrophage and DC generation. Monocytes comprised approximately 20 % of the PBMCs that had been isolated from LRS chamber contents (a by-product from platelet donations). Monocytes were isolated from PBMCs by MACS technology (positive selection). Purity was determined by flow cytometry (FSC/SSC gating and CD14 staining) and was routinely > 95 %. Monocytes were $CD14^+$ / $CD1a^-$ (Figure 11).

Macrophages were obtained after a five day incubation of monocytes with M-CSF and showed the characteristic macrophage phenotype as adherent, $CD14^+$ / $CD1a^-$ cells. DCs were obtained after a five day incubation of monocytes with IL-4 and GM-CSF and exhibited the characteristic DC features of non-adherent, $CD14^-$ / $CD1a^+$ cells. Both, macrophages and DCs, showed immediate phagocytic activity towards *A. fumigatus* conidia (data not shown).

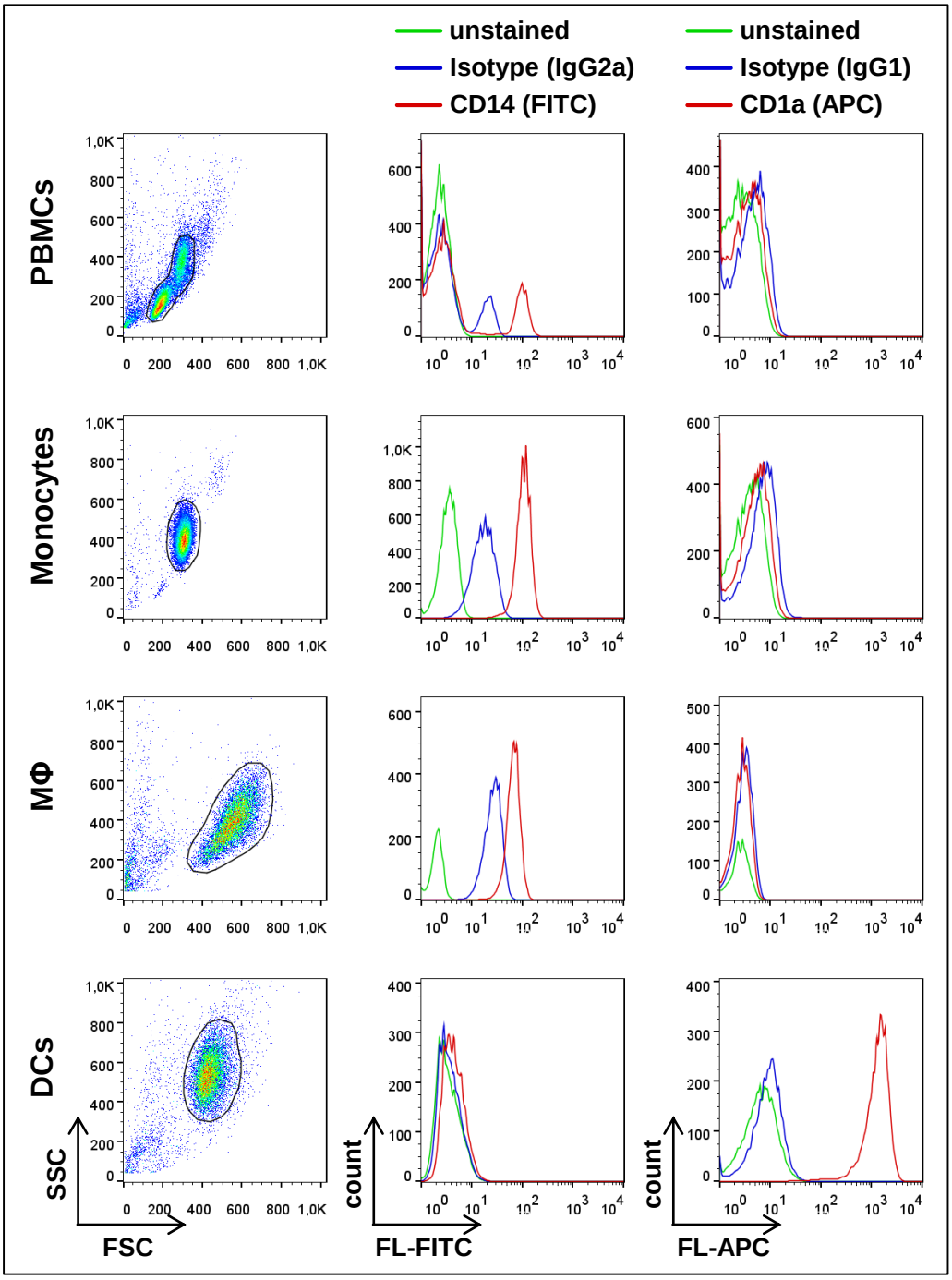

Figure 11 I Generation of monocyte-derived macrophages and DCs.

PBMCs, monocytes, macrophages (MΦ) and DCs were stained for CD14 (middle column) and CD1a (right column) and analyzed by flow cytometry. The first column shows FSC/SSC pseudo color density plots. The histograms show the fluorescence intensity from the cell populations gated according to light scatter characteristics (gates are shown in black in the density plots). The FSC/SSC voltage settings were adjusted for each cell population (as PBMCs and monocytes are much smaller compared to MΦ and DCs). The voltage settings for the fluorochromes remained the same throughout the experiment. Monocytes and MΦ bound unspecifically to the IgG2a FITC isotype antibody (middle column, blue lines). Data are representative for at least three independent experiments. FSC, forward scatter; SSC, side scatter; FL, fluorescence intensity; FITC and APC, fluorochromes.

DCs could be easily harvested and used for further experiments as they are non-adherent in their immature stage at day five after monocyte isolation. Approximately 30-50 % of the monocytes differentiated into DCs. Nonetheless, donor-dependent differences occurred frequently regarding the DC yield. Sometimes, donor-monocytes could not be differentiated into DCs and most of the cells died during the five to six day time-course of DC generation. In addition, DCs derived from other donors sometimes showed uncharacteristic expression of CD1a and were therefore excluded from further experiments (see example in Figure 39, p. 115). However, as the blood samples were anonymized, it was not possible to identify and exclude the respective donors beforehand.

It should be noted that these problems were not observed for macrophages. Comparatively few experiments were performed with this cell type and because of that, possible donor-dependent variations might just have not occurred due to statistical reasons. However, macrophages are adherent cells and various methods of detachment induced significant cell death (Kristin Czakai, unpublished data). Therefore, macrophages were not detached from the culture vessels prior to the experiments.

To verify the comparability of macrophages generated in 12- or 24-well plates within one experiment, gene expression was measured in biological replicates of macrophages derived from the same blood donor. In addition, levels of TNF were quantified in the supernatants of an independent repetition of this experiment. Figure 12 A-C demonstrate that biological replicates of macrophages showed comparable regulation of *HIF1A*, *VEGFA* and *IL6* on transcript level after 6 h stimulation with various PRR ligands or *A. fumigatus*. Furthermore, levels of TNF in the supernatants of the second experiment were equal between the biological replicates (Figure 12 D). These results confirmed the sample-to-sample comparability of macrophages in an experimental setup without cell detachment prior to stimulation experiments.

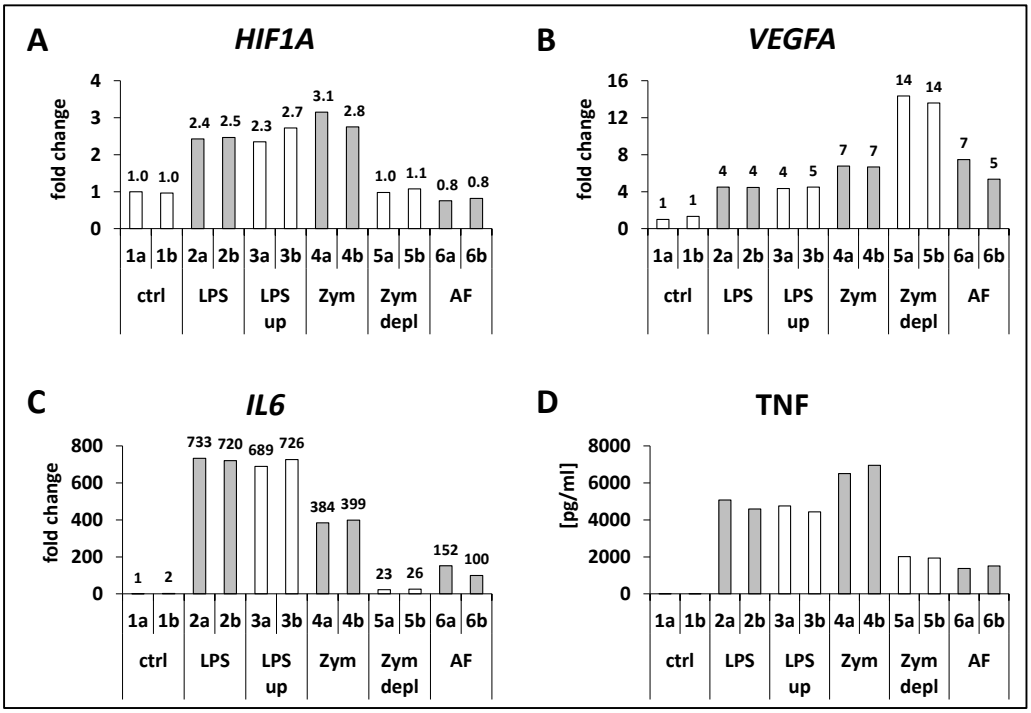

Figure 12 I Biological replicates of macrophages.

Macrophages were cultivated in 12-well plates without stimulation (1, ctrl) or stimulated with LPS (2, 1 µg/ml), ultrapure LPS (3, LPS up, 1 µg/ml), zymosan (4, Zym, 10 µg/ml), depleted zymosan (5, Zym depl, 100 µg/ml) or *A. fumigatus* (6, AF, inactivated germ tubes, 2 x 10^6 / well) for 6 h. Each pair (a, b) represents data from one biological replicate. **(A to C)** Transcript levels of *HIF1A, VEGFA* and *IL6* were measured by real-time RT-PCR, normalized to the reference gene *ALAS1* and are displayed as fold changes relative to unstimulated control macrophages. Fold changes are depicted in numerals above the columns. **(D)** The experiment was repeated independently. Levels of TNF were determined in the culture supernatants by ELISA and are displayed in pg/ml.

3.2 Functional characterization of DCs under hypoxia

3.2.1 DC viability under hypoxic culture conditions

To determine DC viability under conditions of reduced oxygen availability, DCs were incubated under normoxic or hypoxic conditions for 24 h. Hypoxic conditions were 0.1 % O_2 (representing strong hypoxia) and 1 % O_2 (representing moderate hypoxia). DCs were either not stimulated (control DCs) or stimulated with zymosan, LPS or *A. fumigatus*. Zymosan and LPS were used as control substances to stimulate the PRRs TLR2/Dectin-1 and TLR2/TLR4, respectively. All three PRRs are involved in the recognition of *A. fumigatus* (see paragraph 1.2.3.2, p. 23). Among them, the most relevant receptor for *A. fumigatus* on human DCs is Dectin-1. Recognition of *A. fumigatus* via Dectin-1 initiates a pro-inflammatory response in human DCs [69].

DC viability was measured using flow cytometry. Figure 13 shows the results from the DC viability assay. The total numbers of DCs among all events were defined by gating according to light scatter characteristics (see example in Figure 11, p. 68). Percentages of viable DCs ($AnnexinV^-$ / PI^-), apoptotic DCs ($AnnexinV^+$ / PI^-) and dead DCs ($AnnexinV^+$ / PI^+) were defined within the DC gate. Statistical analysis revealed some significant differences comparing DCs stimulated with *A. fumigatus* under normoxic to DCs stimulated under hypoxic culture conditions. This included a significant reduction in viable DCs after stimulation with *A. fumigatus* under 0.1 % O_2 (Figure 13 A, upper right) and a significant reduction in the total numbers of DCs after stimulation with *A. fumigatus* under 1 % O_2 (Figure 13 B, upper left). In addition to the total numbers of DCs and the percentage of viable DCs among these, the percentages of apoptotic and dead DCs were considered as well. There was no significant difference between normoxia and hypoxia regarding the percentages of apoptotic or dead DCs after stimulation with *A. fumigatus*. Taken together, no massive cell death was observed in either treatment condition, leading to the conclusion that DCs tolerated strong and moderate hypoxic culture conditions and stimulation with zymosan, LPS or *A. fumigatus* for culture times up to 24 h.

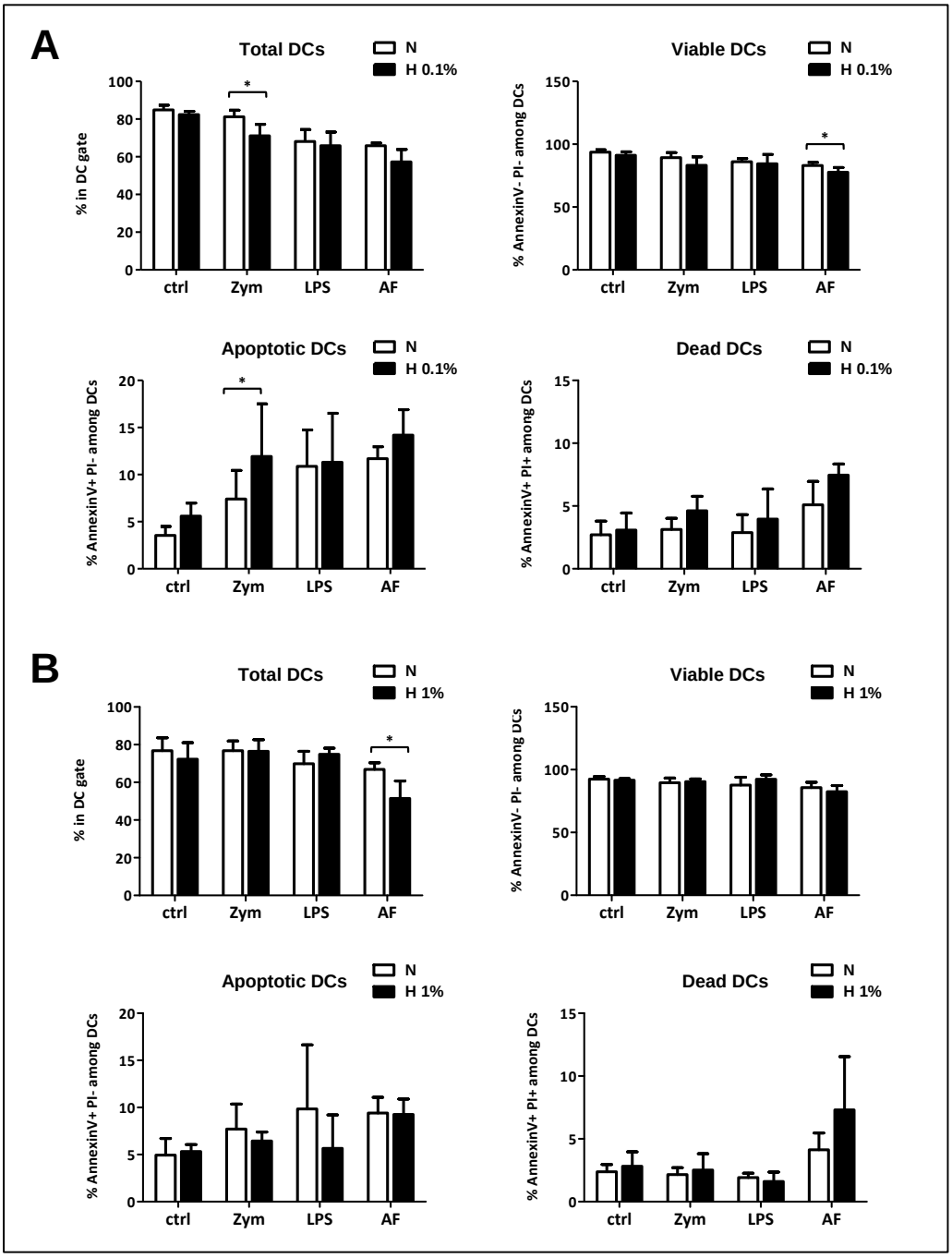

Figure 13 I DC viability under hypoxic culture conditions.

DCs were incubated under normoxia (white bars) or hypoxia (black bars, **(A)** 0.1 % O_2 and **(B)** 1 % O_2) for 24 h without stimulation (ctrl) or stimulated with zymosan (Zym, 10 µg/ml), LPS (1 µg/ml) or *A. fumigatus* (AF, MOI = 1). Flow cytometry was performed to determine DC viability. The DC population was defined by light scatter characteristics (FSC/SSC) to exclude cell debris. To determine apoptotic and/or dead cells, DCs were stained with FITC-conjugated AnnexinV and with PI. The graphs show percentages of total DCs, viable DCs (AnnexinV- PI-), early apoptotic DCs (AnnexinV+ PI-) and dead DCs (AnnexinV+ PI+). Data are shown as mean + SD of n = 3 (0.1 % O_2) or n = 4 (1 % O_2) independent experiments. Significant differences comparing normoxic to hypoxic conditions are indicated with an asterisk (* $p < 0.05$; two tailed, paired t test).

3.2.2 Gene expression profiles of DCs under strong hypoxia (0.1 % O_2)

3.2.2.1 Preparation, performance and validation of the 0.1 % O_2 microarrays

To evaluate the influence of oxygen limitation on DC functions against *A. fumigatus* and to generate a basis for further experiments, genome-wide mRNA expression analyses using microarrays were performed. A first set of experiments was performed under strong hypoxia (0.1 % O_2). The experiment consisted of four treatment groups with three replicates in each group (i.e., DCs derived from three different blood donors). DCs were either cultivated without stimulation under normoxic or hypoxic (0.1 % O_2) conditions or were stimulated with *A. fumigatus* under both culture conditions for 6 h (Figure 14).

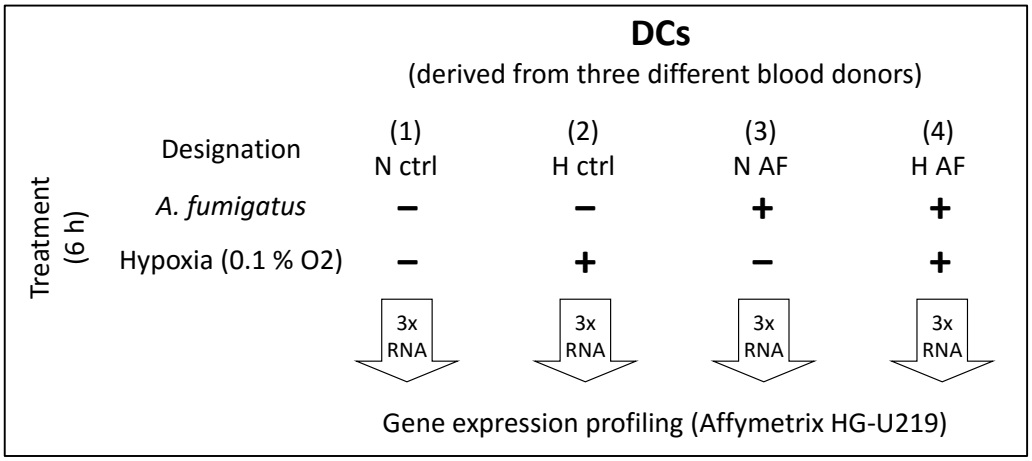

Figure 14 I Schematic outline of the 0.1 % O_2 gene expression profiling experiment.

The gene expression profiling experiment consisted of four treatment groups (1 to 4) with three replicates in each group. DCs were cultivated without stimulation (ctrl) or were stimulated with *A. fumigatus* (AF, MOI = 1) under normoxia (N) or hypoxia (H, 0.1 % O_2) for 6 h. Subsequently, DCs were harvested and stored in an RNA stabilizing agent for RNA isolation and hybridization onto Affymetrix HG-U219 gene expression microarrays. Supernatants were stored separately for cytokine quantification.

The gene expression microarrays were performed by the technical staff at the Microarray Facility Tübingen (MFT). It included RNA isolation, RNA quality control by bioanalyzer, hybridization onto the microarrays and performance of the microarray analysis. The microarray raw data were analyzed in cooperation with Dr. Michael Bonin (at that time head of the MFT). It included the generation of lists of differentially expressed genes (see paragraph 2.2.4.4, p. 59ff. for details). On this basis, analysis of the

microarray data was performed independently, including the use of the web-based microarray gene expression analysis program Ingenuity Pathways Analysis (IPA).

To validate the microarray data, relative transcript levels of several genes were measured by real-time RT-PCR using the same RNA samples applied for hybridization onto the microarrays (Figure 15). For some transcripts (*CCL3, IL1B, IL8, TNF* and *VEGFA*) microarray fold changes were lower compared to real-time RT-PCR fold changes. This indicated a greater sensitivity of the real-time RT-PCR method. Interestingly, under hypoxic control conditions, *HIF1A* was clearly down-regulated on the transcript level. Most importantly, all analyzed transcripts showed the same trend of up- or down-regulation when comparing microarray and real-time RT-PCR results, thus confirming the expression data obtained from the microarrays.

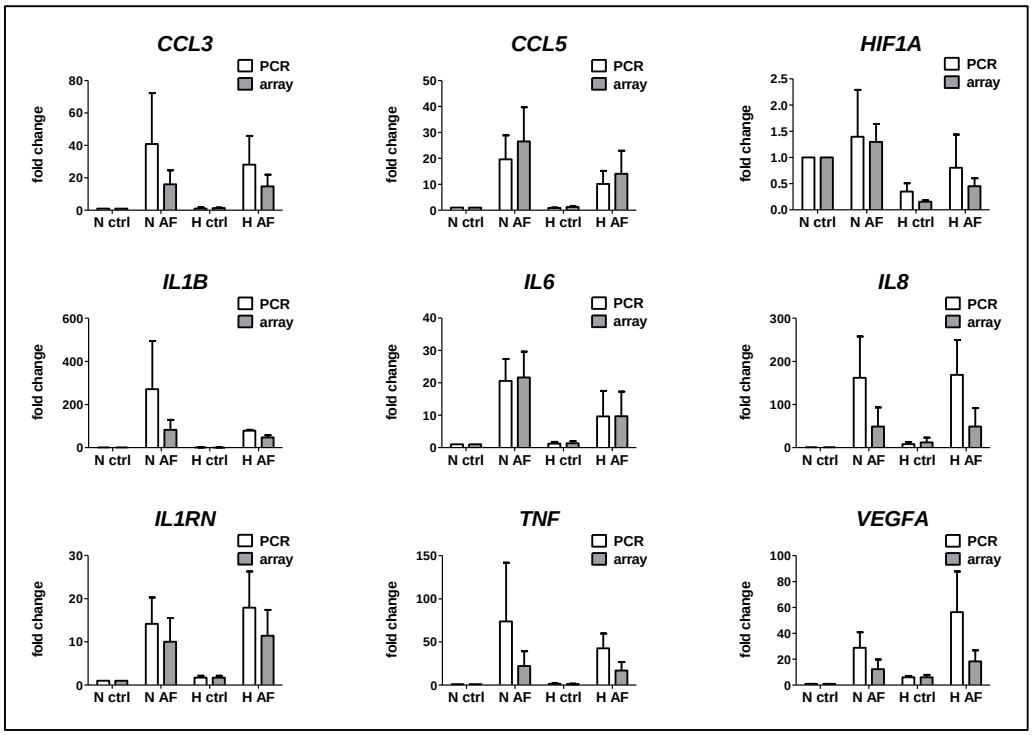

Figure 15 I Validation of the 0.1 % O_2 microarrays by real-time RT-PCR.

Expression levels of selected genes are displayed as fold changes relative to control DCs. **White bars (PCR):** Transcript levels were measured by real-time RT-PCR and normalized to the reference gene *ALAS1*. **Grey bars (array):** Expression levels were calculated using the normalized microarray expression data for the specific transcripts. Data are presented as mean + SD (n = 3). N, normoxia; H, hypoxia (0.1 % O_2); AF, *A. fumigatus* (MOI = 1); 6 h incubation.

Protein levels were quantified in cell culture supernatants of the microarray samples by custom multiplex immunoassays. Levels of 25 analytes are displayed in Figure 16. Full names of the cytokines are listed in paragraph 2.2.5.2, p. 61. Levels of CCL3, CCL4, IL-8 and TNF reached the upper range of the standard curve in some supernatants from DCs stimulated with *A. fumigatus*. In these cases, the concentrations shown in Figure 16 are the upper limit of the standard curve as the real concentrations in the samples could not be determined.

The cytokine levels in the supernatants of the microarray samples revealed great heterogeneity but no clear trend when comparing the three replicates. Stimulation with *A. fumigatus* induced the release of several pro-inflammatory cytokines under normoxic as well as hypoxic culture conditions, including the chemokines CCL2, CCL3, CCL4 and CCL5 as well as IL-8 and TNF. Regulation trends were defined if at least two samples showed increased or reduced levels for a specific cytokine under hypoxia, while the third sample did not show the opposite trend. Comparing supernatants from DCs stimulated with *A. fumigatus* under normoxia to those stimulated under hypoxia, levels of IL-1RA (the receptor antagonist for the IL-1 receptor) were higher under hypoxic conditions (depicted in red in Figure 16). On the other hand, levels of a large range of cytokines, including chemokines (CCL2, CCL5 and CCL7), interleukins (IL-1β, IL-6, IL-10 and IL-18) and other cytokines (CSF2, CSF3, CXCL1 and CXCL10), showed a trend towards reduced concentrations in the supernatants from DCs stimulated under hypoxia compared to those stimulated under normoxia (depicted in green in Figure 16).

In line with reduced levels of CCL5, IL-1β and IL-6 in the supernatants, transcript expression levels of *CCL5*, *IL1B* and *IL6* showed a trend towards lower fold changes in the hypoxia samples (Figure 15). Taken together, measurement of transcript levels by real-time RT-PCR and quantification of cytokine release validated the expression levels determined by microarray analysis. Furthermore, while control DCs under normoxia and hypoxia showed similar transcript and protein expression, hypoxia had an inhibitory effect on the expression and release of cytokines from DCs stimulated with *A. fumigatus*.

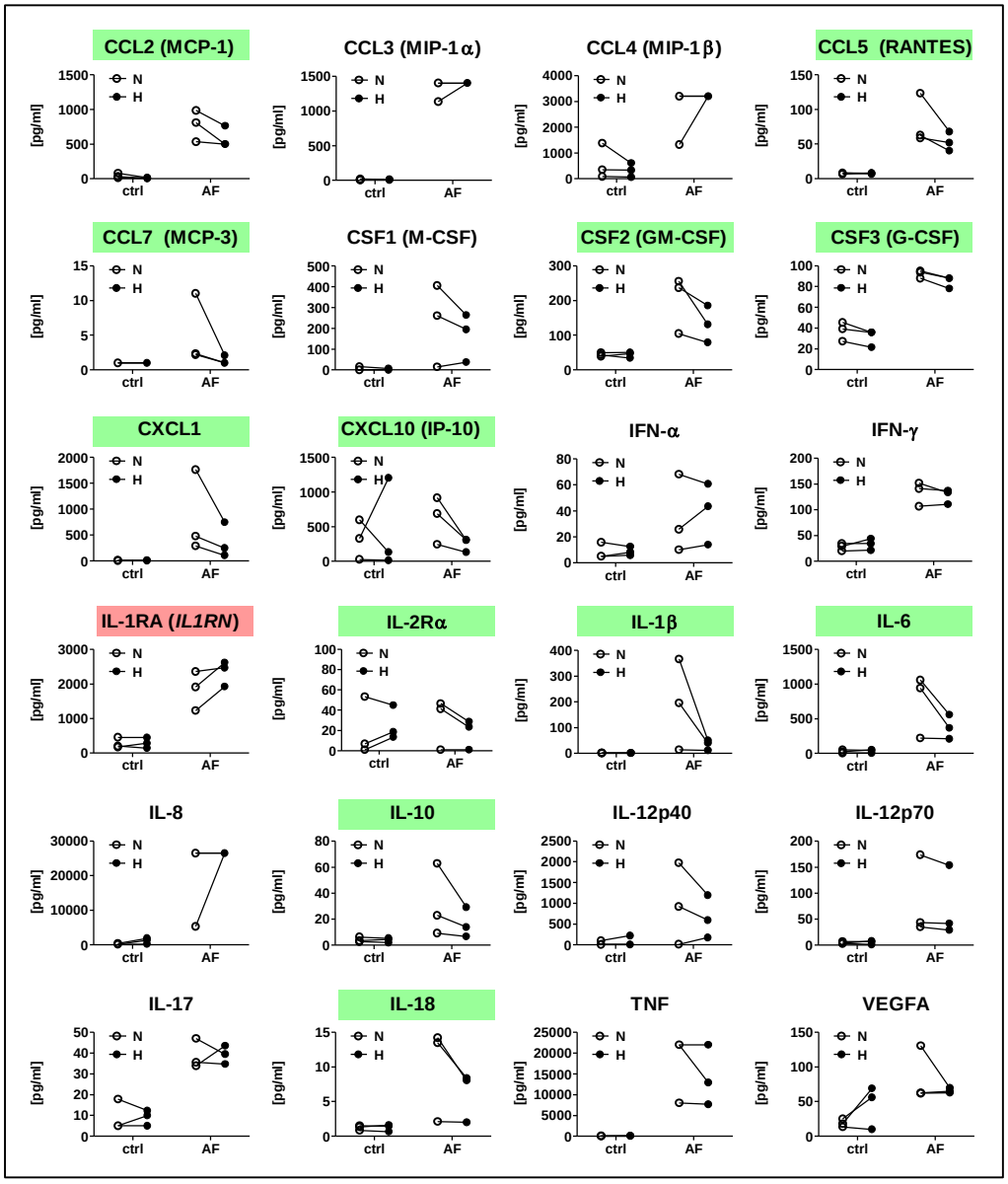

Figure 16 I Cytokine levels in the supernatants of the 0.1 % O_2 microarray samples.

Cytokines were quantified using custom multiplex immunoassays and are shown in pg/ml. Trends comparing normoxic to hypoxic DCs stimulated with *A. fumigatus* are color-coded. Green, trend towards reduced release in H AF; red, trend towards increased release in H AF. N, normoxia; H, hypoxia (0.1 % O_2), ctrl, control; AF, *A. fumigatus* (MOI = 1); 6 h incubation.

3.2.2.2 Analysis of the 0.1 % O_2 microarray data

For a first evaluation of the similarities and differences in the microarray gene expression datasets, principal components analysis (PCA) was performed (Figure 17). The PCA revealed that the replicates in each treatment condition were more closely related compared to the different donors (Figure 17: the colors, i.e. the treatment conditions, lie more closely to each other compared to the symbols, i.e. the different donors). Therefore, the PCA demonstrates that the treatment had a greater influence compared to the donor-specific influence. Interestingly, the unstimulated control DCs under normoxia (green symbols in Figure 17) did not lie as closely to each other in comparison to all other conditions, indicating that the donor-dependent differences are highest in control DCs and become less prominent in DCs under hypoxia and/or stimulation with *A. fumigatus*.

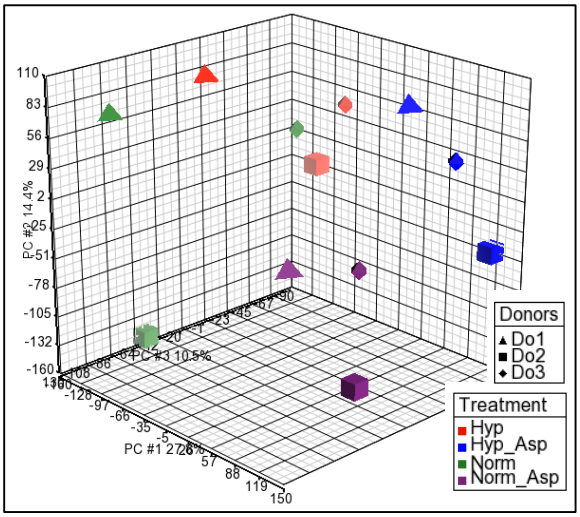

Figure 17 I PCA of the 0.1 % O_2 microarray data.

Principal components analysis (PCA) was performed as an exploratory technique to detect groupings in the microarray data sets. The data used for the PCA were the normalized expression values measured for all transcripts in one sample. The symbols (triangle, big and small square) represent the three replicates (blood donors, Do1 to Do3) and the colors (red, blue, green and purple) represent the four treatment conditions. Norm, normoxia; Hyp, hypoxia, 0.1 % O_2; Asp, DCs stimulated with *A. fumigatus* (MOI = 1). The PCA was performed by Michael Bonin.

Based on the PCA, differentially regulated genes were determined by an unpaired analysis (grouping the datasets according to the treatment condition). Comparing two treatment conditions, probe sets were considered to be differentially expressed with a *p*-value < 0.05 and a fold change > 2 (detailed methods are described in paragraph 2.2.4.4, p. 59ff.). Each probe set corresponds to a specific gene. Most genes are represented by more than one probe set on the HG-U219 microarrays.

Initially, three lists of differentially expressed genes were generated by separately comparing the transcriptome of DCs under hypoxia (2 H ctrl in Figure 14, p. 73), of DCs stimulated with *A. fumigatus* (3 N AF) and of DCs stimulated with *A. fumigatus* under

hypoxia (4 H AF) to control DCs under normoxia (1 N ctrl). These lists were termed "Hypoxia", "*A. fumigatus*" and "Hypoxia + *A. fumigatus*", respectively. Fully annotated lists of the genes in these comparisons are available on the supplementary data CD (file names "*0.1 % O2 Hypoxia*", "*0.1 % O2 A. fumigatus*" and "*0.1 % O2 Hypoxia + A. fumigatus*"). Table 15 to Table 17 list the top ten up- and down-regulated genes on these lists.

Table 15 I Top 10 regulated genes on the list "Hypoxia" (0.1 % O_2 microarrays).

Gene Symbol	Gene Title	FC *
HIF1A	hypoxia inducible factor 1, alpha subunit	-8.62
PPIL1	peptidylprolyl isomerase (cyclophilin)-like 1	-2.91
SDPR	serum deprivation response	-2.71
DCAF4	DDB1 and CUL4 associated factor 4	-2.64
EARS2	glutamyl-tRNA synthetase 2, mitochondrial (putative)	-2.61
FAM92A1/FAM92A2	family with sequence similarity 92, member A1/CG6405-PA-like	-2.49
GPATCH4	G patch domain containing 4	-2.39
SPSB2	splA/ryanodine receptor domain and SOCS box containing 2	-2.33
INPP4A	inositol polyphosphate-4-phosphatase, type I, 107kDa	-2.30
ATF7IP	activating transcription factor 7 interacting protein	-2.30
BNIP3	BCL2/adenovirus E1B 19kDa interacting protein 3	9.78
ANGPTL4	angiopoietin-like 4	10.33
HK2	hexokinase 2	10.37
TMEM45A	transmembrane protein 45A	12.92
ZNF395	zinc finger protein 395	15.39
SLC2A1	solute carrier family 2 (facilitated glucose transporter), member 1	15.46
PLOD2	procollagen-lysine, 2-oxoglutarate 5-dioxygenase 2	16.41
CD300A	CD300a molecule	20.63
ADM	adrenomedullin	25.18
MT1G	metallothionein 1G	26.32

* For genes represented by more than one probe set, the one with the highest fold change (FC) is shown.

Table 16 I Top 10 regulated genes on the list "*A. fumigatus*" (0.1 % O_2 microarrays).

Gene Symbol	Gene Title	FC *
ADORA3	adenosine A3 receptor	-22.00
P2RY14	purinergic receptor P2Y, G-protein coupled, 14	-16.10
CCR2	chemokine (C-C motif) receptor 2	-11.45
FOXQ1	forkhead box Q1	-10.14
KLF4	Kruppel-like factor 4 (gut)	-9.25
FYB	FYN binding protein	-9.23
WNT5B	wingless-type MMTV integration site family, member 5B	-8.69
GCNT1	glucosaminyl (N-acetyl) transferase 1, core 2	-8.66
C10orf54	chromosome 10 open reading frame 54	-8.39
CTSC	cathepsin C	-8.23

Table 16 (continued) I Top 10 regulated genes on the list "*A. fumigatus*" (0.1 % O_2 microarrays).

Gene Symbol	Gene Title	FC *
TNFSF15	tumor necrosis factor (ligand) superfamily, member 15	109.11
CXCL1	chemokine (C-X-C motif) ligand 1	127.95
CSF2	colony stimulating factor 2 (granulocyte-macrophage)	130.67
CXCL3	chemokine (C-X-C motif) ligand 3	131.18
IL12B	interleukin 12B (natural killer cell stimulatory factor 2, cytotoxic lymphocyte	140.17
GEM	GTP binding protein overexpressed in skeletal muscle	152.61
SERPINB2	serpin peptidase inhibitor, clade B (ovalbumin), member 2	168.86
MMP10	matrix metallopeptidase 10 (stromelysin 2)	202.16
PTGS2	prostaglandin-endoperoxide synthase 2	226.53
EDN1	endothelin 1	263.53

* For genes represented by more than one probe set, the one with the highest fold change (FC) is shown.

Table 17 I Top 10 regulated genes on the list "Hypoxia + *A. fumigatus*" (0.1 % O_2 microarrays).

Gene Symbol	Gene Title	FC *
WNT5B	wingless-type MMTV integration site family, member 5B	-13.58
HRH1	histamine receptor H1	-11.33
CCR2	chemokine (C-C motif) receptor 2	-11.08
P2RY14	purinergic receptor P2Y, G-protein coupled, 14	-10.62
CTSC	cathepsin C	-10.31
TRAM2	translocation associated membrane protein 2	-9.26
ADORA3	adenosine A3 receptor	-8.68
MS4A6A	membrane-spanning 4-domains, subfamily A, member 6A	-8.62
PAQR8	progestin and adipoQ receptor family member VIII	-8.19
FYB	FYN binding protein	-7.91
MMP10	matrix metallopeptidase 10 (stromelysin 2)	93.64
CSF2	colony stimulating factor 2 (granulocyte-macrophage)	93.68
CCL20	chemokine (C-C motif) ligand 20	93.69
SERPINB2	serpin peptidase inhibitor, clade B (ovalbumin), member 2	99.88
CXCL3	chemokine (C-X-C motif) ligand 3	103.07
NR4A1	nuclear receptor subfamily 4, group A, member 1	120.70
INHBA	inhibin, beta A	124.19
GEM	GTP binding protein overexpressed in skeletal muscle	131.97
EDN1	endothelin 1	152.79
PTGS2	prostaglandin-endoperoxide synthase 2	223.45

* For genes represented by more than one probe set, the one with the highest fold change (FC) is shown.

Figure 18 visualizes the overlap and differences in these lists of differentially expressed genes in the format of Venn diagrams. Hypoxia (0.1 % O_2) alone did not have a strong influence on DC gene expression. On the other hand, *A. fumigatus* strongly affected gene expression in DCs, either in combination with hypoxia ("Hypoxia + *A. fumigatus*") or under normoxia ("*A. fumigatus*"). There was a great overlap between these two conditions. On the other hand, there were genes that appeared exclusively on the list "*A. fumigatus*" or on the list "Hypoxia + *A. fumigatus*" (Figure 18).

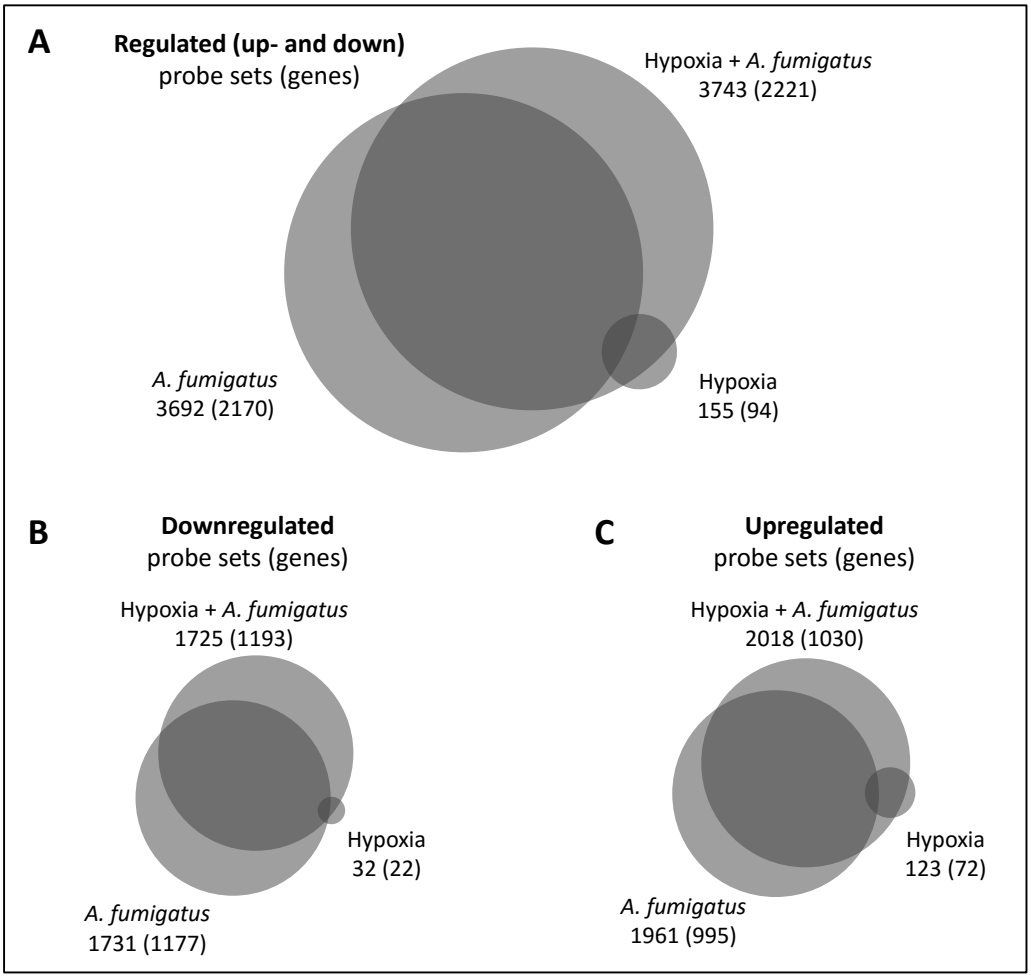

Figure 18 I Overlaps between the lists of differentially expressed genes (0.1 % O_2 microarrays).

Venn diagrams visualize the overlap and differences between the lists of differentially regulated genes. Probe sets (with each probe set corresponding to a specific gene) were considered differentially regulated with a *p*-value < 0.05 and a fold change > 2. Each circle corresponds to one of the three comparisons, and the overlaps between the circles correspond to the overlaps between the data sets. The Venn diagrams are area-proportional, i.e. the sizes of the circles and the overlaps correspond to the number of differentially regulated genes. Numbers indicate the total number of **(A)** all, **(B)** down- and **(C)** up-regulated probe sets (genes) on the respective lists.

In a next analysis step, the three lists of regulated genes were subjected to pathway and upstream regulator analysis using the program IPA. Figure 19 shows the differences and overlaps for this analysis. Because of the large datasets, many pathways and upstream regulators passed the program's significance criteria and made it difficult to interpret the data. Full lists of all pathways and upstream regulators are included on the supplementary data CD (file names "*0.1 % O2 all pathways*" and "*0.1 % O2 Immune relevant pathways*").

Importantly, the HIF-1α signaling pathway was among the four pathways that were significantly involved in all three pathway analyses (Figure 19 A) and HIF-1α was the only upstream regulator predicted to be activated in all three upstream regulator analyses (Figure 19 B). This indicated that HIF-1α signaling not only plays a role in the adaption of DCs to hypoxic conditions but also in the response of DCs against *A. fumigatus* with or without hypoxia.

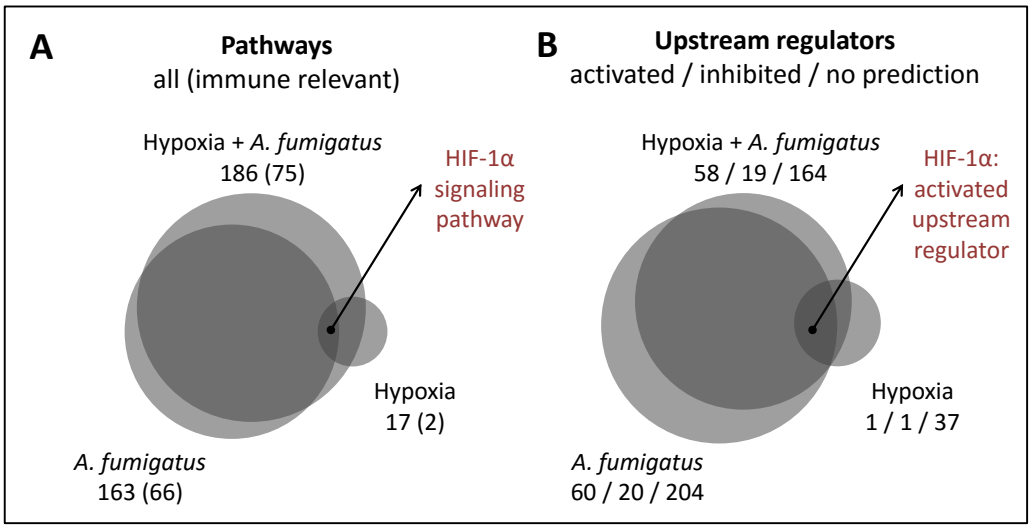

Figure 19 I Visualization of shared and unique pathways and upstream regulators (0.1 % O_2 microarrays).

(A) Pathway analysis. Data sets include all pathways that were significantly enriched in the analysis of the respective list of differentially expressed genes. **(B) Upstream regulator analysis.** Data sets include all upstream regulators that were predicted by the IPA upstream regulator analysis. According to the direction of the upstream regulator's target genes regulation (up or down or not regulated), upstream regulators are predicted to be activated or inhibited or no prediction is made by the software. Data were analyzed using the IPA canonical pathway and upstream regulator analysis tool, $p < 0.05$; scoring method: Fisher's Exact Test.

In order to specifically evaluate the influence of hypoxia on the transcriptome of DCs stimulated with *A. fumigatus*, the gene expression profile of DCs stimulated with *A. fumigatus* under normoxia was compared to the profile of DCs stimulated under hypoxia. The fully annotated list of the genes in this fourth comparison is available on the supplementary data CD (file name "*0.1 % O2 Hypoxia AF vs. Normoxia AF*"). Table 18 lists the top ten up- and down-regulated genes on this list.

Table 18 I Top 10 regulated genes in *A. fumigatus*-stimulated DCs comparing hypoxia (0.1 % O_2) to normoxia.

Gene Symbol	Gene Title	FC *
RGS16	regulator of G-protein signaling 16	-5.83
TSC22D1	TSC22 domain family, member 1	-3.41
HIF1A	hypoxia inducible factor 1, alpha subunit	-3.31
RND3	Rho family GTPase 3	-2.13
SESN2 **	sestrin 2	-2.08
PGM1	phosphoglucomutase 1	5.35
EGLN1	egl nine homolog 1 (C. elegans)	5.76
SLC2A1	solute carrier family 2 (facilitated glucose transporter), member 1	6.02
PFKFB4	6-phosphofructo-2-kinase/fructose-2,6-biphosphatase 4	6.95
PDK1	pyruvate dehydrogenase kinase, isozyme 1	7.22
ANGPTL4	angiopoietin-like 4	9.51
MXI1	MAX interactor 1	11.60
PLOD2	procollagen-lysine, 2-oxoglutarate 5-dioxygenase 2	17.84
C7orf68	chromosome 7 open reading frame 68	20.83
ZNF395	zinc finger protein 395	28.98

* For genes represented by more than one probe set, the one with the highest fold change (FC) is shown.
** Only 5 genes were down-regulated in this comparison.

In a next analysis step, the list of differentially expressed genes under hypoxic conditions without stimulation ("Hypoxia", Table 15) was subtracted from this list (Table 18). The subset of genes that were differentially regulated in *A. fumigatus*-stimulated but not in control DCs was further analyzed (underlined and grey in Figure 20 A). This approach reduced the complexity of the gene expression data sets and allowed to identify relevant genes and pathways that might be influenced by hypoxic conditions specifically in *A. fumigatus*-stimulated DCs.

A pathway analysis of these specific genes was performed (Figure 20 B). No immune-relevant pathways passed the *p*-value criteria in this analysis. However, the pathway analysis revealed hits for several pathways involved in energy generation, including pathways involved in glycolysis (Glycolysis I and Gluconeogenesis I). Most of the genes involved in these pathways were up-regulated in DCs stimulated with *A. fumigatus* under hypoxia compared to normoxia (Figure 20 B, numbers on the right). Therefore, according to the pathway analysis, the major difference when comparing DCs stimulated with *A. fumigatus* under normoxia to hypoxia turned out to be an altered cell metabolism under hypoxic conditions, with an up-regulation of relevant metabolic genes in DCs stimulated with *A. fumigatus* under hypoxia. Interestingly, HIF-1α is known to be involved in regulation of metabolic pathways in many cell types, thus enabling energy generation under conditions of reduced oxygen availability.

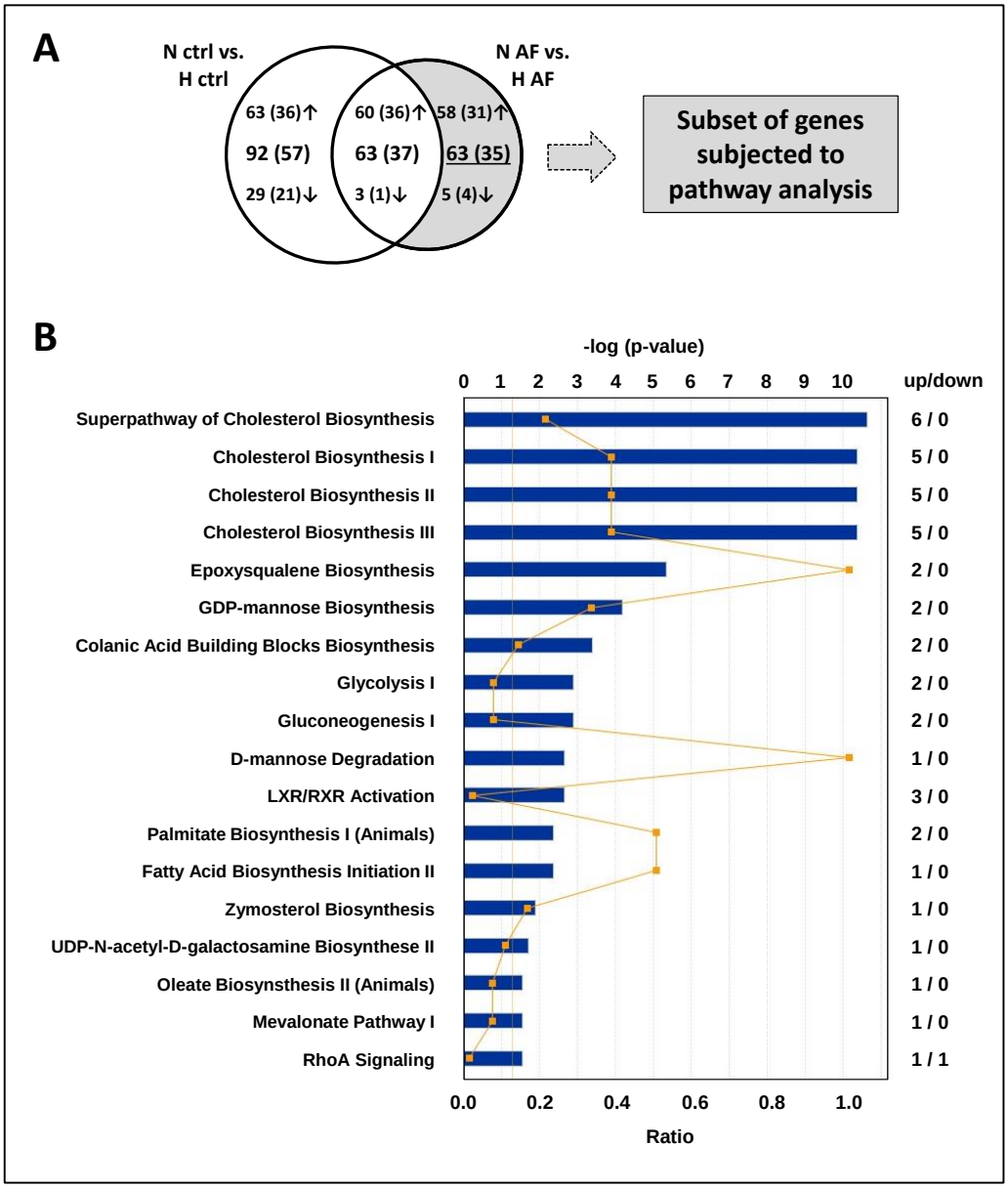

Figure 20 I Pathways specifically involved in DCs stimulated with *A. fumigatus* under 0.1 % O_2.

(A) Gene expression of DCs under hypoxia (0.1 % O_2) was compared to gene expression of DCs under normoxia. The area proportional Venn diagram visualizes the overlap and differences between the two gene lists. Genes that were only regulated in DCs stimulated with *A. fumigatus* under hypoxia were further analyzed (grey and underlined). N, normoxia; H, hypoxia (0.1 % O_2); ctrl, control; AF, *A. fumigatus* (MOI = 1); 6 h stimulation. **(B)** The subset of genes was analyzed using the IPA canonical pathway analysis tool ($p < 0.05$; scoring method: Fisher's Exact Test). All pathways with a –log (*p*-value) > 1.5 are shown. The *p*-value (blue bars) is a measure for the likelihood that the association between the genes in the dataset and the pathway is due to random chance. The ratio (orange squares) is the quotient of the number of genes in the dataset that correspond to one pathway and the total number of genes in the pathway. The numbers on the right indicate how many of the genes corresponding to one pathway were up- or down-regulated in the gene subset.

To sum up the analysis of the 0.1 % O_2 gene expression profiling experiment, the pathway analysis suggested altered metabolism in DCs stimulated with *A. fumigatus* under hypoxic compared to normoxic conditions (Figure 20). Surprisingly, *HIF1A* mRNA was strongly down-regulated under hypoxia (Figure 15, p. 74 and Table 15, p. 78). Nonetheless, pathway and upstream regulator analysis suggested activation of HIF-1α signaling in control DCs under hypoxia as well as in DCs stimulated with *A. fumigatus* under normoxic and hypoxic conditions (Figure 19, p. 81). As a follow-up experiment resulting from the data obtained from this microarray experiment, the DC cell metabolism was further investigated as a potential link between hypoxia, stimulation with *A. fumigatus* and HIF-1α signaling. The results are presented in paragraph 3.2.6, p. 101. Furthermore, analysis of cytokine levels in the supernatants suggested an inhibitory effect of hypoxia on DC cytokine expression and release in response to *A. fumigatus* (Figure 16, p. 76). However, an involvement of cytokine signaling pathways did not become evident from the pathways analysis of the genes specifically regulated in *A. fumigatus*-stimulated DCs under hypoxia (Figure 20).

3.2.3 Gene expression profiles of DCs under moderate hypoxia (1 % O_2)

A second set of experiments for microarray analyses was performed, this time under 1 % O_2. The reason to apply higher oxygen levels was based on a recent publication that demonstrated the presence of hypoxic areas in murine models of invasive pulmonary aspergillosis [93]. In these models, oxygen levels ranged slightly below 1.5 % O_2. This 1 % O_2 microarray gene expression experiment was performed in combination with siRNA based knockdown of *HIF1A* to study the function of HIF-1α signaling in the immune response of DCs against *A. fumigatus*. The confirmatory and validation experiments are described in the HIF-1α section of the results (paragraph 3.3.4, p. 114ff.). The experimental setup was comparable to the 0.1 % O_2 microarrays and is outlined in Figure 38, p. 114. The microarrays and the raw data analysis were again performed in collaboration with the MFT as described in paragraph 3.2.2.1. (p. 73ff.). In the following, the hypoxia-mediated transcriptome will be presented.

Initially, three lists of differentially expressed genes were generated by separately comparing the transcriptome of DCs under hypoxia, of DCs stimulated with *A. fumigatus*

and of DCs stimulated with *A. fumigatus* under hypoxia to control DCs under normoxia. The approach was identical to the one performed for the 0.1 % microarrays (see paragraph 3.2.2.2., p. 77ff.). Fully annotated lists of the genes in these comparisons are available on the supplementary data CD (file names "*1 % O2 Hypoxia*", "*1 % O2 A. fumigatus*" and "*1 % O2 Hypoxia + A. fumigatus*"). Table 19 to Table 21 list the top ten up- and down-regulated genes on these lists.

Table 19 I Top 10 regulated genes on the list "Hypoxia" (1 % O_2 microarrays).

Gene Symbol	Gene Title	FC *
YWHAG	tyrosine 3-monooxygenase/tryptophan 5-monooxygenase activation protein γ	-12.64
DCAF7	DDB1 and CUL4 associated factor 7	-12.34
TLN1	talin 1	-9.51
CCND2	cyclin D2	-8.94
CCDC71	coiled-coil domain containing 71	-8.25
NFAT5	nuclear factor of activated T-cells 5, tonicity-responsive	-7.95
NAA15	N(alpha)-acetyltransferase 15, NatA auxiliary subunit	-7.91
IL6ST	interleukin 6 signal transducer (gp130, oncostatin M receptor)	-7.59
RPS6KA3	ribosomal protein S6 kinase, 90kDa, polypeptide 3	-7.15
HIRA	HIR histone cell cycle regulation defective homolog A (S. cerevisiae)	-7.03
ARRDC3	arrestin domain containing 3	5.04
CD300A	CD300a molecule	5.55
MXI1	MAX interactor 1	5.59
SLC2A1	solute carrier family 2 (facilitated glucose transporter), member 1	5.63
BNIP3	BCL2/adenovirus E1B 19kDa interacting protein 3	6.09
ANGPTL4	angiopoietin-like 4	6.44
SLC2A14/SLC2A3	solute carrier family 2 (facilitated glucose transporter), member 14/solute carrier family 2, member 3	7.34
ADM	adrenomedullin	9.65
DDIT4	DNA-damage-inducible transcript 4	12.10
ZNF395	zinc finger protein 395	14.91

* For genes represented by more than one probe set, the one with the highest fold change (FC) is shown.

Table 20 I Top 10 regulated genes on the list "*A. fumigatus*" (1 % O_2 microarrays).

Gene Symbol	Gene Title	FC *
APOL4	apolipoprotein L, 4	-4.56
CDCA7L	cell division cycle associated 7-like	-4.27
RBMS2	RNA binding motif, single stranded interacting protein 2	-4.27
WNT5B	wingless-type MMTV integration site family, member 5B	-4.22
NFE2	nuclear factor (erythroid-derived 2), 45kDa	-4.18
FOXQ1	forkhead box Q1	-4.08
ADORA3	adenosine A3 receptor	-4.00
NFXL1	nuclear transcription factor, X-box binding-like 1	-3.74
MARCH1	membrane-associated ring finger (C3HC4) 1	-3.53
CTSC	cathepsin C	-3.45

Table 20 (continued) I Top 10 regulated genes on the list "*A. fumigatus*" (1 % O_2 microarrays).

Gene Symbol	Gene Title	FC *
IL1A	interleukin 1, alpha	130.36
MMP10	matrix metallopeptidase 10 (stromelysin 2)	139.46
NR4A2	nuclear receptor subfamily 4, group A, member 2	141.93
CXCL3	chemokine (C-X-C motif) ligand 3	150.00
EGR1	early growth response 1	162.89
IL8	interleukin 8	170.98
CCL20	chemokine (C-C motif) ligand 20	190.00
PTGS2	prostaglandin-endoperoxide synthase 2	198.19
CXCL2	chemokine (C-X-C motif) ligand 2	300.09
IL1B	interleukin 1, beta	348.01

* For genes represented by more than one probe set, the one with the highest fold change (FC) is shown.

Table 21 I Top 10 regulated genes on the list "Hypoxia + *A. fumigatus*" (1 % O_2 microarrays).

Gene Symbol	Gene Title	FC *
DCAF7	DDB1 and CUL4 associated factor 7	-13.37
HIRA	HIR histone cell cycle regulation defective homolog A (S. cerevisiae)	-12.47
TBL1X	transducin (beta)-like 1X-linked	-9.73
YWHAG	tyrosine 3-monooxygenase/tryptophan 5-monooxygenase activation protein γ	-8.56
TLN1	talin 1	-7.23
IL6ST	interleukin 6 signal transducer (gp130, oncostatin M receptor)	-6.81
NAA15	N(alpha)-acetyltransferase 15, NatA auxiliary subunit	-6.77
RPS6KA3	ribosomal protein S6 kinase, 90kDa, polypeptide 3	-6.73
CCND2	cyclin D2	-6.57
NDUFS1	NADH dehydrogenase (ubiquinone) Fe-S protein 1, 75kDa	-6.05
GEM	GTP binding protein overexpressed in skeletal muscle	84.36
CCL3L1/CCL3L3	chemokine (C-C motif) ligand 3-like 1/chemokine (C-C motif) ligand 3-like 3	90.18
INHBA	inhibin, beta A	131.06
NR4A2	nuclear receptor subfamily 4, group A, member 2	132.28
EGR1	early growth response 1	156.33
PTGS2	prostaglandin-endoperoxide synthase 2	158.24
CCL20	chemokine (C-C motif) ligand 20	171.31
IL8	interleukin 8	176.12
CXCL2	chemokine (C-X-C motif) ligand 2	243.72
IL1B	interleukin 1, beta	250.02

* For genes represented by more than one probe set, the one with the highest fold change (FC) is shown.

Figure 21 visualizes the overlap and differences in the lists of differentially expressed genes in the format of Venn diagrams. Hypoxia itself had less influence on the transcriptome of DCs compared to stimulation with *A. fumigatus* under normoxia or hypoxia. Compared to the 0.1 % O_2 microarrays (Figure 18, p. 80), the influence of hypoxia was greater in the 1 % O_2 microarrays. Similar to the 0.1 % O_2 microarrays, the gene expression profiles of DCs stimulated with *A. fumigatus* under hypoxia or normoxia overlapped to some extent and there were also genes that appeared exclusively in one of the two conditions.

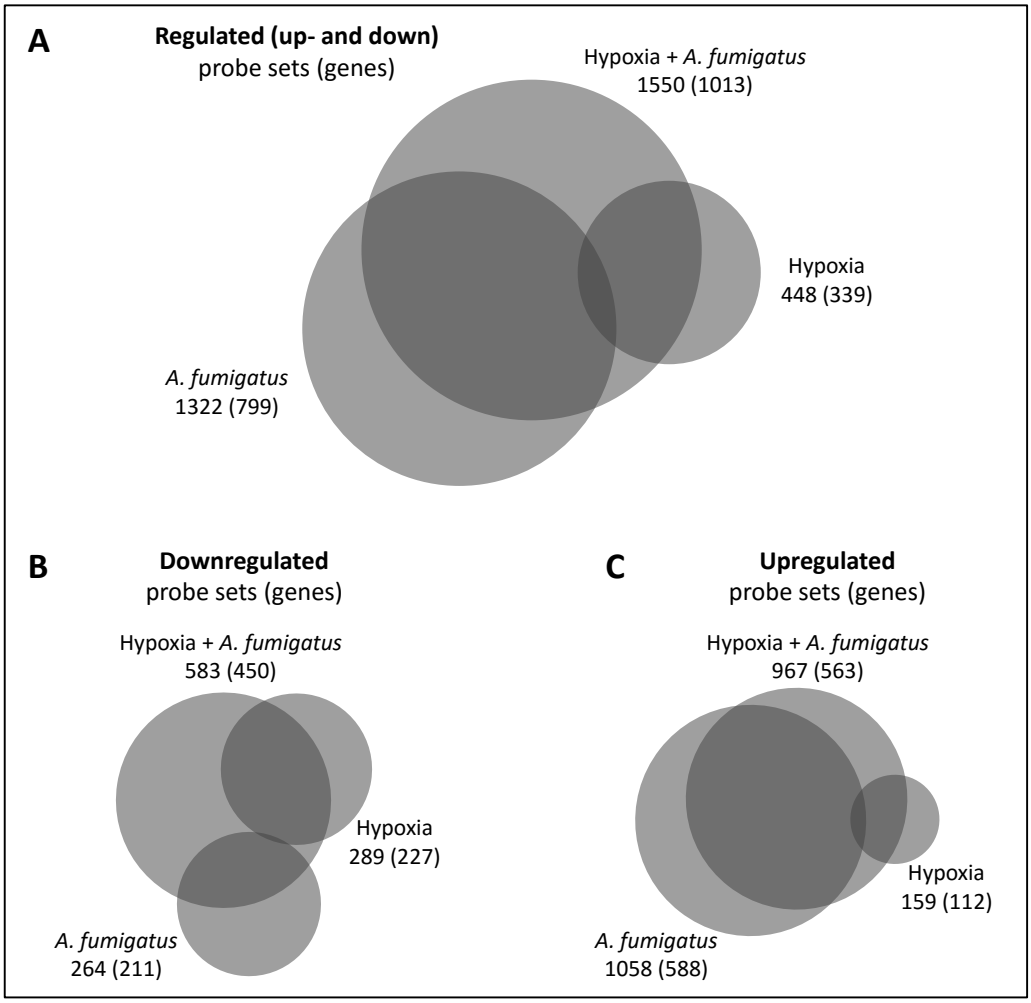

Figure 21 I Overlaps between the lists of differentially expressed genes (1 % O_2 microarrays).

Venn diagrams visualize the overlap and differences between the lists of differentially regulated genes. Probe sets (with each probe set corresponding to a specific gene) were considered differentially regulated with a *p*-value < 0.05 and a fold change > 2. One gene can be represented by more than one probe set. Each circle corresponds to one of the three comparisons, and the overlaps between the circles correspond to the overlaps between the data sets. The Venn diagrams are area-proportional, i.e. the sizes of the circles and the overlaps correspond to the number of differentially regulated genes. Numbers indicate the total number of **(A)** all, **(B)** down- and **(C)** up-regulated probe sets (genes) on the respective lists.

To specifically determine the influence of hypoxia (1 % O_2) on the transcriptome of DCs stimulated with *A. fumigatus*, the normoxic and hypoxic gene expression profiles of *A. fumigatus*-stimulated DCs were directly compared. The fully annotated list of the genes in this comparison is available on the supplementary data CD (file name "*1 % O2 Hypoxia AF vs. Normoxia AF*"). Table 22 lists the top ten up- and down-regulated genes on this list.

Table 22 I Top 10 regulated genes in *A. fumigatus*-stimulated DCs comparing hypoxia (1 % O_2) to normoxia.

Gene Symbol	Gene Title	FC *
HIRA	HIR histone cell cycle regulation defective homolog A (S. cerevisiae)	-7.85
NFAT5	nuclear factor of activated T-cells 5, tonicity-responsive	-7.52
DCAF7	DDB1 and CUL4 associated factor 7	-7.50
YWHAG	tyrosine 3-monooxygenase/tryptophan 5-monooxygenase activation protein, γ	-7.29
IL6ST	interleukin 6 signal transducer (gp130, oncostatin M receptor)	-6.86
RPS6KA3	ribosomal protein S6 kinase, 90kDa, polypeptide 3	-6.67
NAA15	N(alpha)-acetyltransferase 15, NatA auxiliary subunit	-6.59
EPC1	enhancer of polycomb homolog 1 (Drosophila)	-6.23
CCND2	cyclin D2	-6.00
RAD23B	RAD23 homolog B (S. cerevisiae)	-5.82
ANKRD37	ankyrin repeat domain 37	5.32
DDIT4	DNA-damage-inducible transcript 4	5.43
MXI1	MAX interactor 1	5.54
KDM3A	lysine (K)-specific demethylase 3A	5.63
SLC2A1	solute carrier family 2 (facilitated glucose transporter), member 1	5.67
BNIP3	BCL2/adenovirus E1B 19kDa interacting protein 3	6.37
EGLN3	egl nine homolog 3 (C. elegans)	6.97
EGLN1	egl nine homolog 1 (C. elegans)	7.51
C7orf68	chromosome 7 open reading frame 68	8.44
ZNF395	zinc finger protein 395	11.47

* For genes represented by more than one probe set, the one with the highest fold change (FC) is shown.

In a next analysis step, the list of differentially expressed genes under hypoxic conditions without stimulation ("Hypoxia", Table 19) was subtracted from this list. The subset of genes that were differentially regulated in *A. fumigatus*-stimulated but not in control DCs was further analyzed (underlined and grey in Figure 22 A). This was the same approach as for the 0.1 % O_2 microarrays. In contrast to the 0.1 % O_2 microarray data (Figure 20, p. 83), this subset contained several genes encoding immune-relevant mediators, most of which were down-regulated.

Selected genes were displayed in a network analysis (Figure 22 B). This network analysis was performed with *CLEC7A* as the manually set up-stream receptor. *CLEC7A* encodes Dectin-1, the major receptor for *A. fumigatus* on DCs. An analysis of the possible connections between Dectin-1 and the regulated genes in the *A. fumigatus* specific subset revealed TNF and IL-6 as possible mediators in between. Downstream signaling of Dectin-1 can induce release of the pro-inflammatory cytokines IL-6 and TNF. Genes positively regulated by IL-6 and/or TNF signaling were down-regulated in the *A. fumigatus* specific subset (Figure 22 B). This indicated reduced IL-6/TNF signaling in *A. fumigatus*-stimulated DCs comparing normoxia to hypoxia.

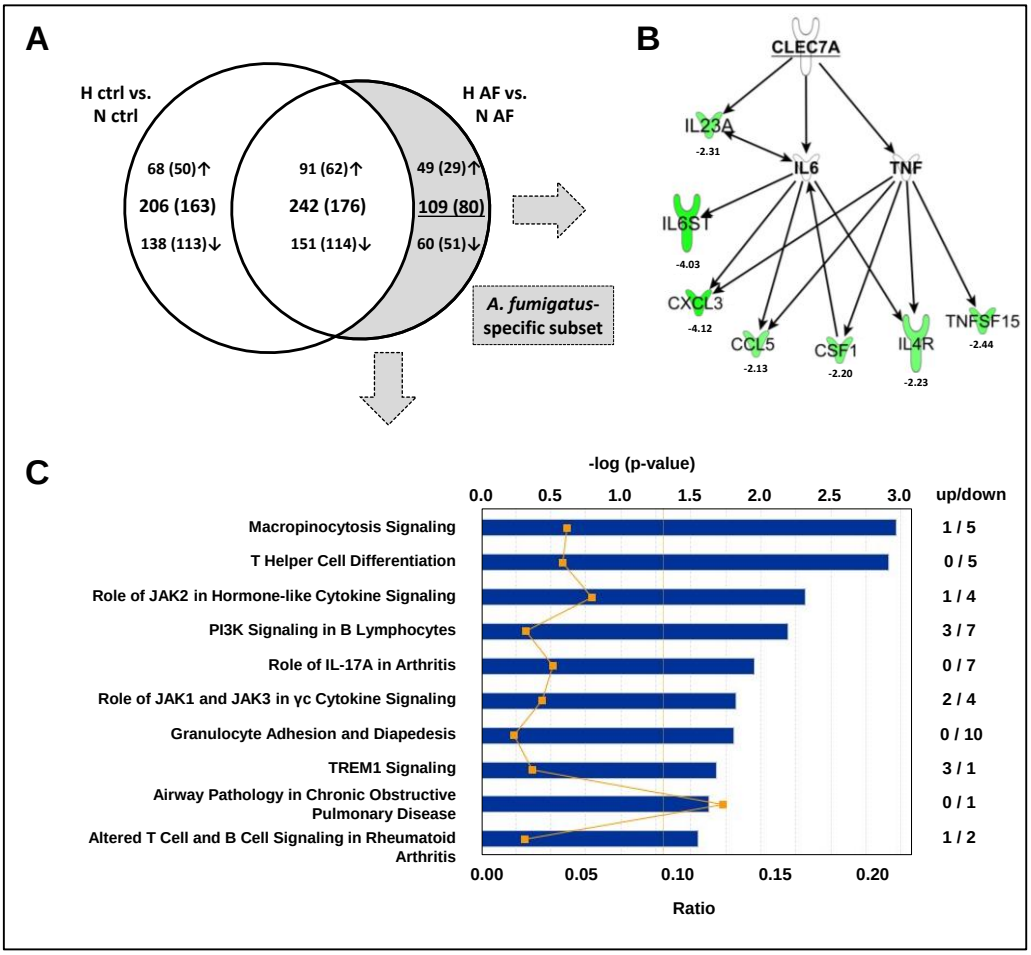

Figure 22 I Network and pathway analysis with genes specifically regulated in *A. fumigatus*-stimulated DCs comparing hypoxia (1 % O_2) to normoxia.

(A) Gene expression of DCs under hypoxia (1 % O_2) was compared to gene expression of DCs under normoxia. The area proportional Venn diagram visualizes the overlap and differences between the two lists. Genes that were only regulated in DCs stimulated with *A. fumigatus* under hypoxia were further analyzed (grey and underlined). N, normoxia; H, hypoxia (1 % O_2); ctrl, control; AF, *A. fumigatus* (MOI = 1). **(B)** Shows a Dectin-1 (CLEC7A) gene network analysis with selected genes from the *A. fumigatus*-specific subset. Fold changes are depicted below the molecule symbols. Green, gene is down-regulated in the subset; white, gene is not regulated in the subset. **(C)** The genes in the *A. fumigatus*-specific subset were analyzed using the IPA canonical pathway analysis tool (scoring method: Fisher's Exact Test, $p < 0.05$). All pathways with a -log (*p*-value) > 1.5 are shown. The *p*-value (blue bars) is a measure for the likelihood that the association between the genes in the dataset and the pathway is due to random chance. The ratio (orange squares) is the quotient of the number of genes in the dataset that correspond to one pathway and the total number of genes in the pathway. The numbers on the right indicate how many of the genes corresponding to one pathway were up- or down-regulated in the *A. fumigatus* specific subset.

In addition to the network analysis, a pathway analysis was performed and revealed hits for several aspects of the immune response (Figure 22 C). Again, most of the genes involved in these pathways were down-regulated under hypoxic conditions. Interestingly, two of the pathways were JAK signaling pathways: "Role of JAK2 in Hormone-like

Cytokine Signaling" and "Role of JAK1 and JAK3 in γc Cytokine Signaling". JAK kinases are tyrosine kinases that transduce cytokine-mediated signals via the JAK-STAT pathway and are initiated upon cell stimulation. In summary, the pathway analysis indicated a difference in the immune-relevant signaling pathways that are induced in DCs upon *A. fumigatus* stimulation under normoxic compared to hypoxic conditions.

To further specify the results from the network and pathway analyses, upstream regulator analysis was performed to predict molecules that could be responsible for the gene expression changes observed in the *A. fumigatus*-specific subset (Figure 22 A). Among the predicted upstream regulators were mostly transcription factors, including immune-relevant signal transduction molecules such as NFKBIA, STAT3, STAT6 and NFKB1 (Table 23). In addition, molecules involved in hypoxia-mediated signaling were also predicted as possible mediators for the observed gene expression levels, including HIF1A itself as well as EPAS1 (encoding HIF-2α). The upstream regulator analysis also predicts an activation z-score. If the numerical value of this score is > 2, the software predicts the respective upstream regulator to be activated or inhibited, respectively. In this case, one upstream regulator passed this criteria: STAT3 (highlighted in green in Table 23).

Table 23 I Upstream regulators enriched in DCs stimulated with *A. fumigatus* in the comparison of hypoxic (1 % O_2) to normoxic conditions.

Upstream Regulator	Description	Type	z-score	-log (*p*-value)
NFKBIA	Nuclear factor of κ light polypeptide gene enhancer in B-cells inhibitor, α	TR	-0.84	7.97
STAT3	Signal transducer and activator of transcription 3	TR	-2.78	6.82
EPAS1	Endothelial PAS domain protein 1	TR	-0.62	6.38
JUN	Jun proto-oncogene	TR	-0.92	5.04
AHR	Aryl hydrocarbon receptor	L-D NR	-0.71	4.77
HIF1A	Hypoxia inducible factor 1α	TR	-0.15	4.51
RELA	V-rel avian reticuloendotheliosis viral oncogene homolog A	TR	-1.96	4.48
ATF6B	Activating transcription factor 6 beta	TR		4.39
SP1	Sp1 transcription factor	TR	1.20	4.31
HLX	H2.0-like homeobox	TR		4.14
RUNX1	Runt-related transcription factor 1	TR		3.89
SMAD1	SMAD family member 1	TR		3.87
STAT6	Signal transducer and activator of transcription 6	TR	-1.93	3.77
NFKB1	Nuclear factor of kappa light polypeptide gene enhancer in B-cells 1	TR		3.61
YAP1	Yes-associated protein 1	TR		3.49

The 15 most significant upstream regulators are shown. Green enhancement, upstream regulator is predicted to be inhibited. Activation z-score, prediction for the activation state of the upstream regulator; overlap *p*-value, measure for a statistically significant overlap between the dataset genes and known targets of the upstream regulator; TR, transcription regulator; L-D NR, ligand-dependent nuclear receptor.

In a next step, a regulator effects analysis was performed with the genes in the *A. fumigatus*-specific subset (Figure 22 A, p. 89). This IPA analytic helps to determine how predicted activated or inhibited upstream regulators might cause increases or decreases in downstream functions. In the present case, STAT3 was predicted to be a relevant regulator for the gene expression observed in the dataset (Figure 23). The regulator effects network is build up on three levels. STAT3 is on top as the upstream regulator and functions and phenotypes predicted by the software are at the bottom. In the middle, there are the genes from the dataset that connect to STAT3 as the regulator above and that are predicted to carry the STAT3 signal to induce the downstream outcomes. In line with the large number of down-regulated immune relevant genes in the dataset (Figure 22), many functions that are induced upon DC activation were predicted to be inhibited in DCs stimulated under hypoxic compared to DCs stimulated under normoxic conditions.

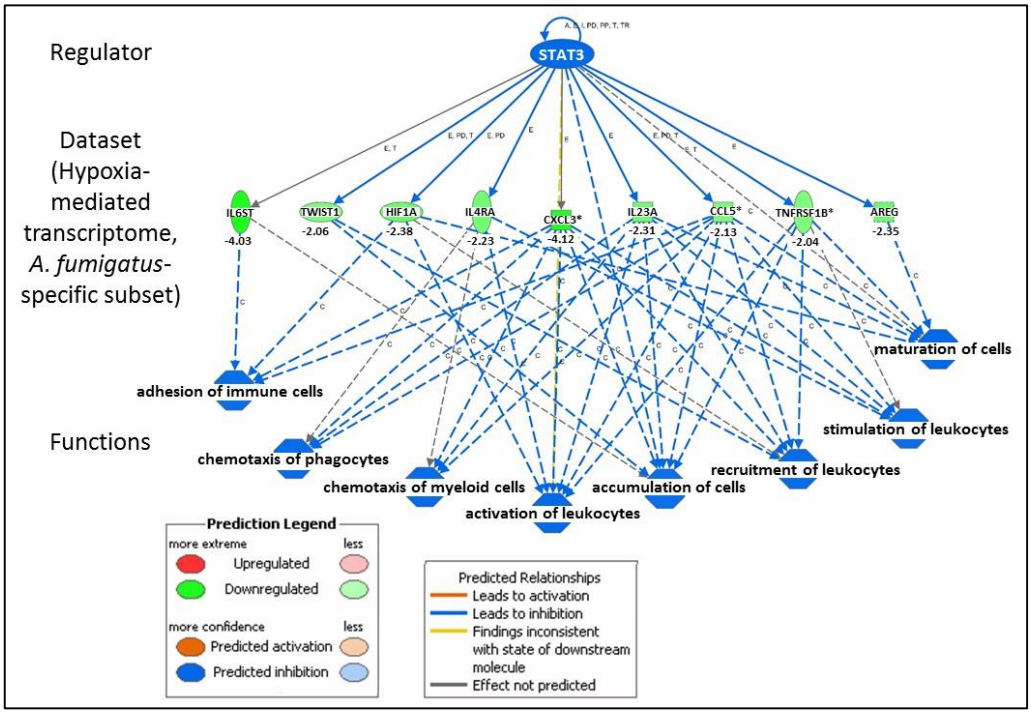

Figure 23 I Possible regulator effects in *A. fumigatus*-stimulated DCs comparing hypoxia (1 % O_2) to normoxia.

Regulators effects analytic was performed with the genes in the *A. fumigatus*-specific subset using IPA. Diseases were excluded from the list of possible downstream outcomes. Scoring method: Fisher's Exact Test, $p < 0.05$, z-score > 2 (regarding the overlap between the regulator and the function dataset molecules).

STAT3 is involved as a transcription factor upon immune cell stimulation and is activated by IL-6. STAT3 in turn activates the JAK/STAT signaling pathway [147]. IL-6 already appeared in the network analysis as a possible mediator between Dectin-1 and a number of down-regulated genes in the dataset (Figure 22 B). In addition, JAK signaling pathways were predicted by the IPA pathway analysis (Figure 22 C). Taken the network (Figure 22 B), the pathway (Figure 22 C), the upstream regulators (Table 23) and the regulator effects (Figure 23) analyses into account, these results suggested altered STAT3 signaling in DCs stimulated with *A. fumigatus* under hypoxic compared to normoxic conditions.

Taken together, the 1 % O_2 microarray data analysis revealed an inhibitory effect of hypoxia on the response of human DCs towards *A. fumigatus* compared to their normoxic counterparts. To confirm this conclusion, DC activation and function under hypoxia were further analyzed and compared to normoxia. This included a cytokine profiling and analysis of maturation marker expression after stimulation under normoxic and hypoxic conditions. Furthermore, the metabolic activity of DCs was investigated, as this function was predicted have been involved in the analysis of the first (0.1 % O_2) microarray experiment. The differences in the data analysis comparing the two sets of microarray experiments (0.1 % vs. 1 % O_2) will be discussed in paragraph 4.1.1. (p. 136ff.).

3.2.4 Influence of hypoxia (1 % O_2) on DC cytokine release

To investigate possible effects of hypoxia on the cytokine release from DCs stimulated with *A. fumigatus*, the cytokines in the cell culture supernatant from the 1 % O_2 microarray samples were analyzed (the cytokine analysis for the 0.1 % O_2 microarrays is shown in Figure 16, p. 76). Cytokines were quantified by a commercially available 27-plex immunoassay. Levels of 24 analytes are displayed in Figure 24. IL-4, IL-5 and IL-15 were excluded from the figure (data not shown). Concentrations of IL-4 in all analyzed samples were so high that the values were out of range of the standard curve, most likely due to the presence of IL-4 in the cell culture media. Although GM-CSF (CSF2) was also present in the culture media, it could be quantified by the assay. Levels of GM-CSF were approximately the same in all samples (Figure 24). IL-5 and IL-15 were excluded because their levels were below 5 pg/ml in all samples analyzed.

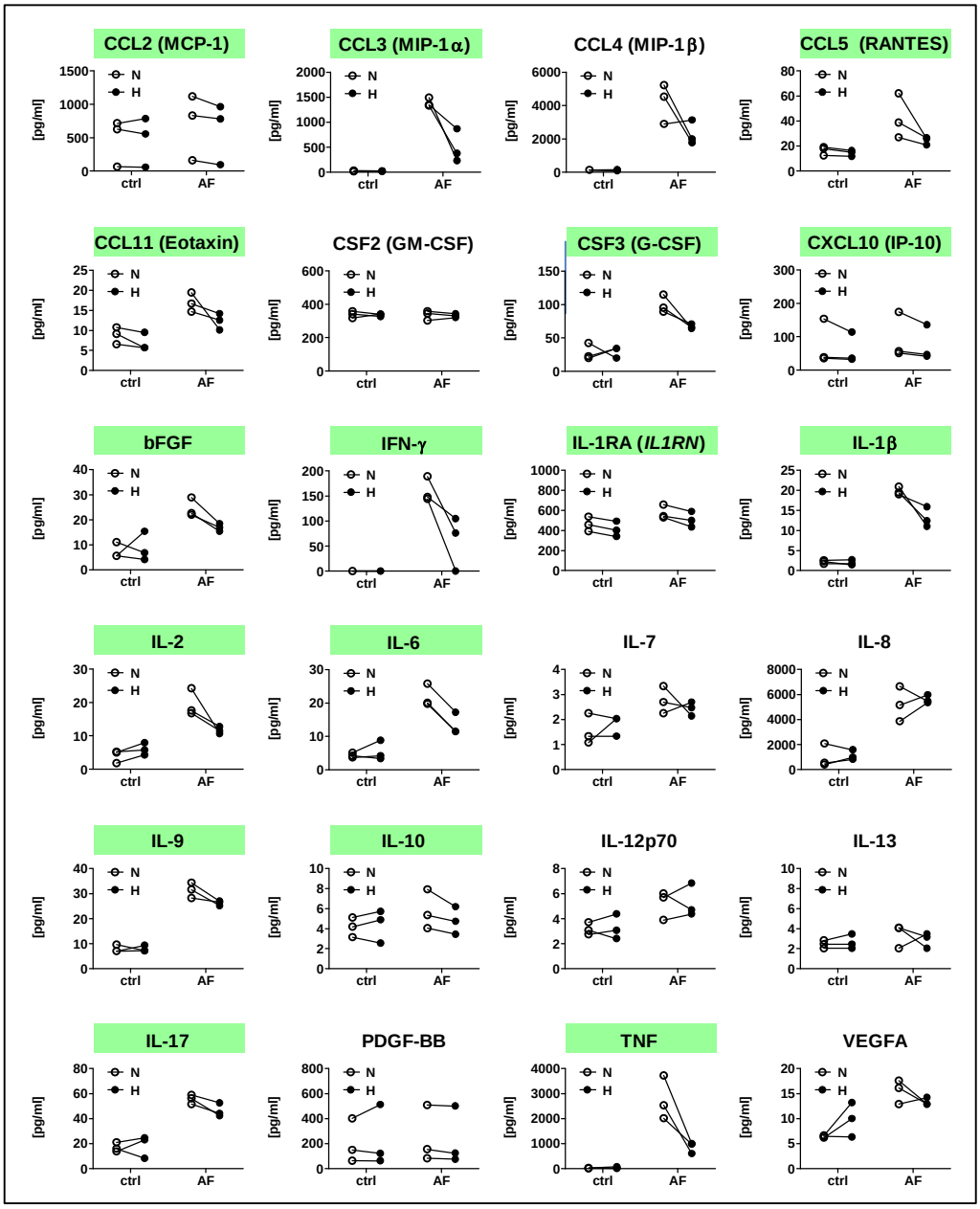

Figure 24 I Quantification of cytokines in the supernatants of the 1 % O_2 microarray samples.

Cytokines were quantified using a 27-plex immunoassay and are shown in pg/ml. Trends towards reduced release of one specific cytokine comparing hypoxic to normoxic DCs stimulated for 6 h with *A. fumigatus* are depicted in green. N, normoxia; H, hypoxia (1 % O_2); ctrl, control; AF, *A. fumigatus* (MOI = 1); n = 3.

Stimulation with *A. fumigatus* induced the release of several pro-inflammatory cytokines under normoxic as well as hypoxic conditions, including the chemokines CCL3, CCL4 and CCL5, the interleukins IL-1β, IL-6, IL-8, IL-9 and IL-17, and TNF (Figure 24). Comparing supernatants from DCs stimulated with *A. fumigatus* under normoxia to those stimulated under hypoxia, regulation trends were defined if at least two replicates

showed increased or reduced levels for a specific analyte under hypoxia while the third replicate did not show the opposite trend. Levels of a range of cytokines, including chemokines (CCL2, CCL3, CCL5 and CCL11), interleukins (IL-1β, IL-2, IL-6, IL-9, IL-10 and IL-17) and other cytokines (CSF3, CXCL10, bFGF, IFN-γ, IL1-RA and TNF) showed a trend towards reduced concentrations in the supernatants from DCs stimulated with *A. fumigatus* under hypoxia compared to normoxia (depicted in green in Figure 24). Whereas transcript expression of *IL6* and *TNF* did not differ between DCs stimulated with *A. fumigatus* under hypoxia compared to normoxia (Figure 22 B, p. 89), the release of IL-6 and TNF was decreased under oxygen limitation. Importantly, IL-6 as well as TNF appeared in the gene expression network as regulators that might be responsible for the reduced expression of several immune-relevant genes in DCs stimulated with *A. fumigatus* under hypoxia (Figure 22 B). Therefore, the cytokine profile confirmed a possible involvement of these mediators in the observed gene regulation and demonstrated that hypoxia reduced the release of pro-inflammatory cytokines from DCs stimulated with *A. fumigatus*.

As a next step, a cytokine time-course profiling was performed after 3, 6, 9 and 12 h stimulation of DCs with *A. fumigatus* under normoxia or hypoxia. Again, cytokines were quantified using a commercially available 27-plex assay. IL-4, IL-5 and IL-7 were excluded from the analysis (IL-4 due to its presence in the culture media, levels of IL-5 and IL-7 were below the limit of detection). Levels of cytokines in the supernatant of unstimulated control DCs were only measured after 12 h incubation under normoxia or hypoxia. These cytokine levels were below 20 pg/ml or did not differ comparing normoxic and hypoxic culture conditions (data not shown). This demonstrates that hypoxia alone did not influence cytokine release from unstimulated (immature) control DCs over a time course of 12 h. Figure 25 shows the levels of 24 cytokines after stimulation with *A. fumigatus*. The levels of almost all of the cytokines increased over the time in the supernatants from DCs stimulated with *A. fumigatus* under normoxia as well as hypoxia. However, levels of some cytokines in the hypoxia samples were constantly lower compared to normoxia. This effect was significant for CCL5, CSF2, IL-10, IL-12p70 and TNF after 12 h stimulation. Thus, the cytokine time-course profiling confirmed the trend to reduced release of some (but not all) inflammation-associated cytokines from DCs stimulated with *A. fumigatus* under hypoxia compared to normoxia.

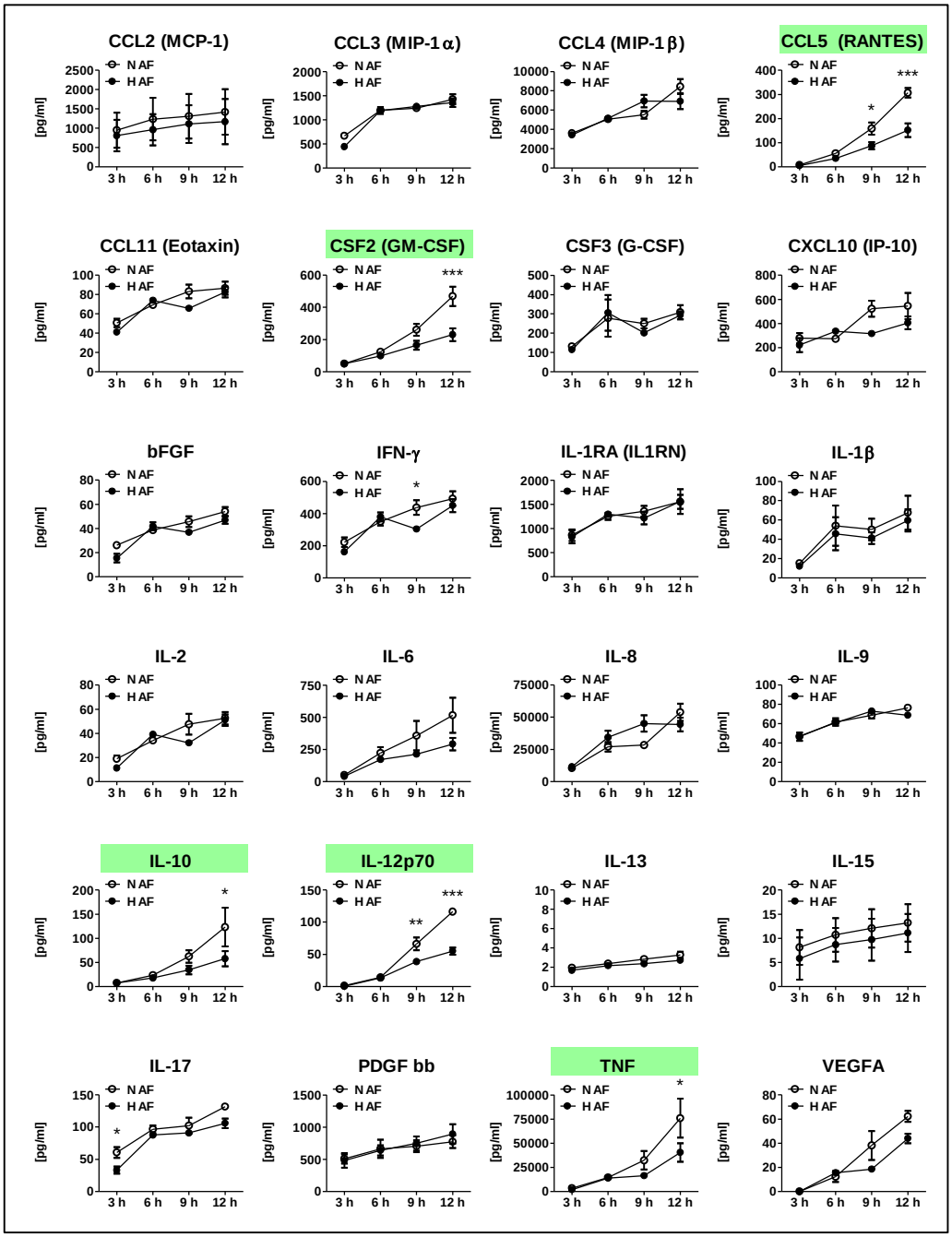

Figure 25 I Time-course cytokine profiling of DCs stimulated with *A. fumigatus* under 1 % O_2.

DCs were stimulated with *A. fumigatus* (AF, MOI = 1) and incubated under normoxia (N, white circles) or hypoxia (H, 1 % O_2, black circles) for 3, 6, 9 and 12 h. Cytokine concentrations in the cell culture supernatants were quantified using a 27-plex immunoassay and are shown in pg/ml. Data is shown as mean + SEM from n = 3 independent experiments. Significant differences comparing normoxia to hypoxia at the respective time are indicated by asterisks (* $p < 0.05$; ** $p < 0.01$; *** $p < 0.001$; two-way repeated measures ANOVA followed by Bonferroni's multiple comparison test).

Taken together, the microarray transcriptome analysis of DCs that were stimulated with *A. fumigatus* under moderate hypoxia (1 % O_2) suggested an inhibitory effect of oxygen limitation on the pro-inflammatory response shortly (6 h) after pathogen contact. The inhibitory effect of hypoxia could be confirmed with the levels of cytokines released from DCs stimulated with *A. fumigatus* (Figure 24). A time-course cytokine profiling over 3, 6, 9 and 12 h confirmed a significantly reduced release of some central pro-inflammatory mediators, including CCL5, IL-10, IL-12p70 and TNF under hypoxic conditions (Figure 25). Although the microarray transcriptome analysis under strong hypoxic conditions (0.1 % O_2) did not reveal immune-relevant mechanisms, levels of several cytokines in the supernatant from DCs stimulated with *A. fumigatus* under 0.1 % O_2 were reduced compared to normoxia (Figure 16, p. 76). Noteworthy, the regulators effects analytic (1 % O_2 microarrays, Figure 23, p. 91) predicted the functions “maturation of cells”, “chemotaxis of myeloid cells” and “stimulation of leukocytes” to be inhibited in DCs stimulated with *A. fumigatus* under hypoxia (Figure 23, p. 91). These are all functions that are relevant for the stimulation of T cells. In the following, the influence of hypoxia on DC functions was further analyzed with a focus on the ability of DCs to activate T cells.

3.2.5 Effects of hypoxia on T cell related DC functions

3.2.5.1 Maturation of DCs under hypoxia

To further explore the possible inhibitory effect of hypoxia on DCs responding to *A. fumigatus* (besides the expression and release of cytokines), the surface expression of several molecules that are typically up-regulated on mature DCs was evaluated using flow cytometry. DCs were stimulated with either zymosan, LPS or *A. fumigatus* under 0.1 % O_2 or 1 % O_2 for 24 h and compared to their normoxic counterparts. The influence of hypoxia on the maturation of DCs was measured through monitoring the surface expression of CCR7, a receptor required for migration of DCs to the lymph nodes [148], of the MHC class II molecule HLA-DR that presents exogenous antigens to T cells, of CD40, CD80 and CD86 as T cell co-stimulatory molecules and of CD83, a marker for mature DCs.

No differences in surface expression of these molecules were observed for unstimulated control DCs (Figure 26). This demonstrated that hypoxia alone did not alter the maturation status of DCs. Stimulation with zymosan, LPS or *A. fumigatus* for 24 h under normoxic and hypoxic conditions enhanced the expression of these molecules on the cell surface, indicating that DC maturation was induced. However, all markers showed significantly reduced levels on DCs stimulated with *A. fumigatus* under hypoxia (0.1 % or 1 % O_2) compared to normoxia. These differences also occurred after stimulation with zymosan or LPS. This experiment revealed an inhibitory effect of hypoxia on the up-regulation of maturation markers on the surface of DCs that undergo maturation upon stimulation with *A. fumigatus*. When comparing strong and moderate hypoxic conditions, the inhibitory effect proved to be similar and occurred under both conditions.

ICAM-1 is an intercellular adhesion molecule that is typically up-regulated on mature DCs and besides other functions, it is involved in cell migration. ICAM-1 was up-regulated on stimulated DCs, however, this up-regulation was significantly lower comparing *A. fumigatus*-stimulated DCs under hypoxia (1 % O_2) to normoxia. This confirmed the inhibitory effect of hypoxic culture conditions DC maturation. Importantly, no significant differences in surface expression of Dectin-1 on DCs after stimulation with *A. fumigatus* under normoxia or hypoxia were observed (Figure 26 B). Therefore, it can be concluded that differences comparing the response of DCs under normoxia and hypoxia are not due to an altered expression of the PRR that recognizes *A. fumigatus*.

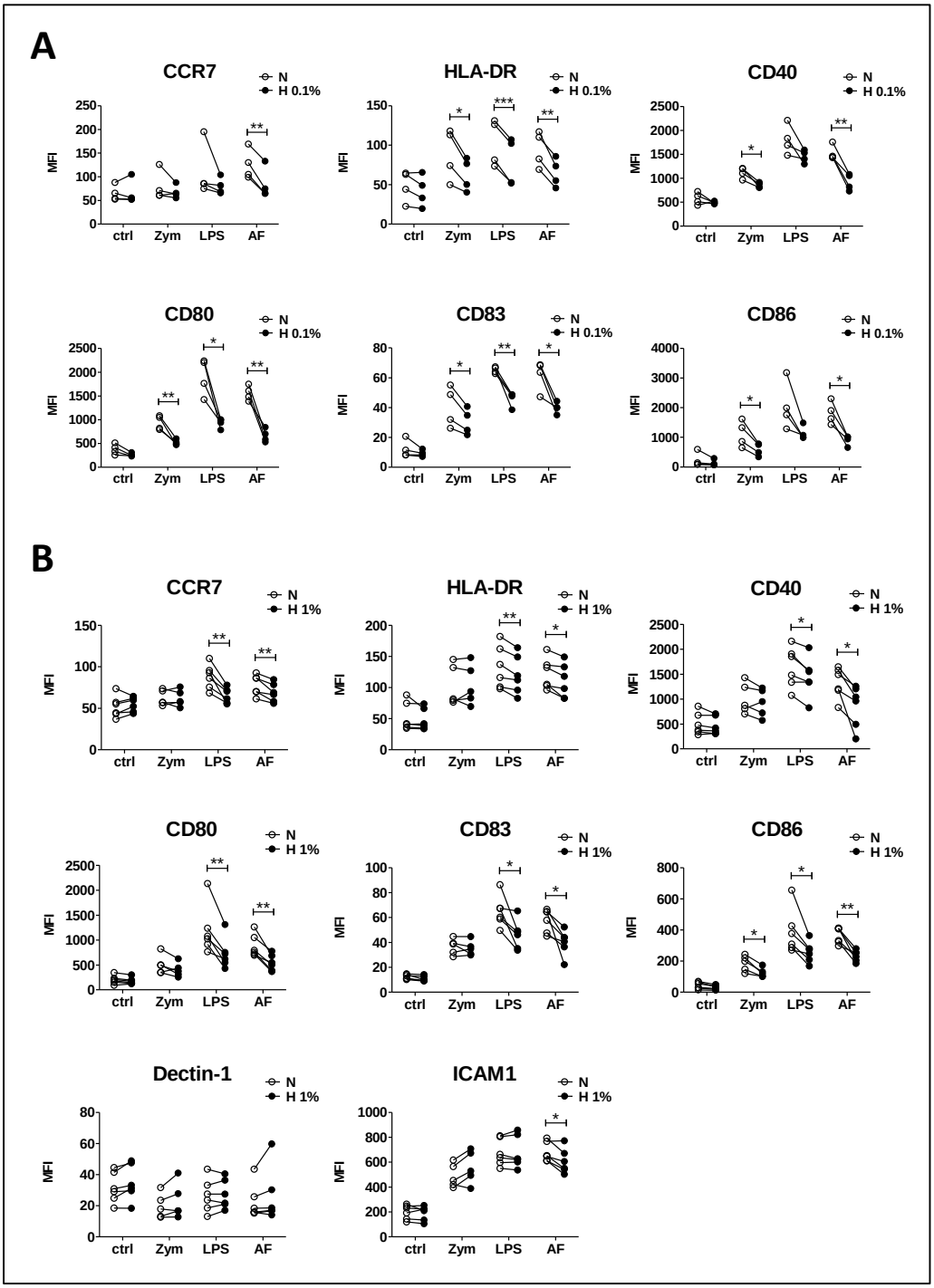

Figure 26 I DCs stimulated under hypoxia show impaired up-regulation of maturation-associated cell surface molecules.

DCs were stimulated with zymosan (Zym, 10 µg/ml), LPS (1 µg/ml) or *A. fumigatus* (AF, MOI = 1) or not stimulated (ctrl) and incubated under normoxia (N) or hypoxia (H, **(A)** 0.1 % O_2 or **(B)** 1 % O_2) for 24 h. Flow cytometry graphs show **(A+B)** CCR7, HLA-DR, CD40, CD80, CD83 and CD86 and **(B)** Dectin-1 and ICAM1 expression on the surface of DCs. Data are the mean fluorescence intensity (MFI) of n = 4 **(A)** and n = 6 **(B)** independent experiments. Significant differences comparing normoxia to hypoxia are indicated by asterisks (* $p < 0.05$; ** $p < 0.01$; *** $p < 0.001$; two-tailed, paired *t*-test).

3.2.5.2 T cell stimulatory capacity of DCs matured under hypoxia

Next, the T cell stimulatory capacity of DCs matured by *A. fumigatus* under either normoxic or hypoxic (1 % O_2) conditions was examined. Therefore, DCs that had been matured for 24 h (as displayed in Figure 26 B) were co-incubated with allogeneic T cells for three additional days, which leads to the production and release of IFN-γ from the T cells as an indicator of T cell activity (Figure 27). The T cell activation assay was performed under normoxic conditions. This protocol was adapted from similar studies which analyzed the T cell stimulatory functions of DCs that had been matured by LPS treatment under normoxic and hypoxic conditions [134, 137].

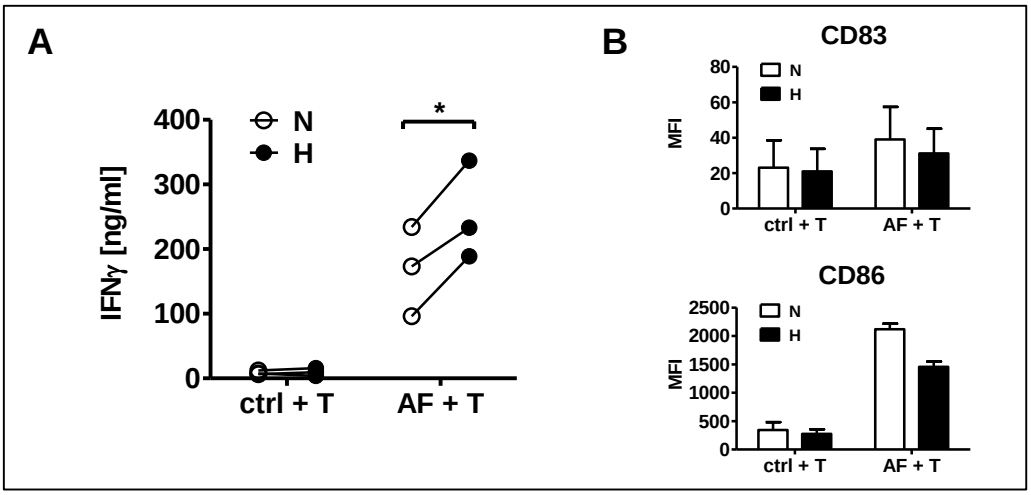

Figure 27 I DCs matured through *A. fumigatus* under hypoxia possess an enhanced T cell stimulatory capacity.

DCs were stimulated with *A. fumigatus* (AF, MOI = 1) or not stimulated (ctrl) and incubated under normoxia (N, white circles) or hypoxia (H, black circles, 1 % O_2) for 24 h. Subsequently, DCs were γ-irradiated and co-cultured for three additional days with allogeneic T cells (T) under normoxia (DC to T cell ratio 1:9). **(A)** IFN-γ concentrations in co-culture supernatants of this T cell activation assay were determined by ELISA and are shown in ng/ml. Data points represent mean values from two biological replicates per condition. Three independent experiments with cells from different blood donors were performed. Significant difference is indicated by an asterisk (* $p < 0.05$; two-tailed, paired *t*-test). **(B)** Flow cytometry graphs show CD80 and CD83 expression on the surface of DCs after three days co-culture with T cells. Data are shown as mean + SD of the geometric mean fluorescence intensity (MFI) of two independent experiments.

IFN-γ was not detectable in the supernatants of T cells and DCs that had been cultured separately (data not shown). Compared to co-culture with immature control DCs, IFN-γ concentrations markedly increased in co-culture supernatants of T cells and DCs matured through stimulation with *A. fumigatus* (Figure 27 A). Surprisingly, IFN-γ concentrations were significantly higher in co-culture supernatants of T cells with DCs

matured under hypoxic compared to DCs matured under normoxic conditions (Figure 27 A). These data demonstrate that DCs matured through exposure to *A. fumigatus* under hypoxic conditions possessed an enhanced capacity to stimulate allogeneic T cells, despite the reduced expression of T cell co-stimulatory molecules on these DCs (Figure 26 B). Nonetheless, the difference in the expression of maturation-associated molecules on the DC surface persisted over the three days co-culture with T cells, as exemplarily shown for CD83 and CD86 in Figure 27 B.

To sum this up, while hypoxia impaired *A. fumigatus*-induced DC maturation on the level of surface marker expression, hypoxia simultaneously enhanced the ability of these DCs to stimulate allogeneic T cells in a T cell activation assay performed under normoxic conditions.

3.2.6 Glycolytic activity in DCs under hypoxia

The 0.1 % O_2 microarray pathway analysis suggested involvement of metabolic pathways in *A. fumigatus*-stimulated DCs under hypoxia (Figure 20, p. 83). To validate this prediction, DC cell metabolism was evaluated by measuring glucose and lactate levels in the cell culture supernatants as indicators of glycolytic activity (Figure 28). Glycolysis requires glucose and fermentation of the by-products of glycolysis produces lactate.

Hypoxia (0.1 % and 1 % O_2) led to significant glucose consumption and lactate accumulation in cell culture supernatants from both control and LPS- or *A. fumigatus*-stimulated DCs after 24 h (Figure 28, white bars vs. grey bars). In the supernatants of DCs stimulated with LPS or *A. fumigatus* under normoxia, there was a significant decrease of glucose and increase of lactate compared to the control DCs under normoxia (white bars). This indicated that DCs enhanced glycolysis not only in the context of reduced oxygen availability, but also during stimulation under normoxic conditions.

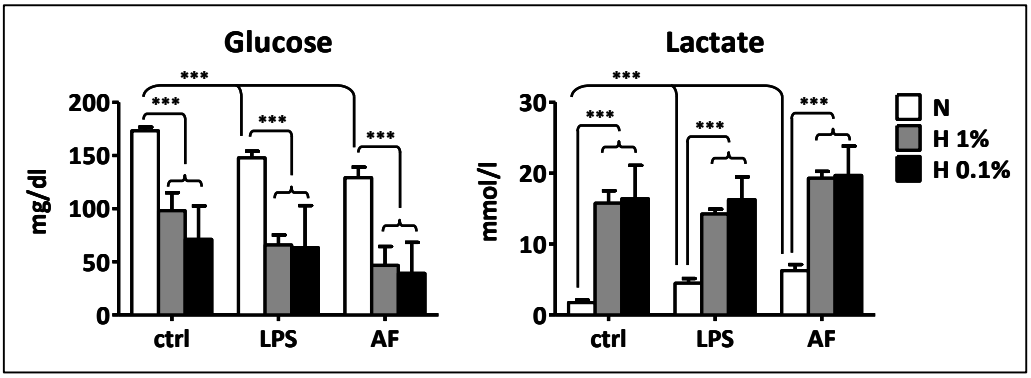

Figure 28 I DCs enhance glycolysis under stimulation in the presence or absence of hypoxia.

DCs were stimulated with LPS (1 µg/ml) or *A. fumigatus* (AF, MOI=1) or were not stimulated (ctrl) and cultivated under normoxia (N) or hypoxia (H, 1 % or 0.1 % O_2). Glucose and lactate concentrations in DC supernatants were quantified after 24 h. The experiment was repeated three times separately under 0.1 % O_2 and 1 % O_2, respectively. Data for cultivation under normoxia was summarized. Data are displayed as mean + SD. Significant differences are indicated by asterisks (*** $p < 0.001$; two-tailed, paired *t*-test).

Taken together, while hypoxia did not influence DC viability to a significant degree, the transcriptome analyses and the follow-up experiments including cytokine quantification in the supernatants, indicated that hypoxia diminished the initial (6 h) pro-inflammatory response against *A. fumigatus*. This inhibitory effect could be confirmed over the time by a cytokine time-course profiling (3, 6, 9, 12 h). A possible mediator involved in the anti-*A. fumigatus* response of DCs under hypoxia might be the transcription factor STAT3. An inhibitory effect of hypoxia could also be observed regarding the expression of maturation-associated molecules on the DC surface. This effect was also present under the stimulation with zymosan or LPS, indicating that this is a general effect of hypoxia on human DCs. However, the T cell stimulatory capacity of these DCs was enhanced (only tested for *A. fumigatus*-stimulated DCs). The metabolic profile of DCs indicated HIF-1α activity under hypoxic conditions, as well as in DCs stimulated with LPS or *A. fumigatus* under normoxia and hypoxia. Regarding the difference between strong and moderate hypoxic culture conditions, there were no major differences and the effects were similar under both conditions. After this comprehensive analysis of the effects of hypoxia on DC functions against *A. fumigatus*, in the next part of the result section, the role of HIF-1α in human DCs directed against *A. fumigatus* is described.

3.3 Role of HIF-1α in DC responses against *A. fumigatus*

3.3.1 Analysis of HIF-1α protein in DCs and macrophages

HIF-1α is stabilized under hypoxia in most human cell types and mediates adaptive responses in conditions of reduced oxygen availability, including metabolic reprogramming to enable energy generation. It was previously shown that in DCs, HIF-1α is also stabilized following TLR stimulation by LPS under normoxia [136]. Stabilization of HIF-1α in DCs upon interaction with *A. fumigatus* has never been investigated so far. Shepardson *et al.* demonstrated that interaction with *A. fumigatus* leads to stabilization of HIF-1α in murine bone-marrow derived macrophages under normoxia [130]. Therefore, in addition to DCs, human macrophages were investigated as a second immune cell type in initial, confirmatory experiments.

3.3.1.1 Establishment of a protocol for the detection of the HIF-1α protein in lysates of human immune cells

To establish a protocol for the detection of HIF-1α protein in human immune cell lysates, DCs were incubated under hypoxia without stimulation or stimulated with LPS. Subsequently, cytoplasmic and nuclear protein fractions were isolated or whole cell lysates were prepared and analyzed by western blot (see paragraph 2.2.5.3, p. 63ff.). Figure 29 demonstrates that HIF-1α was detectable in the nuclear fraction and in whole lysates, but not in the cytoplasmic fraction, thus confirming nuclear localization of the HIF-1α protein after stabilization under hypoxia alone or additional stimulation with LPS. However, in the cytoplasmic fraction, the nuclear protein H3 was detected, indicating cross-contamination of the cytoplasmic with the nuclear fraction (Figure 29). In addition, the volume of the nuclear fraction sample allowed only very limited numbers of immunoblot analyses to detect the HIF-1α protein. Due to these technical difficulties regarding the preparation of separate cytoplasmic and nuclear protein lysates, whole cell lysates of primary immune cells (DCs and macrophages) were used for the detection of HIF-1α. Quantification of HIF-1α protein in total cell lysates is a commonly used method, especially for primary immune cells, where the cell number is a limiting factor [134].

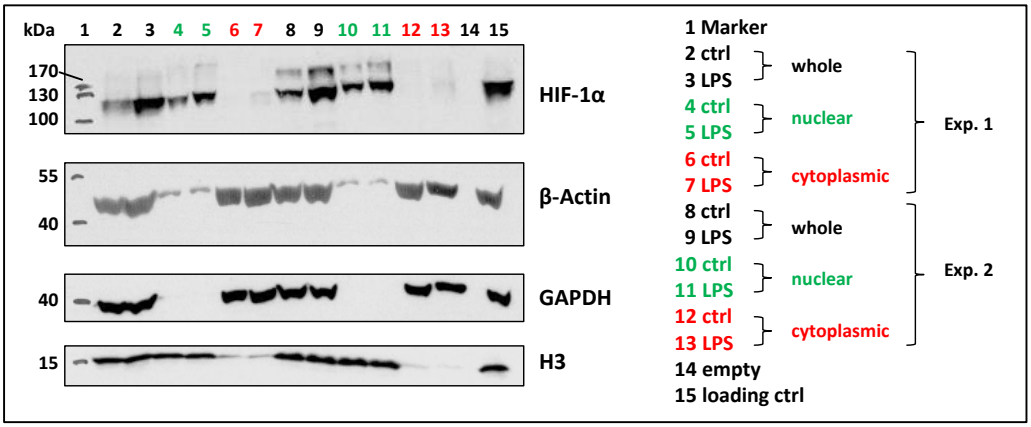

Figure 29 I HIF-1α is localized in the nuclear fraction of DC lysates.

DCs were incubated for 4.5 h under 1 % O_2, either without (ctrl) or with LPS stimulation (1 µg/ml). For each condition, duplicate samples were performed. From one of these replicates, whole cell extracts were prepared and from the other, nuclear and cytoplasmic protein fractions were isolated. Proteins were detected by immunoblotting. β-Actin (predominantly cytoplasmic localization), GAPDH (glyceraldehyde 3-phosphate dehydrogenase, cytoplasmic localization) and H3 (histone H3, nuclear localization) were used as controls for the cell fractions and for equal protein loading. In lane 1, a protein size marker was loaded. Whole cell extracts from DCs treated with 100 µM $CoCl_2$ to chemically stabilize HIF-1α under normoxia served as a loading control (lane 15). Data from two independent experiments (Exp. 1 and 2) are shown.

3.3.1.2 HIF-1α protein levels in macrophages and DCs interacting with *A. fumigatus*

To determine whether interaction with *A. fumigatus* leads to stabilization of the HIF-1α protein in macrophages and DCs, HIF-1α protein levels in immune cells stimulated with *A. fumigatus* under normoxia or hypoxia were analyzed. In addition, several PRR ligands were used to investigate different pathways of HIF-1α activation. LPS is a ligand for TLR2 and TLR4, ultrapure LPS exclusively ligates TLR2, zymosan is a TLR2 and Dectin-1 ligand and depleted zymosan lacks recognition by TLRs and is recognized by Dectin-1.

Initially, to confirm the pro-inflammatory activation induced by stimulation of macrophages and DCs with the different stimuli, levels of TNF were quantified in the cell culture supernatants (Figure 30). TNF was not released by unstimulated immune cells cultivated under normoxia or hypoxia, whereas stimulation induced the secretion of TNF under both culture conditions, thus confirming immune cell activation following PRR stimulation. Levels of TNF in the supernatants varied comparing DCs and macrophages and comparing the different PRR ligands. These different TNF levels demonstrate both cell-type specific as well as ligand-dependent effects on immune cell activation.

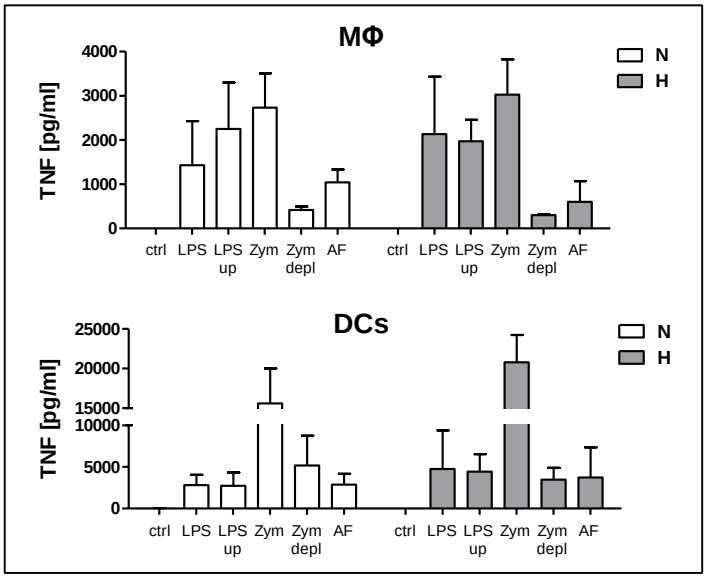

Figure 30 I PRR stimulation induces release of TNF from macrophages and DCs.

Macrophages (MΦ) and DCs were not stimulated (ctrl) or stimulated with LPS (1 µg/ml), ultrapure LPS (LPS up, 1 µg/ml), zymosan (Zym, 10 µg/ml), depleted zymosan (Zym depl, 100 µg/ml) or *A. fumigatus* (AF, MOI = 1) and cultivated under normoxia (N) or hypoxia (H, 1 % O_2) for 6 h. Levels of TNF were quantified in the cell culture supernatants by ELISA. Data are displayed in [pg/ml] as mean + SD and are from n = 3 independent experiments.

Next, HIF-1α protein levels were quantified by immunoblot analyses (Figure 31).

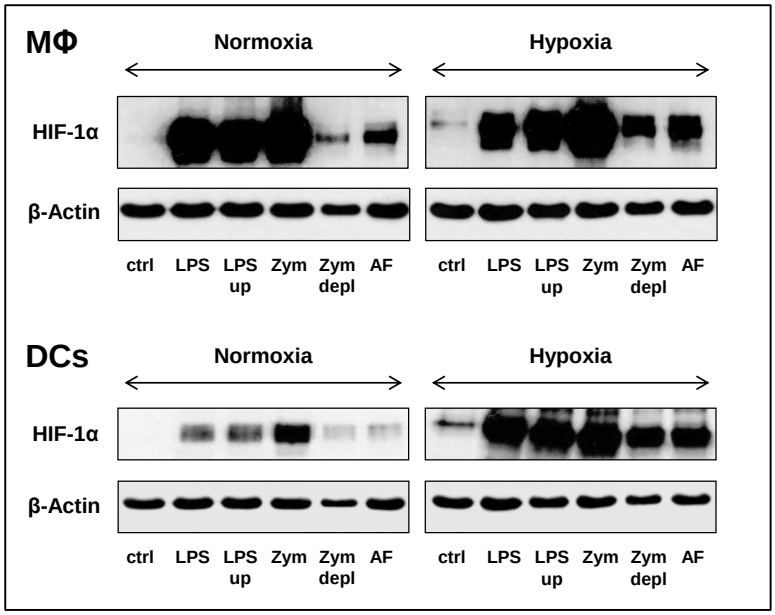

Figure 31 I HIF-1α protein levels in macrophages and DCs.

Macrophages (MΦ) and DCs were not stimulated (ctrl) or stimulated with LPS (1 µg/ml), ultrapure LPS (LPS up, 1 µg/ml), zymosan (Zym, 10 µg/ml), depleted zymosan (Zym depl, 100 µg/ml) or *A. fumigatus* (AF, MOI = 1) and cultivated under normoxia (N) or hypoxia (H, 1 % O_2) for 6 h. Protein levels of HIF-1α and β-Actin were detected in whole cell lysates by immunoblotting. Data are representative of at least n = 3 independent experiments.

The HIF-1α protein was not detected in cell lysates from control macrophages or DCs cultivated under normoxia but it was stabilized under hypoxia This is consistent with its biological function: *HIF1A* mRNA is steadily expressed in mammalian cells but the HIF-1α protein is only stabilized under hypoxic conditions, otherwise it is rapidly degraded in an oxygen-dependent process [107]. Remarkably, these data demonstrate that *A. fumigatus* as well as all PRR stimuli applied stabilized the HIF-1α protein under normoxia and hypoxia in both cell types. The TLR 2/4 ligand LPS, the TLR4 ligand ultrapure

LPS and the TLR2/Dectin-1 ligand zymosan induced higher HIF-1α protein levels under normoxia and hypoxia, whereas the Dectin-1 ligand depleted zymosan (lacking TLR ligands) and *A. fumigatus* induced only weak to moderate HIF-1α levels under normoxia and hypoxia, respectively (Figure 31). These differences in HIF-1α protein levels were similar comparing macrophages and DCs. In summary, interaction with *A. fumigatus* stabilized the HIF-1α protein in macrophages and DCs under normoxic and hypoxic conditions.

3.3.1.3 HIF1A mRNA levels in macrophages and DCs

LPS induced NF-κB leads to enhanced *HIF1A* mRNA transcription and to stabilization of the HIF-1α protein in murine macrophages [128]. To investigate this mechanism of HIF-1α stabilization in human immune cells, levels of *HIF1A* mRNA were measured in macrophages and DCs (Figure 32).

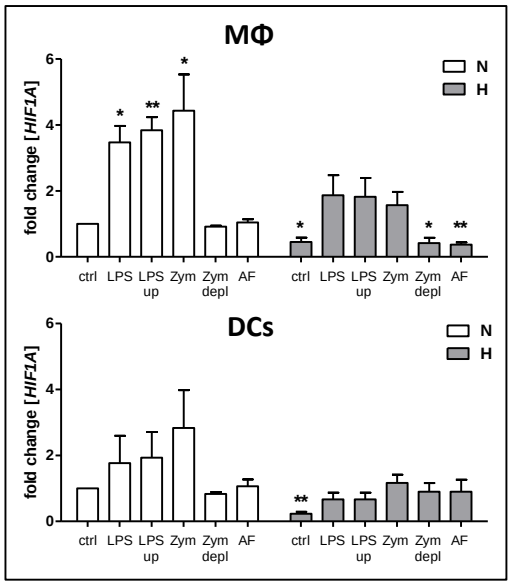

Figure 32 I *HIF1A* transcript levels in macrophages and DCs.

Macrophages (MΦ) and DCs were not stimulated (ctrl) or stimulated with LPS (1 µg/ml), ultrapure LPS (LPS up, 1 µg/ml), zymosan (Zym, 10 µg/ml), depleted zymosan (Zym depl, 100 µg/ml) or *A. fumigatus* (AF, MOI = 1) and cultivated under normoxia (N, white bars) or hypoxia (H, grey bars, 1 % O_2) for 6 h. Transcript levels of *HIF1A* were measured by real-time RT-PCR, normalized to the reference gene *ALAS1* and are displayed as fold changes relative to control cells under normoxia. Data are displayed as mean + SD from n = 3 independent experiments. Statistical analysis was performed compared to control cells under normoxia. Significant differences are indicated by asterisks (* $p < 0.05$; ** $p < 0.01$; two-tailed, paired *t*-test).

Under normoxia, LPS, ultrapure LPS and zymosan induced *HIF1A* transcript expression, while *HIF1A* expression was not enhanced by depleted zymosan or *A. fumigatus*. The effect was significant in macrophages and a trend in DCs. Under hypoxia, *HIF1A* transcript expression was significantly decreased in control macrophages and control DCs. Macrophages stimulated with LPS, ultrapure LPS or zymosan showed a trend to enhanced *HIF1A* mRNA levels under hypoxia, while in macrophages stimulated with depleted zymosan and *A. fumigatus HIF1A* transcript levels were comparable to control macrophages under hypoxia. DCs stimulated under hypoxia with either stimuli

exhibited transcript levels comparable to control DCs under normoxia. These data are evidence of regulation of *HIF1A* mRNA following stimulation with TLR ligands (LPS, ultrapure LPS and zymosan). Stimulation of Dectin-1 (depleted zymosan) or with *A. fumigatus* did not lead to up-regulation of *HIF1A* mRNA.

3.3.1.4 Role of Dectin-1 for HIF-1α stabilization in DCs

To study a possible link between the interaction of *A. fumigatus* with Dectin-1 on human DCs and the stabilization of HIF-1α protein, a siRNA-based partial knockdown of Dectin-1 in human DCs was achieved. This knockdown had already been established in previous work by our group [69]. Real-time RT-PCR and flow cytometric analyses confirmed the knockdown of Dectin-1 on transcript and protein level. On transcript level, knockdown was > 80 % (compared to DCs that had not been electroporated, Figure 33 A). Flow cytometric analyses revealed that the knockdown was only partial on the level of Dectin-1 protein expression on the cell surface (Figure 33 B). To confirm the knockdown functionally, DCs were stimulated with the TLR2/Dectin-1 ligand complete zymosan, the Dectin-1-specific ligand depleted zymosan or with *A. fumigatus* under normoxic and hypoxic conditions. Levels of TNF in the supernatants of stimulated Dectin-1 knockdown DCs were reduced in comparison to their non-silenced counterparts (Figure 33 C).

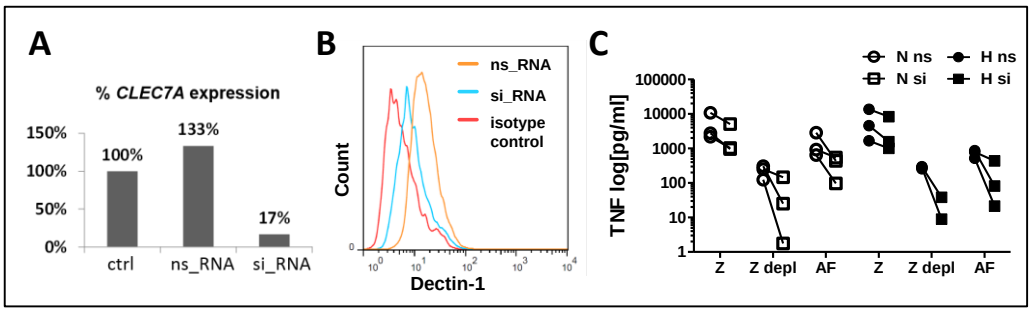

Figure 33 I Dectin-1 knockdown on DCs.

Control non-silencing siRNA (ns) or siRNA directed against *CLEC7A* (encoding Dectin-1, si) was transfected into DCs using electroporation. **(A)** 24 h after electroporation, *CLEC7A* mRNA levels were measured by real-time RT-PCR, normalized to the internal control *ALAS1* and are displayed as % expression relative to control DCs that had not been electroporated. **(B)** 24 h after electroporation, Dectin-1 expression on the DC surface was determined by flow cytometry. **(C)** 24 h after electroporation, DCs were not stimulated (control) or stimulated with zymosan (Z, 10 µg/ml), depleted zymosan (Z depl, 100 µg/ml) or *A. fumigatus* (AF, MOI = 1) and cultivated under normoxia (N) or hypoxia (H, 1 % O_2) for 6 h. Levels of TNF in the supernatants of the DC cultures were quantified by ELISA and are displayed in log [pg/ml]. Control DCs did not release TNF (data not shown). Data from three independent experiments are shown.

To further confirm the Dectin-1 knockdown, Dectin-1 protein levels were measured in DC lysates. DCs that received Dectin-1 siRNA had clearly reduced levels of Dectin-1 protein (Figure 34). These data confirm the partial Dectin-1 knockdown that is leading to reduced Dectin-1 surface expression and a reduced pro-inflammatory response in DCs (Figure 33).

Next, HIF-1α protein levels were analyzed in these DC lysates. Weak baseline levels of HIF-1α protein were detected in cell lysates from unstimulated DCs that received non-silencing control siRNA via electroporation and were cultivated under normoxia (Figure 34, upper panel). In contrast, DCs that had not been transfected with siRNA using electroporation (non-RNAi DCs) did not show baseline HIF-1α protein levels under normoxic conditions (Figure 31, p. 105). Stimulation with *A. fumigatus* as well as complete zymosan and depleted zymosan stabilized HIF-1α protein in normoxic cultures. Complete zymosan induced higher HIF-1α protein levels than depleted zymosan and *A. fumigatus*. This data is in line with the results from non-RNAi DCs (Figure 31, p. 105). Importantly, HIF-1α stabilization was clearly reduced in Dectin-1 knockdown DCs stimulated with depleted zymosan or *A. fumigatus* under normoxic conditions. These findings demonstrate a link between Dectin-1 expression on the surface of DCs and stabilization of HIF-1α following Dectin-1 ligation under normoxic conditions. Under hypoxic conditions, HIF-1α was stabilized in control DCs (Figure 34, lower panel). Signals derived from the different PRR ligands and *A. fumigatus* resulted in higher levels of HIF-1α than under hypoxia alone while there was no obvious difference between Dectin-1 knockdown and non-silenced DCs under hypoxic conditions.

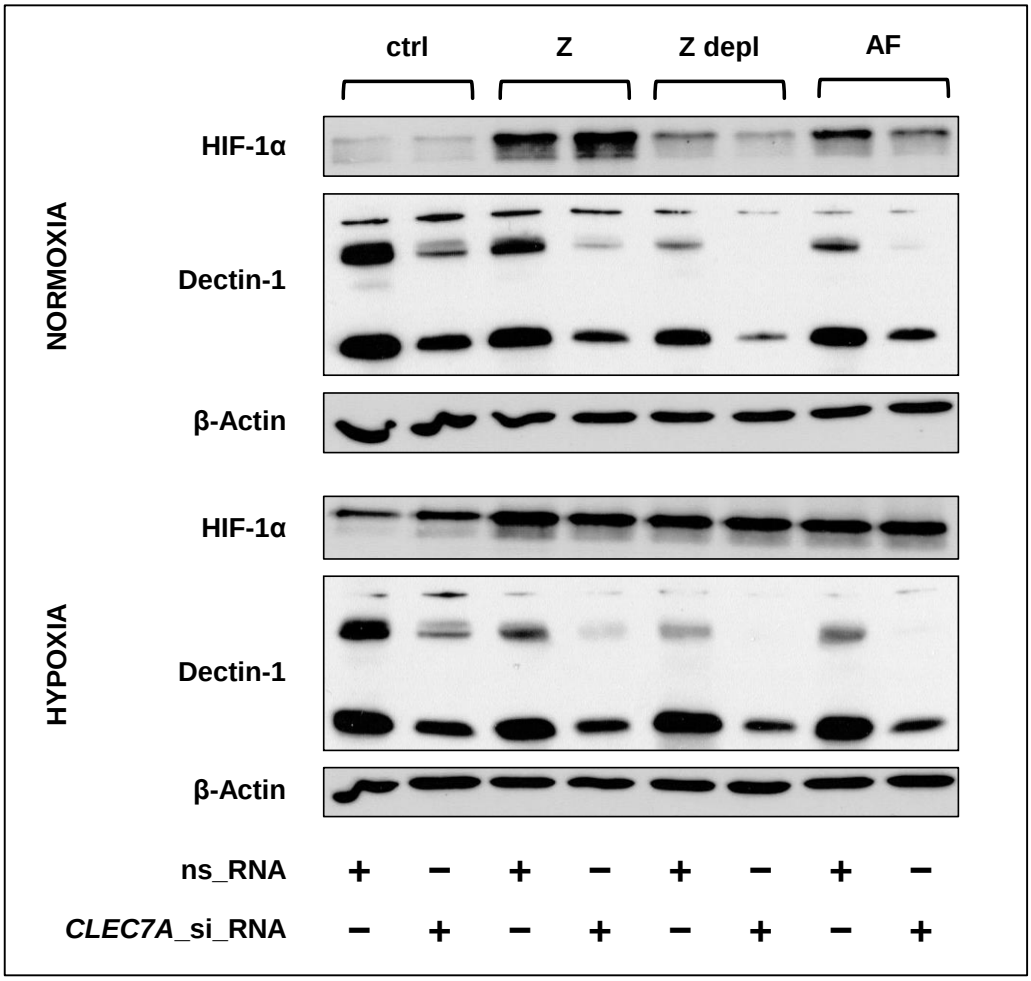

Figure 34 I Partial dependence of HIF-1α stabilization on Dectin-1 expression in DCs.

Control non-silencing siRNA (ns) or siRNA directed against *CLEC7A* (encoding Dectin-1, si) was transfected into DCs using electroporation. 24 h after electroporation, DCs were not stimulated (ctrl) or stimulated with zymosan (Z, 10 µg/ml), depleted zymosan (Z depl, 100 µg/ml) or *A. fumigatus* (AF, MOI = 1) and cultivated under normoxia (N) or hypoxia (H, 1 % O_2) for 6 h. Protein levels of HIF-1α, Dectin-1 and β-Actin were detected in DC lysates by immunoblotting. Data from one out of three representative experiments are shown.

3.3.2 HIF-1α silencing with siRNA

To explore the functional relevance of HIF-1α stabilization in DCs during interaction with *A. fumigatus*, a protocol for a specific, RNAi-mediated knockdown of HIF-1α was established. Therefore, DCs were electroporated with siRNA directed against *HIF1A* mRNA. 24 h after electroporation, *HIF1A* transcript levels were measured in DCs using real-time RT-PCR and compared to levels in DCs that received non-silencing control siRNA or that were not electroporated.

Six different siRNA sequences directed against *HIF1A* were tested. Among them, si_10 induced a mean knockdown of 89 % in comparison to DCs that had not been electroporated (Figure 35 A). Furthermore, HIF-1α protein levels were measured. HIF-1α protein was not detected in cell lysates after siRNA treatment (Figure 35 B). For the following experiments, the siRNA si_10 was used to knock down HIF-1α in DCs.

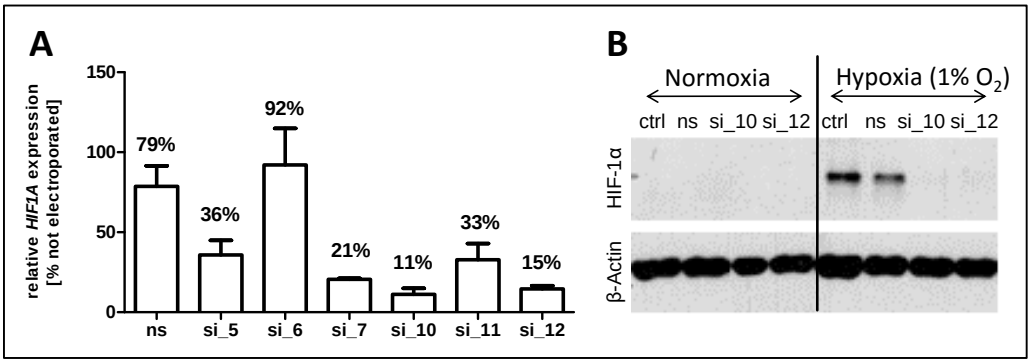

Figure 35 I HIF-1α knockdown in DCs.

Control non-silencing siRNA (ns) or siRNA directed against *HIF1A* (si_x) was transfected into DCs using electroporation. **(A)** 24 h after electroporation, *HIF1A* mRNA levels were measured by real-time RT-PCR, normalized to the internal control *ALAS1* and are displayed as % expression relative to control DCs that had not been electroporated (ctrl). Data from two (si_7, si_12); four (si_5, si_6, si_11) or six (ns, si_10) independent experiments are shown as mean + SD. (**B)** HIF-1α knockdown on protein level is shown. 24 h after electroporation, DCs were cultivated for 4 h under normoxia or hypoxia. Protein levels of HIF-1α and β-Actin were detected in whole cell lysates by immunoblotting. One representative experiment is shown.

Knockdown of *HIF1A* on transcript level was confirmed in DCs cultivated under normoxia or hypoxia and stimulated with LPS or *A. fumigatus* for up to 24 h (Figure 36). In either treatment condition, *HIF1A* transcript levels in siRNA treated DCs were around 20 % compared to their non-silenced counterparts, thus confirming an effective knockdown of HIF-1α for a period of up to 24 h stimulation (i.e., 48 h after

electroporation). Furthermore, levels of two known HIF-1α target genes (*SLC2A1*, encoding the glucose-transporter 1 and *VEGFA*, encoding the vascular-endothelial growth factor) were measured. Both *SLC2A1* and *VEGFA* mRNA levels were lower in HIF-1α silenced DCs (Figure 36). It has to be taken into account that HIF-1α might not be the only transactivator for these genes and that in consequence HIF-1α silencing did not lead to a complete repression of transcriptional activation of these HIF-1α target genes.

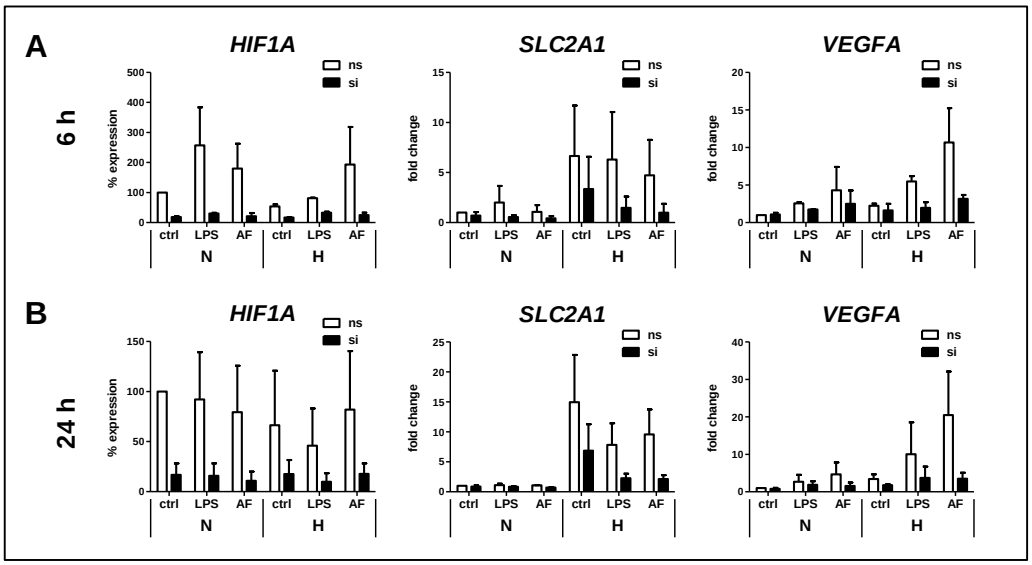

Figure 36 I Transcript levels of *HIF1A*, *SLC2A1* and *VEGFA* after HIF-1α knockdown.

Control non-silencing siRNA (ns) or *HIF1A* silencing siRNA (si) was transfected into DCs using electroporation. 24 h after electroporation, DCs were not stimulated (ctrl) or stimulated with LPS (1 µg/ml) or with *A. fumigatus* (AF, MOI=1) and were cultivated under normoxia (N) or hypoxia (H, 1 % O_2) for **(A)** 6 h or **(B)** 24 h. Transcript levels of *HIF1A, SLC2A1* and *VEGFA* were measured by real-time RT-PCR, normalized to the reference gene *ALAS1* and are displayed as fold changes relative to control DCs under normoxia. Data are displayed as mean + SD from n = 2 (A) or n = 3 (B) independent experiments.

3.3.3 Viability of HIF-1α silenced DCs

Next, viability of HIF-1α knockdown DCs was measured. Therefore, HIF-1α silenced and non-silenced DCs were cultivated under normoxia or hypoxia without stimulation or stimulated with *A. fumigatus* for 24 h. Cell viability was determined using flow cytometry. The total numbers of DCs were defined by gating. Percentages of viable, apoptotic and dead DCs were defined within the DC gate, respectively (Figure 37).

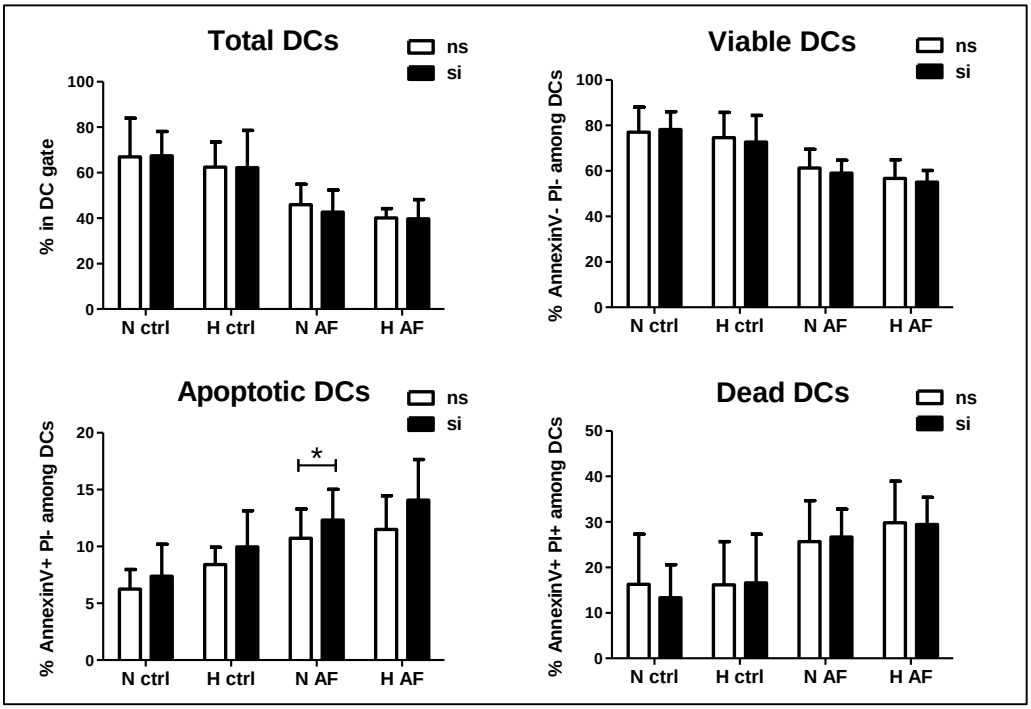

Figure 37 I Viability of HIF-1α silenced DCs.

Control non-silencing siRNA (ns, white bars) or *HIF1A* silencing siRNA (si, black bars) was transfected into DCs using electroporation. 24 h after electroporation, DCs were stimulated with *A. fumigatus* (AF, MOI = 1) or not stimulated (ctrl) and incubated under normoxia (N) or hypoxia (H, 1 % O_2) for 24 h. Flow cytometry was performed to determine DC viability. The DC population was defined by gating according to light scatter characteristics (FSC/ SSC) to exclude cell debris. To determine apoptotic and/ or dead cells, DCs were stained with FITC-conjugated AnnexinV and with PI. Graphs show percentages of total DCs, viable DCs (AnnexinV- PI-), early apoptotic DCs (AnnexinV+ PI-) and dead DCs (AnnexinV+ PI+). Data are shown as mean + SD of n = 4 independent experiments. Significant differences comparing non-silenced and HIF-1α silenced DCs are indicated with an asterisk (* $p < 0.05$; two tailed, paired t test).

DC viability decreased comparing control DCs to DCs stimulated with *A. fumigatus*, as determined by lower numbers of total DCs and lower percentages of viable DCs but increased percentages of apoptotic and dead DCs within the DC gate. This reduction in viability after stimulation with *A. fumigatus* in electroporated DCs is in contrast to DCs

that had not been electroporated (Figure 13, p. 72). Importantly, viability of DCs that were stimulated with *A. fumigatus* was similar when comparing the treatment conditions (HIF-1α silenced and non-silenced DCs as well as cultivation under normoxia and hypoxia). There were significantly higher numbers of apoptotic DCs in HIF-1α silenced DCs compared to non-silenced DCs under normoxia. Apart from that, total numbers, viable DCs, apoptotic DCs and dead DCs were comparable between HIF-1α silenced and non-silenced DCs that had been stimulated with *A. fumigatus*. Therefore, even though HIF-1α mediates adaption to hypoxic conditions, HIF-1α knockdown did not lead to massive DC death under conditions of reduced oxygen availability and simultaneous stimulation for culture times up to 24 h.

3.3.4 Gene expression profiles of HIF-1α silenced DCs

3.3.4.1 Preparation, performance and validation of the 1 % O_2/HIF-1α silenced microarrays

The second set of gene expression microarrays analyzed the role of HIF-1α in anti-fungal immune responses of human DCs under normoxic and hypoxic conditions. The comparison and analysis of the datasets for non-silenced DCs under normoxia and hypoxia are described in detail in paragraph 3.2.3 (p. 84ff.). Figure 38 depicts the eight treatment conditions for this microarray experiment. To verify effective HIF-1α knockdown under these conditions, HIF-1α protein levels were determined by immunoblot analysis and are shown in the upper panel in Figure 38.

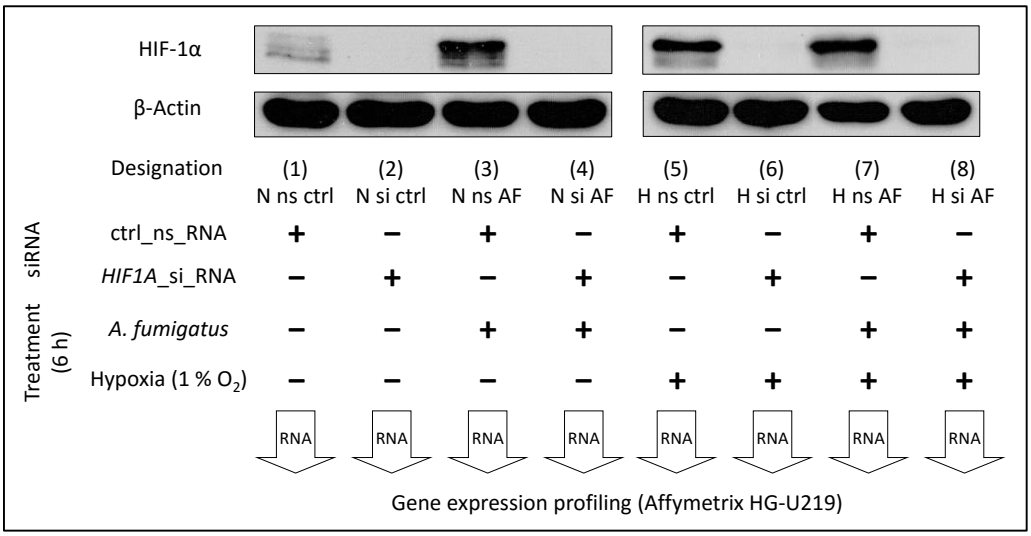

Figure 38 I Schematic outline of the 1 % O_2/HIF-1α silenced microarrays experiment.

The gene expression profiling experiment consisted of eight treatment groups with six replicates in each group (i.e., DCs derived from six different blood donors). Control non-silencing siRNA (ctrl_ns_RNA) or *HIF1A* silencing siRNA (*HIF1A*_si_RNA) was transfected into DCs using electroporation. 24 h after electroporation, DCs were either cultivated without stimulation (ctrl) or were stimulated with *A. fumigatus* (AF) under normoxic (N) or hypoxic (H, 1 % O_2) conditions for 6 h. Subsequently, cells were harvested and stored in a RNA stabilizing agent. Three experiments were chosen for hybridization onto Affymetrix HG-U291 gene expression microarrays. Supernatants were stored separately for cytokine quantification.

A small portion (1/10) of each DC sample was used for RNA isolation prior to gene expression profiling to verify efficient *HIF1A* knockdown (Figure 39 A). Altogether, six independent experiments were performed out of which three were chosen for RNA isolation and hybridization onto the microarrays. As shown in Figure 39 A, in the

experiments 4, 5 and 6 down-regulation of *HIF1A* on transcript level was highest. However, in experiment 5 the expression of the DC cell marker CD1a was clearly distinct compared to the experiments 1-4 and 6 (Figure 39 B). Therefore, the experiments 1, 4 and 6 were chosen for the microarray analysis (depicted in blue in Figure 39 A).

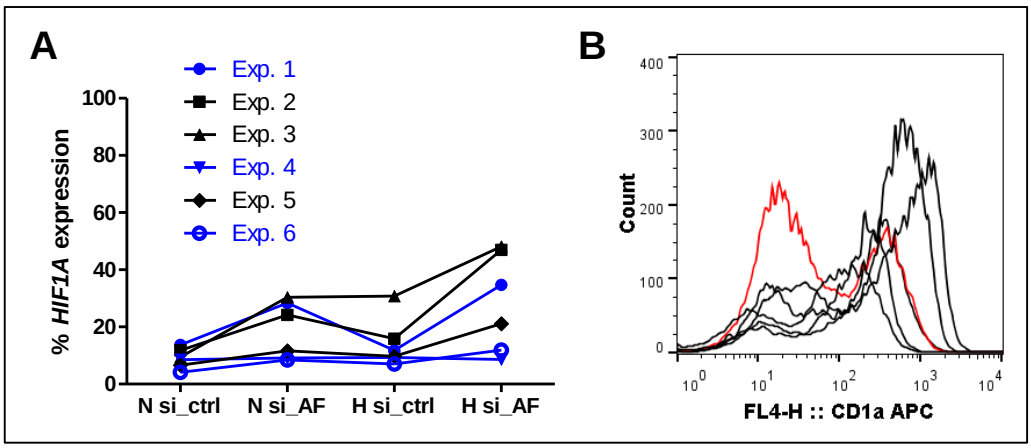

Figure 39 I Selection of samples for microarray analysis (1 % O_2/HIF-1α silenced).

(A) Prior to gene expression profiling, *HIF1A* knockdown was validated by real-time RT-PCR. Therefore, RNA was isolated from a small portion (1/10) of the same samples later used for microarray analyses. Transcript levels of *HIF1A* were measured by real-time RT-PCR, normalized to the internal control *ALAS1* and are displayed as % *HIF1A* expression compared to unstimulated control DCs that received non-silencing RNA and were cultivated under normoxia. **(B)** CD1a expression was monitored on the surface of DCs by flow cytometry. Red line, experiment 5; black lines, all other experiments.

The microarrays and the raw data analysis were performed in cooperation with the Microarray Facility Tübingen (see paragraph 2.2.4.4, p. 59ff.). Initially, a principal component analysis (PCA) of the microarray raw data had been performed to decide for a strategy to determine differentially regulated genes when comparing two treatment conditions (Figure 40).

The PCA demonstrated that the effects of the different treatments (displayed in different colors) were similar. However, there was also a considerable inter-experiment variability (due to donor-dependent differences). The donor-dependent differences are best visible when comparing the pattern of unstimulated (control) DCs (light/ dark blue and light/ dark purple). Therefore, differentially regulated genes were determined by a paired analysis to consider donor-dependent variability. Probe sets with a p-value < 0.05 and a fold change > 1.5 (for the HIF-1α mediated transcriptomes) or a fold change > 2 (for the hypoxia-mediated transcriptomes) were considered to be differentially regulated.

Different cut-offs regarding the fold changes in the hypoxia and the HIF-1α mediated transcriptomes were due to a higher number of regulated genes under normoxic vs. hypoxic conditions than in HIF-1α silenced vs. non-silenced DCs.

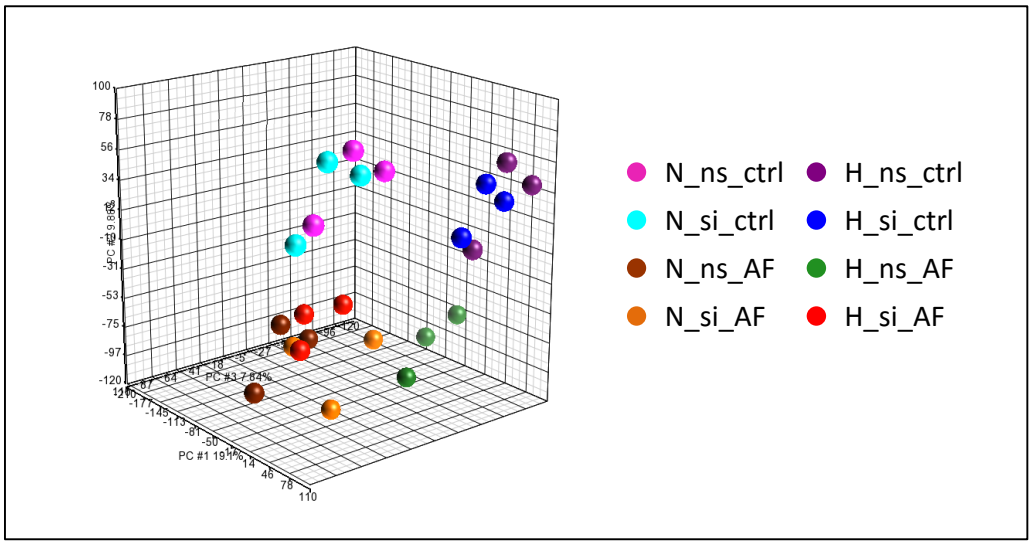

Figure 40 I PCA of the 1 % O_2/HIF-1α silenced microarray data.

Principal components analysis (PCA) was performed as an exploratory technique to detect groupings in the microarray data sets. The data used for the PCA were the normalized expression values measured for all transcripts in one sample. The colors represent the different treatment conditions. N, normoxia; H, hypoxia (1 % O_2); ns, control non-silencing siRNA; si, *HIF1A*-silencing siRNA; ctrl, unstimulated DCs; AF, DCs stimulated with *A. fumigatus* (MOI = 1). PCA was performed by Michael Bonin (Microarray Facility Tübingen).

To verify the levels of transcript expression obtained from the microarray experiment, real-time RT-PCR was performed by reverse transcribing RNA from the same samples used for hybridization onto the microarray and measuring relative expression levels of selected genes (Figure 41). All analyzed transcripts showed the same trend in regulation compared to control DCs (control DCs received non-silencing siRNA and were incubated without stimulation under normoxic conditions) in the microarray and real-time PCR analyses (Figure 41).

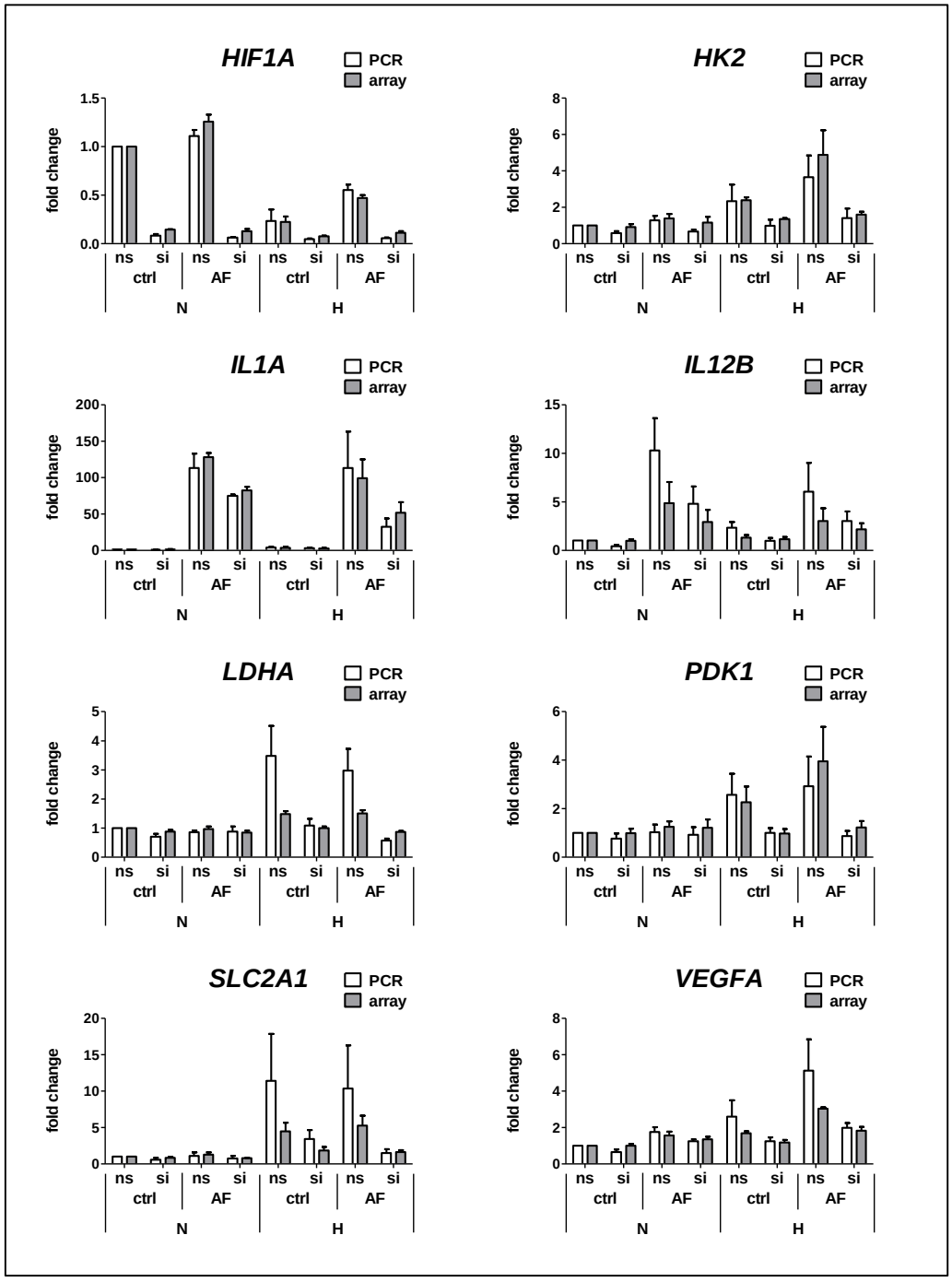

Figure 41 I Validation of the 1 % O_2/HIF-1α silenced microarrays by real-time RT-PCR.

Expression levels of selected genes are displayed as fold changes relative to control DCs. **White bars (PCR):** Transcript levels were measured by real-time RT-PCR and normalized to the reference gene *ALAS1*. **Grey bars (array):** Expression levels were calculated using the normalized microarray expression data for the specific transcripts. Data are presented as mean + SD (n = 3). N, normoxia; H, hypoxia (1 % O_2); AF, *A. fumigatus* (MOI = 1); ns, non-silencing siRNA; si, *HIF1A* silencing siRNA.

3.3.4.2 Analysis of the HIF-1α mediated transcriptomes in DCs under normoxia and hypoxia

To elucidate potential functions of HIF-1α in the immune response of human DCs against *A. fumigatus*, the gene expression profiles of HIF-1α silenced to HIF-1α non-silenced DCs were compared. This resulted in the following comparisons (see Figure 38, p. 114 for the numbers in brackets): "Normoxia": control, HIF-1α silenced (2) vs. control, non-silenced DCs (1); "Normoxia + *A. fumigatus*": *A. fumigatus*-stimulated, HIF-1α silenced (4) vs. *A. fumigatus*-stimulated, non-silenced DCs (3); "Hypoxia (1 % O_2)": control, HIF-1α silenced (6) vs. control, non-silenced DCs (5) and "Hypoxia (1 % O2) + *A. fumigatus*": *A. fumigatus*-stimulated, HIF-1α silenced (8) vs. *A. fumigatus*-stimulated, non-silenced DCs (7). Fully annotated lists of the genes in these comparisons are available on the supplementary data CD (file names "*HIF1a sil Normoxia*", "*HIF1a sil A. fumigatus*", "*HIF1a sil Hypoxia*", "*HIF1a sil Hypoxia + A. fumigatus*"). Table 24 to Table 27 list the top ten up- and down-regulated genes on these lists.

Table 24 I Top 10 regulated genes in the HIF-1α mediated transcriptome "Normoxia".

Gene Symbol	Gene Title	FC *
HIF1A	hypoxia inducible factor 1, alpha subunit	-8.10
MAPRE1	microtubule-associated protein, RP/EB family, member 1	-3.28
PPP1R2	protein phosphatase 1, regulatory (inhibitor) subunit 2	-3.08
C1D	C1D nuclear receptor co-repressor	-3.05
MBTPS2	membrane-bound transcription factor peptidase, site 2	-2.88
C11orf31	chromosome 11 open reading frame 31	-2.84
ALDH1A2	aldehyde dehydrogenase 1 family, member A2	-2.83
DPH3	DPH3, KTI11 homolog (S. cerevisiae)	-2.77
CD1B	CD1b molecule	-2.71
H2AFV	H2A histone family, member V	-2.68
C2orf60	chromosome 2 open reading frame 60	1.64
DRAM1	DNA-damage regulated autophagy modulator 1	1.69
ASNS	asparagine synthetase (glutamine-hydrolyzing)	1.70
CDK5RAP2	CDK5 regulatory subunit associated protein 2	1.73
ASNS	asparagine synthetase (glutamine-hydrolyzing)	1.76
TGFA	transforming growth factor, alpha	1.79
CFI	complement factor I	1.79
PPPDE1	PPPDE peptidase domain containing 1	1.80
THBS1	thrombospondin 1	1.98
PSAT1	phosphoserine aminotransferase 1	2.00

* For genes represented by more than one probe set, the one with the highest fold change (FC) is shown.

Table 25 I Top 10 regulated genes in the HIF-1α mediated transcriptome "Normoxia + *A. fumigatus*".

Gene Symbol	Gene Title	FC *
HIF1A	hypoxia inducible factor 1, alpha subunit	-12.38
H2AFV	H2A histone family, member V	-3.95
C1D	C1D nuclear receptor co-repressor	-3.85
MBTPS2	membrane-bound transcription factor peptidase, site 2	-3.19
PLEKHA1	pleckstrin homology domain containing, family A (phosphoinositide binding specific) member 1	-3.04
MAP1A	microtubule-associated protein 1A	-3.01
PPP1R2	protein phosphatase 1, regulatory (inhibitor) subunit 2	-2.97
C14orf2	chromosome 14 open reading frame 2	-2.96
DPH3	DPH3, KTI11 homolog (S. cerevisiae)	-2.88
EGR4	early growth response 4	-2.86
LRPPRC	leucine-rich PPR-motif containing	1.69
KIAA0090	KIAA0090	1.69
AMACR	alpha-methylacyl-CoA racemase	1.73
C5orf43	chromosome 5 open reading frame 43	1.74
EXOSC2	exosome component 2	1.75
USP46	ubiquitin specific peptidase 46	1.77
PDE3B	phosphodiesterase 3B, cGMP-inhibited	1.80
DDX42	DEAD (Asp-Glu-Ala-Asp) box polypeptide 42	1.88
CCR5	chemokine (C-C motif) receptor 5	1.96
PPPDE1	PPPDE peptidase domain containing 1	2.06

* For genes represented by more than one probe set, the one with the highest fold change (FC) is shown.

Table 26 I Top 10 regulated genes in the HIF-1α mediated transcriptome "Hypoxia (1 % O_2)".

Gene Symbol	Gene Title	FC *
BNIP3	BCL2/adenovirus E1B 19kDa interacting protein 3	-7.64
ALDOC	aldolase C, fructose-bisphosphate	-5.31
DDIT4	DNA-damage-inducible transcript 4	-4.43
C7orf68	chromosome 7 open reading frame 68	-4.42
HIF1A	hypoxia inducible factor 1, alpha subunit	-4.32
PDXP/SH3BP1	pyridoxal (pyridoxine, vitamin B6) phosphatase /// SH3-domain binding protein 1	-3.85
ZC3HAV1L	zinc finger CCCH-type, antiviral 1-like	-3.53
ANKZF1	ankyrin repeat and zinc finger domain containing 1	-3.49
C18orf19	chromosome 18 open reading frame 19	-3.46
MBTPS2	membrane-bound transcription factor peptidase, site 2	-3.38
BNIP1	BCL2/adenovirus E1B 19kDa interacting protein 1	1.83
GINS1	GINS complex subunit 1 (Psf1 homolog)	1.84
SPSB2	splA/ryanodine receptor domain and SOCS box containing 2	1.85
GPR171	G protein-coupled receptor 171	1.88
HMG20A	high-mobility group 20A	1.90
GDF15	growth differentiation factor 15	1.92
SETDB2	SET domain, bifurcated 2	1.94
RSAD2	radical S-adenosyl methionine domain containing 2	2.01
SDS	serine dehydratase	2.20
TAF9B	TAF9B RNA polymerase II, TATA box binding protein (TBP)-associated factor	2.24

* For genes represented by more than one probe set, the one with the highest fold change (FC) is shown.

Table 27 I Top 10 regulated genes in the HIF-1α mediated transcriptome "Hypoxia (1 % O_2) + *A. fumigatus*".

Gene Symbol	Gene Title	FC *
BNIP3	BCL2/adenovirus E1B 19kDa interacting protein 3	-9.75
C7orf68	chromosome 7 open reading frame 68	-6.88
ALDOC	aldolase C, fructose-bisphosphate	-5.92
HIF1A	hypoxia inducible factor 1, alpha subunit	-5.59
DDIT4	DNA-damage-inducible transcript 4	-5.57
EGLN1	egl nine homolog 1 (C. elegans)	-4.90
ANKRD37	ankyrin repeat domain 37	-4.54
PDXP/SH3BP1	pyridoxal (pyridoxine, vitamin B6) phosphatase/SH3-domain binding protein 1	-4.38
SLC2A1	solute carrier family 2 (facilitated glucose transporter), member 1	-3.87
LOC154761	hypothetical LOC154761	-3.56
WASF2	WAS protein family, member 2	5.66
SSH1	slingshot homolog 1 (Drosophila)	5.81
RPS6KA3	ribosomal protein S6 kinase, 90kDa, polypeptide 3	6.01
NAA15	N(alpha)-acetyltransferase 15, NatA auxiliary subunit	6.03
RAD23B	RAD23 homolog B (S. cerevisiae)	6.28
IL6ST	interleukin 6 signal transducer (gp130, oncostatin M receptor)	6.55
HIRA	HIR histone cell cycle regulation defective homolog A (S. cerevisiae)	6.72
NFAT5	nuclear factor of activated T-cells 5, tonicity-responsive	6.76
TLN1	talin 1	7.51
YWHAG	tyrosine 3-monooxygenase/tryptophan 5-monooxygenase activation protein γ	10.03

* For genes represented by more than one probe set, the one with the highest fold change (FC) is shown.

In the following step, the "Normoxia" list was subtracted from the "Normoxia + *A. fumigatus*" list and the "Hypoxia" list was subtracted from the "Hypoxia + *A. fumigatus*" one. For each culture condition (normoxia and hypoxia), this resulted in a subset of genes that were exclusively regulated under the influence of HIF-1α silencing in DCs that had been stimulated with *A. fumigatus* (underlined and grey in Figure 42 A).

For each culture condition (normoxia and hypoxia), network analysis was performed on genes downstream of Dectin-1 that showed HIF-1α dependent regulation after stimulation with *A. fumigatus* (Figure 42 B). Several of those genes were connected to Dectin-1 signaling. Among them were the transcription factors *EGR1* and *EGR3* in the normoxia and *NFAT5* in the hypoxia network. Other genes were involved in immune signaling pathways. Under normoxia, this included the gene encoding the adaptor protein MYD88, which is involved in downstream TLR signaling. Under hypoxia, this included the gene encoding the inflammasome NLRP3 protein complex. These data demonstrated a complex influence of HIF-1α signaling on the transcriptome of *A. fumigatus*-stimulated DCs which involves various genes and signaling pathways.

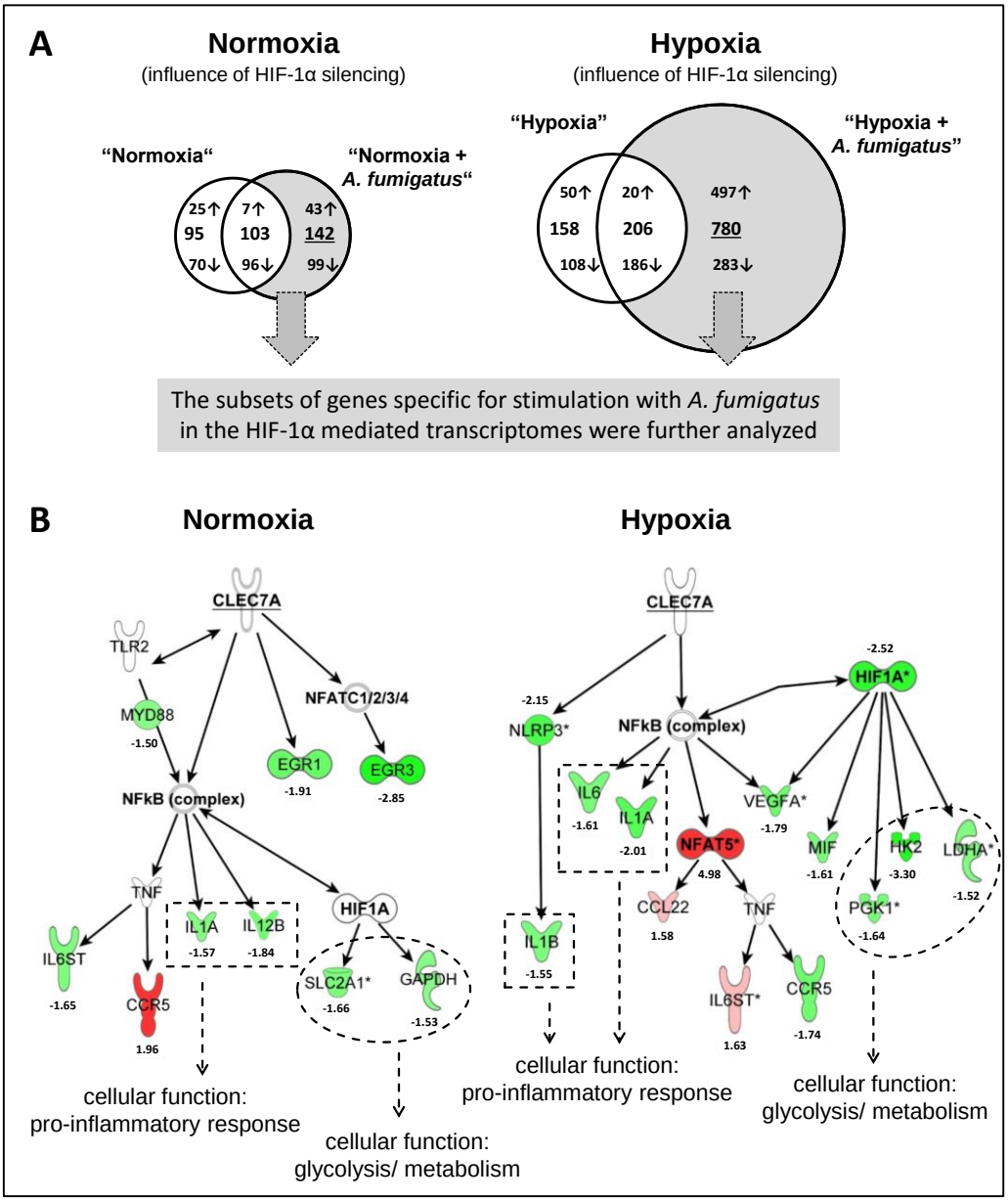

Figure 42 I HIF-1α mediated effects on the transcriptome of DCs stimulated with *A. fumigatus* under normoxia and hypoxia.

(A) Gene expression of HIF-1α silenced DCs was compared to gene expression of non-silenced DCs. Genes with $p < 0.05$ and a fold change > 1.5 were considered to be differentially regulated. The area proportional Venn diagrams visualize the overlap and differences between the lists of differentially regulated genes. Genes that were only regulated in DCs stimulated with *A. fumigatus* in the HIF-1α mediated transcriptomes were further analyzed (grey and underlined). **(B)** Dectin-1 (CLEC7A) / HIF-1α (HIF1A) gene network analyses were performed using IPA. Fold changes are depicted below the molecule symbols. The network is displayed with color-coded gene expression overlay. Green, down-regulated genes; red, up-regulated genes; white, not regulated in the gene subsets.

It is important to point out that both networks contained genes that encode proteins that are involved in glycolysis and that are known to be HIF-1α inducible

(*SLC2A1*, *GAPDH*, *PGK1*, *HK2* and *LDHA*, oval borders) as well as NF-κB inducible genes encoding (pro-) inflammatory mediators (*IL1A*, *IL1B*, *IL12B* and *IL6*, rectangle borders). Therefore, the network analyses of the *A. fumigatus*-specific HIF-1α mediated transcriptomes suggested involvement of HIF-1α in regulating metabolic activity and cytokine production in DCs stimulated with *A. fumigatus* under normoxic as well as hypoxic conditions.

Next, pathways that might be involved in the subsets of genes specific for stimulation with *A. fumigatus* in the HIF-1α mediated transcriptomes were predicted. This pathway analysis resulted in a number of hits for several aspects of the immune response for both the normoxia and the hypoxia datasets (Figure 43). Under normoxia this included the chemokine and TLR signaling pathway. Under hypoxic conditions, several interleukin signaling pathways were enriched in HIF-1α silenced DCs, including the IL-1, IL-6, IL-8 and IL-10 pathways. In summary, the pathway analysis revealed a modulatory effect of HIF-1α on several immune relevant signaling pathways in DCs stimulated with *A. fumigatus.* One common feature of the pathways under normoxia and hypoxia was that many of the pathways belonged to the group of cytokine signaling pathways. This is in line with the network analyses that included several genes encoding cytokines under normoxic as well as hypoxic conditions (Figure 42, rectangle borders).

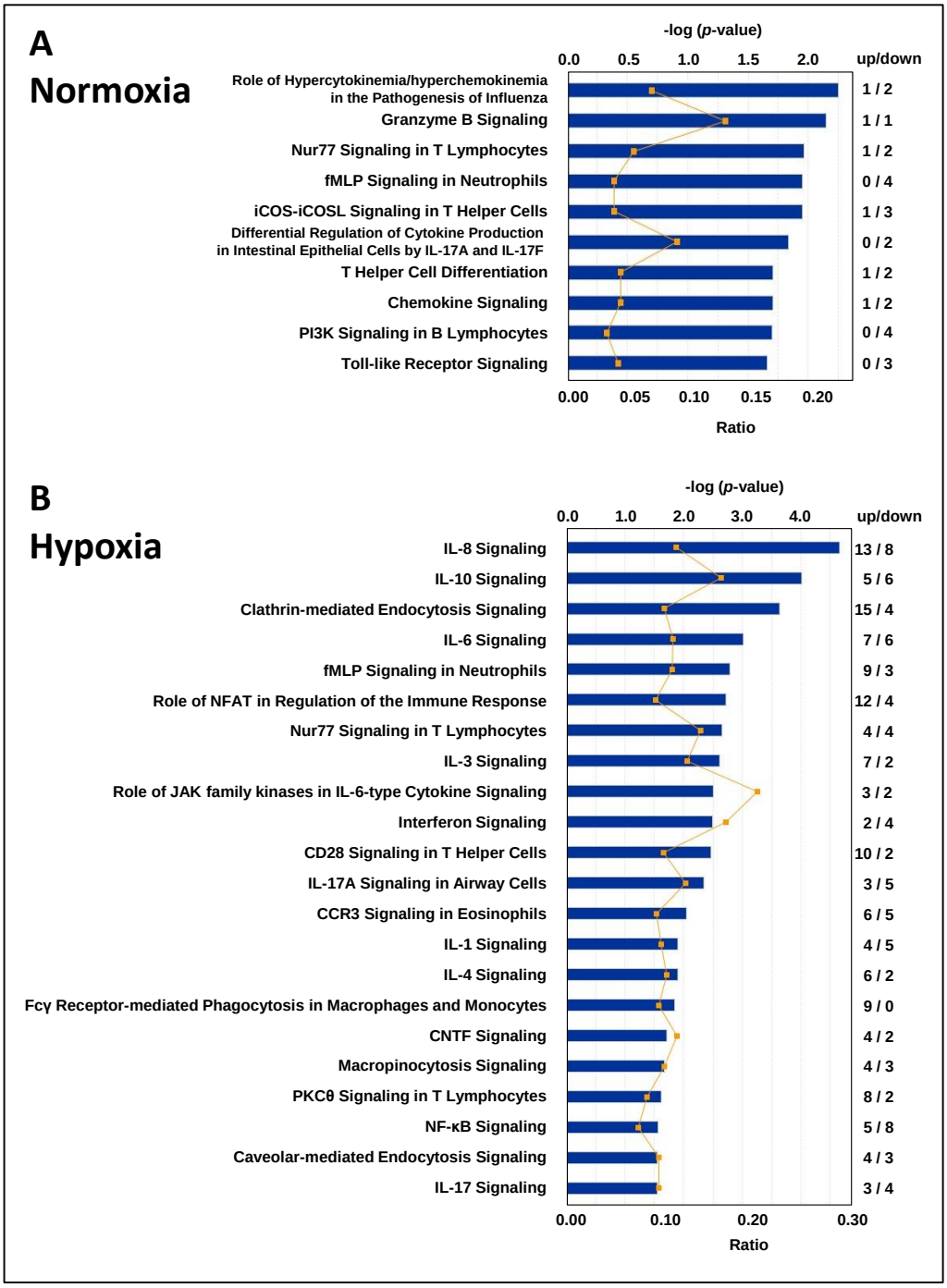

Figure 43 I Immune-relevant pathways enriched in HIF-1α silenced DCs stimulated with *A. fumigatus* under normoxia and hypoxia.

Pathways enriched in HIF-1α silenced DCs stimulated with *A. fumigatus* under normoxic **(A)** or hypoxic **(B)** conditions. All immune relevant pathways with a –log (*p*-value) > 1.5 were included. Immune relevant pathways were among the IPA categories cellular immune response, cytokine signaling, humoral immune response and pathogen influenced signaling. The *p*-value (blue bar) is a measure for the likelihood that the association between the genes in the dataset and the pathway is due to random chance. The ratio (orange squares) is the quotient of the number of genes in the dataset that correspond to one pathway and the total number of genes in the pathway. The numbers on the right indicate how many pathway specific genes in the gene subsets were up- or down-regulated.

Upstream regulator analysis was performed to predict molecules that could be responsible for the gene expression changes observed in the dataset. This analysis was again performed for the specific datasets (Figure 42 A) to compare HIF-1α silenced and non-silenced DCs when stimulated with *A. fumigatus*. Table 28 shows the results for normoxic, Table 29 for hypoxic conditions.

Table 28 I Upstream regulators enriched in DCs stimulated with *A. fumigatus* in the comparison of HIF-1α silenced to non-silenced DCs cultivated under normoxic conditions.

Upstream Regulator	Description	Molecule type	z-score	-log(*p*-value)
BETAESTRADIOL		hormone	-1.52	5.84
DIHYDROTESTOSTERONE		hormone	-1.53	5.23
TCOF1	Treacher Collins-Franceschetti syndrome 1	transporter		4.88
IL5	Interleukin 5	cytokine	-1.77	4.64
LPS	Lipopolysaccharide/ endotoxin	chemical toxicant	-2.14	4.44
NFATC3	Nuclear factor of activated T-cells, cytoplasmic, calcineurin-dependent 3	transcription regulator		4.19
CHRM1	Cholinergic receptor, muscarinic 1	g-protein coupled receptor		4.10
TREM1	Triggering receptor expressed on myeloid cells 1	transmembrane receptor	-0.51	3.98
HNF4A	Hepatocyte nuclear factor 4, alpha	transcription regulator		3.94
TNF	Tumor necrosis factor	cytokine	-2.13	3.90
TLR5	Toll-like receptor 5	transmembrane receptor	-1.94	3.83
CD38	CD38 molecule	enzyme	-1.97	3.82
ERK1/2	Extracellular-signal-regulated kinases (mitogen-activated protein kinases 1 and 3)	group	-0.75	3.81
TRETINOIN	Retinoic acid	chemical	-1.14	3.79
CISPLATIN	Chemotherapy drug	chemical drug	0.88	3.78

The 15 most significant upstream regulators are shown in the table. Green enhancement, upstream regulator is predicted to be inhibited. Activation z-score, prediction for the activation state of the upstream regulator; overlap *p*-value, measure for a statistically significant overlap between the dataset genes and known targets of the upstream regulator.

Table 29 I Upstream regulators enriched in DCs stimulated with *A. fumigatus* in the comparison of HIF-1α silenced to non-silenced DCs cultivated under hypoxic (1 % O_2) conditions.

Upstream Regulator	Description	Molecule type	z-score	-log(*p*-value)
MYC	V-myc avian myelocytomatosis viral oncogene homolog	transcription regulator	0.10	13.33
APP	Amyloid beta (A4) precursor protein	other	0.74	11.91
HIF1A	Hypoxia-inducible factor 1α	transcription regulator	-1.52	11.36
TNF	Tumor necrosis factor	cytokine	-1.28	10.88

Table 29 (continued) I Upstream regulators enriched in DCs stimulated with *A. fumigatus* in the comparison of HIF-1α silenced to non-silenced DCs cultivated under hypoxic (1 % O_2) conditions.

Upstream Regulator	Description	Molecule type	z-score	-log(*p*-value)
CAMPTO-THECIN	Cytotoxic quinoline alkaloid	chemical reagent	-0.69	10.85
OSM	Oncostatin M	cytokine	-1.40	10.32
SP1	Sp1 transcription factor	transcription regulator	-0.08	10.04
F2	Coagulation factor II (thrombin)	peptidase	-0.25	9.84
TGFB1	Transforming growth factor, beta 1	growth factor	-0.40	9.78
FAS	Fas cell surface death receptor	transmembrane receptor	-0.98	9.25
NR3C1	Nuclear receptor subfamily 3, group C, member 1 (glucocorticoid receptor)	ligand-dependent nuclear receptor	1.70	8.76
CSF1	Colony stimulating factor 1 (macrophage)	cytokine	-1.00	8.73
LPS	Lipopolysaccharide/ endotoxin	chemical drug	0.41	8.69
DIHYDROTESTOSTERONE		hormone	1.20	8.50
FSH	Follicle-stimulating hormone	hormone	0.70	8.44

The 15 most significant upstream regulators are shown in the table. Activation z-score, prediction for the activation state of the upstream regulator; overlap *p*-value, measure for a statistically significant overlap between the dataset genes and known targets of the upstream regulator.

Moreover, a regulator effects analysis was performed with the genes of the *A. fumigatus*-specific subsets (Figure 42 A). The analysis helps to determine how predicted activated or inhibited upstream regulators might cause increases or decreases in downstream functions. In comparison to the normoxia dataset, the hypoxia dataset was much larger. Therefore, the regulators effects analysis predicted too many possible regulators and downstream effects with many non-DC related functions. A reduction of the dataset by means of including only genes with a fold change > 2 did not clarify this analysis. Figure 44 shows the regulators effects network with the highest z-score for the normoxia dataset.

The upstream regulators analyses and the regulator effects network predicted a possible inhibiting effect of HIF-1α silencing on the response of DCs against *A. fumigatus* under normoxic conditions. This was indicated by a predicted inhibition of LPS and TNF-induced signaling in the dataset, which might be indicative of a reduced-pro-inflammatory response. Furthermore, the function “maturation of dendritic cells” was predicted to be inhibited in the regulator effects network. However, under hypoxia, none of the 15 most significant upstream regulators were predicted to be activated or inhibited and the regulator effects networks were too unspecific to allow a prediction of possible functions

on the level of a DC-mediated immune response. On the other hand, the network and pathway analyses (Figure 42 and Figure 43) suggested an involvement of HIF-1α in the metabolic activity and cytokine response of DCs stimulated with *A. fumigatus* under normoxic as well as hypoxic conditions. In the following, HIF-1α silenced DCs were further characterized on a functional level, including their maturation and T cell stimulatory capacity as well as metabolic activity and cytokine response.

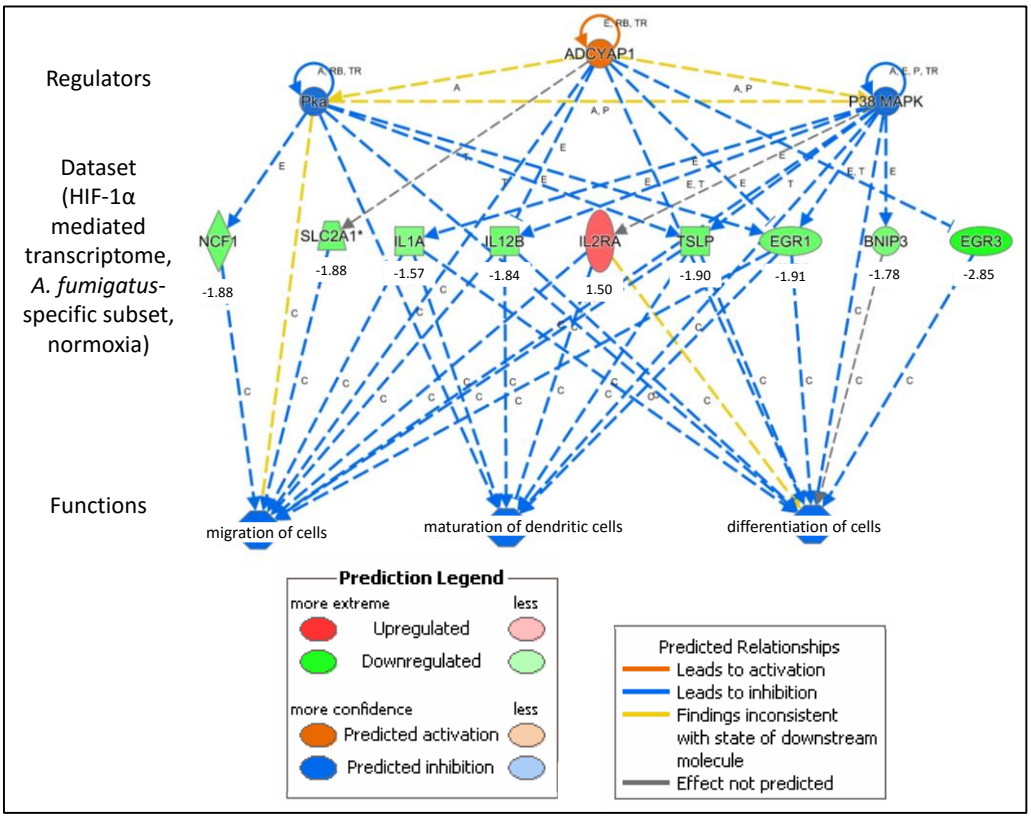

Figure 44 I Possible regulators effects in *A. fumigatus*-stimulated DCs under normoxia comparing HIF-1α silenced to non-silenced DCs.

Genes specifically regulated in HIF-1α silenced DCs stimulated with *A. fumigatus* under normoxia were subjected to regulator effects analysis. One resulting network with possible upstream regulators affecting DC-relevant functions is shown. Diseases were excluded from the list of possible downstream outcomes. Scoring method: Fisher's Exact Test, $p < 0.05$, z-score > 2 (regarding the overlap between the regulator and the function dataset molecules).

3.3.5 Effects of HIF-1α on T cell related DC functions

3.3.5.1 Maturation of HIF-1α silenced DCs

The normoxia regulator effects network predicted an impaired maturation of HIF-1α silenced DCs that had been stimulated with *A. fumigatus* (Figure 44, p. 126). To investigate whether HIF-1α is involved in *A. fumigatus*-induced DC maturation under normoxic or hypoxic conditions, HIF-1α silenced and non-silenced DCs were stimulated with *A. fumigatus*. DC maturation was monitored through flow cytometric analysis of the surface expression of CCR7, a receptor required for migration of DCs to the lymph node, of the MHC class II molecule HLA-DR that presents exogenous antigens to T cells and of the T cell co-stimulatory proteins CD40, CD80 and CD86 (Figure 45).

In addition, CD1a was analyzed as the characteristic marker of DCs to confirm cell identity. The percentage of $CD1a^+$ DCs remained the same in all treatment conditions. It should be noted that the levels of the maturation markers differed when comparing electroporated and non-electroporated DCs (data not shown), thus indicating an unspecific effect of the electroporation method on DC surface marker expression.

Stimulation with *A. fumigatus* for 24 h up-regulated CCR7, HLA-DR, CD40, CD80 and CD86 under all treatment conditions. However, the up-regulation of HLA-DR, CD40 and CD80 was not significant on DCs stimulated with *A. fumigatus* under hypoxic conditions (two-tailed, paired t-test, significance levels not indicated in Figure 45). This was likely due to reduced maturation of DCs under hypoxic conditions (as shown in Figure 26, p. 98). The surface expression of CCR7, HLA-DR, CD40, CD80 and CD86 did not statistically differ when comparing HIF-1α silenced and non-silenced DCs in one respective treatment condition. Taken together, HIF-1α silencing did not influence the expression of DC maturation markers.

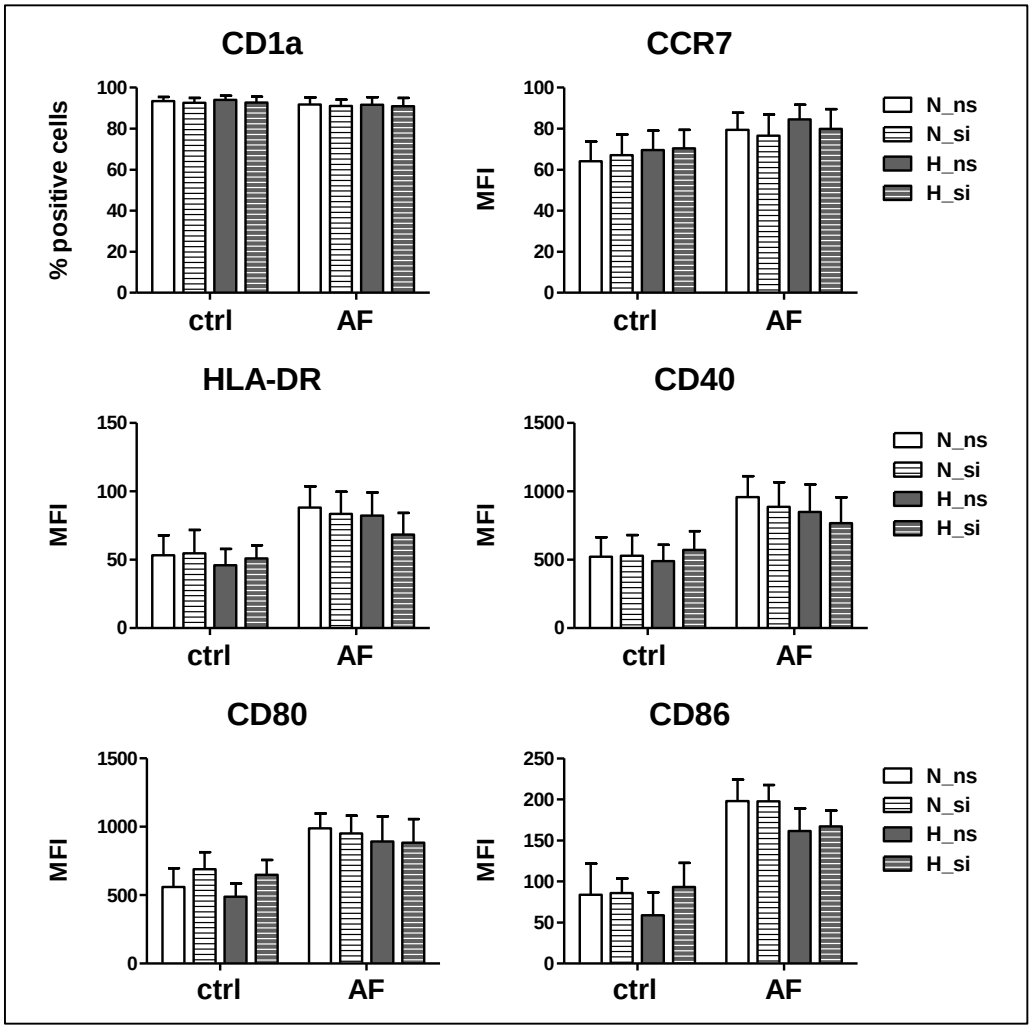

Figure 45 I Expression of DC surface molecules is independent of HIF-1α expression.

Control non-silencing siRNA (ns, bars without pattern) or *HIF1A* silencing siRNA (si, bars with horizontal pattern) was transfected into DCs using electroporation. 24 h after electroporation, DCs were either not stimulated (ctrl) or stimulated with *A. fumigatus* (AF, MOI = 1) and were incubated under normoxia (N, white bars) or hypoxia (H, 1 % O_2, grey bars) for 24 h. Flow cytometry graphs show CD1a, CCR7, HLA-DR, CD40, CD80 and CD86 expression on the surface of DCs. CD1a is shown as the percentage of CD1a positive cells within the live gate. All other markers are shown as mean + SD of the mean fluorescence intensity (MFI) of three independent experiments. Significant testing comparing the pairs of HIF-1α silenced and non-silenced DCs was performed using the two-tailed, paired *t*-test. All *p*-values were > 0.05.

3.3.5.2 T cell stimulatory capacity of HIF-1α silenced DCs

The release of IFN-γ from T cells that was induced after co-incubation of DCs with allogeneic T cells was quantified to determine the T cell stimulatory capacity of HIF-1α silenced or non-silenced DCs. DCs and T cells that were incubated separately did not secrete IFN-γ (data not shown). Compared to co-culture with control DCs that were not

stimulated, IFN-γ concentrations significantly increased in co-culture supernatants of T cells and DCs that were stimulated with *A. fumigatus* (Figure 46). HIF-1α silenced or non-silenced DCs stimulated with *A. fumigatus* under either normoxic or hypoxic conditions induced similar IFN-γ release from allogeneic T cells. Taken together, HIF-1α silencing did not significantly influence *A. fumigatus*-induced DC maturation under normoxic or hypoxic conditions (Figure 45) and did not alter the capacity of these DCs to activate T cells (Figure 46).

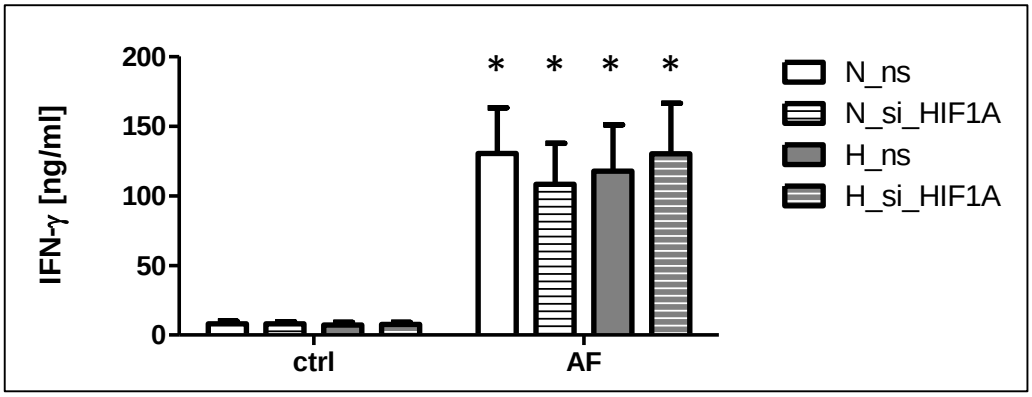

Figure 46 I The T cell stimulatory capacity of DCs is independent of HIF-1α expression.

Control non-silencing siRNA (ns, bars without pattern) or *HIF1A* silencing siRNA (si_HIF1A, bars with horizontal pattern) was transfected into DCs using electroporation. 24 h after electroporation, DCs were stimulated with *A. fumigatus* (AF, MOI = 1) or not stimulated (ctrl) and incubated under normoxia (N, white bars) or hypoxia (H, 1 % O_2, grey bars) for 24 h. Subsequently, DCs were co-cultured for three additional days with allogeneic T cells under normoxia (DC to T cell ratio 1:9). IFN-γ concentrations in co-culture supernatants were determined by ELISA and are shown in ng/ml. Data are shown as mean + SD from n = 3 independent experiments. Significant differences comparing the respective control to *A. fumigatus*-stimulated DCs are indicated by asterisks (* $p < 0.05$; two-tailed, unpaired *t*-test).

3.3.6 Glycolytic activity in HIF-1α silenced DCs

The network analysis suggested involvement of HIF-1α in the regulation of metabolic activity of DCs stimulated with *A. fumigatus* (Figure 42 B, p. 121, oval borders). HIF-1α silencing led to the down-regulation of *SLC2A1* and *GAPDH* in the normoxia dataset and *HK2*, *LDHA* and *PGK1* in the hypoxia dataset. These five genes are known to be inducible by HIF-1α and their protein products are involved in glycolysis [125]. This indicated that HIF-1α enhanced glycolytic activity in DCs stimulated with *A. fumigatus* under both conditions. To confirm the result obtained from the gene expression

microarrays, glucose and lactate levels were measured in the cell culture supernatant as indicators of glycolytic activity. Cultivation under hypoxic conditions increased glucose consumption and lactate accumulation for both stimulated and control DCs compared to the glucose and lactate levels under normoxia (Figure 47). The result is comparable to DCs that had not been electroporated and were cultivated under strong and moderate hypoxia (Figure 28, p. 101). Compared to control DCs under normoxic conditions, stimulation with *A. fumigatus* significantly increased glucose uptake and lactate release from DCs, indicating increased glycolysis. Interestingly, HIF-1α silencing significantly reduced this metabolic shift in DCs stimulated with *A. fumigatus* under normoxic as well as hypoxic conditions. In line with the gene expression data (Figure 42 B), the result confirmed the role of HIF-1α for energy generation in DCs stimulated with *A. fumigatus* under both conditions.

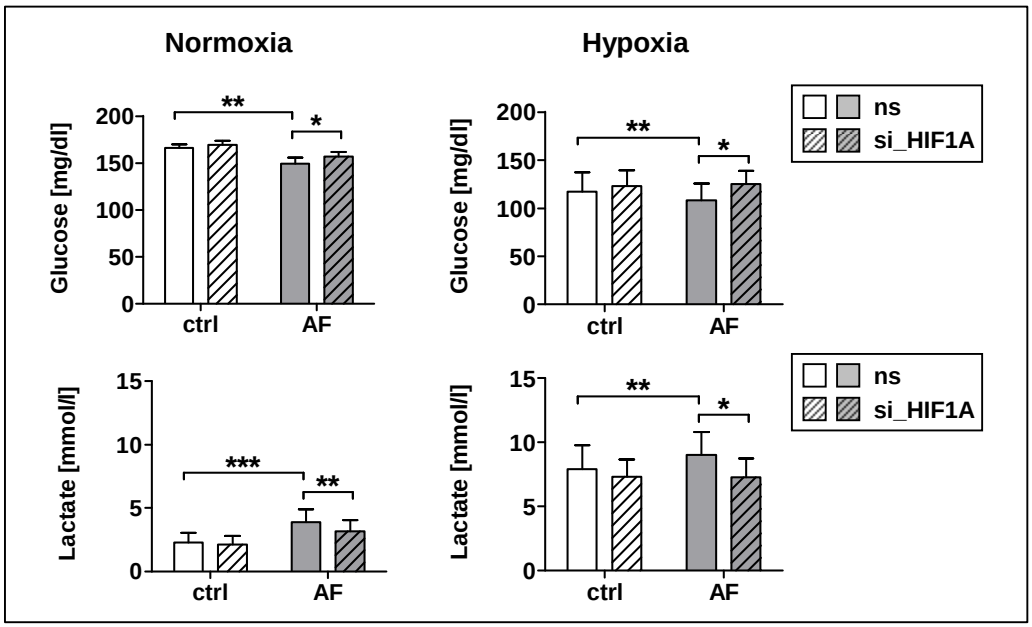

Figure 47 I HIF-1α regulates glycolysis in DCs stimulated with *A. fumigatus* under normoxia and hypoxia.

Control non-silencing siRNA (ns) or *HIF1A* silencing siRNA (si_HIF1A) was transfected into DCs using electroporation. After 24 h, DCs were either stimulated with *A. fumigatus* germ tubes (AF, MOI = 1) or not stimulated (ctrl) and incubated under normoxia or hypoxia (1 % O_2). Glucose and lactate levels were measured photometrically in cell culture supernatants after 24 h stimulation. Data is shown as mean + SD of five independent experiments. Significant differences are indicated by asterisks (* $p < 0.05$; ** $p < 0.01$; *** $p < 0.001$; two-way repeated measures ANOVA followed by Bonferroni's multiple comparison test).

3.3.7 Influence of HIF-1α on DC cytokine release

The HIF-1α mediated transcriptomes in the presence of *A. fumigatus* under both, normoxic and hypoxic conditions, included genes encoding several cytokines that are involved in the pro-inflammatory response of human DCs (network analyses in Figure 42 B, p. 121, rectangle borders and pathways in Figure 43, p. 123). The network analysis specifically included *IL1A* and *IL12B* under normoxia as well as *IL1A*, *IL1B* and *IL6* under hypoxia.

To confirm the involvement of HIF-1α in cytokine release from DCs upon *A. fumigatus* simulation, cytokines were measured in the supernatants from HIF-1α silenced or non-silenced DCs after 3, 6, 9 and 12 h stimulation with *A. fumigatus* under normoxic (Figure 48) or hypoxic (Figure 49) conditions. Levels of several cytokines were significantly reduced in HIF-1α silenced DCs that were stimulated with *A. fumigatus* compared to their non-silenced counterparts. This included IL-12p70 and CCL5 (RANTES) under normoxic and IL-6, IL-12p70, CCL5 and VEGFA under hypoxic conditions. Although release of IL-1β was not statistically different, there was a clear trend towards reduced release in HIF-1α silenced DCs under both conditions. It should be noted that levels of CCL5, IL-10, IL-12p70 and TNF were significantly lower when directly comparing normoxic to hypoxic conditions in non-silenced DCs. This demonstrated an inhibitory effect of hypoxia on the cytokine release in addition to the HIF-1α mediated effect (these data are displayed in Figure 25, p. 95). Overall, the inhibitory effect of HIF-1α silencing on the release of these specific cytokines was similar when comparing the results under normoxic and hypoxic conditions. Therefore, the time-course cytokine release pattern confirmed and complemented the transcriptome analysis and verified the role of HIF-1α in positively regulating DC pro-inflammatory cytokine release during an *A. fumigatus* infection.

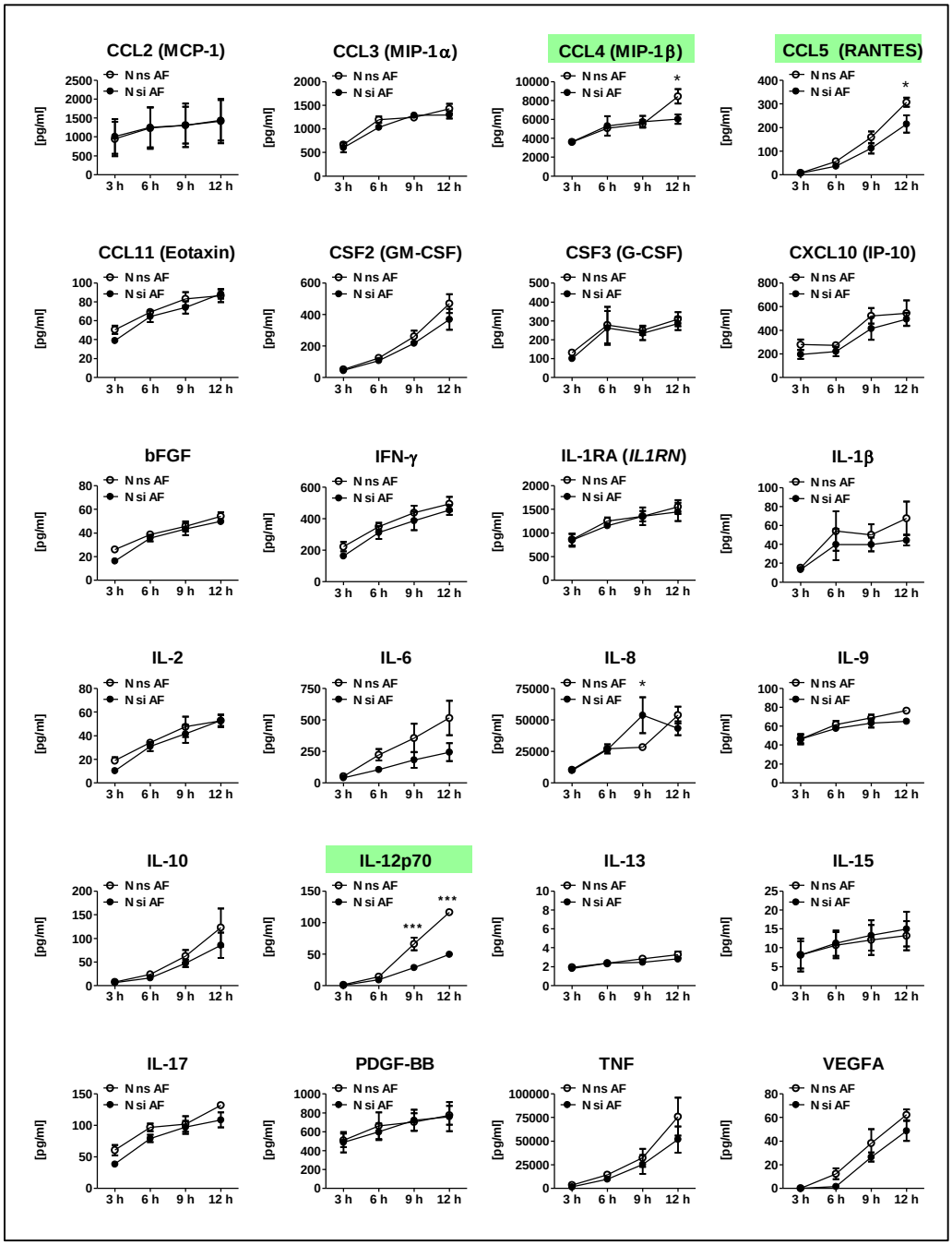

Figure 48 I HIF-1α modulates pro-inflammatory cytokine release from DCs stimulated with *A. fumigatus* under normoxic conditions.

Control non-silencing siRNA (ns, white circles) or *HIF1A* silencing siRNA (si, black circles) was transfected into DCs using electroporation. 24 h after electroporation, DCs were stimulated with *A. fumigatus* and incubated under normoxia. Cytokines were quantified in cell culture supernatants after 3, 6, 9 and 12 h stimulation with *A. fumigatus* by a multiplex immunoassay. Data is shown as mean ± SEM of three independent experiments. Significant differences comparing HIF-1α silenced to non-silenced DCs at the respective time are indicated by asterisks (* $p < 0.05$; ** $p < 0.01$; *** $p < 0.001$; two-way repeated measures ANOVA followed by Bonferroni's multiple comparison test).

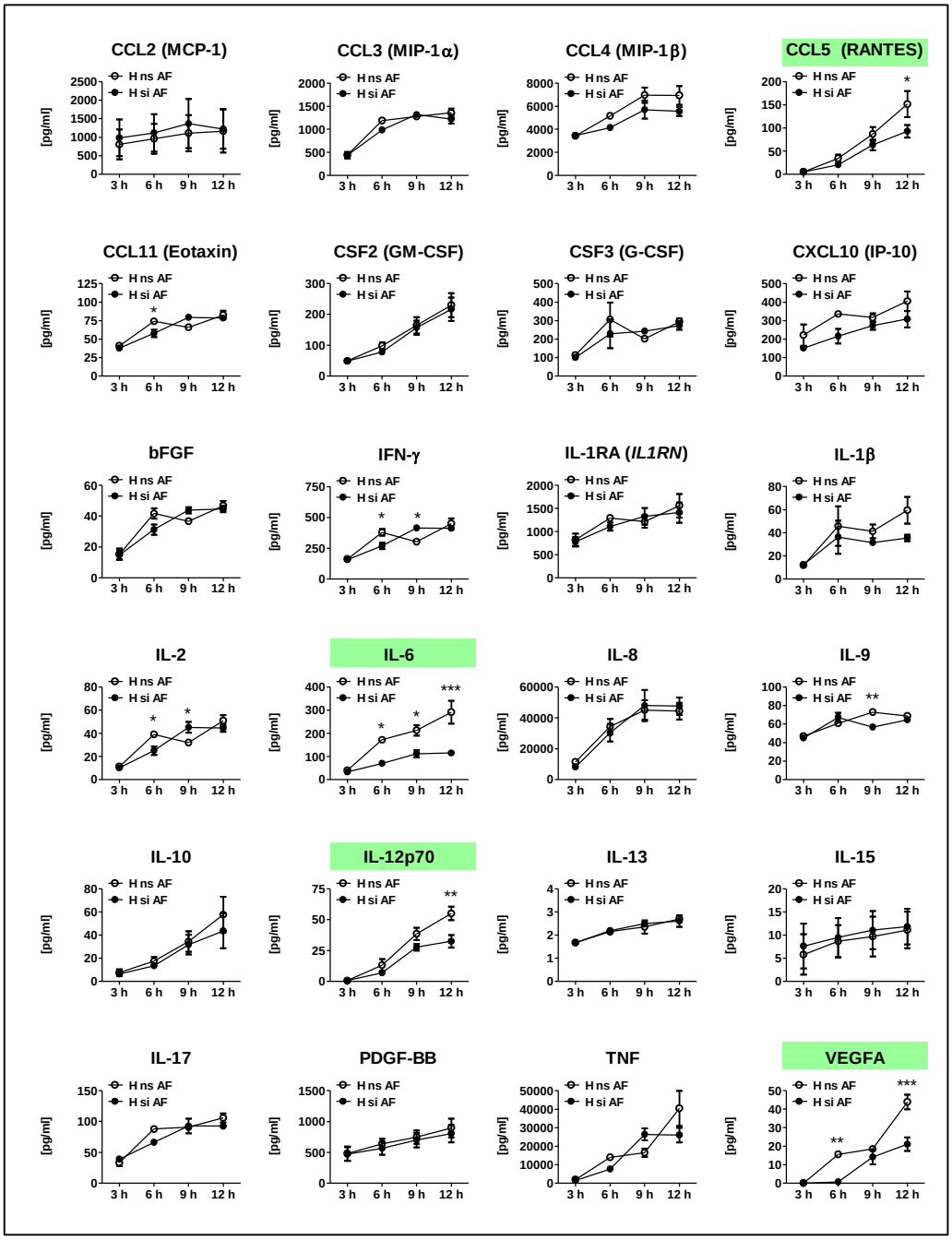

Figure 49 I HIF-1α modulates pro-inflammatory cytokine release from DCs stimulated with *A. fumigatus* under hypoxic (1 % O_2) conditions.

Control non-silencing siRNA (ns, white circles) or *HIF1A* silencing siRNA (si, black circles) was transfected into DCs using electroporation. 24 h after electroporation, DCs were stimulated with *A. fumigatus* and incubated under hypoxia (1 % O_2). Cytokines were quantified in cell culture supernatants after 3, 6, 9 and 12 h stimulation with *A. fumigatus* by a multiplex immunoassay. Data is shown as mean ± SEM of three independent experiments. Significant differences comparing HIF-1α silenced to non-silenced DCs at the respective time are indicated by asterisks (* $p < 0.05$; ** $p < 0.01$; *** $p < 0.001$; two-way repeated measures ANOVA followed by Bonferroni's multiple comparison test).

All in all, in human DCs interaction with *A. fumigatus* induced HIF-1α stabilization under normoxic and hypoxic conditions while *HIF1A* transcript levels remained unchanged. Under normoxia, expression of Dectin-1 on DCs was needed to stabilize the HIF-1α protein upon stimulation with *A. fumigatus*. Under hypoxia, this effect might be obscured by the hypoxia-induced HIF-1α stabilization. The analyses of the HIF-1α mediated transcriptomes by microarrays revealed a possible involvement of HIF-1α in the maturation of DCs under normoxia. Nonetheless, protein analyses revealed that DC maturation and T cell stimulation were independent of HIF-1α expression. On the other hand, an involvement of HIF-1α in metabolic activity and cytokine responses was predicted by the microarray analyses. This could be confirmed by functional downstream analyses. It should be noted that hypoxia itself had an inhibitory effect on the cytokine release from *A. fumigatus*-stimulated DCs. This was independent of expression of HIF-1α. Furthermore, HIF-1α silenced DCs showed similar viability compared to their non-silenced counterparts under hypoxia. Therefore, transcription factors apart from HIF-1α seem to be involved in adaption to hypoxia in human DCs. Nonetheless, *A. fumigatus*-induced HIF-1α contributed to cytokine release and enhanced glycolytic activity in DCs under normoxia and hypoxia. This is a novel aspect of the cellular function of HIF-1α in human DCs that to the best of our knowledge had not been described so far.

4 Discussion

This study analyzed the effect of hypoxia and the functional relevance of HIF-1α signaling on human DCs stimulated with *A. fumigatus.* Hypoxia attenuated the pro-inflammatory response of DCs against *A. fumigatus* during the initial infection, as revealed by genome-wide microarray expression analysis and quantification of the cytokine release upon *A. fumigatus* stimulation. In line with these findings, DCs matured through exposure to *A. fumigatus* under hypoxic conditions showed decreased expression of T cell stimulatory molecules in comparison to their normoxic counterparts. Surprisingly, these hypoxic DCs possessed an enhanced capacity to stimulate allogeneic T cells.

Moreover, this study revealed that HIF-1α is involved in the anti-*A. fumigatus* response in human DCs under both, normoxic and hypoxic conditions. Interestingly, HIF-1α silenced and non-silenced DCs showed similar viability under normoxic and hypoxic conditions, thus indicating that HIF-1α might not be the only factor responsible for adaption to low oxygen levels in DCs. Interaction with *A. fumigatus* stabilized HIF-1α in DCs under normoxia and hypoxia. The HIF-1α mediated transcriptomes (investigated by genome-wide mRNA microarrays) indicated involvement of HIF-1α in regulating metabolic activity and pro-inflammatory cytokine release in response to *A. fumigatus*. These microarray-based results could be confirmed by downstream protein and metabolite analyses. The HIF-1α mediated effects on the immune response were not restricted to hypoxic conditions.

4.1 Hypoxia influences the anti-*A. fumigatus* response of DCs

4.1.1 Differences in the 0.1 % O_2 and 1 % O_2/HIF-1α silenced microarray experiments

The first microarray experiment (0.1 % O_2) was performed to evaluate the influence of strong hypoxia on DCs stimulated with *A. fumigatus* and to guide further downstream analyses. Very strict oxygen limitations were applied to observe a strong phenotype. The major result was an altered metabolism of DCs stimulated with *A. fumigatus* under hypoxia, while an influence on other immune-relevant functions could not be determined. However, quantification of the cytokine release suggested an inhibitory effect of hypoxia (0.1 % and 1 % O_2). Grahl *et al.* demonstrated the presence of hypoxic areas in the lung of mice infected with *A. fumigatus* with oxygen levels ranging below 1.5 % O_2 [93]. Therefore, the second microarray experiment was performed under moderate hypoxia (1 % O_2) and in addition analyzed the function of HIF-1α. In this experiment, DCs were electroporated to transfect them with HIF-1α silencing siRNA. Analysis of the hypoxia-mediated transcriptome of these microarrays indicated that several immune-relevant DC functions are affected. DC metabolism, however, was not among the major predictions.

The most obvious difference when comparing the two microarray experiments are the different oxygen levels. Nevertheless, further analysis of the hypoxia-mediated effects on DC functions indicated similar effects of strong (0.1 % O_2) and moderate (1 % O_2) hypoxia. This included similar effects of hypoxia on DC maturation (Figure 26, p. 98) as well as on DC metabolic activity (Figure 28, p. 101). Therefore, the differences in the predictions based on the two microarray experiments are most likely not attributable to the different oxygen levels. One reason why metabolic pathways had not been predicted in the 1 % O_2/HIF-1α silenced microarray data analysis might have been an unspecific effect of the electroporation method on glycolytic activity in DCs. DCs that had not been electroporated generally showed higher glucose uptake and lactate release than DCs that had been electroporated (the effect can be recognized in the comparison of Figure 28, p. 101 with Figure 47, p. 130). Interestingly, similar results have been observed by

Jonathan Jantsch by comparing the glycolytic activity of electroporated vs. non-electroporated murine DCs (data not published, personal correspondence). Another difference was that the 0.1 % O_2 microarrays were analyzed in an unpaired analysis and the 1 % O_2/HIF-1α silenced microarrays in a paired analysis. The decision for paired or unpaired analyses was based on the PCA analyses, which had demonstrated a greater donor-dependent effect in the 1 % O_2/HIF-1α silenced compared to the 0.1 % O_2 microarrays (Figure 40, p. 116 and Figure 17, p. 77). These differences in the microarray raw data analyses led to differences in the significance of regulated genes. It should be taken into account that the direct comparison between the two microarray experiments is generally hampered by the fact that they were conducted independently, separated in time and with DCs derived from different blood donors. Importantly, downstream analyses that included metabolic and cytokine profiling of DCs could confirm the conclusions drawn from the 0.1 % O_2 as well as the 1 % O_2/HIF-1α silenced microarray experiments though.

4.1.2 Hypoxia: inhibitory or enhancing effects on DC functions?

Up to date, controversial data have been reported regarding the influence of hypoxia on DC functions, including cytokine release, maturation and their capacity to stimulate T cells. To the best of our knowledge, no data have been available so far regarding fungal pathogens and the stimulation of PRRs like Dectin-1 that recognize fungal PAMPs. Nonetheless, some studies have already investigated the effect of hypoxia on the LPS-induced activation of DCs.

Jantsch *et al.* investigated the influence of hypoxia (1 % O_2) on murine bone-marrow derived DCs stimulated with LPS [134]. They observed an increase in the release of IL-6 and TNF and enhanced expression of CD80, CD86 and MHC-II after LPS stimulation under hypoxic conditions. Furthermore, the capacity of these hypoxic DCs to stimulate allogeneic T cells was enhanced. HIF-1α was stabilized in unstimulated DCs under hypoxic conditions and in DCs stimulated with LPS under normoxic as well as hypoxic conditions. Knockdown of HIF-1α by RNAi impaired the up-regulation of CD86 under both, normoxia and hypoxia and reduced the capacity of these DCs to stimulate allogeneic T cells in an assay performed under normoxia. The authors provide evidence that HIF-1α mediated

control of glycolysis in DCs stimulated with LPS under normoxic and hypoxic conditions is responsible for the immune-enhancing effect of hypoxia and the reduced functions of HIF-1α silenced DCs under both, normoxia and hypoxia.

Using human monocyte-derived DCs, Mancino *et al.* reported an increase in the release of TNF and IL-1β but a decrease in IL-10 after stimulation with LPS under hypoxic conditions (1 % O_2) [137]. On the other hand, these DCs showed reduced up-regulation of the maturation markers CD40, CD80, CD83, CD86 and MHC-II and in line with these observations, a reduced capacity to stimulate allogeneic T cells. CCR7 was reduced under hypoxic conditions as well. The authors conclude that hypoxic microenvironments promote an inflammatory DC phenotype by enhancing the release of pro-inflammatory cytokines. Simultaneously, hypoxia inhibits DC functions linked to activation of adaptive immunity by preventing full DC maturation, homing to the lymph node and T cell activation. The authors argue that the inflammatory phenotype of hypoxic DCs is in line with the activation of HIF-1α under hypoxic conditions. They refer to the study published by Cramer *et al.* which demonstrates that HIF-1α is crucial in promoting inflammatory functions of myeloid cells by mediating metabolic adaption under hypoxia [121]. Furthermore, Mancino *et al.* speculate that the reduced DC maturation under hypoxic conditions could be mediated via HIF-1α-induced VEGFA, a factor that might impair DC maturation. However, they did not further analyze the functional relevance of HIF-1α or VEGFA expression and release in hypoxic DCs.

In the present study, the cytokine release and the up-regulation of T cell (co-) stimulatory molecules was reduced under hypoxia. However, DCs that had been matured through exposure to *A. fumigatus* under hypoxic conditions possessed a greater capacity to stimulate allogeneic T cells (Figure 27, p. 99). The T cell activation assay was performed under normoxic conditions as described by Mancino *et al.* and Jantsch *et al.* [134, 137]. This study indicates that hypoxia (at the site of infection) prevents full activation and maturation of DCs, but once these DCs have moved away from the hypoxic area, they possess a greater capacity to stimulate T cells.

Differences between the human and the murine immune system may explain the different effects of hypoxia on the activation and function of DCs. Murine bone-marrow derived DCs as well as human monocyte-derived DCs both comprise well established

model systems to study DC functions *in vitro*; however, *in vivo*, DCs are heterogeneous and comprised of various sub-populations [63]. These sub-populations again differ comparing the human and the murine system [149]. In line with this argumentation, regarding the effect of hypoxia on DC activation and function, the data in the present study are more similar to the data published for human DCs by Mancino *et al.* [137] compared to murine DCs as described by Jantsch *et al.* [134]. Several protocols for the generation of human monocyte-derived DCs exist, but use of IL-4 in combination with GM-CSF is the most widely applied method. It is very well published and also used in commercially available kits for DC generation. However, Mancino *et al.* decided to use a combination of IL-13 and GM-CSF for the generation of DCs, and these differences may explain the different effects of hypoxia on human DC functions compared to the ones found in this study.

Another important aspect that should be considered is the use of LPS, a TLR4 ligand, and *A. fumigatus,* which activates mainly Dectin-1 signaling. In this study, hypoxia had similar inhibitory effects on the expression of maturation markers following stimulation of DCs with zymosan (TLR2/Dectin-1), LPS (TLR4/TLR2) and *A. fumigatus* (Figure 26, p. 98). Nonetheless, differences in the downstream signaling pathways induced upon TLR or CLR activation may fine-tune DC responses and hypoxia may exert different modulating effects. As the focus of this study was on *A. fumigatus* as a fungal pathogen, no comprehensive comparison between zymosan/LPS and *A. fumigatus* stimulation has been performed. To this point, the differences of hypoxia on DC functions when comparing this and other studies [134, 137] cannot be fully explained. The variation in results may be due to differences in stimuli (pathogen or isolated PRR ligand), the model system (murine or human DCs) and the experimental conditions. Likely, the differences in the studies' results reflect complex effects of hypoxia on DC functions that may be dependent on various factors and signaling pathways that yet remain to be fully understood.

4.1.3 Hypoxia-mediated transcriptional changes in DCs

4.1.3.1 Possible involvement of STAT3 in the hypoxia-mediated phenotype

In the present study, transcriptome analyses revealed the transcription factor STAT3 as a possible mediator of the hypoxic phenotype of DCs stimulated with *A. fumigatus* (Figure 23, p. 91). The activity of STAT3 is controlled by the availability of cytokines and growth factors, including IL-6. IL-6 induces STAT3 activation via binding to the membrane-bound or soluble IL-6 receptor. This binding induces homodimerzation of the IL-6 signal transducer, the gp130 receptor (encoded by *IL6ST*). This in turn activates the tyrosine kinase JAK1, which phosphorylates STAT3. Phosphorylated STAT3 forms homodimers that translocate to the nucleus and bind to STAT3-binding elements on STAT3 target gene promotors to activate transcription [147, 150]. Among the STAT3 target genes are *CCL2*, *CCL5*, *CXCL10*, *IL12A*, *IL1B* and *IL8*, the co-stimulatory molecule *CD80* as well as the STAT3 activators *IL6*, *IL10* and *IL17A*, which in turn further activate STAT3 via an autocrine loop [151]. There are several indicators that support altered STAT3 signaling in DCs stimulated with *A. fumigatus* under hypoxia compared to normoxia: reduced levels of IL-6 in the supernatant (Figure 24, p. 93), down-regulation of *IL6ST* (Figure 22, p. 89) and down-regulation of STAT3 target genes (Figure 23, p. 91) accompanied by reduced levels of STAT3 target cytokines (Figure 25, p. 95) in DC culture supernatants.

In solid tumors, hypoxia is a common microenvironment. Interestingly, STAT3 is activated in several tumor cell lines under hypoxia, acting as an oncogene and modulating HIF-1α signaling [152, 153]. Furthermore, it was found that STAT3 cooperates with HIF-1α in the activation of hypoxia-inducible target genes in breast cancer and renal carcinoma cell lines [154]. The study discussed in the previous paragraph by Mancino *et al.* recognized a possible importance of STAT3 signaling in LPS-stimulated DCs in hypoxic microenvironments via cross-talk with hypoxia-induced HIF-1α [137]. However, the authors ruled out the involvement of STAT3 signaling in mediating the hypoxic phenotype of LPS-matured DCs as they did not observe enhanced phospho-STAT3 levels in these DCs.

Overall, the role of STAT3 for DC maturation and function is controversially discussed. Using a conditional hematopoietic knockout mouse model of STAT3, it was shown that DCs from these knockout mice express higher levels of MHC-II, secrete more

IL-12p70, IL-10, and TNF and are better antigen presenters compared to DCs from wild-type mice [155]. STAT3 silenced human monocyte-derived DCs have an enhanced ability to prime IFNγ production by both αβ and γδ T cells. In contrast to the murine model [155], this effect does not seem to be mediated by altered expression of T cell (co-) stimulatory molecules but by an altered cytokine secretion profile, characterized by lower IL-10 and higher IL-12 and TNF levels [156]. In contrast to this data obtained for RNAi treated DCs, chemical inhibition of STAT3 using JSI-124 (cucurbitacin I) leads to increased expression of T cell co-stimulatory molecules and increased activation of allogeneic T cells by human monocyte-derived DCs. This effect seemed to be dependent on increased expression of co-stimulatory molecules rather than altered cytokine release from these DCs [157].

Taken all this literature into account, there seems to be a stronger evidence for an immunosuppressive role of STAT3 in DCs rather than the promotion of pro-inflammatory immune responses. Therefore, if STAT3 activity is inhibited under hypoxic conditions (as predicted in the present study by the microarray data analyses), an enhancing rather than diminishing effect on the DC immune response would be expected. However, the above discussed studies were performed under standard cell culture conditions (normoxia), which hampers the comparison with the present study. Taken together, the relevance of STAT3 in the hypoxia-mediated phenotype of *A. fumigatus*-stimulated DCs remains to be fully elucidated.

4.1.3.2 Hypoxia may control gene regulation in DCs by miRNAs

A relatively new aspect of gene regulation under hypoxia is the control of mRNA transcript expression by the so-called hypoxamirs. These are microRNAs (miRNAs) which are up- or down-regulated under hypoxic conditions [158]. In principle, miRNAs are short, noncoding RNAs and function similar to siRNAs. They regulate gene expression by posttranscriptional mechanisms, including target mRNA degradation or inhibition of translation. In contrast to siRNAs, which are specific to one target sequence, miRNAs do not exclusively bind base-pair specific but can inhibit the translation of many different mRNAs with similar sequences [159]. Several hypoxamirs are already known in the literature [158]. Among them are several miRNAs that are known to be involved in inflammatory responses. For example, miR-146a,b is up-regulated under hypoxic

conditions and has anti-inflammatory effects [160, 161]. Furthermore, miR-155, which is induced under hypoxic conditions, antagonizes HIF-1α mediated effects by targeting *HIF1A* mRNA [162]. This is of special interest as miR-155 was recently reported by our group to be up-regulated in human DCs stimulated with *A. fumigatus* [163].

In conclusion, complex regulatory networks that act on multiple levels could be responsible for the hypoxia mediated changes in the transcriptome of *A. fumigatus*-stimulated human DCs. The large scale genomics datasets provided in this study are a basis for the further elucidation of these signaling networks.

4.2 Role of HIF-1α in anti-*A. fumigatus* DC responses

4.2.1 Stabilization of HIF-1α in response to *A. fumigatus*

Stabilization of HIF-1α occurs in a range of infectious diseases [164] and has also been observed in human DCs stimulated with various TLR ligands [136]. This is the first study to show that interactions with *A. fumigatus* can stabilize the HIF-1α protein in human DCs, even under normoxic conditions (Figure 31, p. 105). In addition, this study confirms the stabilization of HIF-1α in human macrophages following stimulation with *A. fumigatus* [130]. Dectin-1 is the major recognition receptor for *A. fumigatus* on human DCs [69] and stimulation with *A. fumigatus* as well as with depleted zymosan, a specific Dectin-1 ligand, could both induce HIF-1α in DCs as well as macrophages. The HIF-1α levels were lower compared to stimulation of TLR4 (ultrapure LPS) or combined stimulation of TLR2 and TLR4 (LPS) or TLR2 and Dectin-1 (zymosan) (Figure 31, p. 105). This study therefore revealed distinct HIF-1α activation patterns in human DCs and macrophages following TLR or Dectin-1 stimulation. Differences in the signal transduction pathways induced upon TLR or Dectin-1 activation [165] may influence the extent of HIF-1α stabilization in human DCs and macrophages. This in turn may contribute to different immune responses of these cells against bacterial and fungal stimuli. It is important to note that normoxic stabilization of HIF-1α following stimulation of human DCs with *A. fumigatus* or with the Dectin-1 specific ligand depleted zymosan was dependent on Dectin-1 expression (Figure 34, p. 109). This indicates a relationship between Dectin-1/CLR signaling and HIF-1α activation in human DCs. To the best of our knowledge, this connection had not been described previously.

The pathways leading to pathogen-induced HIF-1α stabilization in immune cells are not fully understood yet. In general, *HIF1A* mRNA is steadily expressed in mammalian cells but the HIF-1α protein is only stabilized when required, otherwise it is rapidly degraded [107]. The best characterized degradation mechanism is controlled by oxygen-dependent prolyl hydroxylases, mediating oxygen-dependent regulation of HIF-1α protein levels in most mammalian cells (see paragraph 1.3.3, p. 32). In immune cells, however, enhancement of *HIF1A* mRNA levels following TLR stimulation seems to display an

additional mechanism to stabilize the HIF-1α protein. Rius *et al.* demonstrated in an *in vivo* model that NF-κB is a transcriptional activator of *HIF1A* mRNA in murine macrophages responding to bacterial infections [128]. Jantsch *et al.* confirmed this data for murine DCs stimulated with LPS and provide data indicating that TLR stimulation enhances *HIF1A* transcript expression and induces HIF-1α protein under normoxic and hypoxic conditions [134]. Similar results are published by Frede *et al.* using primary human monocytes and the human monocytic cell line THP-1 [129].

However, in the present study, *HIF1A* mRNA levels could only partially explain HIF-1α protein stabilization in DCs and macrophages. Following TLR2 and/or TLR4 stimulation under normoxia, increased *HIF1A* mRNA levels have been observed (Figure 32, p. 106). On the other hand, stimulation of DCs and macrophages with the Dectin-1-specific ligand depleted zymosan or with *A. fumigatus* did not increase *HIF1A* mRNA levels under normoxia, although the HIF-1α protein was stabilized. As pointed out in a review by Kuschel *et al.*, non-hypoxic stimuli may have an effect on HIF-1α on multiple levels, including transcription, translation, protein stability and transactivation; therefore, it is likely that stabilization of HIF-1α protein following immune cell stimulation is a multi-process mechanism [166]. Recently, a TLR-mediated mechanism leading to stabilization of HIF-1α by mechanisms other than transcriptional enhancement has been described by Tannahill *et al.* [167]. In murine macrophages, LPS increases intracellular succinate levels, leading to HIF-1α stabilization which in turn increases expression of *Il1b* [167]. Furthermore, in cells infected with the intracellular Gram-negative bacteria *C. trachomatis*, HIF-1α is stabilized on the protein level, an important mechanism for the pathogen to protect its host cell from apoptosis. Thereby, HIF-1α mRNA levels remain unchanged, and stabilization of HIF-1α is dependent on MEK/ERK signaling [168].

Hypoxic microenvironments that arise during an infection have an influence on HIF-1α protein stability as well. Dissecting the molecular mechanisms responsible for HIF-1α stabilization under the combination of both “stimuli”, hypoxia and PRR ligands, seems to be even more complex. In this study, *HIF1A* mRNA levels were strongly down-regulated in control cells under hypoxia, accompanied by a stabilization of the HIF-1α protein, thus suggesting a possible negative feedback mechanism (Figure 32, p. 106). However, in DCs as well as macrophages stimulated with either PRR ligands or *A. fumigatus* under hypoxia, *HIF1A* mRNA levels remained on the baseline. This indicates

that stimulation under hypoxia might inhibit the hypoxia-mediated down-regulation of the *HIF1A* transcript and may explain enhanced HIF-1α protein levels when comparing control to stimulated immune cells under hypoxic conditions (Figure 31, p. 105). In murine DCs similar effects were observed regarding the down-regulation of *HIF1A* mRNA under hypoxia [134]. To date, the exact mechanisms leading to HIF-1α stabilization in human DCs (and macrophages) in response to *A. fumigatus* under normoxia or hypoxia remain to be characterized.

4.2.2 The HIF-1α mediated transcriptomes under normoxia and hypoxia

Downstream of Dectin-1, NF-κB is activated as a central transcription factor for both innate and adaptive immune responses [165]. From bacterial infection models, it is known that pathogen-induced HIF-1α contributes to NF-κB signaling [169] and that cross-talk between NF-κB and HIF-1α links cellular responses during hypoxia and bacterial infection [128]. The expression of NF-κB inducible cytokines were influenced by HIF-1α knockdown in human DCs stimulated with *A. fumigatus* under normoxic and hypoxic conditions, indicating NF-κB/HIF-1α cross-talk during *A. fumigatus* infection (Figure 42, p. 121). In murine DCs, under normoxic conditions, LPS-induced HIF-1α cooperates with NF-κB and enhances the expression of TLR-induced, HIF-1α dependent genes including *Ptgs2* (encoding the cyclooxygenase 2) and *Nos2* (encoding the inducible nitric oxide synthase 2) [169]. Hypoxia in the infection microenvironment also contributes to HIF-1α dependent gene expression. Thereby, the genes transactivated by HIF-1α differ depending on whether HIF-1α is induced by LPS under normoxic conditions, or under hypoxic control conditions, or under a combination of both, hypoxia and LPS-stimulation [169].

The HIF-1α mediated transcriptomes suggested cross-talk between HIF-1α and additional transcription factors besides NF-κB, namely EGR1 and EGR3 under normoxic and NFAT5 under hypoxic conditions (Figure 42). Goodridge *et al.* demonstrated that EGR1 and EGR3 are activated via the Dectin-1 pathway in murine macrophages and DCs [170]. Nevertheless, the biological relevance of Dectin-1 induced EGR remained unclear. NFAT5 was recently identified by Buxade *et al.* as a regulator of mammalian anti-pathogen responses and proved to be necessary for an effective *in vivo* response against

Leishmania major [171]. Thereby, Buxade *et al.* were the first to demonstrate an additional function of NFAT5 besides its role as an osmostress responsive factor. In their study, murine NFAT5 knockout macrophages showed reduced release of TNF and IL-6 upon bacterial stimulation. This indicated that NFAT5 contributes to the release of pro-inflammatory cytokines. In HIF-1α silenced DCs stimulated with *A. fumigatus*, however, NFAT5 expression was increased while release of TNF and IL-6 were reduced. Therefore, the functional relevance of NFAT5 up-regulation in HIF-1α silenced DCs stimulated with *A. fumigatus* that has been observed in the present study remains unclear.

As discussed above, hypoxia in the infection microenvironment contributes to differential HIF-1α dependent gene expression [169]. In the present study, however, the transcriptome-based predictions of the immunological functions of HIF-1α activation following interaction with *A. fumigatus* were similar under normoxic as well as hypoxic conditions and included regulation of metabolic activity and cytokine release (Figure 42, p. 121). This indicates that HIF-1α stabilization in human DCs following stimulation with *A. fumigatus* has a functional relevance that is independent of the oxygen level in the infection microenvironment.

4.2.3 Influence of HIF-1α on DC functions

4.2.3.1 HIF-1α and DC metabolism

One function of HIF-1α under hypoxic as well as normoxic conditions was to increase glycolysis in DCs during encounter with *A. fumigatus* (Figure 47, p. 130). This study is the first to show HIF-1α mediated regulation of metabolic activity in human DCs following fungal stimulation. In the context of bacterial infection or TLR-activation on DCs, the functional importance of HIF-1α mediated glycolytic activity for immune responses of DCs and other myeloid cells have already been described. TLR-induced DC activation is accompanied by rapid enhancement of glycolysis and this modification of cellular metabolism can influence innate and adaptive immune responses [172]. Cramer *et al.* demonstrated that HIF-1α regulates glycolysis in murine neutrophils and macrophages and that this function makes HIF-1α essential for a proper immune response in an inflammatory mouse model [121].

In murine DCs stimulated with LPS, HIF-1α silencing reduced glycolytic activity and thereby significantly impaired the release of pro-inflammatory cytokines, DC maturation and the capacity of DCs to activate T cells [134]. These findings are in contrast to the present study, where DC maturation and T cell stimulation was independent on HIF-1α expression in DCs (Figure 45, p. 128 and Figure 46, p. 129). However, data from this study are in line with data published for human DCs. Spirig *et al.* investigated whether HIF-1α stabilization is of functional importance for the maturation of human monocyte-derived DCs. The authors demonstrate that DC maturation induced via LPS, hyaluronic acid (an endogenous TLR4 ligand) or lipoteichoic acid (a TLR2 ligand) is accompanied by a time-dependent stabilization of the HIF-1α protein under normoxic conditions. However, without TLR stimulation, HIF-1α stabilization through either hypoxia (1.5 % O_2) or $CoCl_2$ did not alter the maturation status of DCs. Furthermore, DC maturation was independent of HIF-1α as three different chemical inhibitors of HIF-1α (chetomin, digoxin and YC-1) did neither show an effect on DC maturation nor on cytokine release [136]. Taken together, the functional relevance of HIF-1α mediated control of DC metabolism after stimulation with *A. fumigatus* remains to be elucidated.

4.2.3.2 HIF-1α and DC cytokine release

In this study, HIF-1α knockdown resulted in a reduced release of specific cytokines from DCs stimulated with *A. fumigatus*. This was observed when comparing HIF-1α silenced to non-silenced DCs under normoxic (Figure 48, p. 132) as well as hypoxic (Figure 49, p. 133) conditions. DCs contribute to the antifungal immune response by release of cytokines, including IL-1β, IL-6, IL-12p70 and CCL5 [30, 173-175]. These cytokines displayed reduced levels in HIF-1α silenced DCs stimulated with *A. fumigatus* under normoxic as well as hypoxic conditions. This suggests that HIF-1α contributes to the pro-inflammatory cytokine release that is induced in DCs upon stimulation with *A. fumigatus*. These findings underline the importance of HIF-1α for the ability of human DCs to mount a strong anti-*A. fumigatus* response.

One might speculate that the reduced release of the cytokines is a consequence of reduced glycolytic activity in HIF-1α silenced DCs. However, while enhanced glycolytic activity is needed during initial DC activation, two temporally distinct waves in glycolytic metabolism seem to exist in DCs [172]. Currently, HIF-1α is thought to control the second

signaling pathway that is needed to sustain high glycolytic rates in mature DCs, while the initial enhancement of glycolysis during DC activation occurs independent of HIF-1α [172]. Therefore, the HIF-1α mediated pathways leading to reduced cytokine release shortly after pathogen contact may differ from the HIF-1α mediated pathways that lead to enhanced glycolysis in DCs.

The role of HIF-1α signaling for host immune responses against *A. fumigatus* has only recently begun to be explored. Using immune competent mice with a conditional HIF-1α knockout in neutrophils and macrophages, it has recently been shown that HIF-1α expression in these immune cells is required for survival after pulmonary challenge with *A. fumigatus* [130]. In these mice, the HIF-1α knockdown does not impair fungal conidial killing by neutrophils and macrophages, as had been expected from bacterial infection models [121]. On the contrary, lack of HIF-1α leads to decreased production of the chemokine CXCL1 and increased neutrophil apoptosis during an *A. fumigatus* infection. The present study in human DCs complements and extends the findings in the murine model and strengthens the hypothesis that HIF-1α is a crucial regulator of the pro-inflammatory cytokine release during an *A. fumigatus* infection.

It should be mentioned that hypoxia itself also had an inhibitory effect on cytokine release (Figure 25, p. 95). This inhibitory effect was independent of HIF-1α expression. As discussed above, different transcription factors determine the activation and function of DCs, including a complex signaling network involving HIF-1α, NF-κB and STAT3 and possibly other transcription factors like EGRs or NFAT5 or hypoxia-induced miRNAs. The transcriptional profiles provided in this study may form the platform for further, sophisticated bioinformatics analysis to explore these networks in the context of *A. fumigatus* stimulated DCs under normoxic and hypoxic conditions.

4.3 Clinical relevance

4.3.1 Comparability of *in vitro* studies with *in vivo* physiological and pathophysiological environments

This project started to investigate the impact of hypoxia on the response of DCs against *A. fumigatus*. For the first set of experiments, very strict oxygen limitations were applied (0.1 % O_2) for culture times of up to 24 h. The reason for this was to obtain a strong phenotype as a basis for further experiments. It is difficult to determine actual oxygen levels *in vivo*; however, in similar studies with an infection-immunology background researchers often defined 1 % O_2 as hypoxic condition, while more strict oxygen limitations around 0.1 % O_2 were applied in studies investigating tumor-immunology (reviewed in [138]). A study published by Grahl *et al.* in 2011 visualized hypoxic areas in the *A. fumigatus* infected murine lung by injection of 2-nitroimidazol derivatives (Figure 8, p. 30 and [93]). This method marks areas with oxygen levels below 1.3 % O_2. Follow-up experiments for the present study were therefore performed under 1 % O_2 as a moderate hypoxic culture condition which most likely represents the level of oxygen experienced by immune cells during an *A. fumigatus* infection.

One very important point that is often neglected or misunderstood in tissue culture studies is the fact that the air that surrounds us and fills normal cell culture incubators contains far more oxygen than most cells of the human body would normally encounter *in vivo*. In spite of this fact, 21 % O_2 is usually considered as the normal oxygen level and referred to as “normoxia” in most literature [176]. *In vivo*, physiological oxygen levels range between 3 and 15 %, depending on the tissue. It is very difficult to measure actual oxygen levels *in vivo*, and cell culture models have to be standardized to obtain reliable and comparable results; however, regarding the oxygen level they poorly mimic the physiological *in vivo* situation. This has to be taken into consideration when interpreting results from comparative “normoxia” vs. hypoxia studies.

Together with other studies, this project provides insight how much *in vivo* microenvironmental factors change the response of immune cells in comparison to standard *in vitro* experiments. Besides hypoxia, such microenvironmental factors during

infection with *A. fumigatus* could be nutrient availability, hyperthermia (due to changes of the host's body temperature) or the presence of drugs. To give an example, we previously reported that hyperthermia enhances maturation of DCs that had been stimulated with *A. fumigatus* while the cytokine profile of these DCs remained unaffected [177]. Therefore, hyperthermia may be a useful adjuvant in the generation of DCs for therapeutic approaches to boost the activation and function of DCs targeted against *A. fumigatus*. The effects of microenvironmental factors, such as hypoxia or hyperthermia, on relevant aspects of the anti-*A. fumigatus* DC response may influence the outcome of an infection *in vivo*. Therefore, this study points out the crucial relevance to consider microenvironmental factors such as hypoxia in the translation of cell-culture based results to the *in vivo* situation in the host as well as in the *in vitro* development of cellular antifungal immunotherapies.

4.3.2 Therapeutic potential of strategies targeting oxygen levels and HIF-1α expression in the context of IA

In light of the results of the present study which demonstrated an inhibitory effect of hypoxia on DC functions, it would be interesting to investigate *in vivo* whether enhancing oxygen levels, for example via use of hyperbaric oxygen, would change the outcome of IA, the most severe infection with *A. fumigatus* in immunocompromised patients [178]. Minimizing hypoxic microenvironments at the site of infection could have an impact upon both, the host immune response and the fungus. As DCs response with a more pronounced cytokine release upon stimulation with *A. fumigatus* under normoxic conditions, enhancing oxygen levels may promote a stronger pro-inflammatory response. Up to date, the effect of oxygen levels on the growth of *A. fumigatus* is unclear. *In vitro*, hypoxia (1 % O_2) limits fungal metabolism and growth [106]. Therefore, the supply of oxygen may promote fungal growth in the host. Hyphae grown under hypoxic conditions, however, have an increased β-glucan content in their cell wall. This increase in the fungal cell wall component that is the ligand for Dectin-1 enhances the activation of macrophages, thereby enhancing anti-fungal immunity against hypoxia-grown hyphae [106]. However, the enhanced activity of macrophages against hypoxia-grown hyphae has only been demonstrated in experiments performed under normoxia [106]. Therefore, it remained unclear whether hypoxia had any effects on macrophages in this experiment.

Another aspect to consider is that hypoxia seems to occur *in vivo* at late stages of *A. fumigauts* infections concomitant with massive hyphal growth and severe tissue damage accompanied by massive inflammation [179]. A further enhancement of the immune response by the supply of oxygen may lead to more tissue damage and this might not be beneficial at this stage of the infection. Therefore, a reduced activation of DCs under hypoxic conditions as revealed in the present study may be beneficial for the host to prevent further excessive inflammation. To make the picture even more complex, Hsu *et al.* demonstrated in 2013 that in a murine lung transplant model, *A. fumigatus* shows a growth tropism into ischemic areas of the graft and that invasiveness of the fungal infection increases with growing hypoxic microenvironments [180]. These results seemed to be mediated by hypoxia-induced changes in *A. fumigatus* and not in host cells. Taken together, the therapeutic potential of manipulating oxygen levels during IA is a multi-facetted question that should be investigated in a suitable *in vivo* model.

The present study also provides initial answers to the fundamental question whether HIF-1α is a suitable target to boost host defense against *A. fumigatus*. In a study by Zinkernagel *et al.* use of the HIF-1α agonist mimosine decreased the size of skin lesions in mice following infection with *S. aureus*. Thereby, this study was one of the first to demonstrate that pharmacologically augmenting the host phagocytic function by HIF-1α targeting strategies is effective in the treatment of bacterial infections [181]. Data from this study demonstrate that HIF-1α contributes to cytokine release in DCs upon stimulation with *A. fumigatus* under both, normoxic and hypoxic conditions. Therefore, therapeutic strategies leading to HIF-1α stabilization in DCs may support the immune response towards the fungus. However, in cases were pathology of IA is driven by an overactive immune response (as discussed above), induction of HIF-1α might have disadvantageous effects.

Furthermore, it is not clear whether pharmacological-activated HIF-1α has similar effects compared to pathogen-activated HIF-1α and whether it contributes to the expression of immune-relevant genes. The above discussed study by Jantsch *et al.* clearly showed differential HIF-1α dependent gene expression following stabilization of HIF-1α via TLRs or hypoxia (see paragraph 4.2.2, p. 145 ff. and [169]). In the present study, $CoCl_2$ was used in confirmatory experiments to stabilize HIF-1α under normoxic conditions. This stabilization, however, did not induce cytokine release from DCs (data not shown). These

data are in line with the study by Spirig *et al.* who did not observe DC maturation or cytokine release following the treatment of human monocyte-derived DCs with $CoCl_2$ or the cultivation under hypoxia [136]. In general, most of the chemicals or drugs which stabilize HIF-1α target the oxygen-dependent enzymes that mediate HIF-1α degradation under normoxic conditions. Therefore, these HIF-1α stabilizers are often referred to as hypoxia-mimetics, because the mechanism of stabilization is similar to the process under hypoxic conditions. Furthermore, pharmacological targeting of HIF-1α is not restricted to a specific cell type as HIF-1α is ubiquitously expressed in virtually all body cells. Therefore, unwanted side effects could easily occur [139]. To sum it up, it remains to be investigated how these drugs may alter immune responses against *A. fumigatus in vitro* and *in vivo*.

4.4 Conclusion and perspective

This study revealed a divergent influence of hypoxia on anti-*A. fumigatus* DC functions. It included both, immune suppressing and enhancing effects. Bacterial induced DC activation under hypoxia had already been investigated in previous studies, nonetheless, the results are very divers. The overall picture of the influence of hypoxia on DC functions remains to be fully elucidated and understood. The involvement of HIF-1α in the anti-*A. fumigatus* response initiated by human DCs is a novel aspect revealed in this study. The function of HIF-1α was similar comparing normoxic and hypoxic culture conditions and included enhancing the metabolic response and cytokine release upon *A. fumigatus* encounter. Figure 50 summarizes the effects of hypoxia and HIF-1α signaling on the anti-*A. fumigatus* immune response initiated by human DCs that were revealed in this study.

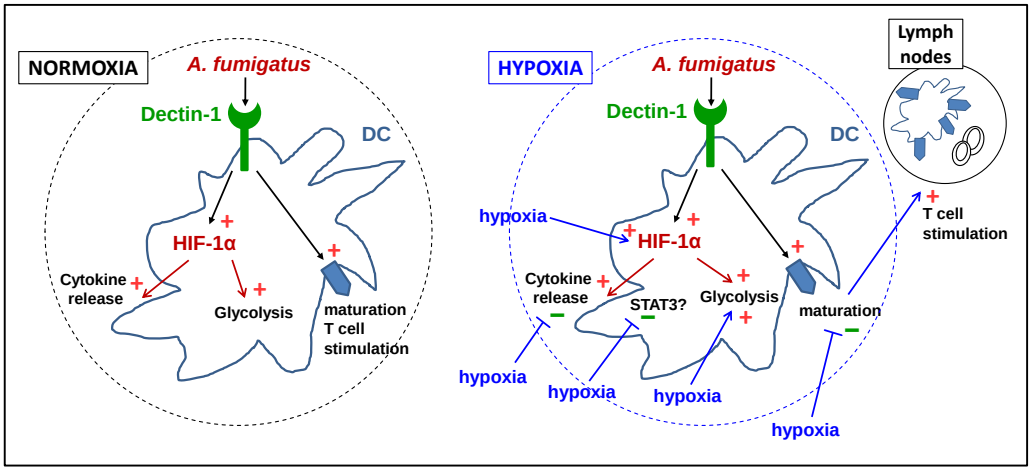

Figure 50 I Graphical summary of hypoxia and HIF-1α mediated effects on the functions of human DCs stimulated with *A. fumigatus*.

Interaction with *A. fumigatus* induces HIF-1α stabilization under normoxia (right) and hypoxia (left) in human DCs. Under normoxic conditions, expression of Dectin-1 is required to stabilize the HIF-1α protein upon stimulation with *A. fumigatus*. *A. fumigatus*-induced HIF-1α contributes to cytokine release and enhances glycolytic activity in DCs under normoxia and hypoxia. DC maturation and T cell stimulation are independent of HIF-1α expression under both conditions. Hypoxia enhances HIF-1α stabilization in *A. fumigatus*-stimulated DCs (right). Furthermore, hypoxia has an inhibitory effect on cytokine release and maturation but enhances glycolytic activity in *A. fumigatus*-stimulated DCs. This effect was independent of HIF-1α expression. Surprisingly, DCs that had been stimulated with *A. fumigatus* under hypoxic conditions show an enhanced capacity to stimulate T cells. Red arrows, influence of HIF-1α; blue arrows, influence of hypoxia.

The relevance of hypoxic microenvironments and the possible involvement of HIF-1α signaling in immune responses during *A. fumigatus* infections have only recently begun to be recognized and explored. Shepardson *et al.* demonstrated the requirement of HIF-1α expression in murine macrophages and neutrophils for the survival of otherwise immune competent mice after pulmonary infection with *A. fumigatus* conidia [130]. To the best of our knowledge, this study is the first to demonstrate that hypoxia and HIF-1α signaling have an impact on the response of human DCs towards *A. fumigatus*. The microarray datasets generated in this study are a platform for further investigations to understand the complex interplay between hypoxia, activation of PRRs and HIF-1α signaling in host responses against *A. fumigatus*. This study complements previous reports that demonstrated functional importance of HIF-1α in murine phagocytes in the context of bacterial and fungal infection. Detailed knowledge of the biological activities of HIF-1α is indispensable to further explore the therapeutic potential of this important signaling molecule in the context of IA and fungal infections in general.

References

1. Brown, G.D. and M.G. Netea, *Exciting developments in the immunology of fungal infections.* Cell Host Microbe, 2012. **11**(5): p. 422-4.
2. McCormick, A., J. Loeffler, and F. Ebel, *Aspergillus fumigatus: contours of an opportunistic human pathogen.* Cell Microbiol, 2010. **12**(11): p. 1535-43.
3. Lass-Florl, C., *The changing face of epidemiology of invasive fungal disease in Europe.* Mycoses, 2009. **52**(3): p. 197-205.
4. Brown, G.D., et al., *Hidden killers: human fungal infections.* Sci Transl Med, 2012. **4**(165): p. 165rv13.
5. Park, S.J. and B. Mehrad, *Innate immunity to Aspergillus species.* Clin Microbiol Rev, 2009. **22**(4): p. 535-51.
6. Latge, J.P., *Aspergillus fumigatus and aspergillosis.* Clin Microbiol Rev, 1999. **12**(2): p. 310-50.
7. Mayr, A. and C. Lass-Florl, *Epidemiology and antifungal resistance in invasive Aspergillosis according to primary disease: review of the literature.* Eur J Med Res, 2011. **16**(4): p. 153-7.
8. Dagenais, T.R. and N.P. Keller, *Pathogenesis of Aspergillus fumigatus in Invasive Aspergillosis.* Clin Microbiol Rev, 2009. **22**(3): p. 447-65.
9. Millner, P.D., et al., *Occurrence of Aspergillus fumigatus during composting of sewage sludge.* Appl Environ Microbiol, 1977. **34**(6): p. 765-72.
10. O'Gorman, C.M., H. Fuller, and P.S. Dyer, *Discovery of a sexual cycle in the opportunistic fungal pathogen Aspergillus fumigatus.* Nature, 2009. **457**(7228): p. 471-4.
11. Zmeili, O.S. and A.O. Soubani, *Pulmonary aspergillosis: a clinical update.* QJM, 2007. **100**(6): p. 317-34.
12. Cornillet, A., et al., *Comparison of epidemiological, clinical, and biological features of invasive aspergillosis in neutropenic and nonneutropenic patients: a 6-year survey.* Clin Infect Dis, 2006. **43**(5): p. 577-84.
13. Cornely, O.A., et al., *Primary prophylaxis of invasive fungal infections in patients with hematologic malignancies. Recommendations of the Infectious Diseases Working Party of the German Society for Haematology and Oncology.* Haematologica, 2009. **94**(1): p. 113-22.
14. Chotirmall, S.H., et al., *Aspergillus-associated airway disease, inflammation, and the innate immune response.* Biomed Res Int, 2013. **2013**: p. 723129.
15. Aimanianda, V., et al., *Surface hydrophobin prevents immune recognition of airborne fungal spores.* Nature, 2009. **460**(7259): p. 1117-21.
16. Morton, C.O., et al., *Direct interaction studies between Aspergillus fumigatus and human immune cells; what have we learned about pathogenicity and host immunity?* Front Microbiol, 2012. **3**: p. 413.
17. Gersuk, G.M., et al., *Dectin-1 and TLRs permit macrophages to distinguish between different Aspergillus fumigatus cellular states.* J Immunol, 2006. **176**(6): p. 3717-24.
18. Latge, J.P., *The pathobiology of Aspergillus fumigatus.* Trends Microbiol, 2001. **9**(8): p. 382-9.
19. Latge, J.P., *Tasting the fungal cell wall.* Cell Microbiol, 2010. **12**(7): p. 863-72.

20. Gresnigt, M.S., M.G. Netea, and F.L. van de Veerdonk, *Pattern recognition receptors and their role in invasive aspergillosis.* Ann N Y Acad Sci, 2012. **1273**(1): p. 60-7.
21. Figueiredo, R.T., L.A. Carneiro, and M.T. Bozza, *Fungal surface and innate immune recognition of filamentous fungi.* Front Microbiol, 2011. **2**: p. 248.
22. van der Velden, W.J., N.M. Blijlevens, and J.P. Donnelly, *Genetic variants and the risk for invasive mould disease in immunocompromised hematology patients.* Curr Opin Infect Dis, 2011. **24**(6): p. 554-63.
23. Cunha, C., et al., *Dectin-1 Y238X polymorphism associates with susceptibility to invasive aspergillosis in hematopoietic transplantation through impairment of both recipient- and donor-dependent mechanisms of antifungal immunity.* Blood, 2010. **116**(24): p. 5394-402.
24. Sainz, J., et al., *Dectin-1 and DC-SIGN polymorphisms associated with invasive pulmonary Aspergillosis infection.* PLoS One, 2012. **7**(2): p. e32273.
25. Carvalho, A., et al., *Polymorphisms in toll-like receptor genes and susceptibility to pulmonary aspergillosis.* J Infect Dis, 2008. **197**(4): p. 618-21.
26. Cunha, C., et al., *Genetic PTX3 deficiency and aspergillosis in stem-cell transplantation.* N Engl J Med, 2014. **370**(5): p. 421-32.
27. Brown, G.D., et al., *Dectin-1 mediates the biological effects of beta-glucans.* J Exp Med, 2003. **197**(9): p. 1119-24.
28. Drummond, R.A. and G.D. Brown, *The role of Dectin-1 in the host defence against fungal infections.* Curr Opin Microbiol, 2011. **14**(4): p. 392-9.
29. Geijtenbeek, T.B. and S.I. Gringhuis, *Signalling through C-type lectin receptors: shaping immune responses.* Nat Rev Immunol, 2009. **9**(7): p. 465-79.
30. Gross, O., et al., *Syk kinase signalling couples to the Nlrp3 inflammasome for anti-fungal host defence.* Nature, 2009. **459**(7245): p. 433-6.
31. Werner, J.L., et al., *Requisite role for the dectin-1 beta-glucan receptor in pulmonary defense against Aspergillus fumigatus.* J Immunol, 2009. **182**(8): p. 4938-46.
32. LeibundGut-Landmann, S., et al., *Syk- and CARD9-dependent coupling of innate immunity to the induction of T helper cells that produce interleukin 17.* Nat Immunol, 2007. **8**(6): p. 630-8.
33. Serrano-Gomez, D., et al., *Dendritic cell-specific intercellular adhesion molecule 3-grabbing nonintegrin mediates binding and internalization of Aspergillus fumigatus conidia by dendritic cells and macrophages.* J Immunol, 2004. **173**(9): p. 5635-43.
34. Chai, L.Y., et al., *Aspergillus fumigatus conidial melanin modulates host cytokine response.* Immunobiology, 2010. **215**(11): p. 915-20.
35. Loures, F.V., et al., *Recognition of Aspergillus fumigatus Hyphae by Human Plasmacytoid Dendritic Cells Is Mediated by Dectin-2 and Results in Formation of Extracellular Traps.* PLoS Pathog, 2015. **11**(2): p. e1004643.
36. Hecht, P.M. and K.V. Anderson, *Genetic characterization of tube and pelle, genes required for signaling between Toll and dorsal in the specification of the dorsal-ventral pattern of the Drosophila embryo.* Genetics, 1993. **135**(2): p. 405-17.
37. Lemaitre, B., et al., *The dorsoventral regulatory gene cassette spatzle/Toll/cactus controls the potent antifungal response in Drosophila adults.* Cell, 1996. **86**(6): p. 973-83.
38. Medzhitov, R., P. Preston-Hurlburt, and C.A. Janeway, Jr., *A human homologue of the Drosophila Toll protein signals activation of adaptive immunity.* Nature, 1997. **388**(6640): p. 394-7.
39. van de Veerdonk, F.L., et al., *Host-microbe interactions: innate pattern recognition of fungal pathogens.* Curr Opin Microbiol, 2008. **11**(4): p. 305-12.
40. Balloy, V., et al., *Involvement of toll-like receptor 2 in experimental invasive pulmonary aspergillosis.* Infect Immun, 2005. **73**(9): p. 5420-5.

41. Bellocchio, S., et al., *The contribution of the Toll-like/IL-1 receptor superfamily to innate and adaptive immunity to fungal pathogens in vivo.* J Immunol, 2004. **172**(5): p. 3059-69.
42. Dubourdeau, M., et al., *Aspergillus fumigatus induces innate immune responses in alveolar macrophages through the MAPK pathway independently of TLR2 and TLR4.* J Immunol, 2006. **177**(6): p. 3994-4001.
43. Rubino, I., et al., *Species-specific recognition of Aspergillus fumigatus by Toll-like receptor 1 and Toll-like receptor 6.* J Infect Dis, 2012. **205**(6): p. 944-54.
44. Wright, S.D., et al., *CD14, a receptor for complexes of lipopolysaccharide (LPS) and LPS binding protein.* Science, 1990. **249**(4975): p. 1431-3.
45. Wang, J.E., et al., *Involvement of CD14 and toll-like receptors in activation of human monocytes by Aspergillus fumigatus hyphae.* Infection and Immunity, 2001. **69**(4): p. 2402-6.
46. Chai, L.Y., et al., *Aspergillus fumigatus cell wall components differentially modulate host TLR2 and TLR4 responses.* Microbes Infect, 2011. **13**(2): p. 151-9.
47. Chai, L.Y., et al., *Modulation of Toll-like receptor 2 (TLR2) and TLR4 responses by Aspergillus fumigatus.* Infect Immun, 2009. **77**(5): p. 2184-92.
48. Gantner, B.N., et al., *Collaborative induction of inflammatory responses by dectin-1 and Toll-like receptor 2.* J Exp Med, 2003. **197**(9): p. 1107-17.
49. Dennehy, K.M., et al., *Syk kinase is required for collaborative cytokine production induced through Dectin-1 and Toll-like receptors.* Eur J Immunol, 2008. **38**(2): p. 500-6.
50. Carvalho, A., et al., *TLR3 essentially promotes protective class I-restricted memory CD8(+) T-cell responses to Aspergillus fumigatus in hematopoietic transplanted patients.* Blood, 2012. **119**(4): p. 967-77.
51. de Luca, A., et al., *Non-hematopoietic cells contribute to protective tolerance to Aspergillus fumigatus via a TRIF pathway converging on IDO.* Cell Mol Immunol, 2010. **7**(6): p. 459-70.
52. Ramirez-Ortiz, Z.G., et al., *Toll-like receptor 9-dependent immune activation by unmethylated CpG motifs in Aspergillus fumigatus DNA.* Infect Immun, 2008. **76**(5): p. 2123-9.
53. Kasperkovitz, P.V., M.L. Cardenas, and J.M. Vyas, *TLR9 is actively recruited to Aspergillus fumigatus phagosomes and requires the N-terminal proteolytic cleavage domain for proper intracellular trafficking.* J Immunol, 2010. **185**(12): p. 7614-22.
54. Madan, T., et al., *Surfactant proteins A and D protect mice against pulmonary hypersensitivity induced by Aspergillus fumigatus antigens and allergens.* J Clin Invest, 2001. **107**(4): p. 467-75.
55. Madan, T., et al., *Protective role of lung surfactant protein D in a murine model of invasive pulmonary aspergillosis.* Infect Immun, 2001. **69**(4): p. 2728-31.
56. Madan, T., et al., *Susceptibility of mice genetically deficient in SP-A or SP-D gene to invasive pulmonary aspergillosis.* Mol Immunol, 2010. **47**(10): p. 1923-30.
57. Neth, O., et al., *Mannose-binding lectin binds to a range of clinically relevant microorganisms and promotes complement deposition.* Infection and Immunity, 2000. **68**(2): p. 688-93.
58. Clemons, K.V., et al., *Resistance of MBL gene-knockout mice to experimental systemic aspergillosis.* Immunology Letters, 2010. **128**(2): p. 105-7.
59. Kaur, S., et al., *Protective role of mannan-binding lectin in a murine model of invasive pulmonary aspergillosis.* Clinical and Experimental Immunology, 2007. **148**(2): p. 382-9.
60. Garlanda, C., et al., *Non-redundant role of the long pentraxin PTX3 in anti-fungal innate immune response.* Nature, 2002. **420**(6912): p. 182-6.
61. Banchereau, J. and R.M. Steinman, *Dendritic cells and the control of immunity.* Nature, 1998. **392**(6673): p. 245-52.

62. Steinman, R.M. and Z.A. Cohn, *Identification of a novel cell type in peripheral lymphoid organs of mice. I. Morphology, quantitation, tissue distribution.* J Exp Med, 1973. **137**(5): p. 1142-62.
63. Collin, M., N. McGovern, and M. Haniffa, *Human dendritic cell subsets.* Immunology, 2013. **140**(1): p. 22-30.
64. Abbas, A.K., A.H. Lichtman, and S. Pillai, *Cellular and molecular immunology*. Vol. 8. 2015, Philadelphia: Elsevier/Saunders.
65. Reizis, B., et al., *Plasmacytoid dendritic cells: recent progress and open questions.* Annu Rev Immunol, 2011. **29**: p. 163-83.
66. Perdiguero, E.G., et al., *Tissue-resident macrophages originate from yolk-sac-derived erythro-myeloid progenitors.* Nature, 2014.
67. Roeder, A., et al., *Toll-like receptors as key mediators in innate antifungal immunity.* Med Mycol, 2004. **42**(6): p. 485-98.
68. Levitz, S.M., *Interactions of Toll-like receptors with fungi.* Microbes Infect, 2004. **6**(15): p. 1351-5.
69. Mezger, M., et al., *Proinflammatory response of immature human dendritic cells is mediated by dectin-1 after exposure to Aspergillus fumigatus germ tubes.* J Infect Dis, 2008. **197**(6): p. 924-31.
70. Bozza, S., et al., *Dendritic cells transport conidia and hyphae of Aspergillus fumigatus from the airways to the draining lymph nodes and initiate disparate Th responses to the fungus.* J Immunol, 2002. **168**(3): p. 1362-71.
71. Park, S.J., et al., *Neutropenia enhances lung dendritic cell recruitment in response to Aspergillus via a cytokine-to-chemokine amplification loop.* J Immunol, 2010. **185**(10): p. 6190-7.
72. Hartigan, A.J., et al., *CCR7 deficiency on dendritic cells enhances fungal clearance in a murine model of pulmonary invasive aspergillosis.* J Immunol, 2009. **183**(8): p. 5171-9.
73. Persat, F., et al., *Binding of live conidia of Aspergillus fumigatus activates in vitro-generated human Langerhans cells via a lectin of galactomannan specificity.* Clin Exp Immunol, 2003. **133**(3): p. 370-7.
74. Ramirez-Ortiz, Z.G., et al., *A nonredundant role for plasmacytoid dendritic cells in host defense against the human fungal pathogen Aspergillus fumigatus.* Cell Host Microbe, 2011. **9**(5): p. 415-24.
75. Lother, J., et al., *Human dendritic cell subsets display distinct interactions with the pathogenic mould Aspergillus fumigatus.* Int J Med Microbiol, 2014. **304**(8): p. 1160-8.
76. Bozza, S., et al., *A dendritic cell vaccine against invasive aspergillosis in allogeneic hematopoietic transplantation.* Blood, 2003. **102**(10): p. 3807-14.
77. Roy, R.M. and B.S. Klein, *Dendritic cells in antifungal immunity and vaccine design.* Cell Host Microbe, 2012. **11**(5): p. 436-46.
78. Segal, B.H., *Aspergillosis.* N Engl J Med, 2009. **360**(18): p. 1870-84.
79. Hebart, H., et al., *Analysis of T-cell responses to Aspergillus fumigatus antigens in healthy individuals and patients with hematologic malignancies.* Blood, 2002. **100**(13): p. 4521-8.
80. Wuthrich, M., G.S. Deepe, Jr., and B. Klein, *Adaptive immunity to fungi.* Annu Rev Immunol, 2012. **30**: p. 115-48.
81. Kreindler, J.L., et al., *Vitamin D3 attenuates Th2 responses to Aspergillus fumigatus mounted by CD4+ T cells from cystic fibrosis patients with allergic bronchopulmonary aspergillosis.* J Clin Invest, 2010. **120**(9): p. 3242-54.
82. Romani, L., *Immunity to fungal infections.* Nat Rev Immunol, 2011. **11**(4): p. 275-88.
83. Zelante, T., et al., *IL-23 and the Th17 pathway promote inflammation and impair antifungal immune resistance.* Eur J Immunol, 2007. **37**(10): p. 2695-706.

84. Rivera, A., et al., *Dectin-1 diversifies Aspergillus fumigatus-specific T cell responses by inhibiting T helper type 1 CD4 T cell differentiation.* J Exp Med, 2011. **208**(2): p. 369-81.
85. Chai, L.Y., et al., *Anti-Aspergillus human host defence relies on type 1 T helper (Th1), rather than type 17 T helper (Th17), cellular immunity.* Immunology, 2010. **130**(1): p. 46-54.
86. Casadevall, A. and L.A. Pirofski, *Immunoglobulins in defense, pathogenesis, and therapy of fungal diseases.* Cell Host Microbe, 2012. **11**(5): p. 447-56.
87. Chaturvedi, A.K., et al., *Monoclonal immunoglobulin G1 directed against Aspergillus fumigatus cell wall glycoprotein protects against experimental murine aspergillosis.* Clin Diagn Lab Immunol, 2005. **12**(9): p. 1063-8.
88. Apostolopoulos, V., et al., *Dendritic cell immunotherapy: clinical outcomes.* Clin Transl Immunology, 2014. **3**(7): p. e21.
89. Satpathy, A.T., et al., *Zbtb46 expression distinguishes classical dendritic cells and their committed progenitors from other immune lineages.* J Exp Med, 2012. **209**(6): p. 1135-52.
90. Rey-Giraud, F., M. Hafner, and C.H. Ries, *In vitro generation of monocyte-derived macrophages under serum-free conditions improves their tumor promoting functions.* PLoS One, 2012. **7**(8): p. e42656.
91. Schaible, B., K. Schaffer, and C.T. Taylor, *Hypoxia, innate immunity and infection in the lung.* Respir Physiol Neurobiol, 2010. **174**(3): p. 235-43.
92. Ben-Ami, R., *Angiogenesis at the mold-host interface: a potential key to understanding and treating invasive aspergillosis.* Future Microbiol, 2013. **8**(11): p. 1453-62.
93. Grahl, N., et al., *In vivo hypoxia and a fungal alcohol dehydrogenase influence the pathogenesis of invasive pulmonary aspergillosis.* PLoS Pathog, 2011. **7**(7): p. e1002145.
94. Varia, M.A., et al., *Pimonidazole: a novel hypoxia marker for complementary study of tumor hypoxia and cell proliferation in cervical carcinoma.* Gynecol Oncol, 1998. **71**(2): p. 270-7.
95. Warn, P.A., et al., *Effect of hypoxic conditions on in vitro susceptibility testing of amphotericin B, itraconazole and micafungin against Aspergillus and Candida.* J Antimicrob Chemother, 2004. **53**(5): p. 743-9.
96. Wezensky, S.J. and R.A. Cramer, Jr., *Implications of hypoxic microenvironments during invasive aspergillosis.* Med Mycol, 2011. **49 Suppl 1**: p. S120-4.
97. Willger, S.D., N. Grahl, and R.A. Cramer, Jr., *Aspergillus fumigatus metabolism: clues to mechanisms of in vivo fungal growth and virulence.* Med Mycol, 2009. **47 Suppl 1**: p. S72-9.
98. Hall, L.A. and D.W. Denning, *Oxygen requirements of Aspergillus species.* J Med Microbiol, 1994. **41**(5): p. 311-5.
99. Taubitz, A., et al., *Role of respiration in the germination process of the pathogenic mold Aspergillus fumigatus.* Curr Microbiol, 2007. **54**(5): p. 354-60.
100. Willger, S.D., et al., *A sterol-regulatory element binding protein is required for cell polarity, hypoxia adaptation, azole drug resistance, and virulence in Aspergillus fumigatus.* PLoS Pathog, 2008. **4**(11): p. e1000200.
101. Hughes, A.L., B.L. Todd, and P.J. Espenshade, *SREBP pathway responds to sterols and functions as an oxygen sensor in fission yeast.* Cell, 2005. **120**(6): p. 831-42.
102. Todd, B.L., et al., *Sterol regulatory element binding protein is a principal regulator of anaerobic gene expression in fission yeast.* Mol Cell Biol, 2006. **26**(7): p. 2817-31.
103. Willger, S.D., et al., *Dsc orthologs are required for hypoxia adaptation, triazole drug responses, and fungal virulence in Aspergillus fumigatus.* Eukaryot Cell, 2012. **11**(12): p. 1557-67.
104. Bien, C.M. and P.J. Espenshade, *Sterol regulatory element binding proteins in fungi: hypoxic transcription factors linked to pathogenesis.* Eukaryot Cell, 2010. **9**(3): p. 352-9.

105. Kroll, K., et al., *Identification of hypoxia-inducible target genes of Aspergillus fumigatus by transcriptome analysis reveals cellular respiration as an important contributor to hypoxic survival.* Eukaryot Cell, 2014. **13**(9): p. 1241-53.
106. Shepardson, K.M., et al., *Hypoxia enhances innate immune activation to Aspergillus fumigatus through cell wall modulation.* Microbes Infect, 2013. **15**(4): p. 259-69.
107. Semenza, G.L., *Regulation of oxygen homeostasis by hypoxia-inducible factor 1.* Physiology (Bethesda), 2009. **24**: p. 97-106.
108. Semenza, G.L. and G.L. Wang, *A nuclear factor induced by hypoxia via de novo protein synthesis binds to the human erythropoietin gene enhancer at a site required for transcriptional activation.* Mol Cell Biol, 1992. **12**(12): p. 5447-54.
109. Wang, G.L., et al., *Hypoxia-inducible factor 1 is a basic-helix-loop-helix-PAS heterodimer regulated by cellular O2 tension.* Proc Natl Acad Sci U S A, 1995. **92**(12): p. 5510-4.
110. Hara, S., et al., *Expression and characterization of hypoxia-inducible factor (HIF)-3alpha in human kidney: suppression of HIF-mediated gene expression by HIF-3alpha.* Biochem Biophys Res Commun, 2001. **287**(4): p. 808-13.
111. Tian, H., S.L. McKnight, and D.W. Russell, *Endothelial PAS domain protein 1 (EPAS1), a transcription factor selectively expressed in endothelial cells.* Genes Dev, 1997. **11**(1): p. 72-82.
112. Palazon, A., et al., *HIF transcription factors, inflammation, and immunity.* Immunity, 2014. **41**(4): p. 518-28.
113. Weidemann, A. and R.S. Johnson, *Biology of HIF-1alpha.* Cell Death Differ, 2008. **15**(4): p. 621-7.
114. McNeill, L.A., et al., *Hypoxia-inducible factor asparaginyl hydroxylase (FIH-1) catalyses hydroxylation at the beta-carbon of asparagine-803.* Biochem J, 2002. **367**(Pt 3): p. 571-5.
115. Ebert, B.L. and H.F. Bunn, *Regulation of transcription by hypoxia requires a multiprotein complex that includes hypoxia-inducible factor 1, an adjacent transcription factor, and p300/CREB binding protein.* Mol Cell Biol, 1998. **18**(7): p. 4089-96.
116. Chilov, D., et al., *Induction and nuclear translocation of hypoxia-inducible factor-1 (HIF-1): heterodimerization with ARNT is not necessary for nuclear accumulation of HIF-1alpha.* J Cell Sci, 1999. **112 (Pt 8)**: p. 1203-12.
117. Iyer, N.V., et al., *Cellular and developmental control of O2 homeostasis by hypoxia-inducible factor 1 alpha.* Genes Dev, 1998. **12**(2): p. 149-62.
118. Greer, S.N., et al., *The updated biology of hypoxia-inducible factor.* EMBO J, 2012. **31**(11): p. 2448-60.
119. Nizet, V. and R.S. Johnson, *Interdependence of hypoxic and innate immune responses.* Nat Rev Immunol, 2009. **9**(9): p. 609-17.
120. Strieter, R.M., *Mastering innate immunity.* Nat Med, 2003. **9**(5): p. 512-3.
121. Cramer, T., et al., *HIF-1alpha is essential for myeloid cell-mediated inflammation.* Cell, 2003. **112**(5): p. 645-57.
122. Zinkernagel, A.S., R.S. Johnson, and V. Nizet, *Hypoxia inducible factor (HIF) function in innate immunity and infection.* J Mol Med (Berl), 2007. **85**(12): p. 1339-46.
123. Peyssonnaux, C., et al., *HIF-1alpha expression regulates the bactericidal capacity of phagocytes.* J Clin Invest, 2005. **115**(7): p. 1806-15.
124. Rupp, J., et al., *Chlamydia pneumoniae directly interferes with HIF-1alpha stabilization in human host cells.* Cell Microbiol, 2007. **9**(9): p. 2181-91.
125. Palsson-McDermott, E.M. and L.A. O'Neill, *The Warburg effect then and now: from cancer to inflammatory diseases.* Bioessays, 2013. **35**(11): p. 965-73.
126. Semenza, G.L., *Regulation of metabolism by hypoxia-inducible factor 1.* Cold Spring Harb Symp Quant Biol, 2011. **76**: p. 347-53.

127. Walmsley, S.R., et al., *Hypoxia-induced neutrophil survival is mediated by HIF-1alpha-dependent NF-kappaB activity.* J Exp Med, 2005. **201**(1): p. 105-15.
128. Rius, J., et al., *NF-kappaB links innate immunity to the hypoxic response through transcriptional regulation of HIF-1alpha.* Nature, 2008. **453**(7196): p. 807-11.
129. Frede, S., et al., *Bacterial lipopolysaccharide induces HIF-1 activation in human monocytes via p44/42 MAPK and NF-kappaB.* Biochem J, 2006. **396**(3): p. 517-27.
130. Shepardson, K.M., et al., *Myeloid derived hypoxia inducible factor 1-alpha is required for protection against pulmonary Aspergillus fumigatus infection.* PLoS Pathog, 2014. **10**(9): p. e1004378.
131. Clausen, B.E., et al., *Conditional gene targeting in macrophages and granulocytes using LysMcre mice.* Transgenic Research, 1999. **8**(4): p. 265-77.
132. Bhandari, T. and V. Nizet, *Hypoxia-Inducible Factor (HIF) as a Pharmacological Target for Prevention and Treatment of Infectious Diseases.* Infect Dis Ther, 2014.
133. Pierobon, D., et al., *Chronic hypoxia reprograms human immature dendritic cells by inducing a proinflammatory phenotype and TREM-1 expression.* Eur J Immunol, 2013. **43**(4): p. 949-66.
134. Jantsch, J., et al., *Hypoxia and hypoxia-inducible factor-1 alpha modulate lipopolysaccharide-induced dendritic cell activation and function.* J Immunol, 2008. **180**(7): p. 4697-705.
135. Kohler, T., et al., *Influence of hypoxia-inducible factor 1alpha on dendritic cell differentiation and migration.* Eur J Immunol, 2012. **42**(5): p. 1226-36.
136. Spirig, R., et al., *Effects of TLR agonists on the hypoxia-regulated transcription factor HIF-1alpha and dendritic cell maturation under normoxic conditions.* PLoS One, 2010. **5**(6): p. e0010983.
137. Mancino, A., et al., *Divergent effects of hypoxia on dendritic cell functions.* Blood, 2008. **112**(9): p. 3723-34.
138. Jantsch, J. and J. Schodel, *Hypoxia and hypoxia-inducible factors in myeloid cell-driven host defense and tissue homeostasis.* Immunobiology, 2015. **220**(2): p. 305-14.
139. Scholz, C.C. and C.T. Taylor, *Targeting the HIF pathway in inflammation and immunity.* Curr Opin Pharmacol, 2013. **13**(4): p. 646-53.
140. Einsele, H., et al., *Immunotherapy for viral and fungal infections.* Bone Marrow Transplant, 2015. **50 Suppl 2**: p. S51-4.
141. Ruijter, J.M., et al., *Amplification efficiency: linking baseline and bias in the analysis of quantitative PCR data.* Nucleic Acids Res, 2009. **37**(6): p. e45.
142. Neron, S., et al., *Characterization of mononuclear cells remaining in the leukoreduction system chambers of apheresis instruments after routine platelet collection: a new source of viable human blood cells.* Transfusion, 2007. **47**(6): p. 1042-9.
143. Edgar, R., M. Domrachev, and A.E. Lash, *Gene Expression Omnibus: NCBI gene expression and hybridization array data repository.* Nucleic Acids Res, 2002. **30**(1): p. 207-10.
144. Benjamini, Y. and Y. Hochberg, *Controlling the False Discovery Rate: A Practical and Powerful Approach to Multiple Testing.* Journal of the Royal Statistical Society. Series B (Methodological), 1995. **57**(1): p. 289-300.
145. Hulsen, T., J. de Vlieg, and W. Alkema, *BioVenn - a web application for the comparison and visualization of biological lists using area-proportional Venn diagrams.* BMC Genomics, 2008. **9**: p. 488.
146. Buettner, M., et al., *Inverse correlation of maturity and antibacterial activity in human dendritic cells.* J Immunol, 2005. **174**(7): p. 4203-9.
147. Garbers, C., S. Aparicio-Siegmund, and S. Rose-John, *The IL-6/gp130/STAT3 signaling axis: recent advances towards specific inhibition.* Curr Opin Immunol, 2015. **34C**: p. 75-82.

148. Forster, R., et al., *CCR7 coordinates the primary immune response by establishing functional microenvironments in secondary lymphoid organs.* Cell, 1999. **99**(1): p. 23-33.
149. Robbins, S.H., et al., *Novel insights into the relationships between dendritic cell subsets in human and mouse revealed by genome-wide expression profiling.* Genome Biol, 2008. **9**(1): p. R17.
150. Hirano, T., K. Ishihara, and M. Hibi, *Roles of STAT3 in mediating the cell growth, differentiation and survival signals relayed through the IL-6 family of cytokine receptors.* Oncogene, 2000. **19**(21): p. 2548-56.
151. Del Corno, M., et al., *HIV-1 gp120 activates the STAT3/interleukin-6 axis in primary human monocyte-derived dendritic cells.* J Virol, 2014. **88**(19): p. 11045-55.
152. Lee, M.Y., et al., *Phosphorylation and activation of STAT proteins by hypoxia in breast cancer cells.* Breast, 2006. **15**(2): p. 187-95.
153. Jung, J.E., et al., *STAT3 is a potential modulator of HIF-1-mediated VEGF expression in human renal carcinoma cells.* FASEB J, 2005. **19**(10): p. 1296-8.
154. Pawlus, M.R., L. Wang, and C.J. Hu, *STAT3 and HIF1alpha cooperatively activate HIF1 target genes in MDA-MB-231 and RCC4 cells.* Oncogene, 2014. **33**(13): p. 1670-9.
155. Assi, H., et al., *Assessing the role of STAT3 in DC differentiation and autologous DC immunotherapy in mouse models of GBM.* PLoS One, 2014. **9**(5): p. e96318.
156. Sanseverino, I., et al., *STAT3-silenced human dendritic cells have an enhanced ability to prime IFNgamma production by both alphabeta and gammadelta T lymphocytes.* Immunobiology, 2014. **219**(7): p. 503-11.
157. Nefedova, Y., et al., *Activation of dendritic cells via inhibition of Jak2/STAT3 signaling.* J Immunol, 2005. **175**(7): p. 4338-46.
158. Nallamshetty, S., S.Y. Chan, and J. Loscalzo, *Hypoxia: a master regulator of microRNA biogenesis and activity.* Free Radic Biol Med, 2013. **64**: p. 20-30.
159. Pillai, R.S., S.N. Bhattacharyya, and W. Filipowicz, *Repression of protein synthesis by miRNAs: how many mechanisms?* Trends Cell Biol, 2007. **17**(3): p. 118-26.
160. Taganov, K.D., et al., *NF-kappaB-dependent induction of microRNA miR-146, an inhibitor targeted to signaling proteins of innate immune responses.* Proc Natl Acad Sci U S A, 2006. **103**(33): p. 12481-6.
161. Chan, S.Y., et al., *MicroRNA-210 controls mitochondrial metabolism during hypoxia by repressing the iron-sulfur cluster assembly proteins ISCU1/2.* Cell Metab, 2009. **10**(4): p. 273-84.
162. Bruning, U., et al., *MicroRNA-155 promotes resolution of hypoxia-inducible factor 1alpha activity during prolonged hypoxia.* Mol Cell Biol, 2011. **31**(19): p. 4087-96.
163. Das Gupta, M., et al., *Aspergillus fumigatus induces microRNA-132 in human monocytes and dendritic cells.* Int J Med Microbiol, 2014. **304**(5-6): p. 592-6.
164. Werth, N., et al., *Activation of hypoxia inducible factor 1 is a general phenomenon in infections with human pathogens.* PLoS One, 2010. **5**(7): p. e11576.
165. Kingeter, L.M. and X. Lin, *C-type lectin receptor-induced NF-kappaB activation in innate immune and inflammatory responses.* Cell Mol Immunol, 2012. **9**(2): p. 105-12.
166. Kuschel, A., P. Simon, and S. Tug, *Functional regulation of HIF-1alpha under normoxia--is there more than post-translational regulation?* Journal of Cellular Physiology, 2012. **227**(2): p. 514-24.
167. Tannahill, G.M., et al., *Succinate is an inflammatory signal that induces IL-1beta through HIF-1alpha.* Nature, 2013. **496**(7444): p. 238-42.
168. Sharma, M., et al., *HIF-1alpha is involved in mediating apoptosis resistance to Chlamydia trachomatis-infected cells.* Cell Microbiol, 2011. **13**(10): p. 1573-85.

169. Jantsch, J., et al., *Toll-like receptor activation and hypoxia use distinct signaling pathways to stabilize hypoxia-inducible factor 1alpha (HIF1A) and result in differential HIF1A-dependent gene expression.* J Leukoc Biol, 2011. **90**(3): p. 551-62.
170. Goodridge, H.S., R.M. Simmons, and D.M. Underhill, *Dectin-1 stimulation by Candida albicans yeast or zymosan triggers NFAT activation in macrophages and dendritic cells.* Journal of Immunology, 2007. **178**(5): p. 3107-15.
171. Buxade, M., et al., *Gene expression induced by Toll-like receptors in macrophages requires the transcription factor NFAT5.* Journal of Experimental Medicine, 2012. **209**(2): p. 379-93.
172. Everts, B. and E.J. Pearce, *Metabolic control of dendritic cell activation and function: recent advances and clinical implications.* Front Immunol, 2014. **5**: p. 203.
173. Cenci, E., et al., *Impaired antifungal effector activity but not inflammatory cell recruitment in interleukin-6-deficient mice with invasive pulmonary aspergillosis.* J Infect Dis, 2001. **184**(5): p. 610-7.
174. Gafa, V., et al., *Human dendritic cells following Aspergillus fumigatus infection express the CCR7 receptor and a differential pattern of interleukin-12 (IL-12), IL-23, and IL-27 cytokines, which lead to a Th1 response.* Infect Immun, 2006. **74**(3): p. 1480-9.
175. Schuh, J.M., K. Blease, and C.M. Hogaboam, *The role of CC chemokine receptor 5 (CCR5) and RANTES/CCL5 during chronic fungal asthma in mice.* FASEB J, 2002. **16**(2): p. 228-30.
176. Semenza, G.L., *Oxygen homeostasis.* Wiley Interdiscip Rev Syst Biol Med, 2010. **2**(3): p. 336-61.
177. Semmlinger, A., et al., *Fever-range temperature modulates activation and function of human dendritic cells stimulated with the pathogenic mould Aspergillus fumigatus.* Med Mycol, 2014. **52**(4): p. 438-44.
178. Wezensky, S.J. and R.A. Cramer, Jr., *Implications of hypoxic microenvironments during invasive aspergillosis.* Medical Mycology, 2011. **49 Suppl 1**: p. S120-4.
179. Brock, M., et al., *Bioluminescent Aspergillus fumigatus, a new tool for drug efficiency testing and in vivo monitoring of invasive aspergillosis.* Applied and Environmental Microbiology, 2008. **74**(22): p. 7023-35.
180. Hsu, J.L., et al., *Aspergillus fumigatus invasion increases with progressive airway ischemia.* PLoS One, 2013. **8**(10): p. e77136.
181. Zinkernagel, A.S., et al., *Pharmacologic augmentation of hypoxia-inducible factor-1alpha with mimosine boosts the bactericidal capacity of phagocytes.* J Infect Dis, 2008. **197**(2): p. 214-7.
182. Morton, C.O., et al., *Gene expression profiles of human dendritic cells interacting with Aspergillus fumigatus in a bilayer model of the alveolar epithelium/endothelium interface.* PLoS One, 2014. **9**(5): p. e98279.

Appendix

Tables and Figures

List of Tables

List of Figures

Abbreviations

ABPA Allergic bronchopulmonary aspergillosis
AIDS Acquired immune deficiency syndrome
APC Allophycocyanin (fluorochrome)
ATCC American type culture collection
BAL Bronchoalveolar lavage
CBP CREB binding protein
CD Cluster of differentiation/Classification determinant
CLR C-type lectin receptor
CNA Chronic necrotizing aspergillosis
DC Dendritic cell
FCS Fetal calf serum
FITC Fluorescein isothiocyanate (fluorochrome)
HIV Human immunodeficiency virus
HLA Human leukocyte antigen
HSCT Hematopoietic stem cell transplantation
IA Invasive aspergillosis
ITAM Immunoreceptor tyrosine-based activation motif
IPA Ingenuity Pathway Analysis
LPS Lipopolysaccharide
MACS Magnetic activated cell sorting
MCSF Macrophage-colony stimulating factor
MHC Major histocompatibility complex
MOI Multiplicity of infection
NLR NOD-like receptor
NOD Nucleotide-binding oligomerization domain
NK Natural Killer
PAMP Pathogen associated molecular pattern
PBMC Peripheral blood mononuclear cell
PE Phycoerythrin (fluorchrome)
PI Propidium iodide
PMN Polymorphonuclear leukocyte
PRR Pattern recognition receptor
RIG Retinoic acid-inducible gene
ROS Reactive oxygen species
rpm Revolutions per minute
RT Room temperature
SD Standard deviation
SEM Standard error of the mean
TLR Toll-like receptor
VHL Von-Hippel Lindau
WT Wild type

Publications

Scientific articles

Data from this study are published as:

- **"Hypoxia-inducible factor 1α modulates metabolic activity and cytokine release in anti-*Aspergillus fumigatus* immune responses initiated by human dendritic cells"**

  Fliesser M, Morton CO, Bonin M, Ebel F, Hünniger K, Kurzai O, Einsele H, Loeffler J. *Int J Med Microbiol.* 2015 Sep 16. pii: S1438-4221(15)30005-9. doi: 10.1016/ j.ijmm.2015.08.036. [Epub ahead of print]

During the time course of this PhD thesis, I was involved in several related projects (apart from this study) that resulted in the following publications:

- **"Gene expression profiles of human dendritic cells interacting with *Aspergillus fumigatus* in a bilayer model of the alveolar epithelium/endothelium interface."** [182]

  Morton CO, **Fliesser M**, Dittrich M, Mueller T, Bauer R, Kneitz S, Hope W, Rogers TR, Einsele H, Loeffler J. *PLoS One*. 2014 May 28;9(5)

- **"*Aspergillus fumigatus* induces microRNA-132 in human monocytes and dendritic cells."** [163]

  Das Gupta M*, **Fliesser M***, Springer J, Breitschopf T, Schlossnagel H, Schmitt AL, Kurzai O, Hünniger K, Einsele H, Löffler J. *Int J Med Microbiol.* 2014 Jul;304(5-6):592-6.

  *These authors contributed equally to the manuscript.

- **"Fever-range temperature modulates activation and function of human dendritic cells stimulated with the pathogenic mould *Aspergillus fumigatus*."** [177]

  Semmlinger A*, **Fliesser M***, Waaga-Gasser AM, Dragan M, Morton CO, Einsele H, Loeffler J. *Med Mycol.* 2014 May;52(4):438-44.

  *A. S. and M. F. contributed equally to the manuscript.

Conference contributions

Data from this study were presented on several national and international conferences.

Oral presentation:

- 65. Jahrestagung der DGHM, Rostock 2013

Poster presentations:

- 6th Advances Against Aspergillosis, Madrid 2014
- 43. Annual meeting of the DGfI, Mainz 2013
- Annual meeting of the DGHO, Stuttgart 2012
- 64. Annual meeting of the DGHM, Hamburg 2012
- Training the innate immunity, Nijmegen 2012

Erklärung

Erklärungen nach §4 Abs. 3 Satz 3, 5, 8 der Promotionsordnung der Fakultät für Biologie

Affidavit

I hereby declare that my thesis entitled: "Hypoxia and hypoxia-inducible factor 1α modulate the immune response of human dendritic cells against *Aspergillus fumigatus*" is the result of my own work.

I did not receive any help or support from commercial consultants. All sources and/or materials applied are listed and specified in the thesis.

Furthermore I verify that the thesis has not been submitted as part of another examination process neither in identical nor in similar form.

Eidesstattliche Erklärung

Hiermit erkläre ich an Eides statt, die Dissertation: „Hypoxie und Hypoxie-induzierter Faktor 1α modulieren die Immunantwort humaner dendritischer Zellen gegenüber *Aspergillus fumigatus*", eigenständig, d. h. insbesondere selbständig und ohne Hilfe eines kommerziellen Promotionsberaters, angefertigt und keine anderen als die von mir angegebenen Quellen und Hilfsmittel verwendet zu haben.

Ich erkläre außerdem, dass die Dissertation weder in gleicher noch in ähnlicher Form bereits in einem anderen Prüfungsverfahren vorgelegen hat.

Würzburg, den 11.08.2015

_____

(Mirjam Fließer)